Modelling evolution of host defence in seasonal environments.

Charlotte Evangeline Ferris

Submitted for the degree of Doctor of Philosophy (PhD)

School of Mathematics and Statistics

University of Sheffield

May 2019

Supervisors: Alex Best, Michael Brockhurst, Dylan Childs

In memory of my aunt, Kitty.

Abstract

Infectious disease is rife throughout the world, with species at risk of infection at every level, from bacteria to humans. These diseases can have devastating effects on populations, which has led to a rich biological and mathematical literature on this topic. There are many factors that can affect the spread and impact of an infectious disease, including environmental heterogeneity and host-parasite evolution. The combination of infection dynamics, heterogeneous environments and evolution could provide powerful insights into real-world systems; however, this has yet to be explored in much detail with regards to temporally heterogeneous environments.

In this thesis I use mathematical models and experimental techniques to investigate the effect of temporally fluctuating environments on host-parasite evolution. Throughout the mathematical analysis, I use the adaptive dynamics framework to study evolution, and implement temporal heterogeneity through a periodic host birth rate. First, I consider host-only evolution through avoidance, and consider how increasingly variable environments affects the end-point of evolution. Second, I investigate the potential for host diversity through three different defence mechanisms in a seasonal environment, with a particular focus on evolution through mortality tolerance. I then conduct an experimental evolution study using the bacteria *P. fluorescens* SBW25 and its parasitic bacteriophage SBW25Φ2, where environmental heterogeneity is implemented through oscillating nutrient concentrations. The results from the experiment are reinforced by a coevolutionary model, which incorporates seasonality through evidence-based assumptions on the bacterial growth.

The work in this thesis is part of a growing field of research investigating temporal environments and evolution in host-parasite systems. It contributes some important results to the field, and demonstrates the power of developing experimental and theoretical work together, which can result in a more cohesive understanding of host-parasite evolution.

Acknowledgements

First and foremost, I want to thank my supervisor Dr. Alex Best for taking me on as a student, for supporting me as I got to grips with research, and for helping me to drastically improve my writing! I couldn't have done this without all of his hard work and encouragement.

Second, I would like to thank Prof. Mike Brockhurst and Dr. Rosanna Wright for their contributions to the experimental work in Chapter 5. Extra special thanks to Rosanna, who spent many hours of her time teaching a mathematician how to work in a wet lab.

Further thanks go to Dr. Dylan Childs, Dr Jonathan Potts, the mathematical biology group and the Brockhurst lab for their conversations, questions and suggestions. Thank you to my family for their support throughout my PhD, including an almost constant supply of chocolate from Uncle Hugh.

Last, but certainly not least, I want to thank Rosie. She has supported me through all the ups and downs, let me incessantly talk at her, helped me to write, encouraged me to work rather than cuddle the cats, bought (yet more) chocolate, has been been a shoulder to cry on and someone I could share my excitement with. The last year has been tough, but I'm glad we can come out of it together.

Contents

List of Tables

List of Figures

Chapter 1

Introduction

§ 1.1 Hosts and Parasites

Infectious disease is rife throughout the world, with species at risk of infection at every level, from bacteria to humans. Infection can have devastating effects on populations, which has led to a rich literature on the spread of infectious diseases, including possible ways to control or limit the detrimental effects of a disease (Colditz et al., 1994; Shepard et al., 2006). This is still an active area of research today, and the field has been expanded to consider many other problems, for example pests in agriculture (Landis et al., 2000; Berg, 2009), conservation (e.g. red squirells, Haller et al., 2014; White et al., 2016), and antibiotic resistance (Neu, 1992; Levy & Marshall, 2004). While the study of infectious disease has a long history, there are many influential aspects that are yet to be fully explored and understood.

Mathematical modelling of infectious diseases has long been used to understand and predict the spread and impact of outbreaks. This approach allows us to consider various drivers and outcomes of infectious diseases theoretically, and can be used to determine effective prevention strategies before they are implemented in real-world situations. This is often done by splitting the interacting species into 'hosts' and 'parasites'. Hosts are species that can be infected, for example humans, bacteria, plants, etc. Many current infection models split these hosts into classes depending on their infectious status, an assumption which is based on the susceptible-infected-recovered (SIR) framework developed by Kermack & McKendrick (1927, 1932, 1933) (see also Anderson & May, 1981). On the other hand, parasites are species that infect and potentially harm hosts, for example bacteria, viruses and fungi. Parasites can be further divided into 'mi-

croparasites' and 'macroparasites'. Microparasites are characterised by small size, short generation times and high multiplication rates within hosts (Anderson & May, 1979, 1981), e.g. viruses and bacteria. In this case, the parasite is only modelled through the number of infected hosts as there can be thousands of individual microparasites within one infected host. In contrast, macroparasites are larger and tend not to multiply within hosts, for example flatworms and nematodes, and so the parasite is modelled as a separate entity since different hosts will have different numbers of parasites (May & Anderson, 1979). The work here will focus on microparasites that are not modelled explicitly, but others have considered the infection dynamics of macroparasites (Fenton et al., 2006a; Crossan et al., 2007; Taylor et al., 2015; McCallum et al., 2017; Orlofske et al., 2018). With these definitions for hosts and parasites, a model can be created to describe a general or specific infection system. Further, empirical data can provide estimates of parameters (Ferguson et al., 2006; Smith et al., 2008; Reynolds et al., 2013; Taylor et al., 2015; Macpherson et al., 2016) which could lead to more accurate infection predictions or information about the system that could not be measured experimentally.

Often we want to know the circumstances that can lead to an endemic infectious disease, whereby a parasite survives and persists in a given host population. This can usually be characterised by how many susceptible hosts are infected by one infectious individual, as this number indicates the relative speed at which the disease can spread through a host population. Many use the basic reproduction number R_0, which is defined to be the number of secondary cases from one infected individual in an otherwise susceptible population (Diekmann et al., 1990). A parasite can invade a population, and potentially become endemic, if $R_0 > 1$, i.e. if an infected individual infects more than one susceptible host. Equally, if $R_0 < 1$, the parasite will not spread through the population and so does not usually invade or become endemic (but see, for example, Roberts, 2007). The basic reproduction number is often used to predict if a disease will spread through a population, and can be calculated from models or data (Diekmann et al., 1990; Roberts, 2007; Imai et al., 2016; Inaba, 2016; Guerra et al., 2017; Klinkenberg et al., 2018; Zhang & Iacono, 2018; Zhou et al., 2019). For example, Measles is estimated to have reproduction number 12–18 (Anderson & May, 1982), making it one of the fastest spreading diseases among humans. However, Measles is not endemic due to wide spread vaccination against the disease. Hence, while the reproduction number is a useful quantity to consider, a closely related, but perhaps more indicative, measure of the spread of a disease is the 'effective' reproduction number (R_e), which estimates the number of secondary cases from one infected individual when there is some level of

immunity in the host population. Many factors can influence the value of the effective reproduction number, for example vaccination and age-structure (Anderson & May, 1985; Diekmann et al., 1990; Cai et al., 2017), with Inaba (2016) finding that when re-infection is possible, bifurcations of the infection dynamics mean that attaining $R_e < 1$ through vaccination may not be enough to prevent the transmission of a disease. Given that the factors which determine R_0 and R_e can be specific to particular diseases or locations, estimates of either reproduction number may need to be redetermined for a given population or area (Johansson et al., 2011; Biggerstaff et al., 2014; Guerra et al., 2017).

While the SIR framework is common throughout infection modelling literature, models have been extended in many different ways to incorporate various aspects of host-parasite dynamics. For example, some have increased complexity by additional species (Venturino, 2001, 2002; Sofonea et al., 2015), while others have used this framework to evaluate the efficacy of different prevention methods (Lipsitch et al., 2003; Ferguson et al., 2006; Porter et al., 2012; Smith? et al., 2017; Díez-Delgado et al., 2018). When modelling a specific disease, we often need to consider how it is transmitted in order to achieve realistic predictions. Generally transmission is assumed to be horizontal through a 'mass-action' principle, whereby the population is well mixed and any infected host can infect any susceptible host (McCallum et al., 2001; Begon et al., 2002). However this is not always accurate, and alternative methods are sometimes needed to reflect the biology of different infections. For example, some parasites are transmitted vertically, whereby infected parents can directly transmit the parasite to their offspring, resulting in an extra infected birth term in differential equation models (Hurst et al., 1994; Teixeira et al., 2008; Jaenike et al., 2010; Fenton et al., 2011; Jones et al., 2011). Alternatively some parasites are transmitted via vectors, which are modelled by adding extra equations to denote the susceptible and infected vector populations (Alizon & van Baalen, 2008; Hartemink et al., 2008; Porter et al., 2012; Simmons et al., 2012; Wilson et al., 2017). Of particular importance for bacteria-phage systems, parasites are often transmitted horizontally but can only infect specific host genotypes (Poullain et al., 2008; Poland et al., 2009), which can be modelled using genetic based methods or through an almost "all-or-nothing" transmission function (Forde et al., 2008; Boots et al., 2009, 2014; Best et al., 2010b, 2017b). Hence, while there are various factors that ought to be considered when studying a specific disease, the way in which transmission is modelled will have important consequences for infection dynamics.

Two other important factors that could impact disease are heterogeneous environments

and evolution. For the former, temporal and spatial changes in environmental conditions can lead to infection dynamics that are periodic in time (Kamo & Sasaki, 2002), spatially distributed (Bhatt et al., 2013), or some combination of both (Dhondt et al., 2005, 2012). Equally, evolution of host defence and/or parasite infectivity means that infection dynamics can change through time purely due to the interaction between the species (Brockhurst et al., 2014). Both of these factors can can have a significant effect on the spread and impact of a disease, and as such will be discussed in more detail.

§ 1.2 Heterogeneous Environments

Many species live in heterogeneous environments, with spatial and temporal changes in climate and resources common throughout the world. This variation can lead to space- or time-dependent life-history traits, and thus determines the ecological dynamics of the species. For example, high migration rates in spatial environments can potentially destabilize metapopulations of *Drosophila* or bacteria (Dey & Joshi, 2006; Vogwill et al., 2009). Elsewhere, Fennoscandian voles have been shown to have multi-year population cycles with periods that depend on their location (Hansson & Henttonen, 1988; Bjørnstad et al., 1995), which can be explained by changes in the abundance of predators at different latitudes (Hanski et al., 1991), or by the length of the breeding season (Taylor et al., 2013). The effect of heterogeneous environments on populations extends to infection dynamics, meaning that outbeaks can be periodic in time and/or spatially distributed (Kamo & Sasaki, 2002; Dhondt et al., 2005, 2012; Bhatt et al., 2013).

Many environments vary spatially, with different habitats and climate conditions dependent on location. The effect of this type of environmental heterogeneity on infection dynamics can be observed empirically. For example, Wommack & Colwell (2000) describe how virioplankton numbers depend on location, and in particular that abundance can peak at certain depths in open-ocean waters due to different processes that determine production and loss. The virioplankton have a significant impact on microbial food webs through infection of bacteria and algae populations, and so the spatial distribution of virioplankton is an important determinant of the infection dynamics in water systems. Additionally, migration between different environments can change population dynamics, and thus will affect the spread of infection (Daversa et al., 2017). Infection dynamics in spatial environments can be modelled using a variety of methods (Keeling & Eames, 2005; Ferguson et al., 2006; Webb et al., 2007), with many incorporating em-

pirical data in order to deduce influential factors in the spread of a particular disease (Bhatt et al., 2013; Gog et al., 2014; Griffiths et al., 2014; Macpherson et al., 2016; White et al., 2016; Charu et al., 2017; Klinkenberg et al., 2018). For example, it has been shown that the spread of influenza in the US is often dominated by short-distance interactions (Gog et al., 2014; Charu et al., 2017). However, a study of Measles in the Netherlands showed that school holidays could lead to a shift towards longer-distance transmission (Klinkenberg et al., 2018). Spatial heterogeneity can also impact how prevention strategies are best implemented. For example, White et al. (2016) found that high intensity control of grey squirrels in key infection corridors could prevent the spread of Squirrel-pox Virus from Southern to Central Scotland, which is predicted to be more effective than previous control methods. Hence spatially heterogeneous environments have an important effect on infection dynamics, which has prompted a range of theoretical research on the topic (Keeling & Eames, 2005; Webb et al., 2007; Griffiths et al., 2014; Parratt et al., 2016; Daversa et al., 2017), including host-parasite evolutionary studies (Hochberg & van Baalen, 1998; Boots & Sasaki, 1999; Haraguchi & Sasaki, 2000; Nuismer & Kirkpatrick, 2003; Thrall & Burdon, 2003; Kamo et al., 2007; Débarre et al., 2012; Horns & Hood, 2012).

Many species live in temporal environments, where changes in conditions can be seasonal and/or stochastic. These temporal changes can affect population sizes (Rowan, 1938; Wommack & Colwell, 2000; Gehrt, 2005; Ketterson et al., 2015; Ewing et al., 2016; Furness, 2016), hence variability in these environments will have an important effect on infection dynamics. Outbreaks of infectious diseases can be seasonal due to temporal changes in a range of different ecological and epidemiologcal processes, including transmission (Turell et al., 2001; Altizer et al., 2006; Jian et al., 2014; White et al., 2014), and life-history traits of either species (London & Yorke, 1973; Fine & Clarkson, 1982; Fels & Kaltz, 2006; Fenton et al., 2006b; Smith et al., 2008; Begon et al., 2009; Knowles et al., 2012; Reynolds et al., 2013). Alternatively direct environmental factors, such as resource availability or rainfall, can drive seasonal infection dynamics (Maurice et al., 2015; Baracchini et al., 2016). Mathematical models of these infection outbreaks will not be accurate if the seasonal peaks and troughs do not occur. Hence many have modelled seasonal diseases by including time-dependent parameters as a proxy for environmental fluctuations, which are often implemented through regular, deterministic oscillations (Dietz, 1976; Aron and Schwartz, 1984; Olsen and Schaffer, 1990; Choisy et al., 2006; He & Earn, 2007; Lello et al., 2008; Smith et al., 2008; Uziel & Stone, 2012; Best, 2013). Of particular importance, it has been found that small perturbations in these models can lead to a switch between distinct attractors

(Smith, 1983; Schwartz, 1985; Keeling et al., 2001; Kamo and Sasaki, 2002; Greenman et al., 2004). In addition, increasing the amplitude of the temporal forcings can lead to chaotic dynamics (Grossman, 1980; Schwartz & Smith, 1983; Greenman et al., 2004; Grassly & Fraser, 2006; Childs & Boots, 2010), although this occurs less often when the forcing is through the host birth rate compared to the transmission rate (White et al., 1996; Begon et al., 2009; Duke-Sylvester et al., 2011; Dorélien et al., 2013; Peel et al., 2014). Similarly to spatial environments, the effectiveness of prevention strategies may depend on when and how they are enforced, but also on the strength of the seasonal fluctuations. For example, Lee & Chowell (2017) showed that some treatments perform equally well in constant and seasonal environments, whereas others can increase the size of the epidemic when transmission is seasonal. Therefore temporal environments have an important effect on infection dynamics, and thus should be taken into account in mathematical models.

Heterogeneous environments, both spatial and temporal, can have a significant impact on infection dynamics empirically and theoretically. Therefore mathematical models may need to include some form of environmental heterogeneity in order to produce accurate predictions for real-world infection systems. In this thesis I focus on seasonal environments since few have considered host-parasite evolution with temporal heterogeneity, while evolution in spatial environments has been relatively well studied (Hochberg & van Baalen, 1998; Boots & Sasaki, 1999; Brockhurst et al., 2003, 2006; Thrall & Burdon, 2003; Forde et al., 2004; Kerr et al., 2006; Boots & Mealor, 2007; Vogwill et al., 2008, 2010, 2011; Lopez-Pascua et al., 2010, 2012; Su & Boots, 2017).

§ 1.3 Host-Parasite Evolution

Host-parasite systems are generally governed by the interactions between the two (or more) species, which has important consequences for population and epidemiological dynamics. These interactions are often antagonistic, and as such promote adaptation in defence/infectivity strategies in response to each other. This results in changes in the species' traits through evolution, as famously described by Darwin in 1859 (see also Darwin & Wallace, 1858). Empirically it has been shown that, for a range of different species, hosts can evolve various defence strategies against parasitism (Fuxa & Richter, 1989; Simms & Triplett, 1994; Råberg et al., 2007; Zbinden et al., 2008; Gerardo et al., 2010; Rohr et al., 2010; Boots, 2011; Medina & Langmore, 2016; Howick & Lazzaro, 2017; Klemme & Karvonen, 2017). It has also been shown that parasites

can evolve different methods to infect hosts (Thrall & Burdon, 2003; Boots & Mealor, 2007; Crossan et al., 2007; Samson et al., 2013), and that in many cases the host and parasite co-evolve in response to each other (Forde et al., 2004; Kerr et al., 2006; Brockhurst et al., 2007, 2014; Laine, 2009; Obbard & Dudas, 2014; Barraclough, 2015; Zeller & Koella, 2017). Therefore evolution is a fundamental process that influences infection dynamics, with one of the most widely recognised problems being the rise of drug-resistance in human and animal diseases (Livermore, 2003; Levy & Marshall, 2004; Davies & Davies, 2010). Hence evolution should be included in mathematical models, as without it theoretical predictions run the risk of missing a key component that may significantly change infection dynamics.

Mathematically, evolution can be studied in a number of different ways. Many use genetic based methods with qualitative traits, where a fixed number of genes are considered that have an associated fitness. These genes are generally categorized into a fixed number of qualitative traits, for example resistant/susceptible for the host, and virulent/avirulent for the parasite. The most common genetic-based approaches are the gene-for-gene (GFG) and matching allele methods (MA; Flor, 1956; Jayakar, 1970; Burdon, 1987; Thompson & Burdon, 1992; Sasaki, 2000; Agrawal & Lively, 2002; Thrall et al., 2016), although these can be extended to investigate more complicated genetic interactions (Fenton & Brockhurst, 2007; Fenton et al., 2009, 2012; Engelstädter, 2015; Ashby et al., 2019). Other evolutionary methods consider quantitative traits, an example of which is the "adaptive dynamics" approach. For this method, a parameter from a set of ecological equations is chosen as the trait that evolves, and a dynamic fitness is derived which determines how the quantitative trait changes through time (Marrow et al., 1996; Dieckmann & Law, 1996; Metz et al., 1996; Geritz et al., 1998). I use this method to study evolution in this thesis, and is described in more detail in Chapter 2.

First, let us consider the evolution of host defence. Hosts can defend themselves against parasitism through many different mechanisms. These are often classified as: (i) resistance, where the host prevents initial infection or recovers once infected (Lambrechts et al., 2006; Poland et al., 2009; Svensson & Råberg 2010; Boots, 2011); (ii) tolerance, such that the host reduces any harmful effects of the parasite (Strauss & Agrawal, 1999; Boots, 2008; Baucom & de Roode, 2011; Hayward et al., 2014; Råberg, 2014; Medina & Langmore, 2016); (iii) acquired immunity, whereby the host cannot be reinfected by the same parasite once recovered from an initial infection (Deerenberg et al., 1997; Zuk & Stoehr, 2002; Gerardo et al., 2010). Any (or all) of these defences can evolve, and there is a wide range of theoretical research on the evolution of each of these defence types

(Boots & Haraguchi, 1999; Boots & Bowers, 1999, 2004; Boots et al., 2009; Débarre et al., 2012; Horns & Hood, 2012; Best et al., 2013, 2015, 2017a; Ashby & Bruns, 2018), including when there are multiple interacting species (Bonsall & Raymond, 2008; Hoyle et al., 2012; Yang et al., 2012; Toor & Best, 2015, 2016; Donnelly et al., 2017). In general, it has been found that infection prevalence, as a proxy for the force of infection, drives selection for host defence (Roy & Kirchner, 2000; Boots et al., 2009). Moreover, changes in ecological and epidemiological model parameters that increase the prevalence of the parasite, for example increased growth rate or transmission, mean that the host invests more in defence (Boots & Haraguchi, 1999; Boots & Bowers, 1999, 2004; Best et al., 2017a). However, the drivers of resistance evolution can be more complicated. For example, when infected hosts are able to reproduce, increasing infected fertility leads to a decrease in selection for resistance, thus lowering evolved defence, despite an increase in the infected population size (Toor & Best, 2015; Best et al., 2017a). This is due to the fact that the overall cost of being infected is lower, as reproduction can still occur even if a higher proportion of the population is infected. Overall there has been little work investigating the evolution of acquired immunity (Boots & Bowers, 2004; Donnelly et al., 2017), possibly due to the long-standing belief that invertebrates and bacteria do not have this type of defence (Rimer et al., 2014). Despite the knowledge that immune priming can occur in plants and invertebrates (Schmid-Hempel, 2005; Jung et al., 2012), this has also recieved little theoretical attention with respect to host evolution (Best et al., 2013). Hence there are many mechanisms through which hosts can evolve defence against parasitism, however, the level of defence critically depends on the specific ecological and epidemiological conditions.

A fairly general result, in a constant environment, is that tolerance and resistance give qualitatively different evolutionary behaviours (Roy & Kirchner, 2000; Boots & Bowers, 1999; 2004; Miller et al., 2005, 2007). This is due to the fact that an increase in resistance negatively impacts the parasite through reduction in growth, while an increase in tolerance either neutrally or positively impacts the parasite through increased infectious period. A common difference between these mechanisms is the occurrence of diversity in host defence. For resistance, diversity has been observed in both theoretical and empirical studies (Frank, 1993; Spiers et al., 2000; Niaré et al., 2002; Lazzaro et al., 2004, 2006; Boots et al., 2012, 2014; Klemme & Karvonen, 2017), with polymorphism found to be more likely in a population with high intrinsic productivity (Boots & Bowers, 1999), although this behaviour is highly dependent on the cost structures involved (Boots & Haraguchi, 1999; Boots & Bowers, 2004; Best et al., 2015). For tolerance, diversity can be observed experimentally (Koskela et al., 2002; Kover & Schaal, 2002;

Råberg et al., 2007; Blanchet et al., 2010; Kause et al., 2012; Sternberg et al., 2012; Hayward et al., 2014; Mazé-Guilmo et al., 2014) but is generally not found theoretically (Roy & Kirchner, 2000; Miller et al., 2005; Best et al., 2014, 2017a) unless there is a trade-off between resistance and tolerance or evolution is through 'sterility tolerance' (Fornoni et al., 2004; Best et al., 2008, 2010a; Carval & Ferriere, 2010). In addition, resistance and tolerance can be linked in some species (Råberg et al., 2007; Howick & Lazzaro, 2017; Klemme & Karvonen, 2017; but see Sternberg et al., 2012; Mazé-Guilmo et al., 2014). This has been studied theoretically (Fornoni et al., 2004; Best et al., 2008; Carval & Ferriere, 2010), with Restif & Koella (2004) finding that, similarly to above, resistance and tolerance respond differently to changes in model parameters. Therefore when modelling host defence it is worth considering the evolution of both resistance and tolerance, as evolution through each mechanism can lead to different outcomes which will have important effects on real-world infection dynamics.

Parasites can evolve different strategies to infect hosts (Thrall & Burdon, 2003; Boots & Mealor, 2007; Crossan et al., 2007; Samson et al., 2013), which has led to the mathematical study of parasite evolution in a range of different contexts (Levin & Pimental, 1981; Bremermann & Pickering, 1983; Bremermann & Thieme, 1989; Boots & Sasaki, 1999; Miller et al., 2006; Gog, 2008; Heilmann et al., 2010, 2012; Morozov & Best, 2012; Bernhauerova, 2016; Su & Boots, 2017). In some cases, the evolution of a parasite can be determined by maximization of the reproduction number R_0 (May & Anderson, 1983; Kucharski & Gog, 2012; Vale et al., 2014), as R_0 is a measure of parasite growth, and therefore can be used as a proxy for parasite fitness. This is not always the case, particularly when R_0 is difficult to calculate or when there are certain environmental feedbacks (Lion & Metz, 2018). Evolutionary frameworks, based on the maximisation of R_0 or other methods, can be used to predict the circumstances that may lead to highly virulent parasites (Haraguchi & Sasaki, 2000; Fenton et al., 2006b; Svennungsen & Kisdi, 2009; Best & Hoyle, 2013), with Boots & Sasaki (1999) finding that, in a spatial model, parasites evolve higher virulence when transmission is increasingly global. Alternatively, parasites can evolve to evade certain drug treatments (Livermore, 2003; Levy & Marshall, 2004; Davies & Davies, 2010), and theoretical studies can determine how best to manage parasite evolution in this context. For example, Restif & Grenfell (2007) found that the persistence of a pathogen is minimised when vaccines provide some level of cross-protection against multiple strains, while Bernhauerova (2016) found that the level of evolved virulence depended on how the parasite evolved to evade the effects of a vaccine. Elsewhere, it has been observed that some parasites can confer resistance to the host against a second parasite (Michalakis et al., 1992; Hughes et al.,

2011; Sternberg et al., 2011; Vorburger & Gouskov, 2011; Ford & King, 2016). Recent theoretical studies of this phenomenon have shown that evolution of host protection by a parasite can occur for a wide range of parameters, although the exact outcome will depend on certain characteristics of the species (Jones et al 2011) or the shape and strength of the underlying trade-off (Ashby & King, 2017). Therefore mathematical models of parasite evolution can provide us with a deeper understanding of the conditions that lead to particularly virulent or transmissible parasites. Models can also be used to explore observed host-parasite interactions, and importantly can warn us about potentially unwanted evolutionary outcomes from infection prevention strategies.

While the study of single-species evolution is useful, many hosts and parasites coevolve due to their interaction with each other, with both species constantly adapting to changes in the other. This has been observed in a wide range of species (Laine, 2009; Bérénos et al., 2011; Obbard & Dudas, 2014; Edger et al., 2015; Zeller & Koella, 2017), including bacteria-phage systems (Buckling & Rainey, 2002; Paterson et al., 2010; Hall et al., 2011; Lopez-Pascua et al., 2014). For example, Lopez-Pascua & Buckling (2008) found that the rate of coevolution between the bacteria *P. fluorescens* SBW25 and its parasitic bacteriophage SBW25Φ2 depended on the productivity of the environment, with greater productivity leading to higher rates of coevolution. As coevolution is such a wide-spread phenomenon, many have studied it theoretically through genetic-based (Leonard, 1977; Sasaki, 2000; Agrawal & Otto, 2006; Fenton & Brockurst, 2007; Peters & Lively, 2007; Tellier & Brown, 2007; Kouyos et al., 2007, 2009; Ashby & Gupta, 2014) and ecology-driven methods (van Baalen, 1998; Gandon & Day, 2009; Best et al., 2010a,b, 2014, 2017b; Carval & Ferriere, 2010; Boots et al., 2014; Ashby & Boots, 2015; Kada & Lion, 2015). Many have observed that results from coevolutionary studies aren't necessarily predictable from single-species evolution (Restif & Koella, 2003), and in fact that coevolution can lead to more highly virulent parasites when compared to parasite-only evolution (Best et al., 2009). Sometimes coevolution can be categorized as "arms race dynamics" (ARD; selection for increasing resistance and infectivity ranges) or "fluctuating selection dynamics" (FSD; selection varies through time). These two types of dynamics can be observed experimentally and theoretically, with costs often determining the extent to which these dynamics play a role in coevolutionary systems (Gomez & Buckling, 2011; Hall et al., 2011; Harrison et al., 2013; Lopez-Pascua et al., 2014). Overall coevolution is a key process in many host-parasite systems which can determine the level of resistance and infectivity obtained. Hence the inclusion of coevolution is often needed in mathematical models to produce accurate evolutionary and epidemiological predictions.

It is commonly observed that underlying ecological dynamics affect evolutionary outcomes. Host-parasite studies often find that the infected population size (or disease prevelence) influences the level of evolved host defence, as this is the predominant selection pressure on the host (van Baalen, 1998; Boots & Haraguchi, 1999; Donnelly et al., 2015). However the opposite can also be true, whereby evolution of the host and/or parasite changes the ecological dynamics of the two species, which in turn affects the evolutionary dynamics and results in "eco-evoutionary feedbacks" (Roy & Kirchner, 2000; Restif & Koella, 2004; Miller et al., 2005, 2007; Boots et al., 2009; Best et al., 2017b; Theodosiou et al., 2019). In some cases, evolution can even drive the underlying ecological dynamics into a parameter region with population cycles that have a different period, which can cause discontinuities in the evolutionary outcomes (Hoyle et al., 2011; Best et al., 2013). Many genetic-based theoretical studies of evolution do not include population or epidemiological dynamics (Leonard, 1977; Sasaki, 2000; Agrawal & Otto, 2006; Peters & Lively, 2007; Tellier & Brown, 2007), and while these studies have important results, it is likely that the addition of ecological dynamics, and therefore eco-evolutionary feedbacks, would change the evolutionary outcomes (Ashby et al., 2019). Therefore models of species that involve variation in population sizes over space or time should take the ecological dynamics into account when studying evolution, as eco-evolutionary feedbacks are likely to play an important role in these environments.

While hosts and parasites evolve greater defence/infectivity, it is often assumed that this comes at a cost in some other life-history trait. The functions that describe these costs are known as trade-offs, and can be observed empirically for both hosts and parasites (Boots & Begon, 1993; Kraaijveld & Godfrey, 1997; Koskela et al., 2002; Thrall & Burdon, 2003; Mealor & Boots, 2006; Poullain et al., 2008; Boots, 2011; Karve et al., 2016; Bartlett et al., 2018; Acevedo et al., 2019; Rafaluk-Mohr, 2019). It is often difficult to evaluate the exact nature of the trade-off experimentally, however it is common to use these costs in theoretical studies as they are important factors that influence host-parasite evolution. Therefore many have considered a range of different trade-off functions to capture all possible evolutionary outcomes, and in fact it has been found that the shape of the trade-off can have an important impact on the type of evolution observed (Boots & Haraguchi, 1999; de Mazancourt & Dieckmann, 2004; Bowers et al., 2005; Kisdi, 2006; Bonsall & Raymond, 2008; Hoyle et al., 2008, 2011; Svennungsen & Kisdi, 2009; Lin et al., 2016). For example, Best et al. (2015) showed that increasing the degree of polynomial trade-offs in the host birth rate can lead to loss of diversity in a host population. Elsewhere, Bonsall & Raymond (2008) found that, when a host is exposed to a lethal pathogen and a non-lethal synergist, the structure

of the underlying trade-offs is critical for the maintenance of polymorphisms in host resistance. Trade-offs can have a significant impact on theoretical evolution results, but since it is difficult to deduce a specific function from experimental data, we have to be careful about our choice of trade-off function and ensure that it is biologically plausible. This can be done by considering empirical evidence when developing trade-off functions, and including enough flexibility within trade-offs to encompass a range of potential scenarios.

Evolution and epidemiological dynamics are closely related and are involved in a continuous feedback with each other. It has been demonstrated that the underlying ecology can often determine host-parasite evolution, which in turn can alter infection dynamics. This can be shown empirically and theoretically, and so it is often crucial to include evolution when modelling infection. This is especially true in heterogeneous environments, as discussed below.

§ 1.4 Evolution in Temporally Hetergeneous Environments

Individually, heterogeneous environments and evolution are important aspects of infection systems, hence the combination and interaction of these two factors could provide even more insight into real world infection dynamics. Many have aready considered the intersection between evolution and spatial environments both experimentally and theoretically (Hochberg & van Baalen, 1998; Boots & Sasaki, 1999; Damgaard, 1999; Haraguchi & Sasaki, 2000; Brockhurst et al., 2003, 2006; Nuismer & Kirkpatrick, 2003; Thrall & Burdon, 2003; Forde et al., 2004; Kerr et al., 2006; Boots & Mealor, 2007; Kamo et al., 2007; Vogwill et al., 2008, 2010, 2011; Heilmann et al., 2010, 2012; Lopez-Pascua et al., 2010, 2012; Débarre et al., 2012; Horns & Hood, 2012; Ashby et al., 2014; Su & Boots, 2017), but overall temporal evironments have received less attention. Here I summarize the current experimental and theoretical literature about host-parasite evolution in temporal environments, and consider where there may be gaps in this growing area of research.

Experimentally, some have considered how temporal abiotic environmental factors affect (co)evolution in various different species (Blanford et al., 2003; Laine, 2007; Blanchet et al., 2010; Friman et al., 2011; Friman & Laakso, 2011; Hiltunen et al., 2012, 2015 Dallas & Drake, 2016; Mazé-Guilmo et al., 2016), including bacteria-phage systems (Zhang & Buckling, 2011; Harrison et al., 2013; Duncan et al., 2017). These studies range from wild populations in stochastic heterogeneous environments (Blanchet

et al., 2010; Mazé-Guilmo et al., 2016) to populations in experimentally altered periodic conditions (Hiltunen et al., 2012, 2015; Harrison et al., 2013; Duncan et al., 2017), and so provide an array of experimental evidence as to how temporal environments may affect host-parasite evolution. The type of environmental fluctuations can have different effects on coevolution of the same host-parasite species depending on how the fluctuations affect the individuals or their interaction. For example, for the bacteria *P. fluorescens* SBW25 and its parasitic bacteriophage SBW25Φ2, rapid fluctuations in resource concentration significantly affects the bacteria population sizes and constrains coevolution (Harrison et al., 2013). In contrast, oscillations in temperature primarily affect the phage population sizes, and coevolution is constrained for slower oscillations (Duncan et al., 2017). For many different infection systems, experimental studies generally find that temporal environments have an effect on host-parasite evolution, however there has been a lack of attention paid to how the amplitude of regular oscillations in conditions may impact evolution. This is possibly due to the comparatively large number of individual conditions that are needed to make up the oscillating environments, which could be limited by equipment and resource availablility. However, the consideration of seasonal amplitude is particularly important for real-world infection systems, as natural seasonal variations are more likely to vary in amplitude than period. Only Blanford et al., (2003) consider this, finding that pea aphids, *Acyrthosiphon pisum*, evolved greater resistance against a fungal pathogen, *Erynia neoaphidis*, when periodically exposed to high temperatures, although how the level of resistance changed as amplitude increased varied between pea aphid clones. Hence there is plenty of scope for more experimental work that considers host-parasite evolution in temporal environments, in particular focussing on the potential effects of increasing the amplitude of regular environmental fluctuations.

Mathematically, both parasite-only evolution (Koelle et al., 2005; Sorrell et al., 2009; van den Berg et al., 2010, 2011; Hamelin et al., 2011; Donnelly et al., 2013; Baker et al., 2018) and host-parasite coevolution (Nuismer et al., 2003; Mostowy & Engelstädter, 2011; Poisot et al., 2012; Gibson et al 2018) have been considered in a temporal environment. These studies use genetic- or ecology-based methods to study evolution, and temporal heterogeneity is incorporated in a variety of different ways. Given the small number of studies that exist, the main results are summarised below.

First let us review the theoretical literature on parasite-only evolution in temporal environments. When considering an increasingly variable climate implemented through transmission, Koelle et al. (2005) found that the parasite evolved lower sensitivity to en-

vironmental variability in transmission and virulence as climate fluctuations increased, i.e. the parasite evolved such that fluctuations in transmission due to the environment were dampened as the amplitude increased. Elsewhere, Sorrell et al. (2009) investigated the evolution of covert infection as a parasite strategy, finding that covert infection does not evolve in a constant environment, but seasonal host birth rate or transmission can select for low levels of covert infection for high enough amplitudes. In many plant-parasite systems, seasonal conditions mean that the plant host is regularly absent, so the parasite has to survive in the environment for a certain period of the year. Some have theoretically studied the evolution of parasite transmission in such a system (van den Berg et al., 2010, 2011; Hamelin et al., 2011), finding that evolutionary divergence of the parasite can occur (Hamelin et al., 2011), and that the type of trade-off (virulence or inter-season survival) determines the direction of selection as the length of host absence is varied (van den Berg et al., 2011). In a similar vein, Donnelly et al. (2013) considered how a fluctuating host birth rate affected parasite evolution through transmission and virulence. Initially they found that the parasite was not affected by the seasonality, although the inclusion of density-dependent virulence meant that high amplitudes could lead to greater parasite investment in transmission. Alternatively, parasites can evolve to evade treatment strategies, and it has been suggested that pulsed management schemes could be used to exploit competition between different strains (Garrison et al., 2014; Enriquez-Navas et al., 2016; Hackett & Bonsall, 2016). Baker et al. (2018) considered this in relation to antibiotic resistance, finding that reducing treatment pulse duration led to lower levels of drug-resistance in the parasite, although high dose concentrations were needed to decrease pathogen load within individual hosts. All of these studies consider different types of parasite evolution in a range of temporal environments, and generally find that the amplitude and/or period of the fluctuations has a significant effect on parasite evolution.

Coevolution between hosts and parasites has also been studied theoretically in a temporal environment. Nuismer et al. (2003) considered stochastic fluctuations between mutualistic and antagonistic interactions between the host and parasite. Using a genetic-based method, they found that matching traits coevolved when the geometric mean of the interaction was mutualistic, but otherwise there was trait mismatching and possibly coevolutionary cycles. In another study, Mostowy & Engelstädter (2011) introduced deterministic environmental variation through the specificity of the interaction between the host and parasite. They found that, when the velocity of the environmental change was high, the impact of the oscillations on coevolution could be seen through both short- and long-term effects, which could produce rapid allele fluctuations. For slower

environmental oscillations, the short- and long-term effects merged, and the coevolutionary dynamics became similar to those observed in a constant environment. While the results from the two studies above are important, they both use genetic-based evolutionary methods without population dynamics, despite the fact that ecological dynamics have an important effect on coevolution (Papkou et al., 2016; Ashby et al., 2019). In contrast, Poisot et al. (2012) used a genetic evolution method within an ecological infection framework, with temporal heterogeneity incorporated through the input of a dynamic host resource. They found that high amplitude and duration of the productive season led to large host and parasite investment in defence and infectivity when there is no recovery, with minimal investment in host defence occuring at intermediate amplitudes.

The studies above considered evolution through a range of different mechanisms in temporal environments, and generally found that these environments have a significant effect on evolution. Therefore predictions of infection outbreaks should take both evolution and temporal environments into account, as their interaction can have important consequences. However, I found no theoretical studies of host-only evolution in a temporal environment, no adaptive dynamics studies of coevolution, and limited studies on parasite-only evolution, so there is clearly more scope for theoretical work in this area, especially investigating the effects on host defence. In the experimental literature, many either consider pulsed environments with fixed amplitude and period (Friman et al., 2011; Friman & Laakso, 2011; Hiltunen et al., 2015) or temporal environments with different periods (Harrison et al., 2013; Dallas & Drake, 2016; Duncan et al., 2017). Only Blanford et al. (2003) consider how the amplitude of environment impacts evolution, so more empirical research could be done to explore this further. Given the importance of infection dynamics, and the influence of evolution and temporal environments on infection, more research could be done in this area to fill the gaps in our current knowedge. Therefore, I use a mathematical infection model to study host-parasite evolution in a temporal environment, and conduct an experimental study to investigate the effect of the amplitude of environmental oscillations on coevolution in a bacteria-phage system.

§ 1.5 Thesis Outline

In this thesis, I investigate the effects of temporally heterogeneous environments on host-parasite evolution, specifically through a fluctuating birth rate in the host species.

I consider different mechanisms of host defence, present an experimental bacteria-phage study, and explore coevolution of the host and parasite. This work contributes to the growing field of host-parasite evolution in temporally heterogeneous environments, reinforcing the argument that temporal environments should be considered more generally, and generates further questions for future research.

In Chapter 2, I introduce the mathematical methods used throughout this thesis. I formulate a mathematical model of the infection dynamics and explain how seasonality is incorporated into this model, with a brief discussion on how the temporal heterogeneity affects the epidemiological dynamics. I then describe the adaptive dynamics method that I use to study host evolution, using trade-off functions to represent costs of defence in reproduction. I detail the numerical procedures used to adapt this method for the time-dependent infection equations, which are used in Chapters 3, 4 and 6.

In Chapter 3, I consider evolution of host defence through avoidance. I find that seasonality does in fact have a quantitative effect on evolution, with avoidance decreasing as the amplitude of seasonality increases. The effect of seasonality on evolution critically depends on the presence or absence of recovery, with the qualitative behaviour of evolved host defence changing in the absence of recovery. I also find regions of bistabilty between two different defence strategies, which often occurs in conjunction with a period-doubling bifurcation in the population dynamics. This means that the bistable defence strategies often give different periods of oscillation in the population dynamics, highlighting the importance of eco-evolutionary feedbacks in temporally heterogeneous systems.

In Chapter 4, I investigate how seasonality affects the possibility for the evolution of diversity through branching processes. I consider three types of host defence, namely avoidance, recovery and tolerance, as previous theoretical work has found qualitatively different evolutionary behaviour for resistance (avoidance/recovery) and tolerance mechanisms (Roy & Kirchner, 2000; Boots & Bowers, 1999, 2004; Miller et al., 2005, 2007). I find that, while tolerance branching does not occur in a constant environment, seasonality allows for diversity in tolerance to emerge. In a seasonal environment, tolerance continues to have qualitatively different evolutionary behaviours when compared to the two resistance mechanisms, and in particular that greater seasonal amplitudes appear to 'stabilise' tolerance evolution while having the opposite effect on resistance.

To test the model predictions from Chapter 3, in Chapter 5 I present a bacteria-phage evolution experiment where the nutrient resource oscillates between high and low concentrations. I measured the resistance of the bacteria at the end of the evolution

experiment, finding that highest bacterial resistance and phage infectivity evolved at intermediate amplitudes due to differences in growth rates in the various resource concentrations. This result is reinforced by a theoretical coevolution model, but only when the seasonal forcing is based on the bacterial growth rates in the individual environments.

In Chapter 6, I give more details about the coevolutionary model that is introduced in Chapter 5, incorporating three different types of seasonality and a specific infection process. I find that for symmetric seasonality functions, the host and parasite evolve monotonically decreasing defence and infectivity as the amplitude of oscillations increase, which does not match the results for the bacteria and phage. The model only replicates the experimental evolution results when evidence-based growth rates are incorporated into the model. This has important consequences for future modelling, as I show that individual environments within the oscillating environment can have a large impact on evolutionary outcomes.

Some of the work in this thesis has previously been published or has been submitted for publication at international journals:

- Chapter 3: Ferris C, Best A. 2018 The Evolution of Host Defence To Parasitism in Fluctuating Environments. Journal of Theoretical Biology. 440, 58–65. (doi: 10.1016/j.jtbi.2017.12.006)
- Chapter 4: Ferris C, Best A. Can temporal fluctuations select for diversity in host tolerance to parasitism? *Submitted.*
- Chapter 5: Ferris C, Wright RC, Best A, Brockhurst MA. The intensity of host-parasite coevolution peaks in seasonal environments that oscillate at intermediate amplitudes. *In prep.*

Chapter 2

Mathematical Methods

In this chapter, I give a thorough discussion of the mathematical methods used for the majority of the work produced in this thesis. First, I consider how to form an appropriate infection model that incorporates seasonality. Second, I define trade-offs within the model so that there are costs/benefits as evolution occurs. Third, I provide a detailed explanation of the adaptive dynamics method used to investigate host evolution within the infection model framework, with a focus on the system with time-dependent coefficients. Additional details are given in Chapters 3, 4 and 6, with further discussion of the method when applied to coevolution provided in Chapter 6.

§ 2.1 Infection Model

In infection modelling, a common approach is to separate the host population into categories depending on their infection status (Anderson & May, 1981). Susceptible (S) and infected (I) hosts are those which are susceptible to infection or are currently infected with a parasite. Other categories can be defined, for example immune or exposed (infected but not infectious) hosts, or infection and demographic related parasite categories. I do not consider these categories here, as I assume that the host does not have acquired immunity, that there is no exposed stage of infection, and that the parasite can be considered to be uniform and is transmitted horizontally by contact between infected and susceptible hosts. These assumptions simplify the initial model that I build upon later. I define parameters to describe the rate at which individuals enter, leave and transfer between the susceptible and infected categories, Figure 2.1, and use this framework to build the mathematical model below.

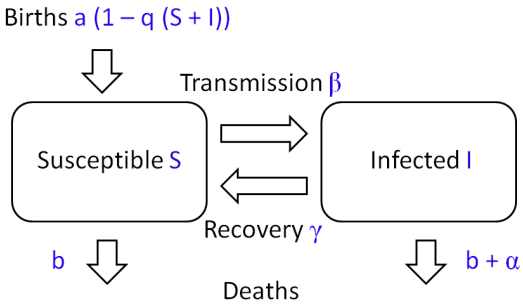

Figure 2.1: Flow chart demonstrating the infection system, modelled by the differential equations (2.1), (2.2).

The population is modelled using an SIS (susceptible-infected-susceptible) framework with the following set of ordinary differential equations:

$$\frac{dS}{dt} = a(1 - qN)S - bS - \beta SI + \gamma I, \tag{2.1}$$

$$\frac{dI}{dt} = \beta SI - (b + \alpha + \gamma)I, \tag{2.2}$$

where S and I are the susceptible and infected population sizes respectively, and $N = S + I$ is the total population size (Anderson & May, 1981; Ferris & Best, 2018). All offspring are born susceptible at rate a, and only susceptible hosts are able to reproduce, i.e. the parasite renders the host (temporarily) sterile (this assumption can be relaxed, see Boots & Bowers, 1999; Best et al., 2008; Tidbury et al., 2012; Best, 2013). The births are limited by density with crowding coefficient q, so that birth rate is low when competition is high. All hosts die at baseline mortality rate b, with an additional infected death rate α. The parasite is transmitted to susceptible hosts at rate βI due to contact with infected individuals. I assume a mass-action infection process, although other types of infection exist (Anderson & May, 1981; Childs & Boots, 2010; Strauß & Telschow, 2015; Cai et al., 2017). Hosts recover from the parasite at rate γ and return to the susceptible class with no acquired immunity. These parameters are summarized in Table 2.1, and default values are given for each model in Chapters 3, 4 and 6.

For this model there are three equilbria: (i) the extinction state $(0, 0)$, (ii) the disease-free state $(S_0^*, 0) = (\frac{a-b}{aq}, 0)$, and (iii) the positive infection equilibrium (S^*, I^*):

$$(S^*, I^*) = \left(\frac{\Gamma}{\beta}, \frac{b\Gamma - a\Gamma(1 - \frac{q\Gamma}{\beta})}{(\gamma - \Gamma)\beta - a\Gamma q} \right) \tag{2.3}$$

where $\Gamma = \alpha + b + \gamma$. To guarantee that infection is maintained in the population, we need to find parameters such that the extinction state and disease-free equilibrium are unstable while the positive infection equilibrium is stable. The stability of the extinction and disease-free equilibria can be determined by considering the eigenvalues of the Jacobian of equations (2.1) and (2.2) evaluated at each equilibrium. If at least one of the eigenvalues is positive, then the equilibrium point is unstable. For the extinction state, the Jacobian has eigenvalues $\lambda_1 = a - b$, $\lambda_2 = -\Gamma$, so the equibirium is unstable for $a - b > 0$. The first eigenvalue for the disease-free equilibrium is $\lambda_1 = b - a$, which is negative as long as $S_0^* > 0$. Therefore for $(S_0^*, 0)$ to be unstable, we need the second eigenvalue λ_2 to be positive, i.e.:

$$\lambda_2 = \frac{(a-b)\beta}{aq} - \Gamma > 0. \tag{2.4}$$

To determine if the positive infection equilibrium (S^*, I^*) is stable, we can consider the basic reproduction number R_0, defined to be the number of secondary cases from one infected individual in an otherwise susceptible population (Diekmann et al., 1990). Infection persists in the population for parameters where the parasite can grow in the population, i.e.:

$$R_0 = \frac{\beta S_0^*}{\Gamma} = \frac{\beta(a-b)}{aq\Gamma} > 1\,. \tag{2.5}$$

Parameter	Definition
a_0	Average birth rate
$\hat{a_0}$	Relative size of the average birth rate
p	Gradient of the average birth rate
c	Curvature of the average birth rate
α	Virulence/additional death rate due to parasite
β	Transmission coefficient
γ	Recovery Rate
s	Evolving parameter (α, β or γ)
$s_{\min}$	Minimum value of s (α, β or γ)
$s_{\max}$	Maximum value of s (α, β or γ)
δ	Amplitude of the oscillating birth rate
ϵ	Period of the oscillating birth rate
q	Crowding coefficient acting on births
b	Baseline mortality rate

Table 2.1: Parameter definitions for the general infection model, where different parameters are allowed to evolve (namely β, α or γ).

Condition (2.5) is actually the same as (2.4), therefore for parameters that satisfy $a > b$ and (2.4), the population always tends towards the positive-infection equilibrium.

§ 2.2 Seasonality

Periodic birth rates have been observed in a large number of species (Rowan, 1938; Ketterson et al., 2015), and a sinusoidal function has been used many times to model a time-varying birth rate (He & Earn, 2007; Donnelly et al., 2013; Dorélien et al., 2013) or transmission rate (Schwartz & Smith, 1983; Grassly & Fraser, 2006; Childs & Boots, 2010). Complex dynamical behaviour is often associated with time-dependent coefficients in differential equations, although it has been shown to occur less frequently for forcings in the birth rate compared to the transmission rate (White et al., 1996; Begon et al., 2009; Duke-Sylvester et al., 2011; Dorélien et al., 2013; Peel et al., 2014). Therefore I incorporate seasonality through the birth rate a by letting it depend on time t periodically. I assume that seasonality occurs on the ecological timescale in the following way:

$$a = a(t) = a_0(1 + \delta \sin(2\pi t/\epsilon)), \tag{2.6}$$

where a_0 is the average birth rate, $\delta \in [0, 1]$ is the amplitude and $\epsilon > 0$ is the period of the forcing. This function causes continuous fluctuations in the birth rate, which in turn impacts the population dynamics. For $\delta > 0$, equations (2.1),(2.2) are non-linear with time-dependent coefficients and I cannot find the limit cycle of the population dynamics analytically, although numerically this is less of a challenge. Nevertheless, I can find the average population sizes semi-analytically. Let T be the period of the host dynamics (generally some integer multiple of ϵ) such that $S(t + T) = S(t)$ and $I(t + T) = I(t)$. Taking the average of equations (2.1), (2.2) over this period gives:

$$\frac{1}{T}\int_{P_0}^{P_1} \frac{dS}{dt} dt = [S(t)]_{P_0}^{P_1} = 0\,, \tag{2.7}$$

$$\frac{1}{T}\int_{P_0}^{P_1} \frac{dI}{dt} dt = [I(t)]_{P_0}^{P_1} = 0\,, \tag{2.8}$$

where $P_1 = P_0 + T$ for some arbitrary time $P_0 > 0$ after the population has reached a dynamic attractor. Similarly, I can also find that:

$$\frac{1}{T}\int_{P_0}^{P_1} \frac{1}{S}\frac{dS}{dt} dt = [\ln(S(t))]_{P_0}^{P_1} = 0\,. \tag{2.9}$$

$$\frac{1}{T}\int_{P_0}^{P_1}\frac{1}{I}\frac{dI}{dt}dt = [\ln(I(t))]_{P_0}^{P_1} = 0\,. \tag{2.10}$$

By using equations (2.2) and (2.10), the average susceptible population size $\hat{S}$ can be found as follows:

$$0 = \frac{1}{T}\int_{P_0}^{P_1}\frac{1}{I}\frac{dI}{dt}dt \tag{2.11}$$

$$= \frac{1}{T}\int_{P_0}^{P_1}\beta S - (\alpha+b+\gamma)dt \tag{2.12}$$

$$= \beta\hat{S} - (\alpha+b+\gamma)\,, \tag{2.13}$$

giving

$$\hat{S} = \frac{1}{T}\int_{P_0}^{P_1} S(t)dt = \frac{\alpha+b+\gamma}{\beta}\,. \tag{2.14}$$

Using equations (2.2) and (2.8), the average infected population size $\hat{I}$ can be found semi-analytically:

$$0 = \frac{1}{T}\int_{P_0}^{P_1}\frac{dI}{dt}dt \tag{2.15}$$

$$= \frac{1}{T}\int_{P_0}^{P_1}\left[\beta SI - (\alpha+b+\gamma)I\right]dt \tag{2.16}$$

$$= \frac{\beta}{T}\int_{P_0}^{P_1} SIdt - (\alpha+b+\gamma)\hat{I}\,, \tag{2.17}$$

giving

$$\hat{I} = \frac{1}{T}\int_{P_0}^{P_1} I(t)dt = \frac{\beta}{(\alpha+b+\gamma)T}\int_{P_0}^{P_1} S(t)I(t)dt\,. \tag{2.18}$$

From equations (2.7) and (2.18), there is an alternative form for $\hat{I}$:

$$\hat{I} = \frac{1}{(\alpha+b)}\left[\frac{1}{T}\int_{P_0}^{P_1}\left\{a(t)S(t)(1-qN(t))\right\}dt - b\hat{S}\right]. \tag{2.19}$$

Note that the equation for the average susceptible population (2.14) is valid for all values of the seasonal parameters δ and ϵ. For the average infected population size $\hat{I}$, there is no fully analytic expression for positive amplitudes ($\delta > 0$) as I cannot compute the integral in equation (2.18) or (2.19), so numerical methods must be used to calculate this average.

The population averages above change with the model and seasonal parameters, as

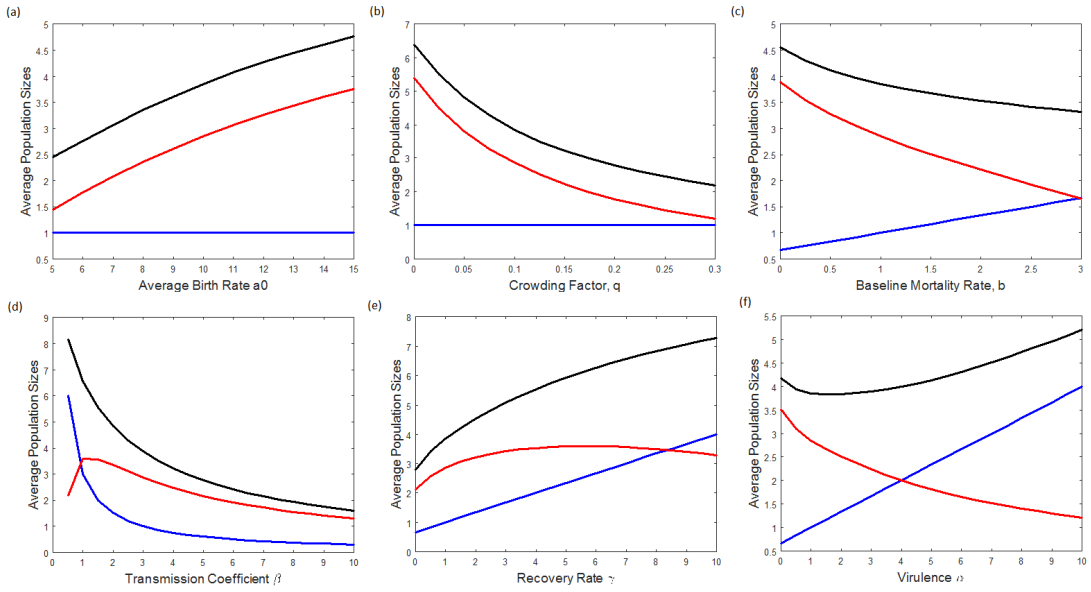

Figure 2.2: Average population sizes as model parameters vary when there is no trade-off. (a) Average birth rate a_0; (b) Crowding factor q; (c) Baseline mortality rate b; (d) Transmission coefficient β; (e) Recovery rate γ; (f) Virulence α. Blue: Average susceptible population $\hat{S}$; Red: Average infected population $\hat{I}$; Black: Average total population $\hat{N}$. Parameters: $a_0 = 10$, $q = 0.1$, $b = \gamma = \alpha = 1$, $\beta = 3$, $\delta = 0.5$, $\epsilon = 1$.

plotted in Figures 2.2 and 2.3. These plots are for when there is no trade-off (see section 2.3), although the qualitative behaviour is generally the same when one is included in the model. In Figure 2.2, the average susceptible population behaves as expected from equation (2.14), with no change for varying a_0 or q, a linear increase with b, γ and α, and a monotonic decrease for increasing β. The average infected population $\hat{I}$ is largest for high a_0, or low q, b and α. This is due to increased numbers of susceptible hosts that can become infected (a_0, q, b), or greater infectious period (b, α). For varying transmission coefficient β, $\hat{I}$ peaks at a relatively small value then gradually decreases as β is increased. This decrease occurs because there is a decrease in the number of susceptibles that are able to reproduce, but also an increase in the number of hosts that die from infection. When the recovery rate γ varies, $\hat{I}$ is largest for intermediate values, as the loss of infected hosts through recovery is balanced by the increased size of the susceptible population that can become infected.

The effects of changing the seasonal parameters on the average population sizes can be seen in Figure 2.3. The average susceptible population size $\hat{S}$ is constant as both seasonal parameters vary, as they do not appear in equation (2.14). Generally, $\hat{I}$ increases

with the amplitude of seasonality δ (Figure 2.3(a)), and hence the average prevalence $\left(\frac{1}{T}\int_{P_0}^{P_1}\frac{I(t)}{N(t)}dt\right)$ of the parasite also increases since $\hat{S}$ is constant. When the period ϵ is varied, for the parameter values specified in Figure 2.3, $\hat{I}$ increases to a peak at $\epsilon \approx 1.25$ due to resonance with the unforced system, then decreases as ϵ continues to increase. This peak may occur at a different value of ϵ when the parameters are altered, as the inherent period of the unforced system is likely to change. The behaviour of the average population sizes may impact evolution of the host in different seasonal environments, which is discussed further in Chapters 3, 4 and 6.

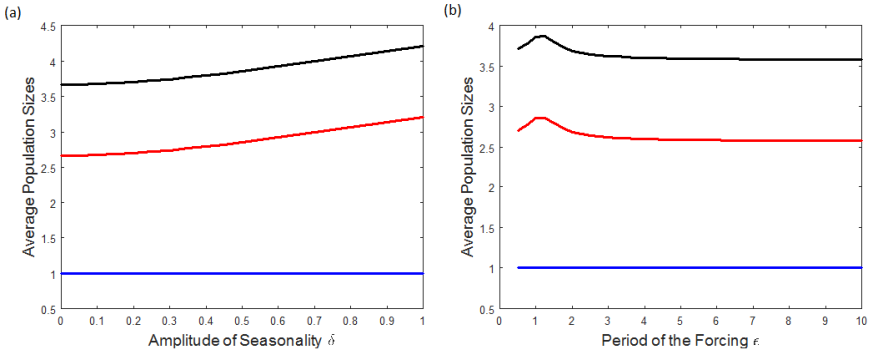

Figure 2.3: Average population sizes as seasonal parameters vary when there is no trade-off. (a) Amplitude δ; (b) Period ϵ. Blue: Average susceptible population $\hat{S}$; Red: Average infected population $\hat{I}$; Black: Average total population $\hat{N}$. Parameters: $a_0 = 10$, $q = 0.1$, $b = \gamma = \alpha = 1$, $\beta = 3$, $\delta = 0.5$, $\epsilon = 1$.

For most parameter sets, the period of the population dynamics is equal to that of the forcing in the birth rate, i.e. $T = \epsilon$. However, there are regions where the population undergoes a period-doubling bifurcation, whereby a small change in a parameter causes the dynamics to switch to a cycle with double the period of the original system (Kuznetsov, 1998). The bifurcations mean that in some parameter regions I find population cycles of period $T = \lambda\epsilon$, where λ is some positive integer. There can also be cases of multiple attractors, often with different periods, which can have an effect on host evolution (Chapter 3).

§ 2.3 Trade-Offs

It is important to remember that species cannot invest in every aspect of their survival simultaneously, meaning that evolution of a particular fitness trait is constrained by reduction in some other life-history trait (Stearns, 1992; Roff, 2002). For example, hosts

may trade-off investment in defence against a parasite with some other life-history trait, and there is empirical evidence for such a trade-off between host defence and reproduction (Boots & Begon, 1993; Kraaijeveld & Godfray, 1997; Koskela et al., 2002; Mealor & Boots, 2006; Bartlett et al., 2018). Approximations of these trade-offs are regularly used in theoretical literature (Miller et al., 2007; Carval & Ferriere, 2010; Toor & Best, 2015, 2016; Donnelly et al., 2015, 2017), however it is often hard, if not impossible, to deduce the exact nature of the trade-off experimentally. The choice of trade-off function can have a large impact on evolution (Boots & Haraguchi, 1999; de Mazancourt & Dieckmann, 2004; Bowers et al., 2005; Kisdi, 2006; Best et al., 2015; Ashby & King, 2017), so it important to be able to consider different trade-off shapes to capture the full range of possible evolutionary outcomes.

Suppose the host evolves defence through trait s, which has lower and upper limits fixed at $s_{\min}$ and $s_{\max}$ respectively (i.e. $s \in [s_{\min}, s_{\max}]$). I let the average birth rate a_0 depend on this evolving parameter so that there is a cost of defence against the parasite. I use the following trade-off function, based on that used by White et al. (2006) (see also Ferris & Best, 2018):

$$a_0 = a_0(s) = \hat{a_0} - p\frac{(1 + \frac{s - s_{\min}}{s_{\max} - s_{\min}})}{(1 + c\frac{s - s_{\min}}{s_{\max} - s_{\min}})}, \tag{2.20}$$

where $a_0(s)$ has relative size $\hat{a_0}$, gradient p and curvature c such that as the host invests in defence against the parasite, less can be invested in reproduction. The parameter $\hat{a_0}$ determines the relative size of the average birth rate a_0. I can use the trade-off parameters to pick a particular shape for the trade-off function depending on biological and theoretical constraints. Figure 2.4 shows a few examples of the possible trade-off shapes I can choose from, including positive/negative gradients with accelerating or decelerating costs. This trade-off function is used in Chapters 3, 4 and 6 when considering host-only evolution or coevolution of the host and parasite.

§ 2.4 Adaptive Dynamics

I use the adaptive dynamics method to model evolution of host defence in the host-parasite system (2.1), (2.2) (see Chapter 6 for coevolution with parasite infectivity). The method was originally developed from a game theoretic point of view, using the concept of an evolutionary stable (unbeatable) strategy ESS (EUS) which is a fitness optimum (Hamilton, 1967; Maynard Smith & Price, 1973). This theory was developed

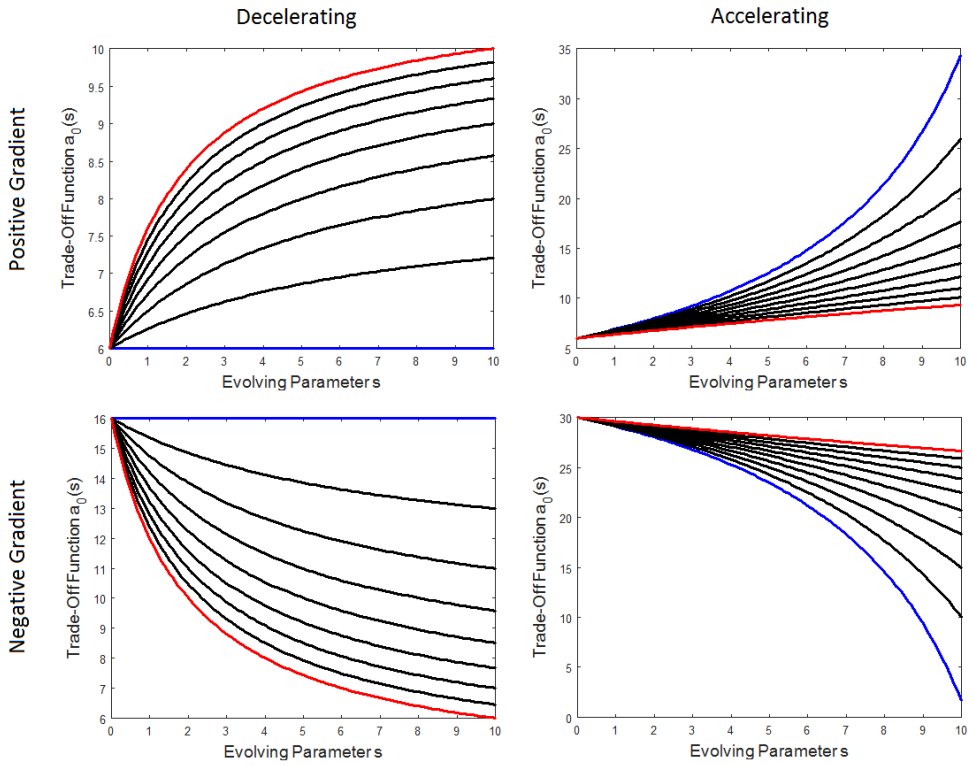

Figure 2.4: Trade-off function $a_0(s)$ for positive (top row) or negative (bottom row) gradients, with decelerating (left column) or accelerating (right column) costs of defence. In all cases, the limits on s were fixed at $s_{\min} = 0$ and $s_{\max} = 10$. Top left: $\hat{a_0} = 12$, $p = 6$, c varied between 1 (blue) and 5 (red) with gaps of 0.5. Bottom left: $\hat{a_0} = 1$, $p = -15$, c varied between 1 (blue) and 5 (red) with gaps of 0.5. Top right: $\hat{a_0} = 1$, $p = -5$, c varied between -0.7 (blue) and 0 (red) with gaps of 0.1. Bottom right: $\hat{a_0} = 35$, $p = 5$, c varied between -0.7 (blue) and 0 (red) with gaps of 0.1.

further to include convergence stability (Eshel, 1983; Taylor, 1989; Christiansen, 1991; Abrams et al., 1993), which has resulted in the adaptive dynamics method that is commonly used today (Marrow et al., 1996; Dieckmann & Law, 1996; Metz et al., 1996; Geritz et al., 1998). This approach has been used to study evolution in a wide range of contexts since its development, including predator-prey systems (Abrams, 2000; Geritz et al., 2007; Litchman & Klausmeier, 2008), spatially structured populations (Doebeli & Ruxton, 1997; Kisdi & Geritz, 1999; Ernande & Dieckmann, 2004) and coevolutionary host-parasite models (van Baalen, 1998; Best et al., 2009; Kada & Lion, 2015; Ferris et al., in prep). I give key details of the method in relation to the models studied in this thesis, including key assumptions and definitions that are used in Chapters 3, 4 and 6.

2.4.1 General Method and Assumptions

The adaptive dynamics method is a way to track long-term evolutionary changes in a trait value. The resident population is defined as that which currently exists with trait s, and a mutant is a similar population with trait s_m which arises due to a small mutation in the resident trait. It is assumed that all mutant population sizes are initially small (rare), and that the resident remains at its equilibrium or limit cycle as long as this is the case (Geritz et al., 1998). I assume that mutations occur infrequently so that the population reaches the dynamic attractor of the population dynamics (generally a limit cycle here) before the next mutant is introduced (Geritz et al., 1998), giving a separation of timescales between the ecological and evolutionary dynamics. I also assume that hosts reproduce clonally such that offspring have the same trait as the parent.

The method itself involves repeatedly adding rare mutants with traits close to that of the resident population and following the growth of these mutants. For host evolution in the infection model here, this means that I add a rare host with defence very close to that of the resident. I then use the mutant's fitness (exponential growth rate; sections 2.4.2 and 2.5.1) to determine what happens next. For positive fitness, the mutant grows and invades the current population, resulting in survival of either both populations or only the mutant. If the mutant's fitness is negative, the population dies out and only the resident remains. Another mutant is then added to the current resident population, and the process repeats. The evolutionary trajectory can be found by tracking the changes in the defence parameter through time, for example through simulations (section 2.6).

2.4.2 Fitness

To analyse how the host evolves, I consider the mutant's fitness r, defined as the long-term exponential growth rate of the mutant in the current environment (Metz et al., 1992). When there is no seasonality, i.e. amplitude $\delta = 0$ in equation (2.6), I can find the fitness as follows (see section 2.5.1 for $\delta > 0$). As an example, let the host evolve defence through lowered transmission β with an associated cost in birth rate $a_0(\beta)$, such that a mutant will have transmission coefficient β_m and birth rate $a_0(\beta_\mathrm{m})$. Adding this mutant to the resident population, I can write equations to describe the dynamics of the mutant susceptible and infected populations S_m, I_m:

$$\frac{dS_{\mathrm{m}}}{dt} = a_0(\beta_{\mathrm{m}})(1 - q(N^* + N_{\mathrm{m}}))S_{\mathrm{m}} - bS_{\mathrm{m}} - \beta_{\mathrm{m}}S_{\mathrm{m}}(I^* + I_{\mathrm{m}}) + \gamma I_{\mathrm{m}}, \tag{2.21}$$

$$\frac{dI_{\mathrm{m}}}{dt} = \beta_{\mathrm{m}}S_{\mathrm{m}}(I^* + I_{\mathrm{m}}) - (b + \alpha + \gamma)I_{\mathrm{m}}, \tag{2.22}$$

where $N_{\mathrm{m}} = S_{\mathrm{m}} + I_{\mathrm{m}}$ is the total mutant population, and S^*, I^* are the stable equilibrium resident population sizes evaluated before the mutant is introduced (equation (2.3)). Assuming that the mutant population is initially small ($N_{\mathrm{m}} \ll N$, section 2.4.1), the mutant equations become:

$$\frac{dS_{\mathrm{m}}}{dt} = a_0(\beta_{\mathrm{m}})(1 - qN^*)S_{\mathrm{m}} - bS_{\mathrm{m}} - \beta_{\mathrm{m}}S_{\mathrm{m}}I^* + \gamma I_{\mathrm{m}} + \mathcal{O}(N_{\mathrm{m}}^2), \tag{2.23}$$

$$\frac{dI_{\mathrm{m}}}{dt} = \beta_{\mathrm{m}}S_{\mathrm{m}}I^* - (b + \alpha + \gamma)I_{\mathrm{m}} + \mathcal{O}(N_{\mathrm{m}}^2), \tag{2.24}$$

where $\mathcal{O}(N_{\mathrm{m}}^2)$ indicates that the error in the differential equations after linearization is of order of magnitude $N_{\mathrm{m}}^2 \ll N^2$, and can therefore be ignored. As these equations are approximately linear with constant coefficients, they can be rewritten in the form:

$$\frac{d\mathbf{X}}{dt} = A\mathbf{X}, \tag{2.25}$$

where $\mathbf{X} = (S_{\mathrm{m}}(t), I_{\mathrm{m}}(t))$ and A is the 2 x 2 matrix containing the coefficients from equations (2.23), (2.24), i.e. A is the Jacobian matrix of (2.23), (2.24). The solution of equation (2.25) is of the form $\mathbf{X} = c_1 e^{\lambda_1 t}\mathbf{v}_1 + c_2 e^{\lambda_2 t}\mathbf{v}_2$, where c_1, c_2 are constants, λ_1, λ_2 are non-equal real eignvalues of A, and $\mathbf{v}_1$, $\mathbf{v}_2$ are the corresponding eigenvectors. Therefore the mutant fitness (exponential mutant growth rate) is the maximum of the eigenvalues λ_i for $i \in \{1, 2\}$. For both λ_i negative, the mutant population decays to zero and is eliminated. If one of the λ_i is positive, then the mutant population grows and potentially takes over the resident population.

Alternatively, I can use the negative determinant of the matrix A as a proxy for the fitness, as it is sign equivalent to the maximum eigenvalue but is simpler to calculate (Hoyle et al, 2012; Toor & Best, 2015). This can be seen by considering the Jacobian matrix A:

$$A = \begin{pmatrix} a_0(\beta_{\mathrm{m}})(1 - qN^*) - b - \beta_{\mathrm{m}}I^* & \gamma \\ \beta_{\mathrm{m}}I^* & -(b + \alpha + \gamma) \end{pmatrix} = \begin{pmatrix} B & C \\ D & E \end{pmatrix}, \tag{2.26}$$

where $C > 0$, $D > 0$, $E < 0$, and the sign of B is unknown. The eigenvaues of A are

given by:

$$\lambda_+, \lambda_- = \frac{1}{2}\left[B + E \pm \sqrt{(B+E)^2 - 4(BE - CD)}\right] \tag{2.27}$$

$$= \frac{1}{2}\left[B + E \pm \sqrt{(B-E)^2 + 4CD)}\right] . \tag{2.28}$$

Due to the sign of C and D, the discriminant is always positive and so there are two distinct real eignevalues. First, consider the sign of λ_-. Since $E < 0$, if $B < 0$, then it follows that $\lambda_- < 0$. If $B \geq 0$, we know that $|B + E| \leq |B - E|$, and so again $\lambda_- < 0$. Hence λ_- is always negative. Given that $\lambda_+ > \lambda_-$, we know that λ_+ is the largest eigenvalue and so it is the mutant fitness r. We can use the property $\mathrm{Det}(A) = \lambda_+\lambda_-$ to show that:

- if fitness $r = \lambda_+ > 0$, then $\mathrm{Det}(A) < 0$;
- if fitness $r = \lambda_+ < 0$, then $\mathrm{Det}(A) > 0$.

Therefore the negative determinant is sign equivalent to the fitness and we can use it as a proxy. It can be shown that derivatives of the fitness and the negative determinant are also sign equivalent, which will be important when considering singular points and the type of evolutionary behaviour observed (section 2.4.3). Hence for no seasonality ($\delta = 0$) and evolving transmission coefficient β, I have host fitness:

$$r = r(\beta, \beta_\mathrm{m}) = -\mathrm{Det}(A) = (b + \alpha + \gamma)\left[a_0(\beta_\mathrm{m})(1 - qN^*) - b\right] + (b + \alpha)\beta_\mathrm{m} I^*. \tag{2.29}$$

It is worth noting that for equal resident and mutant traits (here $\beta = \beta_\mathrm{m}$, generally $s = s_\mathrm{m}$) the fitness is always zero (i.e. $r(s, s) = 0$), since the introduced mutant is the same as the resident and so the population remains at equilibrium with no change in the mutant dynamics.

The fitness in equation (2.29) can only be used when there is no seasonality in the model. For positive amplitudes ($\delta > 0$), the assumption of the form of the solution to (2.25) is no longer correct because the matrix A is time-dependent. Therefore I developed an alternative method to find the fitness in seasonal environments, as detailed in section 2.5.

2.4.3 Singular Points

When studying evolution theoretically, I want to find end points of evolution, traits that promote divergence, etc. This is done by finding singular points s^*, defined as the value of the evolving trait where the fitness gradient with respect to the mutant trait s_m is zero, i.e.:

$$\left.\frac{\partial r}{\partial s_\mathrm{m}}\right|_{s=s_\mathrm{m}=s^*} = 0. \tag{2.30}$$

The value of the singular point s^* can be demonstrated using a pairwise invasion plot (PIP). In these plots, both the resident and mutant traits are varied and the sign of the fitness plotted for each point, for examples see Figure 2.5. There are often two zero fitness lines in a PIP, with one always at $s = s_\mathrm{m}$ as the fitness is zero by defnition on this line. The value of s where these lines cross is the singular point s^*, since the fitness gradient with respect the mutant trait changes sign at this point.

In the case where the fitness gradient in equation (2.30) is never zero, the singular point s^* does not exist and the population evolves towards s_max for positive fitness gradients (maximisation) or s_min for negative gradients (minimisation). In the PIP, this behaviour occurs when there is only one zero-fitness line, or the lines do not cross (Figure 2.6).

Equation (2.30) can be used to find the singular point, but this does not tell us how evolution proceeds. The type of the singular point must also be determined, which can be done using second order derivatives or the PIP. I focus on four different types of singular point, which are determined by two stability conditions: evolutionary stability and convergence stability.

The singular point is defined to be evolutionarily stable (ES) if no nearby mutant can invade a resident population with trait s^*. Mathematically, this is defined:

$$\left.\frac{\partial^2 r}{\partial s_\mathrm{m}^2}\right|_{s=s_\mathrm{m}=s^*} < 0. \tag{2.31}$$

This condition means that the singular point is a fitness maximum with respect to the mutant trait. In the PIP, this can be seen by looking at the vertical line through the singular point in the neighbourhood of $s = s_\mathrm{m}$ (e.g. Figure 2.5, top left). If the line passes through only white (negative) regions, then the singular point is ES as it is a fitness maximum. However, if the line passes through the blue (positive) region near the singular point, then a nearby mutant can invade and the singular point is not ES

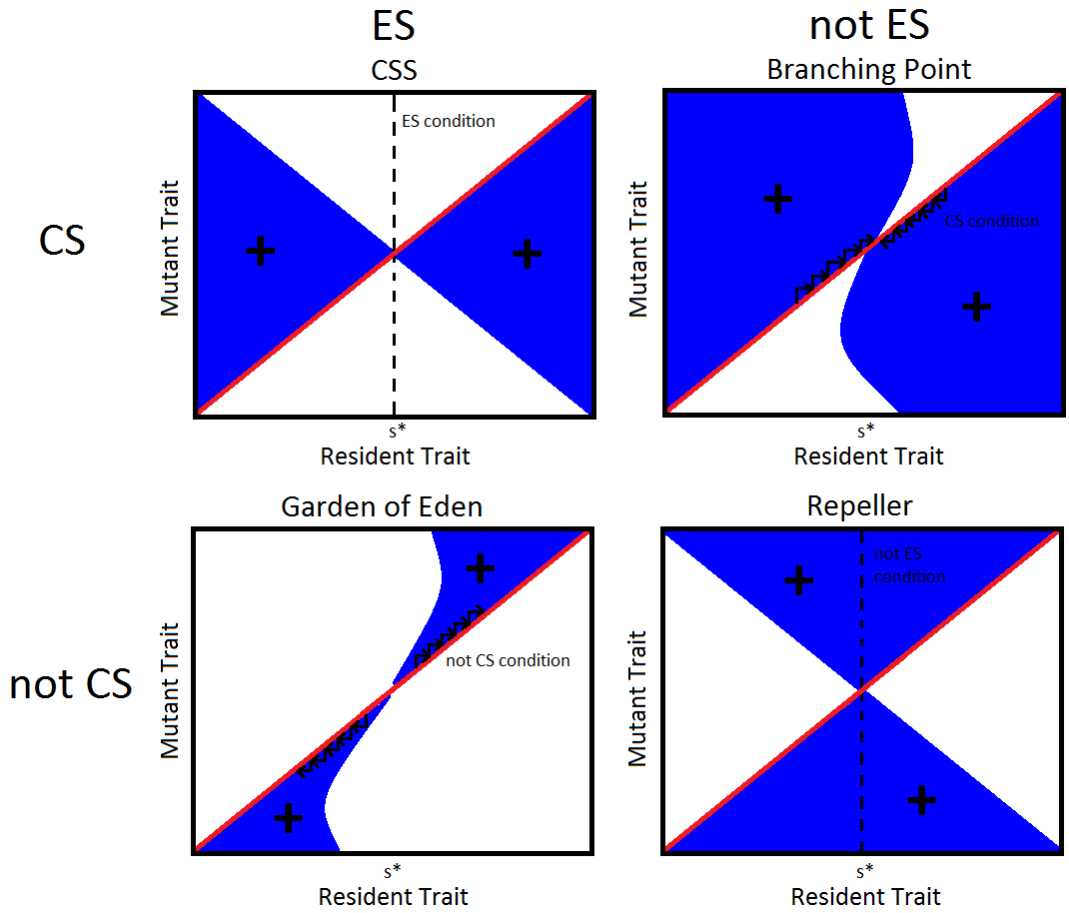

Figure 2.5: Examples of PIPs for the four different types of evolutionary behaviour described, where blue indicates positive mutant fitness, and white negative mutant fitness. The red line shows $s = s_{\mathrm{m}}$ where the mutant fitness is zero by definition, and s^* is the point where the two zero fitness lines cross. Top left: CSS point and ES condition, showing that no nearby mutant can invade the current population at the singular point. Top right: Branching point and CS condition, showing that the population trait moves towards the singular point. Bottom left: Garden of Eden point and when the CS condition isn't satisfied, showing that the population trait moves away from the singular point. Bottom right: Repeller point and when the ES condition isn't satisfied, so a nearby mutant can invade the resident population at the singular point. Left column: ES condition satisfied; Right column: ES condition not satisfied; Top row: CS condition satisfied; Bottom row: CS condition not satisfied.

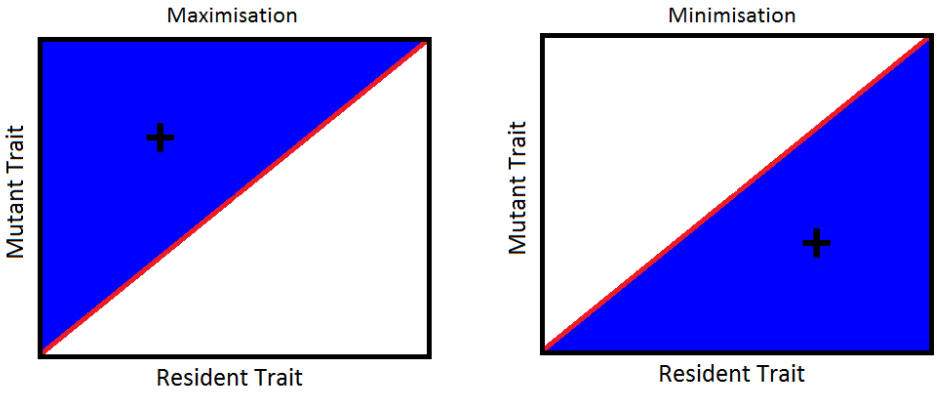

Figure 2.6: Examples of PIPs for maximisation (left) and minimisation (right), where blue indicates positive mutant fitness, and white negative mutant fitness. The red line shows $s = s_{\mathrm{m}}$ where the mutant fitness is zero by definition. In these two cases, a singular point s^* does not exist.

(i.e. it is a fitness minimum; Figure 2.5, bottom right).

The singular point is convergence stable (CS) when evolution of the trait is driven towards the singular point. Mathematically, this is defined:

$$\frac{\partial^2 r}{\partial s_{\mathrm{m}}^2} + \frac{\partial^2 r}{\partial s \partial s_{\mathrm{m}}}\bigg|_{s=s_{\mathrm{m}}=s^*} < 0, \tag{2.32}$$

or alternatively

$$\frac{\partial^2 r}{\partial s_{\mathrm{m}}^2} - \frac{\partial^2 r}{\partial s^2}\bigg|_{s=s_{\mathrm{m}}=s^*} < 0. \tag{2.33}$$

This means that the fitness is a locally decreasing function of the resident trait s, such that the singular point is a local minimum. In the PIP, this is true if there is a blue positive fitness region just above the $s = s_{\mathrm{m}}$ line for $s < s^*$ and below the line for $s > s^*$ (e.g. Figure 2.5, top right). This can also be seen by considering how the population evolves from an initial point along the $s = s_{\mathrm{m}}$ line. For example, choose a resident population with $s < s^*$. A mutant introduced with $s_{\mathrm{m}} < s$ has negative fitness and so the mutant dies out. For a mutant with trait $s_{\mathrm{m}} > s$, the fitness is positive, so the mutant invades the resident population and a single population survives with trait $s = s_{\mathrm{m}}$. This continues, with s increasing over time and eventually the population has trait $s = s^*$. Equally, an initial population with $s > s^*$ can be considered, and following a similar process the population evolves gradually lower trait values and again ends up with trait $s = s^*$. When the singular point is not convergence stable, the same

argument can be used to demostrate that the trait evolves away from the singular point, potentially leading to a population with an extreme trait that depends on its initial value (Figure 2.5, bottom left).

The combination of these two conditions (ES and CS) leads to four main types of singular point, namely:

- Continuously Stable Strategy (CSS): the singular point satifies both ES and CS conditions. The population evolves towards s^* and remains there for all time (top left in Figure 2.5).
- Branching point: The singular point is continuously stable but not evolutionarily stable (CS but not ES; top right in Figure 2.5). The population evolves towards the singular point, which is a fitness minimum, then 'branches' and becomes a dimorphic population with two distinct traits.
- Repeller point: the singular point doesn't satisfy either stability condition. Evolution drives the trait away from the singular point (bottom right in Figure 2.5).
- Garden of Eden (GoE): the singular point is ES but not CS. The population evolves away from s^*, unless the initial population has trait $s_0 = s^*$, in which case it will remain there for all time (bottom left in Figure 2.5). In practice, this type of point acts like a repeller as the population is unlikely to start with trait value at the singular point.

§ 2.5 Evolution when parameters are time-dependent

2.5.1 Fitness in a Seasonal Environment

For the model here, I introduced seasonality through a time-dependent birth rate. This means that I cannot find the fitness through conventional methods (e.g. via the Jacobian in section 2.4.2) as the assumption of the solution to the mutant equations does not hold. Instead, I use Lyapunov exponents as the mutant fitness (Metz et al., 1992; Klausmeier, 2008; Ferris & Best, 2018), which are found numerically as detailed below.

Above I showed the case for host defence evolving through β when there is no seasonality (section 2.4.2). As an alternative example, here I describe how to find the fitness when the host evolves defence through tolerance by reducing the infected mortality α,

although the case for evolving recovery γ can easily be extended from these examples. First, I add a rare mutant with susceptible and infected population sizes S_m, I_m and virulence α_m close to the resident virulence α, with a trade-off in the average birth rate $a_0(\alpha_\mathrm{m})$. This gives equations for the mutant population:

$$\frac{dS_\mathrm{m}}{dt} = a_0(\alpha_\mathrm{m})(1+\delta\sin(2\pi t/\epsilon))(1-q(N^*+N_\mathrm{m}))S_\mathrm{m} - bS_\mathrm{m} - \beta S_\mathrm{m}(I^*+I_\mathrm{m}) + \gamma I_\mathrm{m}, \quad (2.34)$$

$$\frac{dI_\mathrm{m}}{dt} = \beta S_\mathrm{m}(I^* + I_\mathrm{m}) - (b + \alpha_\mathrm{m} + \gamma)I_\mathrm{m}, \quad (2.35)$$

where $N_\mathrm{m} = S_\mathrm{m} + I_\mathrm{m}$ is the total mutant population, and $S^* = S^*(t)$, $I^* = I^*(t)$, $N^* = N^*(t)$ are the resident dynamics from equations (2.1), (2.2) evaluated on the limit cycle found before a mutant is introduced. Equations (2.34) and (2.35) can be simplified using the assumption that the mutant is initially rare ($N_\mathrm{m} \ll N$), giving:

$$\frac{dS_\mathrm{m}}{dt} = a_0(\alpha_\mathrm{m})(1 + \delta\sin(2\pi t/\epsilon))(1 - qN^*)S_\mathrm{m} - bS_\mathrm{m} - \beta S_\mathrm{m}I^* + \gamma I_\mathrm{m} + \mathcal{O}(N_\mathrm{m}^2), \quad (2.36)$$

$$\frac{dI_\mathrm{m}}{dt} = \beta S_\mathrm{m}I^* - (b + \alpha_\mathrm{m} + \gamma)I_\mathrm{m} + \mathcal{O}(N_\mathrm{m}^2). \quad (2.37)$$

For $\delta \geq 0$, the mutant's growth is determined by the largest Lyapunov exponent, which I use as the fitness (Metz et al., 1992; Klausmeier, 2008; Ferris & Best, 2018). This is found in the following way (see also Klausmeier, 2008; Ferris & Best, 2018).

First, suppose that I have a fundamental solution $\mathbf{X}(t) = (S_\mathrm{m}(t)\, I_\mathrm{m}(t))$ of the simplified mutant equations (2.36), (2.37) (Grimshaw, 1990, pp. 27). I can then rewrite the problem as:

$$\frac{d\mathbf{X}(t)}{dt} = A(t)\mathbf{X}(t) \quad (2.38)$$

where $A(t)$ is a 2 x 2 matrix containing the periodic coefficients. This is similar to equation (2.25), except that here A is time-dependent rather than constant. The solution $\mathbf{X}(t)$ may not be periodic, but I can write the linearly independent solutions to (2.38) in the form:

$$\mathbf{X}_i(t) = e^{\mu_i t}\mathbf{p}_i(t) \quad (2.39)$$

where $i \in \{1, 2\}$, the $\mathbf{p}_i$ are unknown periodic vector functions with period T, T is the period of the resident population dynamics, and the constants μ_i determine the extent of growth or decay of the population (Grimshaw, 1990, pp. 50). The mutant fitness is therefore the largest of the μ_i: if the μ_i are both negative, the mutant ultimately dies out; if at least one is positive, the mutant grows. As I cannot solve the equations

analytically, I use numerical methods to find the growth rate μ_i. Hence the growth of the mutant depends on the sign of the fitness, i.e. if $\max\{\mu_1, \mu_2\}$ is greater or less than zero.

Using the form of the solution in equation (2.39), I can write:

$$\mathbf{X}(t+T) = \mathbf{X}(t)\mathbf{C} \quad \forall\ t \geq 0, \tag{2.40}$$

where $\mathbf{C}$ is a non-singular constant 2 x 2 matrix (Grimshaw, 1990, pp. 47) that can be found numerically, with eigenvalues denoted ρ_1, ρ_2. The fitness is related to the eigenvalues of $\mathbf{C}$ by $\rho_i = e^{\mu_i T}$ from (2.40), therefore I can use the maximum of these eigenvalues as a proxy for the fitness, since the sign of μ_i is equivalent to considering whether or not ρ_i is greater or less than 1. Therefore I define the fitness for the seasonal system as the largest eigenvalue of $\mathbf{C}$ minus 1.

I cannot find the eigenvalues of $\mathbf{C}$ analytically because the mutant equations cannot be solved analytically (Klausmeier, 2008). However, I can find $\mathbf{C}$ numerically by setting $t = 0$ in (2.40), then choosing two linearly independent initial conditions $\mathbf{X}(0)$. By running the linearised mutant equations with the current resident dynamics for these initial conditions, I can find four equations for the elements of $\mathbf{C}$ in the numerically found components of $\mathbf{X}(T)$. The simplest initial conditions to implement are $(S(0), I(0)) = (1\,0), (0\,1)$, which are what I use in this thesis. The fitness can then be found from this numerically acquired $\mathbf{C}$ by finding its eigenvalues.

Often the transient dynamics of the linearised mutant equations are not representative of the actual growth, and so it is useful to be able to run the dynamics for longer than one period. Therefore I run the mutant dynamics up to time kT for some positive integer k, which still finds the correct sign for the fitness. To understand this, we begin by noting that $\mathbf{C}$ is a non-negative matrix, as its components are determined by exponentials from equations (2.39) and (2.40). Hence the Perron-Frobenius theorem applies and the largest eigenvalue ρ of $\mathbf{C}$ is non-negative. I set $t = t' + (k-1)T$ in equation (2.40) to obtain:

$$\mathbf{X}(t' + kT) = \mathbf{X}(t')\mathbf{C}^k \quad \forall\ t' \geq 0. \tag{2.41}$$

By setting $t' = 0$, I can find the elements of $\mathbf{C}^k$ numerically by running the mutant dynamics up to time kT. From linear algebra results, I know that the eigenvalues of $\mathbf{C}^k$ are ρ_i^k. The fitnesses $(\rho - 1)$ and $(\rho^k - 1)$ obtained from equations (2.40) and (2.41) respectively are of the same sign when ρ is non-negative, hence I find the correct sign for

the fitness when the mutant dynamics are run up to time kT for some positive integer k. I also have the correct sign for the fitness derivatives needed to find the singular point and evaluate ES and CS conditions (Table 2.2). For the second order derivatives, the fitness obtained from $\mathbf{C}^k$ gives the same sign as that from $\mathbf{C}$ when evaluated at the singular point ($\frac{\partial \rho}{\partial s_{\mathrm{m}}}\Big|_{s=s_{\mathrm{m}}=s^*} = 0$).

Quantity	Eigenvalue from $\mathbf{C}$	Eigenvalue from $\mathbf{C}^k$	Same sign?
r	$\rho - 1$	$\rho^k - 1$	✓
$\frac{\partial r}{\partial s_{\mathrm{m}}}$	$\frac{\partial \rho}{\partial s_{\mathrm{m}}}$	$k\rho^{k-1}\frac{\partial \rho}{\partial s_{\mathrm{m}}}$	✓
$\frac{\partial^2 r}{\partial s_{\mathrm{m}}^2}\Big\|_{s=s_{\mathrm{m}}=s^*}$	$\frac{\partial^2 \rho}{\partial s_{\mathrm{m}}^2}\Big\|_{s=s_{\mathrm{m}}=s^*}$	$k\rho^{k-1}\frac{\partial^2 \rho}{\partial s_{\mathrm{m}}^2}\Big\|_{s=s_{\mathrm{m}}=s^*}$	✓
$\frac{\partial^2 r}{\partial s \partial s_{\mathrm{m}}}\Big\|_{s=s_{\mathrm{m}}=s^*}$	$\frac{\partial^2 \rho}{\partial s \partial s_{\mathrm{m}}}\Big\|_{s=s_{\mathrm{m}}=s^*}$	$k\rho^{k-1}\frac{\partial^2 \rho}{\partial s \partial s_{\mathrm{m}}}\Big\|_{s=s_{\mathrm{m}}=s^*}$	✓

Table 2.2: Table showing that the signs of the fitnesses and its derivatives obtained from $\mathbf{C}$ and $\mathbf{C}^k$ are the same, where k is some positive integer and ρ is a positive eigenvalue of $\mathbf{C}$. Note that the second-order derivatives have the same sign at the singular point, which is where I evaluate them for the ES and CS conditions.

2.5.2 Singular Points in a Seasonal Environment

I can use the numerical method above to approximate the fitness gradients needed to find singular points and the CS and ES conditions. To find the fitness gradient with respect to the mutant trait, I use the following scheme:

1. Pick a trait value s and run the resident population dynamics (2.1), (2.2) to equilibrium (or limit cycle).

2. Set $s_{\mathrm{m}} = s$, and find the fitness $r(s, s)$ using the numerical methods above, which should find $r(s, s) = 0$.

3. Set $s_{\mathrm{m}} = s + \Delta$ for small Δ, and find the fitness $r(s, s + \Delta)$.

4. Approximate the fitness gradient with respect to the mutant trait as follows:

$$\left.\frac{\partial r}{\partial s_{\mathrm{m}}}\right|_{s=s_{\mathrm{m}}} \approx \frac{r(s, s+\Delta) - r(s, s)}{\Delta} + \mathcal{O}(\Delta). \tag{2.42}$$

5. Repeat steps 1 - 4 for multiple values of s until there is a change in the sign of the fitness gradient. This gives the approximate position of the singular point s^*.

I use a similar method to approximate the second order derivatives needed to evaluate the ES and CS conditions from section 2.4.3, specifically:

$$\left.\frac{\partial^2 r}{\partial s_{\mathrm{m}}^2}\right|_{s=s_{\mathrm{m}}} \approx \frac{r(s, s+2\Delta) - 2r(s, s+\Delta) + r(s, s)}{\Delta^2} + \mathcal{O}(\Delta)\,, \tag{2.43}$$

and

$$\left.\frac{\partial^2 r}{\partial s \partial s_{\mathrm{m}}}\right|_{s=s_{\mathrm{m}}} \approx \frac{r(s+\Delta, s+\Delta) - r(s+\Delta, s) - r(s, s+\Delta) + r(s, s)}{\Delta^2} + \mathcal{O}(\Delta)\,. \tag{2.44}$$

§ 2.6 Simulations

In order to confirm the evolutionary results, I ran stochastic simulations in MATLAB of the evolutionary process that relax the separation of timescales assumption. Initially, there is a single population with trait s_0. The dynamics are run for a fixed length of time, by the end of which the population should have reached an equilibrium or limit cycle. At this point, a mutant is added with small population size and trait value close to s_0 (50% chance the trait is above or below s_0). The dynamics for the whole population (resident and mutant) are run for a fixed length of time. At the end of the run, if the size of one of the populations is lower than a given threshold then that population is removed. Another mutant is added, and the process is repeated until a fixed number of evolutionary time steps have been completed. If more than one population persists at the end of a run, no populations are removed and the new mutant trait is weighted by the relative densities of the remaining populations, i.e. the mutant trait is more likely to be close to the trait belonging to the largest population. Examples of the output from this method can be found in Chapters 3, 4 and elsewhere (Bowers et al., 2003; Hoyle et al., 2011; Ashby & King, 2017; Best et al., 2017b).

Chapter 3

The evolution of host avoidance to parasitism in fluctuating environments

In this chapter, I consider evolution of host defence through avoidance. This mechanism is a form of resistance, and involves defending against a parasite by preventing infection, i.e. by avoiding the parasite through changes in physiological traits or behaviour. Here the focus is on evolution of a continuous phenotype through the transmission coefficient β, such that higher defence leads to lower transmission, which is generally more applicable to changes in physiological traits rather than avoidance behaviours. In particular, I consider how a fluctuating host birth rate affects evolution through transmission. The majority of this work has previously been published (Ferris & Best, 2018).

§ 3.1 Introduction

Given the ubiquity of infectious diseases in natural systems there is strong selection pressure on host organisms to evolve costly defence mechanisms. A wide range of theoretical work has been developed to understand the evolution of host defence against parasitism, with much of this work focused on the ecological/epidemiological feedbacks that drive selection of quantitative host defence (van Baalen, 1998; Boots & Haraguchi, 1999; Boots & Bowers, 1999, 2004; Restif & Koella, 2003; Miller et al., 2005, 2007; Bonds, 2006; Best et al., 2008, 2009; Carval & Ferriere, 2010). These

studies have explored how long-term, stable investment in host defence varies with ecological/epidemiological parameters, as well as determining the conditions that can lead to coexistence of strains through evolutionary branching. However, the vast majority of these studies assume that the populations live in a temporally static environment. In reality, almost all natural systems are subject to some degree of temporal environmental heterogeneity, in particular fluctuations caused by seasonality. For example, many natural species exhibit seasonal reproductive strategies driven by regular environmental fluctuations (Rowan, 1938; Stawski et al., 2014; Ketterson et al., 2015; Furness, 2016). It is therefore essential to consider the impact of fluctuating environmental conditions on the evolution of host defences.

It is well established that variable climates affect ecological systems (Taylor et al., 2013; Ketterson et al., 2015; Ewing et al., 2016), including the spread and impact of diseases (Fine & Clarkson, 1982; Finkenstädt & Grenfell, 2000; Wommack & Colwell, 2000; Altizer et al., 2006; Knowles et al., 2012). Many theoretical studies have considered the effects of seasonality in purely epidemiological models (i.e., non-evolutionary), often through a periodic transmission rate (Schwartz & Smith, 1983; Aron & Schwartz, 1984; Olsen & Schaffer, 1990). Increasing the amplitude of the transmission rate can generate sub-harmonic oscillations or cause the population dynamics to move through a series of period-doubling bifurcations, eventually leading to chaotic dynamics (Grossman, 1980; Schwartz & Smith, 1983; Greenman et al., 2004; Grassly & Fraser, 2006; Childs & Boots, 2010). Small perturbations in these seasonal models can also trigger the system to switch between distinct attractors, often due to resonance, potentially leading to significant changes in the population dynamics and different patterns of outbreaks (Smith, 1983; Schwartz, 1985; Keeling et al., 2001; Kamo & Sasaki, 2002; Greenman et al., 2004). These complex dynamics have been found to exist less frequently when seasonality is assumed to occur in the host birth rate rather than transmission (White et al., 1996; Begon et al., 2009; Duke-Sylvester et al., 2011; Dorélien et al., 2013; Peel et al., 2014), and so evolutionary dynamics may be more tractable when birth rate rather than transmission rate is assumed to be periodic. Predictions about the impact of a disease are likely to be more accurate when either of these types of seasonality are included in the model (White et al., 1996; Kamo & Sasaki, 2002), so it follows that evolutionary results from these seasonal models may also be more reliable.

There is an increasing appreciation of the importance of temporal heterogeneity in host-enemy interactions within the experimental evolution literature (Blanford et al., 2003; Friman & Laakso, 2011; Hiltunen et al., 2012), for example showing that rapidly

fluctuating environments constrain co-evolutionary arms races in a bacteria-phage system (Harrison et al., 2013). Theoretically, however, evolution and seasonality have rarely been studied together in a host-parasite context. The few studies that do exist have either investigated evolution of only the parasite (Koelle et al., 2005; Sorrell et al., 2009; Donnelly et al., 2013), or used a genetic-based, rather than ecology-driven, model for coevolution between the host and parasite (Nuismer et al., 2003; Mostowy & Engelstädter, 2011; but see Poisot et al., 2012). For example, seasonality in the host's birth rate does not affect the evolution of the parasite's transmission/virulence strategy unless a density-dependence is applied to virulence (parasite-induced mortality) (Donnelly et al., 2013). This occurs because the average susceptible density, and therefore the parasite fitness, doesn't depend on the seasonal parameters unless this density-dependence is included. Elsewhere, step-wise environmental variation implemented through a dynamic resource was found to change the coevolutionary outcomes in a gene-for-gene based host-parasite system (Poisot et al., 2012). In particular, they found that both the host and parasite invest more in resistance and infectivity respectively for higher amplitudes in the seasonality. However, currently there is no theory specifically addressing the impact that seasonality has on the evolution of host defence to parasitism.

Here I investigate the impact of a continuous seasonal birth rate on the evolution of quantitative host avoidance through small mutation steps using an evolutionary invasion (adaptive dynamics) method, as detailed in Chapter 2. I focus on how the amplitude and period of the implemented seasonality impacts the ecological/epidemiological dynamics, and therefore the evolution of the host. I find that recovery plays an important role in avoidance evolution, and in particular that at very low recovery rates a period-doubling bifurcation can exist for high amplitude oscillations that may result in evolution driving the population dynamics to a different ecological attractor.

§ 3.2 Methods

In this chapter I use the methods as described in Chapter 2, specifically an SIS model for the infection dynamics and adaptive dynamics to investigate evolution. Here I give details specific to this chapter, including model parameter values, the trade-off used, and an additional discussion of the fitness when recovery is absent.

3.2.1 General Model Specifics

Here I investigate the evolution of host avoidance through reduction in the transmission coefficient β. I let the average birth rate depend on the transmission coefficient as a trade-off, so that there is a cost to resisting the parasite, using the following trade-off function (Chapter 2; see also White et al., 2006; Ferris & Best, 2018):

$$a_0 = a_0(\beta) = \hat{a_0} - p\frac{(1 + \frac{\beta-\beta_{\min}}{\beta_{\max}-\beta_{\min}})}{(1 + c\frac{\beta-\beta_{\min}}{\beta_{\max}-\beta_{\min}})}, \tag{3.1}$$

where $\hat{a_0} > 0$, $0 < p < \hat{a_0}$, $c > 1$ and $\beta \in [\beta_{\min}, \beta_{\max}]$. The birth rate $a_0(\beta)$ has minimum $\hat{a_0} - p$, and parameters p, c determine the gradient and curvature of the trade-off, which needs to have positive gradient: as the host invests in defence against the parasite (β decreases), less can be invested in reproduction ($a_0(\beta)$ decreases) (Boots & Haraguchi, 1999; Geritz et al., 2007). The constraints on the trade-off parameters give accelerating costs of defence, so that it is more costly to invest in resistance when defence is already high $\left(\frac{d^2a_0(\beta)}{d\beta^2} < 0\right)$. Figure 3.1 shows this trade-off function against transmission coefficient β, showing that increased defence (lower β) leads to a decrease in the birth rate a_0, and that defence becomes more costly as it increases. Accelerating trade-offs generally lead to evolutionary attractors (Hoyle et al., 2008), which will be the focus in this chapter (but see Chapter 4 for discussion of other behaviours). Parameter values for this chapter are defined in Table 3.1.

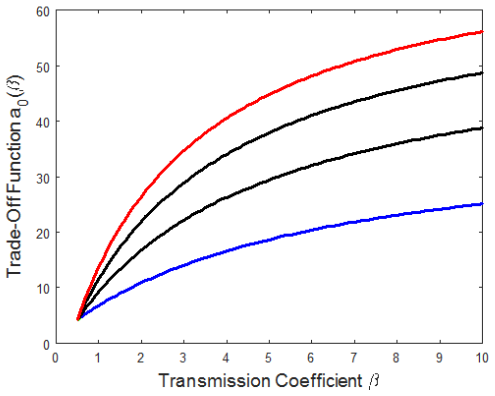

Figure 3.1: Trade-off function $a_0(\beta)$ as defined in equation (3.1) for varying transmission coeffieicnt β and different values of c increasing from 1.5 (blue) to 3 (red) in steps of size 0.5. Otherwise default parameters from Table 3.1 were used.

Here I only consider continuously stable strategies (CSSs) unless stated otherwise, i.e.

singular points that are both evolutionarily stable (ES) and convergence stable (CS) as defined by Geritz et al. (1998) which lead to long-term evolutionary attractors. This behaviour was confirmed using pairwise-invasion plots (PIPs) and simulations over a range of parameters, an example of which is given in Figure 3.5 for $\gamma > 0$.

Parameter	Definition	Default Value
a_0	Average birth rate	Varies
$\hat{a_0}$	Relative size of the average birth rate $a_0(\beta)$	108
p	Gradient of the average birth rate $a_0(\beta)$	103.75
c	Curvature of the average birth rate $a_0(\beta)$	1.5
β	Transmission coefficient	Varies
$\beta_{\min}$	Minimum transmission coefficient	0.5
$\beta_{\max}$	Maximum transmission coefficient	10
B	Avoidance $(\beta_{\max} - \beta)$	Varies
δ	Amplitude of the birth rate forcing	Varies
ϵ	Period of the birth rate forcing	1
q	Crowding coefficient acting on births	0.1
b	Baseline mortality rate	1
γ	Recovery Rate	Varies
α	Virulence/additional death rate due to parasite	1

Table 3.1: Parameter definitions and default values.

3.2.2 Evolution for No Recovery ($\gamma = 0$)

In the case where $\gamma = 0$, the fitness can be found analytically for $\delta \geq 0$. Infected mutants cannot re-enter the suscepetible mutant class due to the lack of recovery, and as such act as a sink for the mutant population. Therefore the infected mutants do not contribute to the host fitness, which can be derived from the single equation for the mutant susceptible hosts. Using the assumption that the mutant population is small ($N_{\mathrm{m}} \ll N$) with transmission coefficient β_{m}, the equation for the dynamics of the mutant susceptible hosts can be simplified to give:

$$\frac{dS_{\mathrm{m}}}{dt} = a_0(\beta_{\mathrm{m}})(1 + \delta \sin(2\pi t/\epsilon))(1 - qN^*)S_{\mathrm{m}} - bS_{\mathrm{m}} - \beta_{\mathrm{m}} S_{\mathrm{m}} I^* + \mathcal{O}(N_{\mathrm{m}}^2), \tag{3.2}$$

where $I^* = I^*(t)$ and $N^* = N^*(t)$ denote the resident infected and total population densities on their limit cycle. Equation (3.2) can be used to read off the time-varying growth rate $r(t)$ of the mutant host:

$$r(t) = a_0(\beta_{\mathrm{m}})(1 + \delta \sin(2\pi t/\epsilon))(1 - qN^*(t)) - b - \beta_{\mathrm{m}} I^*(t)\,, \tag{3.3}$$

where $\frac{dS_\mathrm{m}}{dt} = r(t)S_\mathrm{m}$. Following the method from Donnelly et al. (2013), the mutant fitness can be found by taking the average of this over one period:

$$r = \frac{1}{T}\int_{P_0}^{P_1} r(t)dt = \frac{a_0(\beta_\mathrm{m})}{T}\int_{P_0}^{P_1}\left\{\left[1+\delta\sin\left(\frac{2\pi t}{\epsilon}\right)\right][1-qN^*(t)]\right\}dt - b - \beta_\mathrm{m}\hat{I}\,, \quad (3.4)$$

where T is the period of the system, P_0 is an arbitrary time after the resident dynamics have reached a limit cycle, $P_1 = P_0 + T$ and $\hat{I}$ is the average of the resident infected population over one cycle (equation (2.18)). The integral can be simplified further by using the fact that sin is a periodic function. This gives:

$$r = a_0(\beta_\mathrm{m})\left[1 - q\hat{N} - \frac{\delta q}{T}\int_{P_0}^{P_1}\sin\left(\frac{2\pi t}{\epsilon}\right)N^*(t)dt\right] - b - \beta_\mathrm{m}\hat{I}\,, \quad (3.5)$$

with derivatives of the fitness given by:

$$\frac{\partial r}{\partial\beta_\mathrm{m}} = \frac{\partial a_0(\beta_\mathrm{m})}{\partial\beta_\mathrm{m}}\left[1 - q\hat{N} - \frac{\delta q}{T}\int_{P_0}^{P_1}\sin\left(\frac{2\pi t}{\epsilon}\right)N^*(t)dt\right] - \hat{I}\,, \quad (3.6)$$

$$\frac{\partial^2 r}{\partial\beta_\mathrm{m}^2} = \frac{\partial^2 a_0(\beta_\mathrm{m})}{\partial\beta_\mathrm{m}^2}\left[1 - q\hat{N} - \frac{\delta q}{T}\int_{P_0}^{P_1}\sin\left(\frac{2\pi t}{\epsilon}\right)N^*(t)dt\right]. \quad (3.7)$$

$$\frac{\partial^2 r}{\partial\beta\partial\beta_\mathrm{m}} = \frac{\partial a_0(\beta_\mathrm{m})}{\partial\beta_\mathrm{m}}\left[-q\frac{\partial\hat{N}}{\partial\beta} - \frac{\delta q}{T}\int_{P_0}^{P_1}\sin\left(\frac{2\pi t}{\epsilon}\right)\frac{\partial N^*(t)}{\partial\beta}dt\right] - \frac{\partial\hat{I}}{\partial\beta}\,. \quad (3.8)$$

When equation (3.6) is set to zero with $\beta = \beta_\mathrm{m}$, this gives the position of the singular point $\beta = \beta^*$. When equation (3.7) is evaluated at $\beta = \beta_\mathrm{m} = \beta^*$, its sign determines if the singular point is evolutionarily stable (ES if $\left.\frac{\partial^2 r}{\partial\beta_\mathrm{m}^2}\right|_{\beta=\beta_\mathrm{m}=\beta^*} < 0$; Chapter 2). For my default parameters with $\beta \in [\beta_\mathrm{min}, \beta_\mathrm{max}]$ and $\delta \in [0, 1]$, the term inside the square brackets in equation (3.7) is positive. Given that I have already chosen trade-off parameters such that $\frac{d^2 a_0(\beta)}{d\beta^2} < 0$, the second-order gradient (3.7) is negative, and so the singular point is ES for all values of the amplitude δ and period ϵ with the default parameter set.

For the convergence stability (CS) condition to hold, the sum of equations (3.7) and (3.8) evaluated at $\beta = \beta_\mathrm{m} = \beta^*$ needs to be negative (equation (2.32)). For my default parameter set, the gradients of $\hat{N}$ and $N^*(t)$ with respect to β are negative (Figure 2.2), hence the first term in equation (3.8) is positive since $a_0'(\beta_\mathrm{m}) > 0$. The sign of the last term $-\frac{\partial\hat{I}}{\partial\beta}$ depends on the relative position of the singular point and the peak in

the average infected population size as β varies (Figure 2.2). Hence the singular point β^* may not be convergence stable for all δ and ϵ, and so should be checked numerically.

§ 3.3 Results

In this section I consider how the seasonal parameters δ (amplitude) and ϵ (period) affect evolution of the host, and investigate if the inclusion of seasonality alters previously found trends in a constant environment. I separate results when there is no recovery ($\gamma = 0$), and generally find that the interaction between recovery and the amplitude of seasonality plays an important role in the evolutionary dynamics. For clarity, I present the results in terms of avoidance $B = \beta_{\max} - \beta$ (i.e. reduction in transmission), where $\beta_{\max}$ is the maximum value of β.

3.3.1 Evolution for No Recovery

When there is no recovery ($\gamma = 0$) and the amplitude δ is increased from 0, the average infected population increases and so does the investment in defence, shown by an increase in B^* in Figure 3.2(a),(b). This is what we would naively expect: as the average infected population increases (Figure 3.2(b)), the host has to invest more in resistance against the parasite to reduce the proportion of infected individuals (Boots & Haraguchi, 1999; Boots et al., 2009).

In Chapter 2 it was mentioned that for particular parameter sets, period-doubling bifurcations and bistability between different attractors in the population dynamics can occur. Figure 3.2(c),(d) shows an example of this phenomenon together with host selection. I found that for varying amplitude δ, the 1-year population dynamics solution (black line in Figure 3.3(a)) remains stable up to $\delta = 0.63$, at which point it undergoes a period-doubling bifurcation (and the 1-year solution is then unstable). The red curve that emerges in Figure 3.3 is the 2-year solution. This is stable for a very short time but then has a fold, becomes unstable, and goes back until about $\delta = 0.57$ where another fold produces the stable 2-year solution that continues up to $\delta = 1$. The stable solutions each give different singular points, and bistability between the 1- and 2-year cycles or between the two different 2-year cycles for $\delta \in (0.57, 0.63)$ causes overlap of the singular points given by each cycle, giving a discrete change in the CSS resistance B^* and the average infected population, Figure 3.2(c),(d). This jump in the average infected population and singular point occurs whenever a period-doubling bifurcation

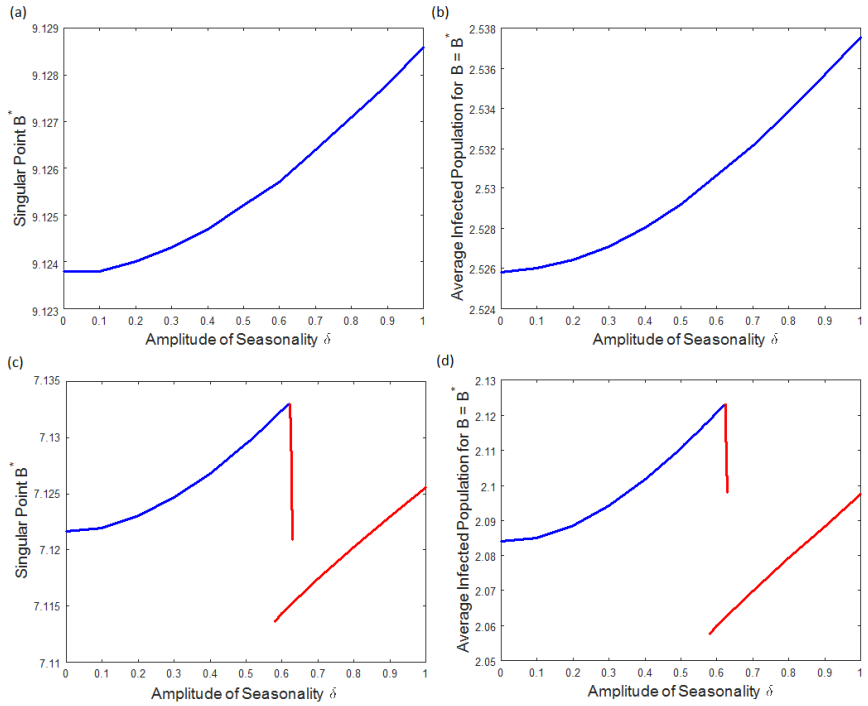

Figure 3.2: Change in (a),(c) the singular point $B^* = \beta_{\max} - \beta^*$ and (b),(d) the average infected population for $B = B^*$ as the amplitude of seasonality δ varies for $\gamma = 0$. Default parameters were used in (a),(b), with lower birth rate ($\hat{a_0} = 104$) in (c),(d). In (c),(d), on the left only the 1-year solution is stable, and on the right only the 2-year solution. In the centre there is bistability between the 1- and 2-year cycles or between the two different 2-year cycles. Blue: period $T = 1$; Red: period $T = 2$.

and bistability between attractors exists for $\gamma = 0$. Singular points from the unstable solutions in Figure 3.3 could not be shown due to the numerical method used, as this relies on the population converging to a limit cycle which cannot be found if it is unstable.

Both singular points were found to be CSSs, although for amplitudes within the bistability region, the $T = 2$ singular point can only be reached by evolution from initial avoidance B_0 lower than the upper bound of the bistability region in Figure 3.3(b). This is due to the fact that for initial B_0 greater than this point, the population never reaches the period-doubling bifurcation and so it doesn't switch between the attractors, and hence the host evolves towards the higher singular point with period $T = 1$.

Overall the impact of the amplitude of seasonality δ on the singular point for $\gamma = 0$ is weak for a wide range of parameters as seen in Figure 3.2. Seasonality has a much

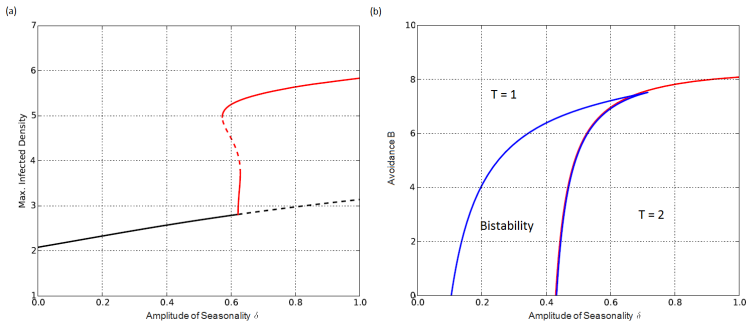

Figure 3.3: (a) Stability of solutions to the population equations (2.1), (2.2) when amplitude δ varies. Black lines - solution with period 1; Red lines - solution with period 2; Solid lines - stable solution; Dashed lines - unstable solution. (b) 2D bifurcation plot of avoidance B vs amplitude δ. The region inside the blue lines indicates where there is bistability between the 1- and 2-year solutions or between the two different 2-year solutions. Red: period-doubling bifurcation; Blue: fold bifurcations. Both graphs use $\hat{a_0} = 104$ and $\gamma = 0$, with $B = 7.13$ in (a) and otherwise default parameter values. These graphs were created using AUTO-07p (Doedel & Oldman, 2009).

stronger effect for higher recovery rates, as discussed below.

3.3.2 Evolution with Recovery

In the last section, there was no recovery and so I could use a semi-analytic version of the host fitness (section 3.2.2). In contrast, when there is recovery ($\gamma > 0$), the form of the solution to the mutant equations cannot be found analytically, so I use a numerical approximation to find the host fitness (method in Chapter 2). When γ is relatively close to zero, I find one singular point B^* such that avoidance increases with δ, as seen in section 3.3.1. However for positive but small values of γ, this behaviour changes direction. The singular point B^* starts to decrease while the average infected population increases (e.g. Figure 3.4 for $\gamma = 1$). This in contrast to the case of no recovery $\gamma = 0$, where the trends go in the same direction. As recovery increases, selection for defence is weakened, and so at this small recovery maintaining a large population size through births becomes more important than resistance to the parasite, causing the change in evolutionary direction.

As the recovery rate continues to increase, there is a region of γ values where three singular points exist, two CSSs with a repeller between them, for examples see Figures 3.5 and 3.6(a),(b). Here there is evolutionary bistability between two CSSs, with the evolutionary behaviour near the singular points confirmed using PIPs and simulations,

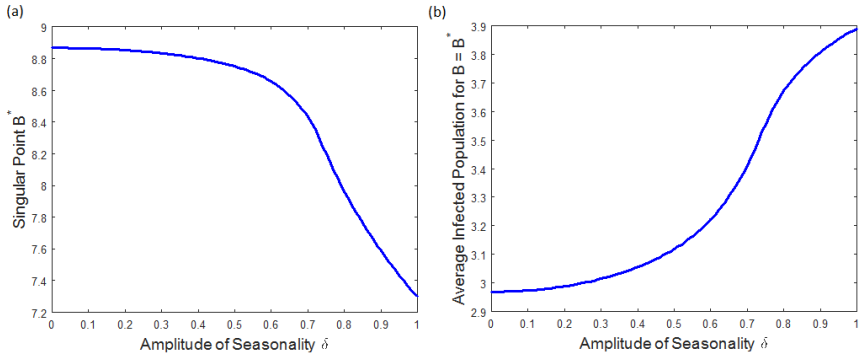

Figure 3.4: Change in (a) the singular point B^* and (b) the average infected population for $B = B^*$ as the amplitude of seasonality δ varies for $\gamma = 1$. Otherwise prameters were fixed at default values.

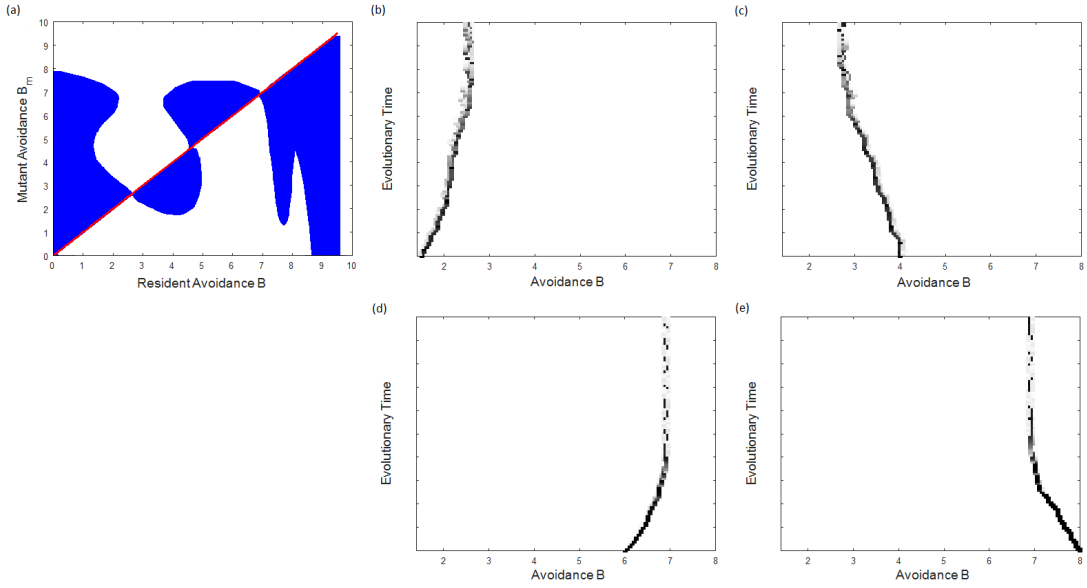

Figure 3.5: (a) Pairwise-invasion plot, where blue indicates positive mutant fitness, and the red line is $B = B_{\mathrm{m}}$. The PIP shows that three singular points exist, specifically two CSSs ($B^*_{\mathrm{H}} = 6.9059$ and $B^*_{\mathrm{L}} = 2.6236$) separated by a repeller ($B^*_{\mathrm{R}} = 4.6489$). (b)–(e) Simulations of the evolutionary behaviour for initial resident avoidance (b) $B_0 = 1.5$, (c) $B_0 = 4$, (d) $B_0 = 6$ and (e) $B_0 = 8$. The simulations confirm the singular point types seen in the PIP, with the host evolving towards B^*_{L} for initial avoidance $B_0 < B^*_{\mathrm{R}}$ (Figures (b) and (c)) and towards B^*_{H} for $B_0 > B^*_{\mathrm{R}}$ (Figures (d) and (e)). Darker squares indicate a higher proportion of the population with the corresponding avoidance B. Parameters were set at default values except $\hat{a_0} = 104$, $\gamma = 0.03$ and $\delta = 0.75$.

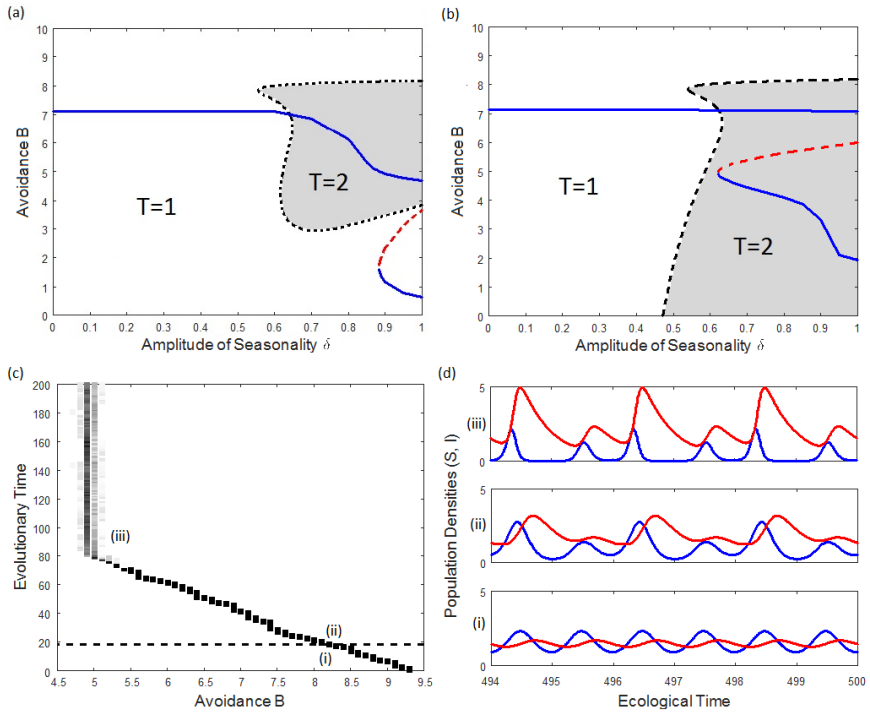

Figure 3.6: (a),(b) Change in the singular points B^* as δ varies for $\hat{a_0} = 104$ and (a) $\gamma = 0.005$ or (b) $\gamma = 0.0001$. Blue lines indicate the CSS points, red dashed lines the repeller point and black dashed lines the switch between attractors. The period of the population dynamics is 2 in the shaded region and 1 (ϵ) elsewhere. (c) Simulation example corresponding to (a) with initial transmission coefficient $B_0 = 9.3$ and $\delta = 0.9$, which evolves towards the highest CSS $B^*_{\mathrm{H}} = 4.933$. Darker squares indicate a higher proportion of the population with avoidance B, and the dashed line marks the point where evolution drives the population to switch to an attractor with period $T = 2$. (i)-(iii) correspond to sample population dynamics of the resident strain shown in (d), with blue for the susceptible population S and red for the infected population I at evolutionary times (i) 10, (ii) 20 and (iii) 100.

as shown in Figure 3.5. For certain parameter sets, the bistable CSSs have different cycle lengths due to the stability of the attractors in the population dynamics, e.g. Figure 3.6. In this case the host could start in a 1-year cycle, but evolution would drive it into a 2-year regime, i.e. evolution can drive changes in the population dynamics, Figure 3.6(c),(d). There can also be the situation where all three singular points give period two population dynamics (Figure 3.6(b)), so that the final population dynamics after evolution will have a 2-year period for any initial avoidance B_0.

Figure 3.7 shows two-dimensional contour plots for two bistable CSS points in the

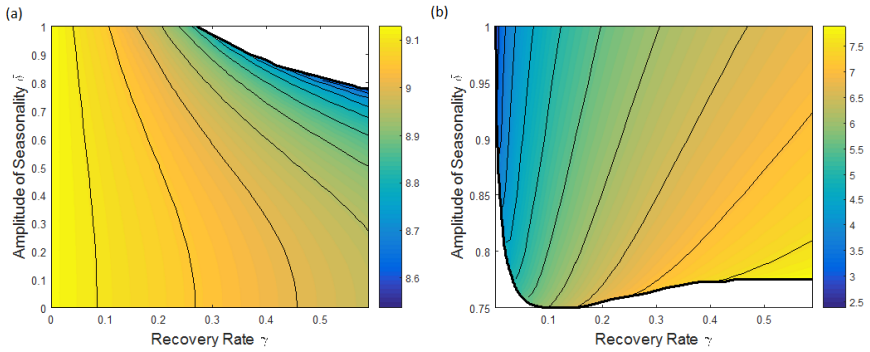

Figure 3.7: Two-dimensional contour plots showing the change in the two bistable CSS points that occur as γ and δ vary for default parameters. (a) B^*_{H}, the highest CSS point; (b) B^*_{L}, the smallest CSS point. White areas indicate where each singular point does not exist.

parameter regions where they occur. Both CSS points decrease as the amplitude δ increases, as argued above, but they move in opposite directions as γ increases. This occurs because at high levels of defence (Figure 3.7(a)), selection for even higher defence weakens as recovery increases, and so the host decreases its resistance. However, when the host has a relatively low level of defence (Figure 3.7(b)), the susceptible hosts become infected more quickly and an increase in recovery raises the infected population further, hence there is strong selection for defence and the host invests more in resistance. Recovery therefore has a much more complicated effect on evolution when seasonality is included in the model, since most of these bistability regions occur for large amplitudes.

As γ is increased further, the size of the interval of δ values where bistability occurs decreases to zero. For all γ values above this point, there is only one singular point B^* that decreases as δ increases, Figure 3.8(a), for the same reasons as explained above.

Figure 3.8(a) shows a two-dimensional contour plot for the singular point B^* as δ and γ vary in the region where one singular point exists. For the majority of amplitudes, the average infected population decreases with increasing recovery (not shown), and hence the host invests less in defence. However, there is slightly more complicated behaviour for high δ. Initially the host increases defence B^*, then at an intermediate recovery the trend turns and the host decreases its defence. This behaviour is due to changes in the average infected population, which peaks for intermediate γ since initially the increase in susceptible individuals available to be infected outweighs the loss from recovery (e.g. Figure 2.2).

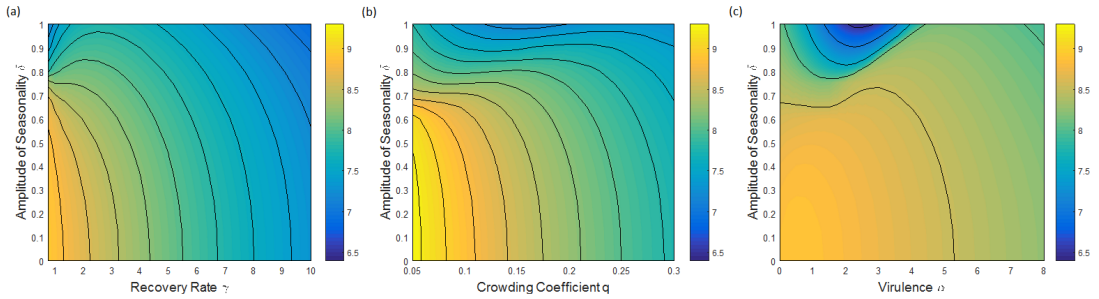

Figure 3.8: Two-dimensional contour plots showing the value of the singular point B^* as amplitude of seasonality δ and (a) recovery rate γ, (b) crowding factor q and (c) virulence α vary. Other parameters were fixed at default values from Table 3.1 with $\gamma = 1$.

Alterations to other model parameters also cause variation in the host's evolution. Figure 3.8(b) shows the change in the singular point B^* as δ and the crowding coefficient q are varied. As above, host defence B^* decreases as δ increases for all values of q. As q is increased for fixed δ, the infected population size decreases. Therefore, we would expect the host to invest less in defence as q increases, which is exactly what I found for most values of δ. However, for very high amplitudes the level of defence has a more complicated relationship with q, and in particular that defence is minimal for intermediate and very high values of q. For low q, the average infected population decreases as q increases, hence the host invests less in defence as for lower δ. However, there comes a point where the susceptible population is relatively low due to the decreased resistance, and so the host invests more in defence rather than births to increase the average susceptible population. As q continues to increase, the average infected population becomes small enough that selection for defence is weakened, and so the host returns to its previous behaviour and invests less in defence for very high q.

I find similar results when the virulence α varies, Figure 3.8(c). As α increases, the average infected population decreases and the host can afford to invest less in defence, which is exactly what I found for δ up to intermediate values. However, as for varying q, the trend becomes more complicated for highly seasonal birth rates. In this region, there is a large trough in B^* for an intermediate value of α, followed by a peak and a small decrease in B^* for high α. For small and very large α, the decrease in defence is due to the average infected population decreasing and therefore the host can afford to invest less in defence. However, the behaviour at small α causes the total population to decrease, leading to a region of α values where the host needs to evolve in such a way that the population size increases. Therefore the host has to balance changes

in the infected and total population sizes, giving the more complicated evolutionary behaviour for high amplitudes.

3.3.3 Longer-lived Hosts

The results discussed above are for a parameter set where the host lifespan is equal to the period of the forcing (one year). In this section I let the parameters take default values with baseline mortality rate decreased to $b = 0.5$ (longer-lived hosts).

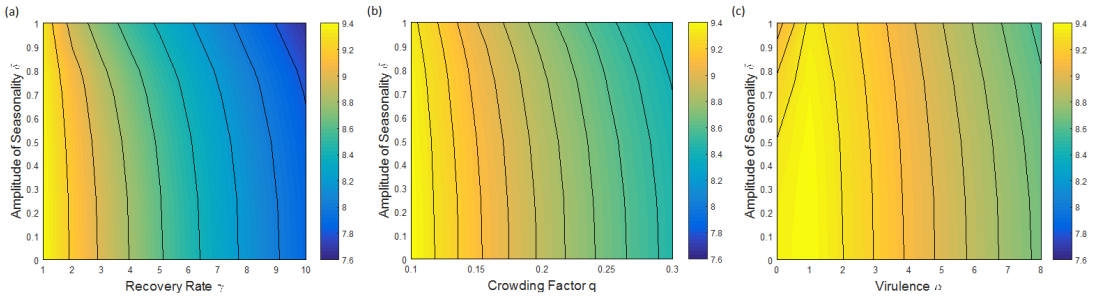

Figure 3.9: Two-dimensional contour plots showing the change in the singular point B^* as amplitude δ and (a) recovery rate γ, (b) crowding factor q and (c) virulence α vary. Other parameters were fixed at default values from Table 3.1 with $\gamma = 1$ and $b = 0.5$.

Figure 3.9 shows the CSS singular point B^* for varying amplitude δ with recovery rate γ, crowding factor q and virulence α (corresponding to Figure 3.8 for short-lived hosts). In this case, the evolutionary behaviour of the host as parameters vary remains the same for all values of δ and is caused by changes in the average infected population in all three cases. These results are in contrast to those above (Figure 3.8), where I found that the evolutionary behaviour changes for high amplitudes. Note in particular that the host evolves highest defence for an intermediate virulence for all values of δ as seen elsewhere (van Baalen, 1998), although the peak is smaller for low amplitudes (Figure 3.9(c)).

Therefore, the effects of a seasonal environment on host evolution seen in section 3.3.2 are dampened for longer lived hosts (smaller b), and there can even be no difference in the evolutionary behaviour with γ, q or α at different amplitudes. Hence the effect of the amplitude on the host's evolutionary behaviour with other parameters depends on context. In particular, for short-lived hosts we cannot rely on the evolutionary behaviour remaining the same when the amplitude of the birth rate is increased.

3.3.4 Varying the Period of the Forcing ϵ

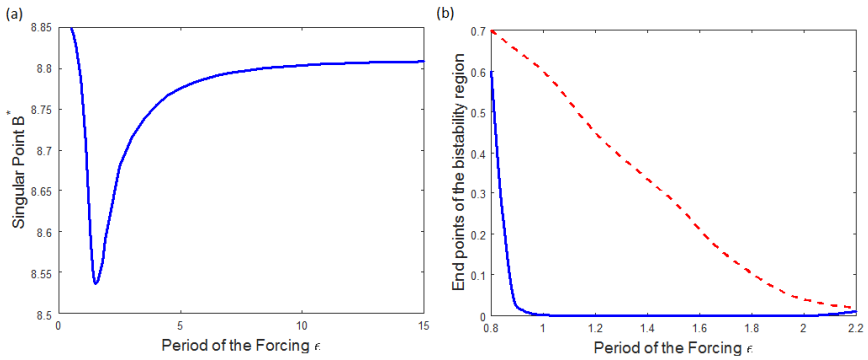

Figure 3.10: (a) Change in the CSS singular point B^* as ϵ varies for default parameters with $\delta = 0.5$ and $\gamma = 1$. (b) Change in the size of the bistability region in recovery rate γ as ϵ varies. Blue: γ value where bistability starts; Red dashed: γ value where bistability ends.

The population dynamics have period determined by that of the forcing ϵ, as discussed in Chapter 2. It is worth investigating how changing this period over a wide range of values affects the evolution of the host, Figure 3.10(a), although in many systems a 1-year cycle ($\epsilon = 1$) may be the most appropriate. I found that there is a peak in the average infected population (Figure 2.3), with a corresponding trough in the singular point B^*, caused by resonance with the natural timescale of the model. After this point, the average infected population decreases slowly as ϵ is increased further, with defence B^* gradually increasing. Hence for rapidly changing environments (ϵ low), any alteration to the period would have a significant impact on the host's evolution. In comparison, for slowly varying environments any change in the period barely alters the host's evolution. This behaviour with ϵ stays roughly the same for all parameters tested. Similarly, when both the period and other parameters are varied simultaneously, the period doesn't affect the evolutionary behaviour found as other parameters change and vice versa.

The bistability region studied in section 3.3.2 changes in size for varying period ϵ. Figure 3.10(b) shows this, indicating that the region of γ values that gives bistability is largest for $\epsilon \approx 1$, slightly lower than the peak seen in Figure 3.10(a). Above and below this value the bistability region decreases in size and quickly disappears. The period of the seasonality therefore has a large impact on whether or not these bistability regions occur.

§ 3.4 Discussion

In this chapter I have shown that seasonality in the ecological dynamics, specifically the birth rate, has a clear quantitative and qualitative effect on the evolution of host resistance against a parasite. The relative size and nature of the impact depends crucially on the underlying epidemiological model, and particularly on the potential for recovery from infection. I found regions of parameter space where there is bistability between two distinct evolutionary strategies (CSS points), which can occur alongside a switch between attractors in the population dynamics. In these regions, evolution could drive the population to a different attractor, fundamentally altering the population dynamics the host experiences. Crucially, I also found that well known patterns for the host's evolutionary strategy in a constant environment don't necessarily hold for variable birth rates, particularly when the amplitude of fluctuations is high.

For the model presented here, I found that the amplitude of seasonality and recovery rate are key processes affecting the evolution of the host's defence for a seasonal host birth rate. When recovery is absent, the host invests more in defence as the amplitude of seasonality increases as this leads to an increase in the average infected population and thus selection for increased defence. The trends observed were weak, but are consistent with existing theory on the evolution of avoidance in the absence of recovery (Boots & Haraguchi, 1999; Donnelly et al., 2015). When the host can recover from the parasite, the evolutionary dynamics become more complicated. The trend of host investment with the amplitude of seasonality switches direction at a low recovery rate, above which the host decreases its defence as the amplitude increases, since the host is now balancing reduced transmission against the increased contribution to fitness made by infected hosts through recovery. These results emphasise the importance of recovery in host-parasite infections as they prevent the parasite from being a 'functional predator' (Boots, 2004; Donnelly et al., 2015; Best et al., 2017a). It should also be noted that the results with recovery for host evolution are similar to the findings of Donnelly et al. (2013) for parasite evolution, where the parasite invests more in infectivity as the amplitude of seasonality increases. This suggests a robust result that in many systems increased seasonal amplitude will lead to higher transmission, though a full coevolutionary study that includes recovery would be needed to confirm this, which I will explore later (Chapter 6).

There has been a lack of attention to how seasonality might affect host evolution in theoretical studies, even though it has been shown that epidemiological dynamics can

be greatly impacted by a variable environment (Altizer et al., 2006; Grassly & Fraser, 2006). In addition, it is well known that a wide range of species reproduce seasonally due to environmental fluctuations, for example in bats (Stawski et al., 2014), killifish (Furness, 2016) and birds (Ketterson et al., 2015). The theoretical studies that do consider seasonality are generally co-evolutionary with a gene-for-gene based infection interaction (Nuismer et al., 2003; Mostowy & Engelstädter, 2011; Poisot et al., 2012). Of particular relevance to this study, Poisot et al. (2012) include explicit ecological dynamics in their model, using an additional resource variable with discrete fluctuations to implement seasonality, as well as a partial gene-for-gene infection mechanism. Despite these different underlying assumptions, they too find that the host invests more in defence when the amplitude of the seasonality is high and there is no recovery. Moreover, in an experimental study, Blanford et al. (2003) showed that pea aphids, *Acyrthosiphon pisum*, evolved higher resistance against a fungal pathogen, *Erynia neoaphidis*, when periodically exposed to higher temperatures. Since the fecundity of aphids varies with temperature (Ramalho et al., 2015) and aphids lack many of the genes associated with immune response to microbes (Gerardo et al., 2010), these results agree with the theoretical results found here and by Poisot et al. (2012), that increased seasonality leads to increased resistance in the absence of recovery (but see Chapter 6).

Interestingly, I found that evolutionary bistability can exist between two convergence stable strategies for small recovery rates. When the amplitude of the birth rate is high, the host may evolve towards either of two levels of defence depending on initial conditions. This bistability only occurs for a finite range of amplitudes, meaning that a small change in the amplitude could lead to a large change in the level of defence that the host evolves. Furthermore, the bistability can occur in conjunction with a switch between attractors with different cycle lengths. In many cases the higher level of defence tends to give a regime of two-year cycles in the population dynamics, whereas the lower defence tends to be in a one-year regime, meaning that evolution can in fact drive the population dynamics into a cycle with a different period. This effect of evolution moving host-parasite systems into regions of qualitatively different population dynamics has also been shown in systems which assume a constant environment but population cycles occur naturally (Hoyle et al., 2011; Best et al., 2013). These results emphasize that ecology/epidemiology and evolution are involved in a two-way feedback, as not only does ecology drive selection, but evolution can determine the nature of the population dynamics.

There have been many studies considering the evolution of host defence against para-

sites that did not include seasonality (van Baalen, 1998; Boots & Bowers, 1999; Boots & Haraguchi, 1999). I have shown here that many classic results are likely to be true in a weakly seasonal system, but may not hold for an increasingly variable birth rate. For example, as virulence varies, investment in resistance decreases as found previously (van Baalen, 1998; Boots & Haraguchi, 1999; Best et al. 2017a) for low amplitudes of seasonality, but at high amplitudes is maximized at either minimum or relatively high virulence. Similar behaviour can be observed for varying crowding factor, in that the results here agree with those found by Boots & Haraguchi (1999) for low amplitudes, but disagree for high amplitudes. These differences are a result of complicated feedbacks between seasonality, population sizes and selection which alter the costs/benefits of resistance and births. However, I have shown that this effect is dampened for hosts with longer lifespans, returning to the behaviours seen in previous work for all amplitudes of the seasonality (see section 3.3.3). It is clear that while many results found for constant environments remain true when the birth rate is variable in time, this may not be the case when the amplitude is particularly high, especially for short-lived hosts.

I also investigated the impact of changing the period of the forcing on the evolution of the host's defence. I found that changing the period induces a peak in the infected density, caused by resonance in the population dynamics with the unforced system. Naively we would expect this to lead to a maximum level of investment in defence, however, as with varying amplitude in the presence of recovery, the host evolves towards a minimum level of defence in order to maintain a large overall population size through increased birth rate. Near the peak, small alterations in the period will lead to relatively large changes in the evolutionary investment in defence. Away from the peak, the curve is almost flat and so the host's evolution is barely affected by changes in the period when it is already large. In an experimental study, Harrison et al. (2013) found that resistance of *P. fluorescens* SBW25 to a phage was constrained most strongly in rapidly fluctuating environments, while Duncan et al. (2017) showed that resistance of the same bacteria evolved more quickly in environments with rapidly fluctuating temperatures. It is unclear to what extent my theoretical results agree with these experimental studies, in part due to these systems being co-evolutionary with genetic specificity, and in part because it is difficult to ascertain which side of the resonance peak these studies may be focusing on. It is clear, though, that the time-frame of the fluctuations has important consequence to the evolutionary outcome.

Temporal heterogeneity, including seasonal fluctuations, is a fundamental aspect of all natural ecological systems. However, both experimental and theoretical studies have

rarely investigated the impact of fluctuating environments on evolutionary patterns. Here I have shown that a seasonal birth rate has a significant qualitative impact on the evolution of host defence in an SIS model, which is highly dependent on the presence and size of recovery. It is clear that key features of evolutionary dynamics may be missed by assuming a constant environment, and therefore it is important to consider how seasonality may impact host-parasite evolution more widely.

Chapter 4

Can temporal fluctuations select for diversity in host tolerance to parasitism?

In this chapter I consider evolution of host defence through tolerance, whereby the host alleviates harmful effects of the parasite. Here I do this through the parasite-induced mortality rate α, where increased tolerance leads to lower infected mortality. I consider how seasonal fluctuations in the host birth rate affects the possibility for evolutionary branching, and compare tolerance evolutionary results to two resistance mechanisms (avoidance and recovery). The majority of the results from this chapter have been submitted for publication (Ferris & Best, submitted).

§ 4.1 Introduction

Understanding the processes that create and maintain diversity in host defence and parasite infection is extremely important given its implications at both the population (Lively, 2010a) and evolutionary (Schmid-Hempel, 2011) scales. This has led to a wide range of both empirical (Laine, 2009; Lazzaro & Little, 2009; Wolinska & King, 2009; Bérénos et al., 2011; Penczykowski et al., 2016) and theoretical studies (Frank, 1993; Boots & Haraguchi, 1999; Sasaki, 2000; Miller et al., 2005; Tellier & Brown, 2007; Best et al., 2009, 2010b, 2017a,b; Boots et al., 2014) focussed on the evolutionary drivers of diversity in host-parasite interactions. Many natural communities live in spatially and/or temporally heterogeneous environments, and it has been suggested that

this heterogeneity could maintain variation in a population if different environmental conditions select for certain traits (Thompson, 1994; Byers, 2005; Lazzaro & Little, 2009). Although this may apply in general contexts, theoretically there is conflicting evidence for this hypothesis with regards to temporal heterogeneity, with studies showing delayed diversification (Johansson & Ripa, 2006), or the promotion of diversity in the population (Ives et al., 1999; Fuentes & Ferrada, 2017) when there are stochastic fluctuations. Additionally, increased plasticity and bet-hedging are alternative evolutionary outcomes to polymorphism (Leimar, 2005; Rueffler et al., 2006). However, I am unaware of any studies that investigate the effect of experimentally determined regular fluctuations on the static diversity of host defence (i.e. a polymorphism of different strains that is maintained through time). Hence it remains unclear how this type of temporal environmental variation affects population-level diversity, as models may oversimplify important biological processes, while experiments with wild species have a possibly unknown evolutionary history that will impact current levels of diversity, and as such observers might only observe a snapshot of the full evolutionary trajectory.

Hosts may defend themselves from parasitism through a number of different mechanisms, which can be broadly classified as either tolerance or resistance (Boots & Bowers, 1999; 2004; Strauss & Agrawal, 1999; Roy & Kirchner, 2000; Boots et al., 2009). Resistance mechanisms are usually defined as those that directly decrease the prevalence of the parasite, for example through decreased transmission or increased recovery (by decreasing the infectious period). However, here I focus on defence through tolerance where a host alleviates some of the harmful effects of a parasite, for example by decreasing infected mortality, but with no deleterious impact on parasite growth. In fact, 'mortality tolerance' has a positive effect on parasite fitness by increasing the infectious period, hence the parasite prevalence increases which in turn selects for higher tolerance in the host. This induces a positive feedback between host defence and parasite prevalence, with theoretical studies showing that this leads the host to evolve to extremes (in the absence of costs) or to an optimal monomorphic strategy (Roy & Kirchner, 2000; Miller et al., 2005; Best et al., 2008, 2014, 2017a). Only a few theoretical studies of tolerance have found the potential for diversification, for example when 'sterility tolerance' evolves (Best et al., 2008; 2010a), or when trade-offs between resistance and tolerance are included with an additional life-history cost (Fornoni et al., 2004; Best et al., 2008; Carval & Ferriere, 2010). Therefore it seems that under standard assumptions, including a constant environment, theory predicts that diversity in host tolerance is usually not expected to emerge.

There is a growing field of experimental studies of tolerance to parasitism in both plant and animal systems. In contrast to the theory, while some studies have found fixation of tolerance (Lefèvre et al., 2011; Parker et al., 2014), genetic variation in tolerance within populations has been observed across a wide range of different species (Koskela et al., 2002; Kover & Schaal, 2002; Råberg et al., 2007; Kause et al., 2012; Sternberg et al., 2012), including when the environment is heterogeneous for sheep and wild fish populations (Blanchet et al., 2010; Hayward et al., 2014; Mazé-Guilmo et al., 2014). Reconciling the theoretical and experimental results is clearly important for understanding of the drivers of diversity in host populations, especially for accurate predictions of the effects of external changes to these populations. One interesting theory put forward, based on empirical evidence, is that variation in host defence may be maintained through temporal environmental heterogeneity (Thomas & Blanford, 2003), at least temporarily (Lazzaro & Little, 2009). Many studies, both theoretical and empirical, have shown that temporally varying environments affect host-parasite evolution (Blanford et al., 2003; Koelle et al., 2005; Sorrell et al., 2009; Friman & Laakso, 2011; Donnelly et al., 2013; Harrison et al., 2013; Hiltunen et al., 2015; Duncan et al., 2017), however very few theoretical studies have considered host evolution, and all of those have focussed on resistance (Nuismer et al., 2003; Mostowy & Engelstädter, 2011; Poisot et al., 2012; Ferris & Best, 2018; Chapter 3). Since resistance and tolerance often lead to qualitatively different evolutionary outcomes (Boots & Bowers, 1999; Roy & Kirchner, 2000; Miller et al., 2005; Best et al., 2017a), it is still unclear how a temporally fluctuating environment will affect host tolerance evolution and diversity.

In this chapter, I analyse the mathematical model from Chapter 2 to investigate how seasonal temporal variation in the environment, specifically through a periodic host birth rate, impacts the potential for diversification through evolutionary branching and sustained polymorphism in host tolerance to parasitism. I focus on how increasing the amplitude of seasonality changes the evolutionary behaviours observed, and consider evolution of the host through two resistance mechanisms, namely avoidance (Chapter 3) and recovery, as a comparison to tolerance.

§ 4.2 Methods

In this chapter I closely follow the model and methods from Chapter 2, the main difference being evolution through different parameters with a focus on the type of evolutionary behaviour found. Here I highlight parts of the methods given in Chapter

2 that will influence the evolutionary results in section 4.3.

4.2.1 Trade-Offs and Other Parameters

I assume that the host evolves defence through reduced virulence α, lowered transmission β, or increased recovery γ separately, as seen elsewhere for a constant environment (Boots & Bowers, 1999; Roy & Kirchner, 2000; Miller et al., 2005; Best et al., 2017a). I let the average birth rate a_0 depend on the evolving parameter so that there is a cost of defence against the parasite (equation (2.20)), to reiterate:

$$a_0 = a_0(s) = \hat{a_0} - p\frac{(1 + \frac{s-s_{\min}}{s_{\max}-s_{\min}})}{(1 + c\frac{s-s_{\min}}{s_{\max}-s_{\min}})}, \tag{4.1}$$

where $a_0(s)$ has relative size given by $\hat{a_0}$, the gradient and curvature of $a_0(s)$ are determined by p and c, $s \in \{\alpha, \beta, \gamma\}$, and s takes values between $s_{\min}$ and $s_{\max}$. Trade-off parameter values are chosen such that the gradients $a_0'(\alpha), a_0'(\beta) > 0$ and $a_0'(\gamma) < 0$, since increasing α or β results in lower defence and therefore higher investment in births, while increasing γ improves defence and so the host has a lower birth rate. Figure 4.1 shows how this trade-off changes with each of the evolving parameters for fixed trade-off parameters $\hat{a_0}$ and p with varying c.

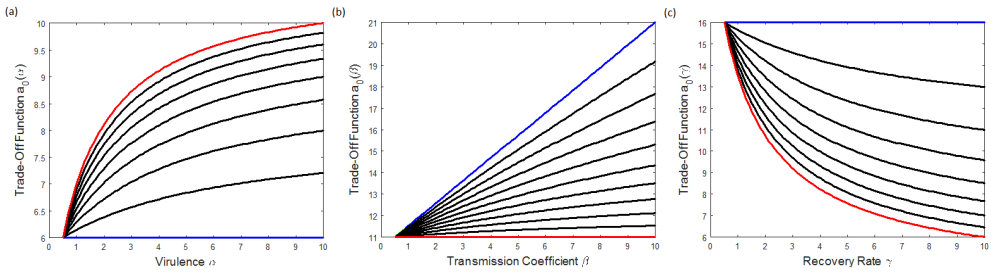

Figure 4.1: Trade-off function $a_0(s)$ for each of the three evolving parameters. (a) Virulence α varies for $\hat{a_0} = 12$, $p = 6$ and c taking values between 1 (blue) and 5 (red). (b) Transmission coefficient β varies for $\hat{a_0} = 1$, $p = -10$ and c taking values between 0 (blue) and 1 (red). (c) Recovery rate γ varies for $\hat{a_0} = 1$, $p = -15$ and c taking values between 1 (blue) and 5 (red).

I chose default parameter values such that for evolving α and β, the trade-off is accelerating ($a_0'(s) > 0$ and $\frac{\partial^2 a_0(s)}{\partial s^2} < 0$). This is so that, as more is invested in defence (i.e. α, β decrease), it becomes increasingly costly to the host and the gradient of the trade-off is steeper. Additionally, I chose accelerating trade-offs for these evolving parameters because decelerating trade-offs in constant and seasonal environments give

singular points that are always repellers when evolution is through tolerance, or only gives repellers and branching points for evolution through avoidance (Figure 4.13). In particular, branching in tolerance only appears if I assume the trade-off is accelerating (Figure 4.3).

For evolution through recovery rate γ, I chose parameters so that the trade-off is decelerating ($a_0'(\gamma) < 0$ and $\frac{\partial^2 a_0(\gamma)}{\partial \gamma^2} < 0$). In this case, I would normally choose parameters such that the trade-off is accelerating for the biological reasons given above. However, for this model I find only CSS behaviour for accelerating trade-offs, and more interesting behaviour (e.g. repellers, branching, etc) only occurs for decelerating trade-offs (Figure 4.13). As branching behaviour is the focus of this study, I used a decelerating trade-off for recovery. Biologically, decelerating trade-offs could arise through defence mechanisms that, while costly to produce, lead to small additional costs as defence is increased further (Boots & Haraguchi, 1999), hence giving increasingly less costly defence.

Default parameter values for this chapter are given in Table 4.1.

Parameter	Definition	α Model	β Model	γ Model
a_0	Average birth rate	Varies	Varies	Varies
$\hat{a_0}$	Relative size of the average birth rate $a_0(s)$	Varies	Varies	Varies
p	Gradient of the average birth rate $a_0(s)$	6	-10	-15
c	Curvature of the average birth rate $a_0(s)$	2.7	0.2	3.7
α	Virulence/additional death rate due to parasite	3	1	1
β	Transmission coefficient	3	3	3
γ	Recovery Rate	1	1	3
A	Tolerance ($\alpha_{\max} - \alpha$)	7	-	-
B	Avoidance ($\beta_{\max} - \beta$)	-	7	-
s	Evolving Parameter (α, β or γ)	3	3	3
$s_{\min}$	Minimum value of s (α, β or γ)	0.5	0.5	0.5
$s_{\max}$	Maximum value of s (α, β or γ)	10	10	10
δ	Amplitude of the oscillating birth rate	0.5	0.5	0.5
ϵ	Period of the oscillating birth rate	1	1	1
q	Crowding coefficient acting on births	0.1	0.1	0.1
b	Baseline mortality rate	1	1	1

Table 4.1: Parameter definitions and default values for each model.

4.2.2 Notes on the Evolutionary Method

In Chapter 2, I detailed how to find host fitness using a numerical method by assuming that the linearly independent solutions of the simplified mutant equations were of the form $\mathbf{X}_i(t) = e^{\mu_i t}\mathbf{p}_i(t)$ for $i \in \{1, 2\}$ (Grimshaw, 1990). I take the largest μ_i as the mutant fitness, as this governs the overall growth. Note that $\mathbf{X}_i(t)$ is composed of a bounded fluctuating vector $\mathbf{p}_i(t)$ multiplied by an exponential $e^{\mu_i t}$, and so the coefficient of the exponential term μ_i (host fitness) describes the envelope that the mutant cycles are encased in (Figure 4.2). This will be used to explain some of the evolutionary results in section 4.3.

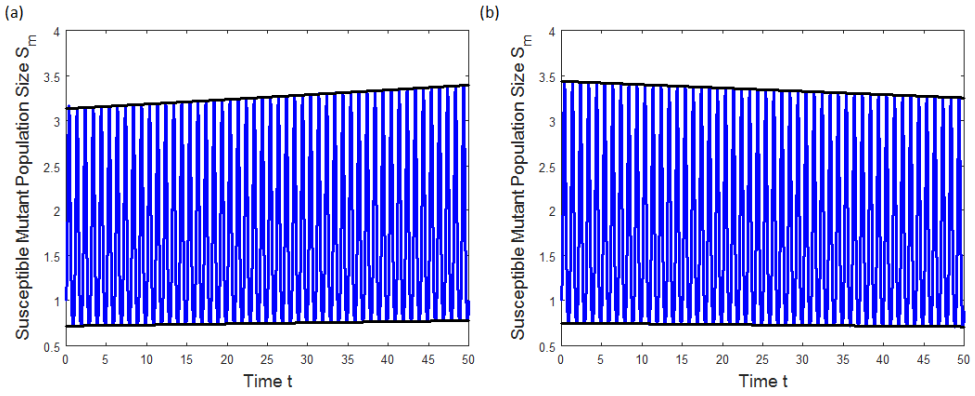

Figure 4.2: Trajectory of the susceptible mutant population $S_{\mathrm{m}}(t)$ (blue) through time for initial conditions $S_{\mathrm{m}}(0) = 1$, $I_{\mathrm{m}}(0) = 0$ with resident virulence $\alpha = 4$ and mutant virulence (a) $\alpha_{\mathrm{m}} = 3.5$, (b) $\alpha_{\mathrm{m}} = 4.5$. Black lines show how the trajectories are bounded by $pe^{\mu t}$ from equation (2.39), where p is the periodic function evaluated at the maximum or minimum of its cycle, and μ is the fitness. (a) $\mu = 0.0016 > 0$, $p_{\max} = 3.1332$ and $p_{\min} = 0.7193$; (b) $\mu = -0.0011 < 0$, $p_{\max} = 3.4374$ and $p_{\min} = 0.7512$. Otherwise parameters were fixed at default values from Table 4.1. Similar limits can be observed when the mutant infected population is plotted rather than the susceptible population.

In this chapter I am primarily interested in the creation and maintenance of diversity, which theoretically arises through evolutionary branching. A summary of the conditions under which this occurs was given in Chapter 2, but I reiterate here. Branching behaviour occurs when the host initially evolves towards an intermediate defence strategy (i.e. the singular point s^*) which is a fitness minimum and so any phenotypically similar mutant may coexist with the current resident. This is defined by s^* being convergence stable (CS; the population evolves defence such that s gets closer to s^*) but not evolutionary stable (not ES; any mutant with defence s_{m} close to the resident defence $s = s^*$ can invade/coexist with the resident population) (Geritz et al., 1998).

I also find different behaviours (continuously stable strategy (CSS), garden of eden (GoE) and repeller), definitions and examples of which can be found in Chapter 2.

§ 4.3 Results

In this section I present results for evolving host tolerance (reduction in virulence), concentrating on the potential for evolutionary branching points. I find that branching can occur for positive amplitudes ($\delta > 0$), explaining why and when this happens. I also consider resistance evolution, specifically avoidance (Chapter 3) and recovery, and investigate how the seasonal environment affects the type of evolutionary behaviour observed. I compare the resistance and tolerance results, finding that, similar to constant environment studies, there are many qualitative differences between the defence mechanisms.

I assume that the host evolves through parameters α, β or γ as stated above, but for clarity I present the results in terms of tolerance $A = \alpha_{\max} - \alpha$ (reduction in additional infected death rate), avoidance $B = \beta_{\max} - \beta$ (reduction in transmission coefficient), or recovery γ, where $\alpha_{\max}$, $\beta_{\max}$ denote the maximum values of α, β respectively.

4.3.1 Tolerance Branching Can Exist in Seasonal Environments

In a constant environment, i.e. when the amplitude of seasonality $\delta = 0$, there is no branching behaviour in tolerance for any parameter values or trade-off shapes (i.e. for any gradient and curvature of the trade-off $a_0(\alpha)$ determined by p and c). This is shown in Figure 4.3(a) for fixed singular point $A^* = \alpha_{\max} - \alpha^* = 7$, where blue regions indicate continuously stable strategies (CSS; CS and ES), red repellers (not CS and not ES) and black Garden of Eden points (GoE; ES but not CS). Therefore host evolution through tolerance in a constant environment will result in a monomorphic population with minimum, intermediate or maximum defence depending on the shape of the trade-off and initial tolerance.

Once I introduce seasonality in the birth rate, branching for tolerance evolution can occur for a small range of trade-off parameters, shown in Figure 4.3(b),(c) by the appearance of the light blue areas. This behaviour can be demonstrated through PIPs and simulations, for example see Figure 4.4 for high amplitude $\delta = 1$. For these accelerating trade-offs, the singular point is (locally) convergence stable so the host evolves towards the branching point A^*. However, the singular point is not evolutionarily sta-

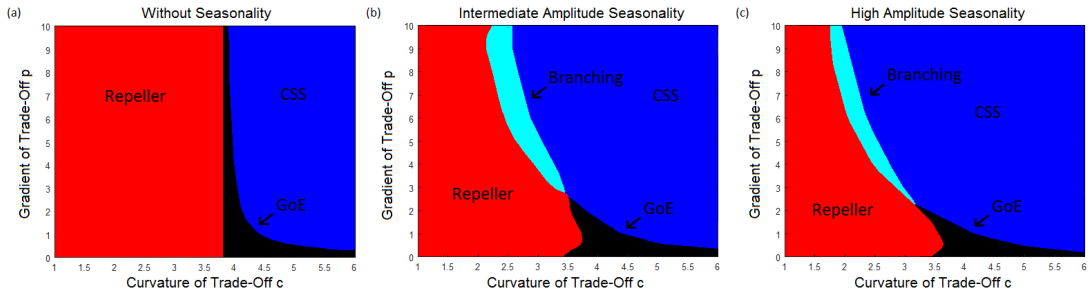

Figure 4.3: Evolutionary behaviour as the curvature of the trade-off c and the gradient of the trade-off p vary, with the value of $\hat{a_0}$ determined at every point (c, p) by the singularity condition such that the singular point $A^* = 7$. The amplitude of the seasonality is taken to be (a) $\delta = 0$ (without seasonality), (b) $\delta = 0.5$ (intermediate amplitude seasonality), and (c) $\delta = 1$ (high amplitude seasonality). Otherwise parameters were set at default values. Dark blue - CSS; Red - Repeller; Light blue - Branching; Black - GoE.

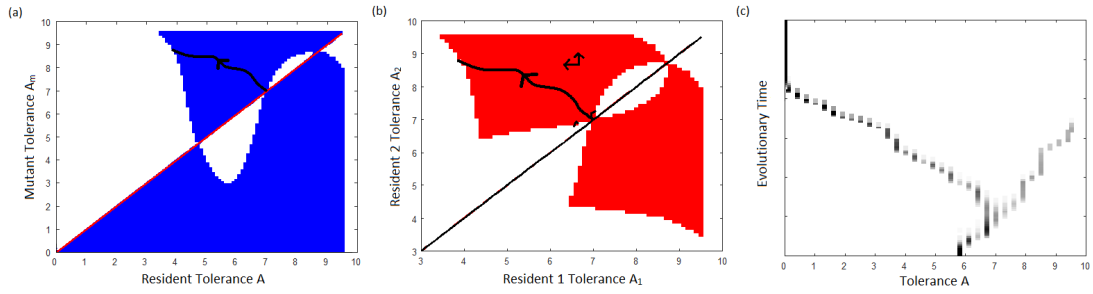

Figure 4.4: (a) PIP where blue indicates positive fitness for a mutant with tolerance $A_\mathrm{m} = \alpha_\mathrm{max} - \alpha_\mathrm{m}$ in a resident population with tolerance A. The red line shows $A = A_\mathrm{m}$, and the thick black line shows the evolutionary path after the population has reached the branching point. (b) Region of protected dimorphisms, where the thick black line indicates the evolutionary path taken by the population from the branching point, and the thin black lines are the nullclines. Arrows show the direction of evolution. (c) Evolutionary simulation starting from a monomorphic population with tolerance $A_0 = 5.8$, where darker squares indicate a higher proportion of the population with tolerance A. Throughout, $A^* = 7$, $\delta = 1$, $p = 8$, $c = 2$, $\hat{a_0} = 12.4007$, but otherwise parameters were set at default values.

ble, i.e. a mutant with similar tolerance A_m can coexist with the resident population at the singular point, hence the population branches and a dimorphic population emerges (Figure 4.4(c)). It should be noted that if the population does not start within the basin of attraction for the branching point (i.e. between the repeller points in Figure 4.4(a)), the population will converge towards one of the boundary strategies $A = 0$ and $A = 9.5$ and stay there for all time. As such, these strategies are potentially important

end-points of evolution.

Once there is a dimorphic population, there are two possible outcomes. The most common outcome for this model with tolerance evolution is where one branch eventually dies out, giving a monomorphic population again. This was determined through simulations, all of which showed extinction of a branch as seen in Figure 4.4(c) when the limits on α take default values. In this case, polymorphism is transient and eventually the resulting monomorphic population tends towards maximum or minimum defence. To understand this, consider the region of protected dimorphisms (red region in Figure 4.4(b)), i.e. the combinations of traits that can coexist, and the evolutionary trajectory of the dimorphic population through this region. For an evolutionary stable coalition to exist, the nullclines in this region need to cross. However here, as seen in the example shown, the nullclines do not cross within the protected dimorphism (red) region, and hence there is no evolutionary stable coalition. Therefore, after branching the host evolves towards the edge of the dimorphic region, at which point one of the branches dies out, leaving only one tolerance strain. By looking at the PIP where the monomorphic population emerges, the model predicts that it will evolve towards minimum tolerance, as shown in the simulation in Figure 4.4(c). This is a common result for the default limits on α ($\sim \frac{4}{5}$ simulations result in a monomorphic population with minimum tolerance, $\sim \frac{1}{5}$ result in maximum tolerance), which is to be expected since the basin of attraction for $A = 0$ is much larger than that for $A = 10$ (Figure 4.4(a)).

The second possible outcome from a branching event is fixation of the dimorphic population, often with extreme trait values, as seen elsewhere for this evolutionary behaviour (Boots & Haraguchi, 1999; Kisdi, 1999). While this behaviour is not common for the default parameter set, when the limits on α are altered some evolutionary branching simulations can demonstrate fixation of the dimorphic population, Figure 4.5. For the example shown, the evolutionary trajectory after branching does not leave the region of protected dimorphisms (Figure 4.5(b)), and so both branches survive. Hence there are cases where variability is maintained, although these are predominantly when there are tighter restrictions on the range of tolerance values allowed, which could be determined by physiological/biological limits.

4.3.2 Why Does Seasonality Allow for Branching in Tolerance?

Given that branching in tolerance has generally not been observed for simple models in constant environments (Figure 4.3(a); Roy & Kirchner, 2000 Miller et al., 2005), it

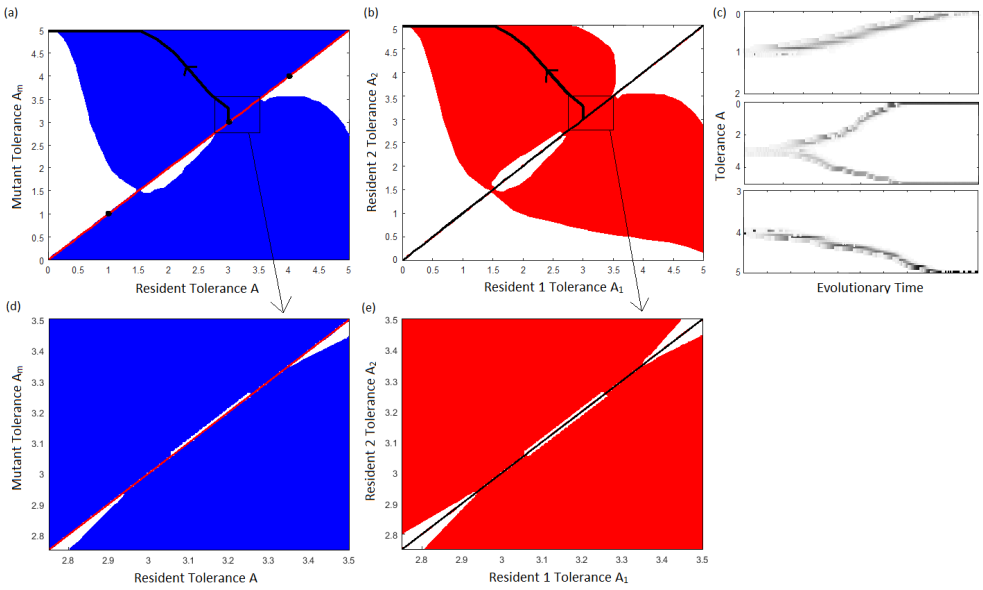

Figure 4.5: (a),(d) PIP where blue indicates positive mutant fitness, the red line is $A = A_{\mathrm{m}}$ and the black dots show where the simulations start from in (c). The thick black line shows the evolutionary path taken from the branching point. The square indicates the region that is enlarged in (d) to demonstrate the presence of a branching and repeller point in close proximity. (b),(e) Regions of protected dimorphisms, where the thick black line indicates the evolutionary path taken by the population from the branching point and arrows show the direction of evolution. The square indicates the region that is enlarged in (e). (c) Evolutionary simulations starting from a monomorphic population with tolerance $A_0 = 1$ (top), $A_0 = 3$ (middle) and $A_0 = 4$ (bottom). Darker squares indicate a higher proportion of the population with tolerance A. Parameters were fixed at $\delta = 0.85$, $p = 8$, $c = 1.3$, $\hat{a_0} = 11.9484$, $\alpha_{\min} = 1$ and $\alpha_{\max} = 6$, with default values used otherwise.

is important to understand why seasonality can allow for this behaviour. I discuss two mechanisms below, the first being strictly mathematical, while the second provides a more intuitive explanation.

The appearance of branching in tolerance is due to saddle-node bifurcations of the singular points from adaptive dynamics when the amplitude of seasonality δ is large enough. This is demonstrated in Figure 4.6(a), where numbers denote the number of singular points that exist, the dashed black lines the saddle-node bifurcations, and the light blue region where branching points occur. Branching predominantly occurs in parameter regions where there are three singular points, although note that it can also be found for fewer points if one or both of the repellers move out of the tolerance values considered (i.e. outside $[0, A_{\max}]$ where $A_{\max} = \alpha_{\max} - \alpha_{\min}$, e.g. Figure 4.6(b)).

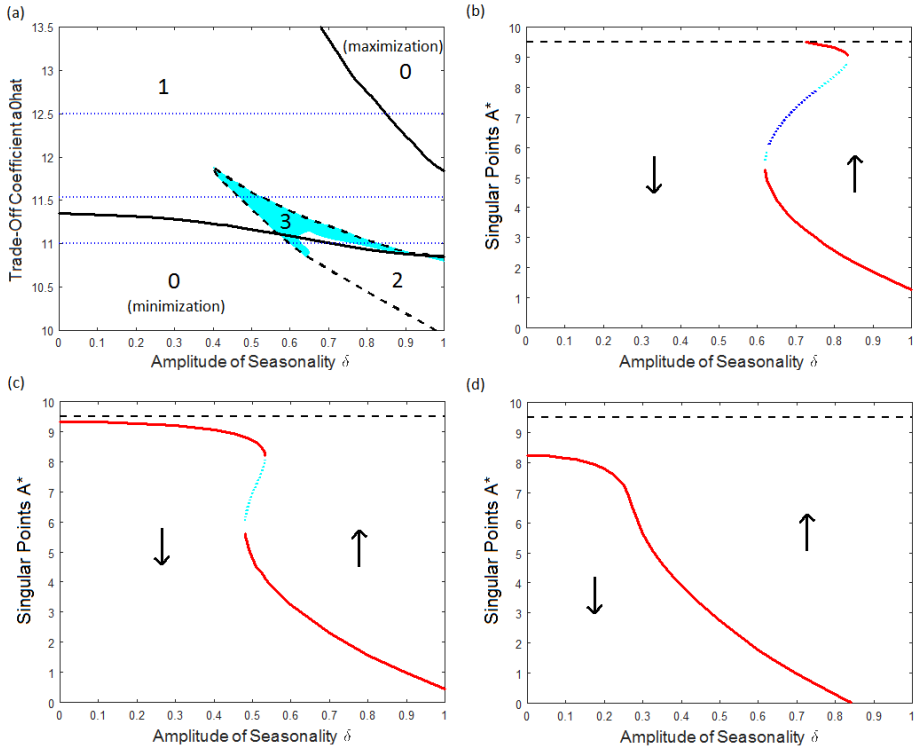

Figure 4.6: (a) Number of tolerance singular points $A^* \in [0, A_{\max}]$ for varying trade-off parameter $\hat{a_0}$ and amplitude δ, where $A_{\max} = \alpha_{\max} - \alpha_{\min}$. Populations in the regions with zero singular points either evolve towards maximum or minimum tolerance as labelled. Black lines show the boundaries of the different regions, with the dashed lines showing the saddle-node bifurcations. Light blue shading indicates where branching occurs, and the dark blue dotted lines the values of $\hat{a_0}$ used for (b)-(d). (b)-(d) Variation in the tolerance singular point(s) A^* as the amplitude δ varies with trade-off parameter (b) $\hat{a_0} = 11$, (c) $\hat{a_0} = 11.5308$, and (d) $\hat{a_0} = 12.5$. Arrows show the direction of evolution, including minimization/maximization of tolerance when no singular points exist. Red solid - repeller; Light blue dotted - branching point; Dark blue dotted - CSS; Black dashed - maximum tolerance $A_{\max} = 9.5$. Parameters were otherwise fixed at default values.

Therefore there can be three singular points occuring simultaneously, with the outer points being repellers while the central point is a branching point or a CSS (e.g. Figure 4.4). For parameters near the bifurcations, two new singular points will emerge as the amplitude δ is increased, while the second fold at higher δ values removes two singular points (Figure 4.6(b),(c)). For parameter values away from the bifurcations, there may be only one singular point as δ increases (Figure 4.6(d)). Note that in all three cases shown in Figure 4.6, the trade-off has exactly the same shape but with a greater value

as $\hat{a_0}$ is increased. Also note that the predominant direction of evolution depends on the amplitude δ, whereby low amplitudes tend to give evolution towards $A = 0$ (completely intolerant), while high amplitudes lead to evolution towards $A = A_{\max}$ (completely tolerant; Figure 4.6).

I have considered how the trade-off parameter $\hat{a_0}$ alters the saddle-node bifurcations (Figure 4.6), but changing other model parameters also affects this behaviour. Figure 4.7 shows how varying other model parameters and the amplitude δ changes the saddle-node bifurcations observed in the singular point. In all cases, branching can occur between the bifurcations near the cusp where three singular points exist. Examples of how the singular point changes with each parameter are shown to exhibit the saddle-node bifucations. Therefore, the bifurcations leading to branching can be found for a range of different parameter values, so tolerance diversity appears more generally for $\delta > 0$. Additionally, when there are no singular points, high amplitudes tend to give maximization of tolerance, suggesting that highly variable environments promote populations that are completely tolerant to the parasite.

Intuitively, it is generally understood that evolutionary branching occurs when there is a negative feedback between host defence and parasite prevalence (Roy & Kirchner, 2000; Miller et al., 2005; Boots et al., 2009). Mortality tolerance often induces a positive feedback with disease prevalence in constant environments (increasing tolerance increases disease prevalence), and so branching is rarely observed theoretically. However, here I found a non-linear relationship between tolerance and the maximum infected density on a cycle when the amplitude δ is large enough, giving a negative feedback in certain regions (Figure 4.8(a)). For tolerance near the singular point ($A \sim 7$), as defence increases the maximum infected population decreases, which in turn selects for lower tolerance and increases the maximum infected population, thus creating a negative feedback. This can be seen in Figure 4.8(a), as the gradient of the maximum infected population size with tolerance A is negative near the branching singular point. This infected maximum impacts host evolution through the assumption of the form of the mutant's trajectory. In Chapter 2, I assumed that the solution of the mutant equations is given by $\mathbf{X}(t) = e^{\mu t}\mathbf{p}(t)$, where $\mathbf{p}(t)$ is a periodic vector with fixed amplitude and μ is the host fitness. Therefore the exponential term $e^{\mu t}$ determines the limits of the mutant dynamics (Figure 4.2), and as such the fitness μ is impacted by the maximum infected population size. Hence the maximum infected population size gives a significant negative feedback in the host fitness that can lead to branching in tolerance, which is backed up by simulations that are purely multi-strain population

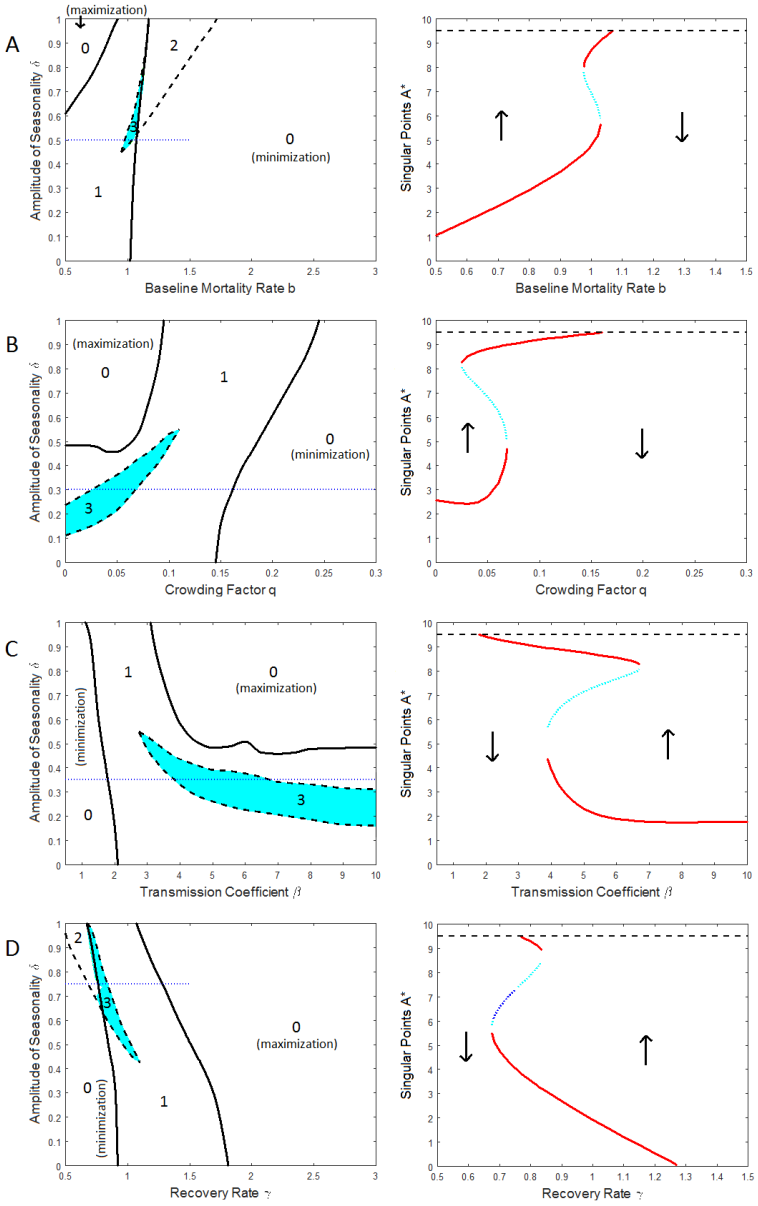

Figure 4.7: Left column: Number of singular points $A^* \in [0, A_{\max}]$ for varying parameters and amplitude δ. Otherwise parameters took defualt values with $\hat{\alpha_0} = 11.5308$ throughout. Populations in the regions with zero singular points either evolve maximum or minimum tolerance as labelled. Black lines show the boundaries of the different regions, with the dashed lines showing the saddle-node bifurcations. Light blue shading indicates where branching occurs, and the blue dotted lines the value of δ used for the singular point trends on the right. Right column: Variation of the singular points A^* with (A) baseline mortality rate b for $\delta = 0.5$, (B) crowding factor q for $\delta = 0.3$, (C) transmission coefficient β for $\delta = 0.35$ and (D) recovery rate γ for $\delta = 0.75$. Arrows show the direction of evolution, including minimization/maximization of tolerance when no singular points exist. Red solid - repeller; Light blue dotted - branching; Dark blue dotted - CSS; Black dashed - maximum tolerance $A_{\max} = 9.5$.

dynamics (Figure 4.4). Note that I also considered the average infected population size, which increases with amplitude δ but does not provide a negative feedback with tolerance (not shown), however this does not directly influence the host fitness and so I do not focus on it. For parameters where branching doesn't occur, I found that either the negative feedback didn't appear (e.g. Figure 4.8(b), the gradient of the maximum infected population size with tolerance A is always positive), or the singular point didn't enter the negative feedback region and so didn't become a branching point (e.g. Figure 4.8(c)).

4.3.3 When does Branching in Tolerance Occur?

So far I have established that branching can occur for evolution in tolerance when seasonality is included in the model. However, this behaviour is dependent on the choice of parameters. Figure 4.9 shows the regions of parameter space where there exists at least one trade-off of the form in equation (4.1) such that the singular point A^* is a branching point. This was done by creating behaviour graphs such as in Figure 4.3 for each parameter combination shown, then categorizing the point as 'Branching' if a light blue region appeared in the graphs, or 'Not Branching' if no light blue region appeared. Examples of these graphs can be seen in Figures 4.10 and 4.11, which are expansions of Figures 4.9(a) and (d), where I show a number of behaviour plots for different parameter sets. The graphs within the dark grey lines show where branching is possible (indicated by the presence of light blue areas), i.e. the top left corner for Figure 4.10 and the top right corner for Figure 4.11, imitating the regions shown in

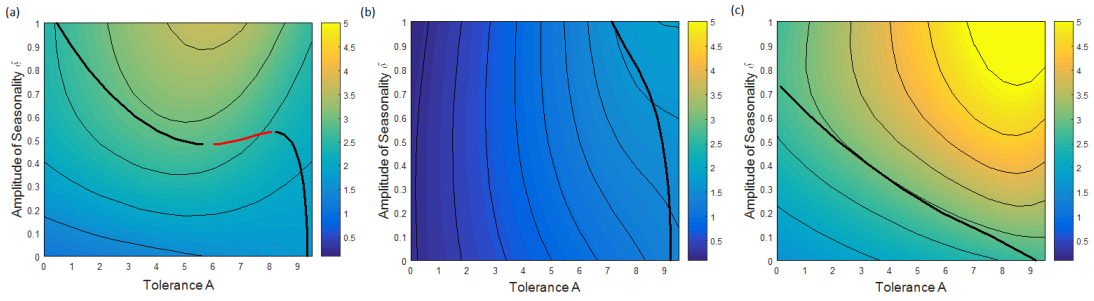

Figure 4.8: Maximum infected population size as tolerance A and amplitude of seasonality δ vary. Parameters were otherwise fixed at (a) $\hat{a_0} = 11.5308$ and default values (branching), (b) $\hat{a_0} = 12.1$ and crowding factor $q = 0.2$ (no branching), or (c) $\hat{a_0} = 18.7$ and baseline mortality rate $b = 2$ (no branching). Thick black lines show the path of the singular point(s) A^*, with red lines showing where it is a branching point in (a).

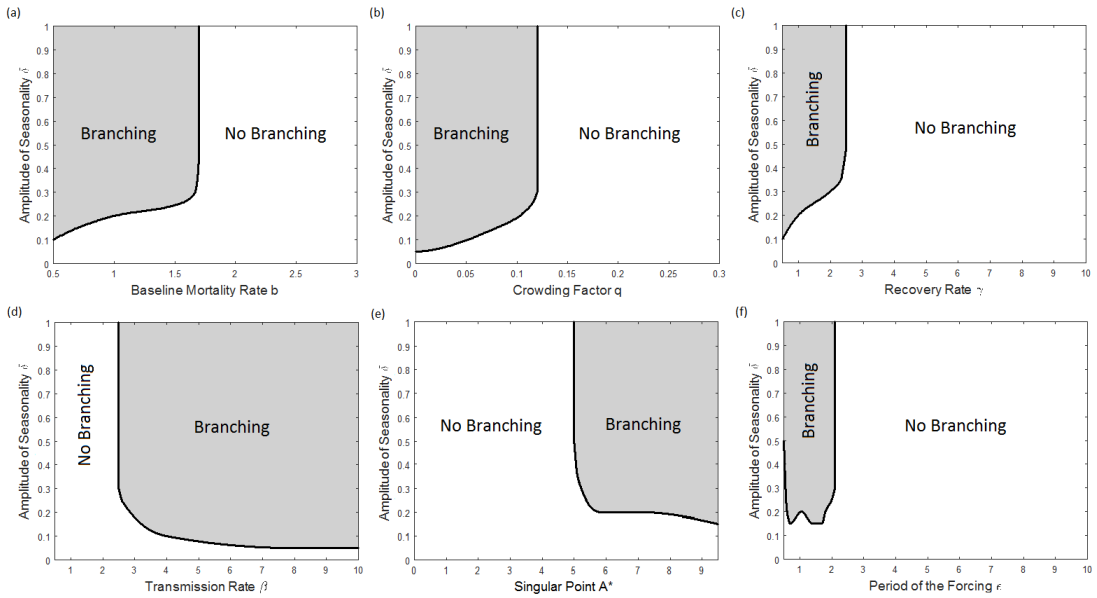

Figure 4.9: Regions of parameter space where there exists at least one trade-off function of the form defined in equation (4.1) such that branching in tolerance occurs, i.e. there are some values of $\hat{a_0}$, p and c such that A^* is a branching point ($A^* = 7$ in all but (e)). Amplitude δ varies with (a) baseline mortality rate b, (b) crowding factor q, (c) recovery rate γ, (d) transmission coefficient β, (e) tolerance singular point A^*, and (f) period ϵ. Otherwise parameters were fixed at default values.

Figure 4.9.

The parameter regions where branching can occur coincides with relatively high average infected population size (low b, q, γ and ϵ, intermediate/high β and A^* - see Figures 2.2 and 2.3), suggesting that the size of the infected population could be a driver of host diversity in tolerance in a seasonal environment. This is reinforced by the expanded graphs (Figures 4.10 and 4.11), since the branching area (light blue) increases in size as mortality rate b decreases and as the transmission coefficient β increases, corresponding to relatively large infected population sizes.

Another important feature of the branching regions is that once the amplitude reaches a certain threshold δ_{T}, then for $\delta \geq \delta_{\mathrm{T}}$ I can always find a trade-off such that A^* is a branching point. This is due to how the maximum infected population changes with tolerance A and amplitude δ. Above I showed that branching occurs when there is a negative feedback between tolerance and the maximum infected population size. Figure 4.8(a) demonstrates this, but it also shows that the non-linear trend with tolerance appears near the singular point value $A^* = 7$ for all δ greater than some threshold.

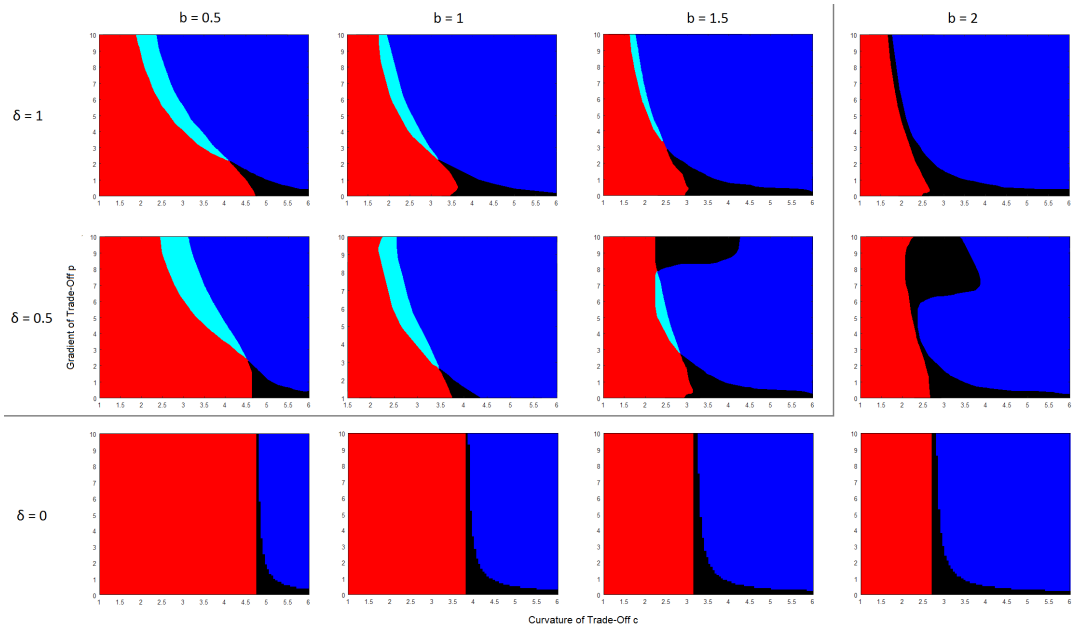

Figure 4.10: Exanded version of Figure 4.9(a), showing evolutionary behaviour as trade-off coefficients p and c vary, with $\hat{a_0}$ determined by the singularity condition at each point (c, p) such that $A^* = 7$ throughout. Amplitude δ varies vertically and baseline mortality rate b varies horizontally. Grey lines show the branching boundary from Figure 4.9(a). Bottom row: $\delta = 0$; Middle row: $\delta = 0.5$; Top row: $\delta = 1$. Left column: $b = 0.5$; Middle left column: $b = 1$ (default); Middle right column: $b = 1.5$; Right column: $b = 2$. Dark blue - CSS; Red - Repeller; Light blue - Branching; Black - GoE.

This threshold (likely) corresponds to that in Figure 4.9, so above the threshold I am always able to find a trade-off that gives branching behaviour at the singular point. For parameters where there is no branching, either the negative feedback does not exist (e.g. Figure 4.8(b)), or it occurs for tolerance values greater than the singular point (e.g. Figure 4.8(c)).

4.3.4 Branching Still Occurs if the Trade-Off is in Baseline Mortality Rate

One possible explanation for why I found evolutionary branching is that I have the trade-off and the environmental fluctuations in the same term (i.e. the birth rate). I can check this by considering trade-offs in other parameters, and investigate if branching still occurs. For example, I instead put the trade-off in the baseline mortality rate b

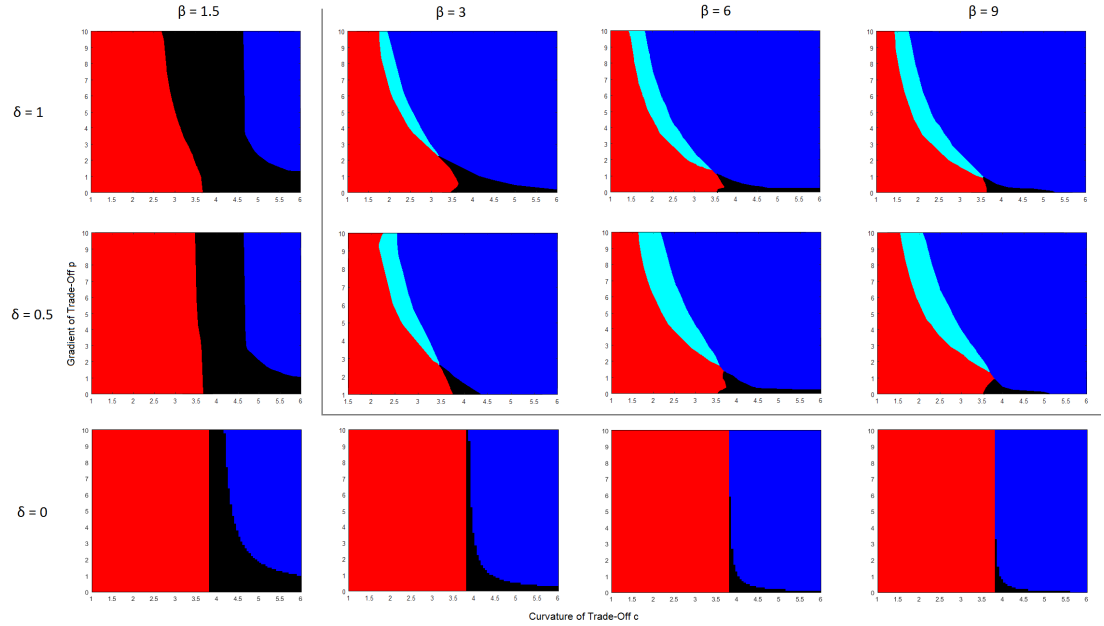

Figure 4.11: Expanded version of Figure 4.9(d), showing evolutionary behaviour as trade-off coefficients p and c vary, with $\hat{a_0}$ determined by the singularity condition at each point (c, p) such that $A^* = 7$ throughout. Amplitude δ varies vertically and transmission coefficient β varies horizontally. Grey lines show the branching boundary from Figure 4.9(d). Bottom row: $\delta = 0$; Middle row: $\delta = 0.5$; Top row: $\delta = 1$. Left column: $\beta = 1.5$; Middle left column: $\beta = 3$ (default); Middle right column: $\beta = 6$; Right column: $\beta = 9$. Dark blue - CSS; Red - Repeller; Light blue - Branching; Black - GoE.

using the following function:

$$b = b(\alpha) = \hat{b} - p_b \frac{(1 + \frac{\alpha - \alpha_{\min}}{\alpha_{\max} - \alpha_{\min}})}{(1 + c_b \frac{\alpha - \alpha_{\min}}{\alpha_{\max} - \alpha_{\min}})}, \tag{4.2}$$

where, similarly to the trade-off function in the average birth rate, p_b and c_b determine the gradient and curvature of the trade-off, and $\hat{b}$ is chosen such that $A^* = 7$. In this case, I still find branching in host tolerance evolution for $\delta > 0$. Figure 4.12 shows how the PIPs change for increasing δ, with $A^* = 7$ a repeller in (a), branching point in (b),(c) and finally a CSS in (d). This means that branching in host tolerance can occur more generally when seasonality is included in the model, and isn't necessarily dependent on where the cost of defence is implemented.

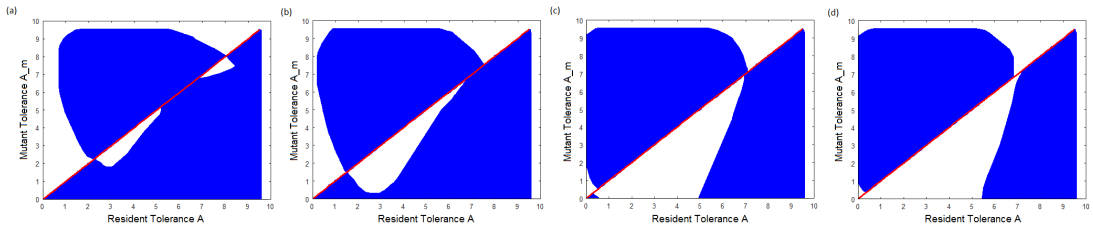

Figure 4.12: PIPs for trade-off in baseline mortality rate $b = b(\alpha)$, with $A^* = 7$ for (a) $\delta = 0.25$, $\hat{b} = -2.0935$ (repeller), (b) $\delta = 0.275$, $\hat{b} = -2.0615$ (branching), (c) $\delta = 0.35$, $\hat{b} = -1.9555$ (branching) and (d) $\delta = 0.375$, $\hat{b} = -1.9175$ (CSS - singular point is CSS for all δ values above this). The $\hat{b}$ values were chosen such that $A^* = 7$ with $\beta = 6$, $a_0 = 6$, $p_b = -4$ and $c_b = 1.75$, but otherwise default parameters were used.

4.3.5 Resistance Evolution in a Seasonal Environment

Previously, I have considered avoidance evolution in a fluctuating environment (Chapter 3; Ferris & Best, 2018), however I primarily investigated the behaviour of CSS points (end points of evolution) as seasonal parameters varied. Here I consider evolution of both avoidance and recovery, and investigate all four types of behaviour, with a focus on how seasonality affects the occurrence of branching.

For constant environments, branching occurs for decelerating trade-offs when evolution is through either resistance mechanism (avoidance B or recovery γ), Figure 4.13(a),(b). Once seasonality is introduced, branching behaviour can still occur, although the behaviour regions move and trade-offs that previously gave branching may now give CSS or repeller behaviour (Figure 4.13(c),(d)). For avoidance evolution, seasonality means that I can now find branching for both decelerating and accelerating costs (for the values of p considered, $c < 0$: decelerating costs; $c > 0$: accelerating costs). For recovery evolution, branching only occurs for decelerating costs at all amplitudes (for the values of p considered, $c > 0$: decelerating costs). In both cases, seasonality has a stronger effect on the evolutionary behaviour for large negative p, i.e. for steeper trade-off functions.

4.3.6 Tolerance vs Resistance Evolution in a Seasonal Environment

In a constant environment, it has been shown that evolution through resistance mechanisms (i.e. avoidance and recovery) gives qualitatively different results to evolution through tolerance (Boots & Bowers, 1999; Miller et al., 2005; Best et al., 2010, 2017a). Here I compare how varying the amplitude of seasonality δ and other parameters change

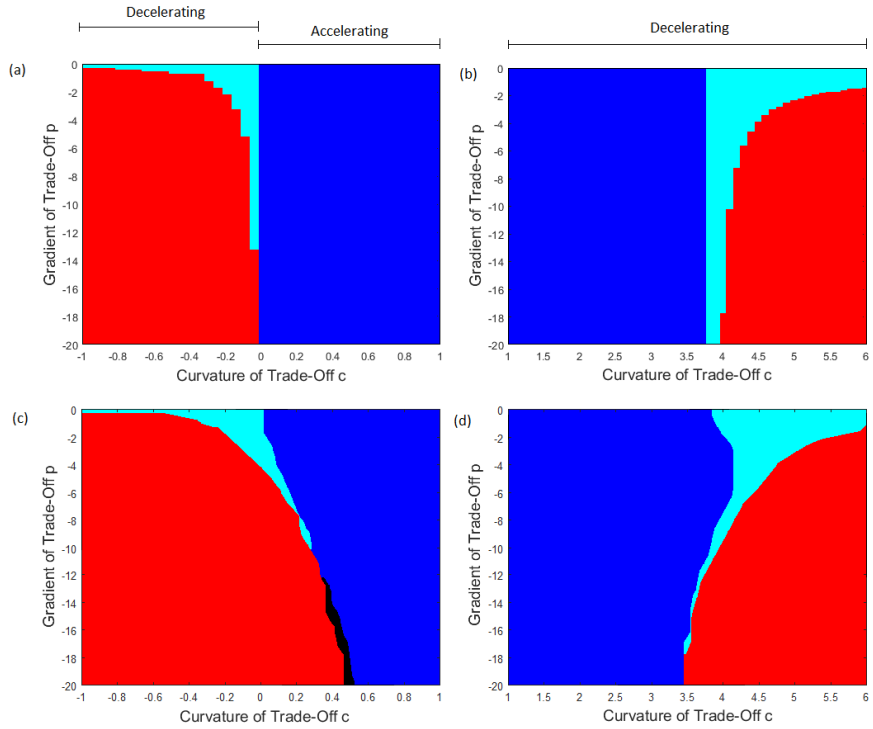

Figure 4.13: Evolutionary behaviours for resistance as trade-off parameters p and c vary, with $\hat{a_0}$ chosen at each point (c, p) such that the singular points $B^* = \beta_{\max} - \beta^* = 7$ and $\gamma^* = 3$. Left: Avoidance B evolution; Right: Recovery γ evolution; Top row: Constant environment $\delta = 0$; Bottom row: High amplitude environment $\delta = 1$. Parameters were otherwise fixed at respective default values. Dark blue - CSS; Red - Repeller; Light blue - Branching; Black - Garden of Eden.

the regions of branching behaviour for all three defence mechanisms.

For the tolerance model, increasing the amplitude δ appears to stabilise evolution, and CSSs are more likely to appear for very high amplitudes, Figure 4.14(a). In contrast, for fixed trade-off shapes that do not give branching behaviour in a constant environment, increasing the amplitude of seasonality δ can destabilise resistance evolution and cause the host to evolve to extreme defences via branching or repeller behaviour. This can be seen in Figure 4.13, where the introduction of seasonality leads to larger regions of parameter space that give branching or repeller points rather than CSS evolutionary behaviour. Figure 4.14(b),(c) also shows this, as CSS behaviour is more likely at lower amplitudes. Therefore intermediate defence strategies are more likely to evolve through tolerance in a highly variable environment, whereas intermediate resistance can evolve in a wide range of varying environments.

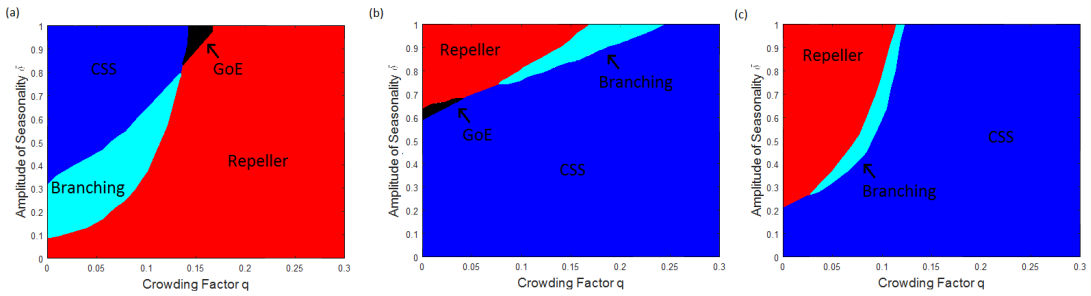

Figure 4.14: Evolutionary behaviour as the amplitude of seasonality δ and crowding factor q vary, for defence through (a) tolerance A, (b) avoidance B, and (c) recovery γ. The trade-off parameter $\hat{a_0}$ varies such that the respective singularity conditions hold at each point ($A^* = B^* = 7$, $\gamma^* = 3$), but otherwise parameters were fixed at default values in all three models. The trade-off is accelerating for (a),(b) and decelerating for (c). Dark blue - CSS; Red - Repeller; Light blue - Branching; Black - Garden of Eden.

I can also consider how varying other model parameters affects the evolutionary outcomes, as seen in Figure 4.14 for varying crowding factor q and Figure 4.15 as other parameters vary. As crowding increases, all three models agree that branching occurs at higher amplitudes. However, the size of the branching region decreases in the tolerance model, whereas in the resistance models it either increases (avoidance) or stays a similar size (recovery) until it disappears at $\delta = 1$. This could be related to the size of the infected population, in that less branching occurs for tolerance as the infected population decreases (q increases), whereas the resistance mechanisms act oppositely. The models also disagree as to the behaviour that occurs in a highly competitive environment: for resistance, high crowding leads to a CSS and therefore intermediate levels of defence for all amplitudes, whereas for tolerance the singular point is a repeller and so the host will evolve to minimum/maximum defence.

Similar to varying crowding factor q, the models for evolving resistance and tolerance often disagree when considering changes in other parameters. Figure 4.15 shows how changing the model parameters affects the evolutionary behaviour found for each of the defences studied. Generally, as stated above, I find that as the amplitude δ increases CSS are more likely to occur for evolving tolerance across a wide range of parameter scenarios. In contrast, for evolution in either of the resistance mechanisms, repellers and branching points are more likely for high amplitudes. This reinforces the result above over a wide range of parameters, that increased amplitude 'stabilises' tolerance evolution, but destabilises resistance evolution.

It is worth considering in more detail how the seasonal period ϵ alters the evoutionary

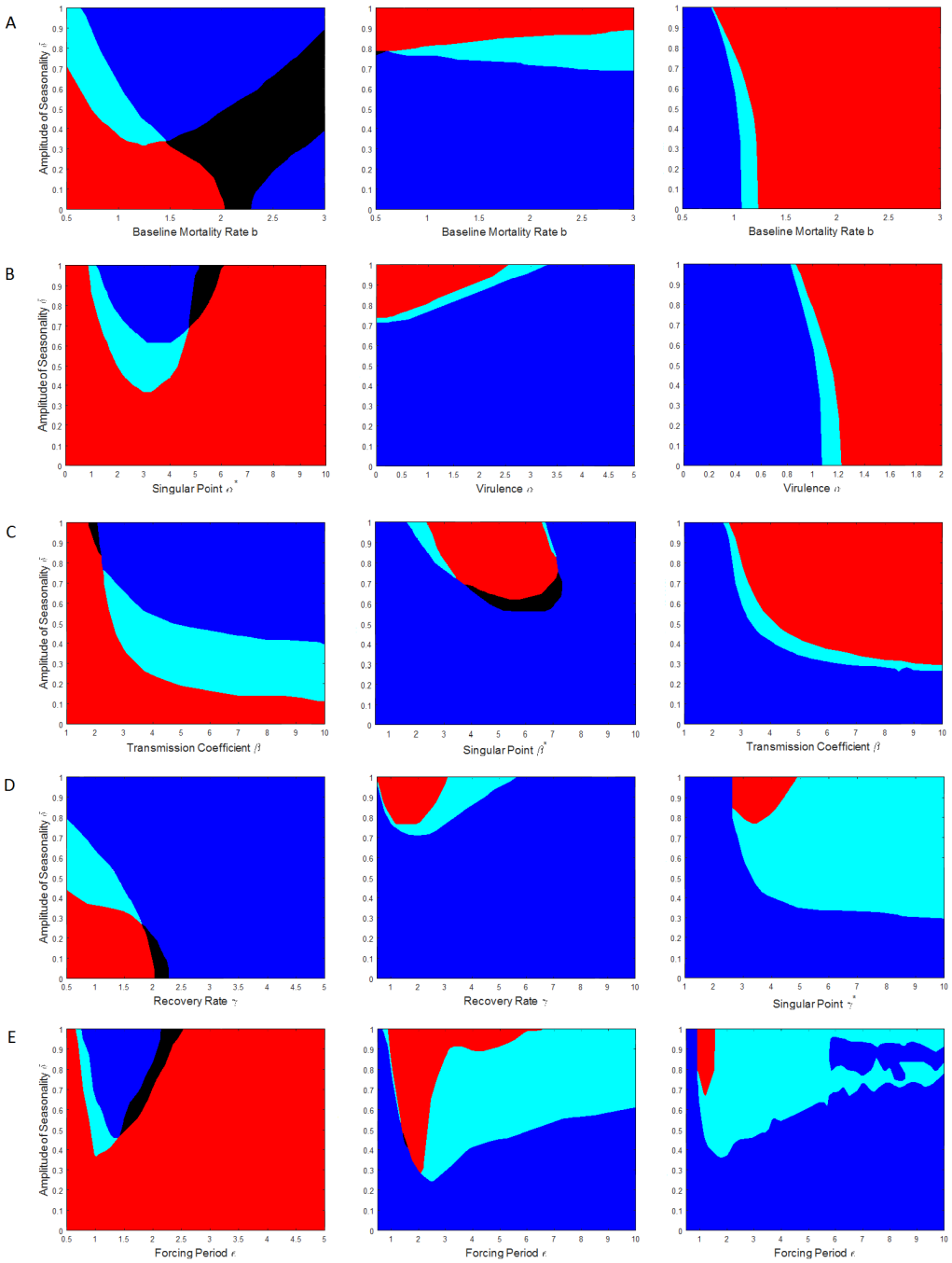

Figure 4.15: Evolutionary behaviours for varying amplitude δ and other model parameters for evolution through each of the three defence mechanisms studied. Trade-off parameter $\hat{a_0}$ was chosen at each point such that the respective singularity conditions hold, but otherwise parameters were fixed at default values. Left column: Evolution in tolerance A; Middle column: Evolution in avoidance B; Right column: Evolution in recovery γ. A: Baseline mortality rate b; B: Virulence α; C: Transmission coefficient β; D: Recovery rate γ; E: Seasonal period ϵ. Dark blue - CSS; Red - Repeller; Light blue - Branching; Black - Garden of Eden.

behaviour of all three defence mechanisms, Figure 4.15E. Similar to results from Chapter 3 (Figure 3.10), intermediate ϵ values lead to a greater range of amplitudes that give CSS behaviour for tolerance, and repeller or branching behaviour for resistance. Note that branching only occurs for low ϵ when evolution is through tolerance, compared to the wide range of periods that give branching through resistance. This suggests that only rapidly oscillating environments promote branching in tolerance (see also Figure 4.9), while branching in resistance is more likely to occur in environments with relatively slow fluctuations. It should also be noted that in the right hand column of row E, the irregular dark blue region inside the light blue area is likely due to numerical inaccuracies in the approximations used for the computations.

§ 4.4 Discussion

The aim of this chapter was to determine whether a temporally variable environment may create and maintain polymorphism in host tolerance, as suggested by empirical literature (Thomas & Blanford, 2003; Lazzaro & Little, 2009). This is in contrast to standard theoretical models which often find no branching to polymorphism in a constant environment (Roy & Kirchner, 2000; Miller et al., 2005; Best et al., 2008, 2014, 2017a). I found that branching in tolerance indeed emerged when a temporally varying environment was introduced through a seasonal birth-rate, and that sufficiently high amplitudes are needed to observe this behaviour. Mathematically, the branching occurs due to saddle-node bifurcations in the evolutionary dynamics, similar to those found in Chapter 3 for avoidance evolution (Ferris & Best, 2018). These bifurcations cause two singular points to simultaneously appear, thus creating a region where three singular points can exist (two evolutionary repellers surrounding a branching or CSS point). In line with previous work, a negative feedback can be associated with the branching behaviour (Roy & Kirchner, 2000; Miller et al., 2005; Best et al., 2008; Boots et al., 2009). Usually this is through the parasite prevalence, but due to the fitness method used here, it emerges in the maximum infected population on a cycle when the amplitude of seasonality is large enough. In this region, increasing tolerance leads to a decrease in the maximum infected population size. This selects for lower tolerance, which in turn gives a greater maximum infected population, hence a negative feedback emerges and branching is possible.

Interestingly, I observed that the dimorphic population resulting from branching is often temporary and so there is no long term guarantee of diversity, as predicted by

Lazzaro & Little (2009). Here this is due to the high cost of defence in the birth rate, so the branch with larger tolerance is often unable to maintain a high enough population size and dies out. Additionally, the high tolerance population will have a longer infectious period, resulting in a greater proportion of the population being infected and thus fewer susceptible hosts that can reproduce. The branch with lowest defence frequently survives in the long term, despite having higher overall mortality rate, because the larger investment in birth rate can keep up with the additional deaths from infection. Extinction of branches has also been observed for constant environments, for example when resistance evolves with sufficiently complex trade-offs (Best et al., 2015). The potential for both monomorphic and dimorphic populations agrees with the range of experimental literature on tolerance, including those that find diversity, as these populations may fixate or eventually lose their diversity (Blanchet et al., 2010; Sternberg et al., 2012; Hayward et al., 2014; Mazé-Guilmo et al., 2014; Parker et al., 2014). Evolutionary branching is very slow theoretically, so the population modelled here would remain dimorphic for a very long time on ecological timescales before any eventual extinctions. However, it is possible that stochastic processes may remove a strain prematurely and thus shorten the time spent as a polymorphic population. It is also worth noting that evolutionary branching through adaptive dynamics is only one way to describe diversity in empirical systems, and that this method often results in two (or more) genotypes that are very different. There are alternative methods, such as population or quantitative genetics, which describe diversity as the number of genetic characteristics or phenotypes within a species. Each of these approaches may be more suited to different empirical studies, depending on how diversity is measured and whether or not this results in major or minor differences between the genotypes.

In this chapter I have shown that variation in host tolerance is more likely in a fluctuating environment when the average infected population is high. In these regions, the maximum infected population has a significant impact on the mutant fitness and therefore the negative feedback can cause branching. When the infected population size is low, if the negative feedback appears it doesn't have as large an influence on the fitness (compared to, say, the maximum susceptible population) and so branching is less likely to occur. Theoretically, it is unclear how influential infected population size is to the potential for tolerance branching more generally since few studies have found mortality tolerance diversity in a constant environment. However, Best et al. (2010a) found that a wider range of trade-off shapes give branching behaviour at low mortality rates for evolving sterility tolerance. This leads to high infected population sizes, and therefore agrees with the result here for mortality tolerance. This relation-

ship has also been shown in an experimental study by Blanchet et al. (2010), where they found more variation in host tolerance when parasite burden was high in a wild dace population. However, I found no other experimental studies that relate tolerance diversity and parasite burden explicitly, mainly due to the fact that tolerance is often defined as the slope of host fitness against infection intensity (Simms & Triplett, 1994; Koskela et al., 2002; Råberg et al., 2007; Hayward et al., 2014). Since linear statistical methods are commonly used to analyse empirical data, results do not consider how infection intensity may impact the variation in tolerance, only stating whether or not diversity is present. Infected population size is a driver of host evolution in general, and specifically for tolerance diversity, although more empirical and theoretical work needs to be done to confirm this relationship.

The differences between host tolerance and resistance have been theoretically and empirically studied in great depth (Boots & Bowers, 1999; Strauss & Agrawal, 1999; Roy & Kirchner, 2000; Miller et al., 2005; Råberg et al., 2009; Baucom & de Roode, 2011; Best et al., 2017a), but not yet in a temporally varying environment. Here I showed that the amplitude of seasonality can have qualitatively different effects on the two defences: for tolerance, temporal variation stabilises evolution and intermediate strategies are more common; for resistance, higher amplitudes destabilise evolution and extreme traits are more likely to occur (see also Chapter 6). I found no empirical tolerance studies in a fluctuating environment, but predictions here may relate to those conducted in a temporally stationary environment by considering variation in other parameters, for example Sternberg et al. (2012) found a relationship between tolerance and mortality rate in Monarch butterflies reared on different species of plant. However, since I have shown that seasonality may change evolutionary outcomes, it is unclear how comparable the results are in these environments. There are more experimental studies that consider how a temporally fluctuating environment influences resistance evolution (Blanford et al., 2003; Friman & Laakso, 2011; Friman et al., 2011; Harrison et al., 2013; Hiltunen et al., 2015; Duncan et al., 2017), but diversity of resistance is rarely measured. Only Harrison et al. (2013) consider the variation in evolved resistance, finding that when bacteria *P. fluorescens* SBW25 are competed against phage from different treatments, those grown in rapidly oscillating resource evolved the narrowest range of resistance. This outcome broadly agrees with my result for avoidance evolution, that there is less diversification in fluctuating environments with small periods (Section 4.3.6).

The work in this chapter provides theoretical support for the hypothesis that heterogeneous environments may maintain polymorphic host defences. Specifically, I found

that a periodically oscillating birth rate makes diversity in host tolerance possible, and that this environment has qualitatively different effects on host tolerance and resistance evolution. Given this and the lack of previous work on how tolerance evolves in a fluctuating environment, there is plenty of scope for future theoretical and empirical work in this area. In particular, the effect of infected reproduction or joint evolution of resistance and tolerance could be investigated, which may give more insight into potential drivers of diversification.

Chapter 5

The Intensity of Host-Parasite Coevolution Peaks in Seasonal Environments That Oscillate at Intermediate Amplitudes

In this chapter I present a joint experimental and theoretical study of host-parasite coevolution in an oscillating environment, with particular attention paid to how the amplitude of the oscillations changes the evolutionary outcomes. I use a bacteria-phage experimental system with oscillations in the concentration of the nutrient resource, and measure the resistance of the bacteria at the end of the evolution experiment. I model the experiment with a theoretical coevolution model, which I then use to explain the experimental evolutionary results. The model is briefly summarized here, with more details given in Chapter 6. A version of this chapter will soon be submitted for publication (Ferris et al., In prep.).

§ 5.1 Introduction

It has long been recognised that environmental factors affect host-parasite coevolution, with experimental evidence showing that host defence, parasite transmission, and the type of evolutionary dynamics observed can be influenced by the environment (Fels & Kaltz, 2006; Vale et al., 2008; Lopez-Pascua et al., 2012; 2014; Zeller & Koella, 2017).

One important feature of many eco-systems is that the environment is heterogeneous, often varying in both space and time. This heterogeneity has been shown to have direct implications for host-parasite coevolution both empirically (Laine, 2009; Wolinska & King, 2009; Koskella & Brockhurst, 2014; Brunner & Eizaguirre, 2016; Parratt et al., 2016) and theoretically (Hochberg & van Baalen, 1998; Best et al., 2011; Mostowy & Engelstädter, 2011; Poisot et al., 2012). While the impact of spatial heterogeneity on host-parasite coevolution has been intensively studied (Rand et al., 1995; Haraguchi & Sasaki, 2000; Thompson, 2005; Gandon et al., 2008; Laine, 2009; Best et al., 2011; Débarre et al., 2012), the effects of temporal heterogeneity have received less attention, especially theoretically. This is despite the fact that many species experience seasonal oscillations in environment, which can lead to time-dependent effects upon infection rates (Altizer et al., 2006; Fine & Clarkson, 1982; Finkenstädt & Grenfell, 2000), and life-history traits such as reproduction (Rowan, 1938; Stawski et al., 2014; Ketterson et al., 2015; Furness, 2016) and mortality (Summers-Smith, 1956; Gehrt, 2005; Gogarten et al., 2012).

In host-parasite systems, temporally heterogeneous seasonal environments can affect coevolution in a number of different ways. For example, hosts may evolve greater resistance against a pathogen when exposed to oscillating temperatures (Blanford et al., 2003), but this may come at a cost to host survival (Dallas & Drake, 2016). However, different types of environmental oscillations can result in other evolutionary outcomes, and it has been reported that oscillations in resources can constrain antagonistic coevolution in two different predator-prey systems (Friman & Laakso, 2011; Hiltunen et al., 2015), and that such oscillations may skew the symmetry/asymmetry of coevolution by imposing stronger selection on one of the species (Friman et al., 2011). Even within the same study system, different environmental oscillations can change how the interacting species evolve. For the bacterium *Pseudomonas fluorescens* SBW25 and associated lytic bacteriophage SBW25Φ2, Harrison et al. (2013) showed that rapidly oscillating nutrient resource levels constrained coevolution, whereas Duncan et al. (2017) showed the opposite effect for the same species in oscillating temperature environments. Many of these studies only consider how different periods of oscillation in environmental variables affect evolutionary outcomes for fixed amplitudes (but see Blanford et al., 2003), however natural seasonal variations are more likely to differ in amplitude than period, yet the effect of the former remains untested. An important unanswered question is, therefore, how the amplitude of environmental oscillation affects host-parasite coevolution.

As well as empirical work, there is a growing body of mathematical modelling of host-parasite coevolution in temporally heterogeneous seasonal environments. Ecologically based models have shown that oscillating environments affect both host (Ferris & Best, 2018, *submitted*; Chapters 3 and 4) and parasite evolution (Koelle et al., 2005; Sorrell et al., 2009; Donnelly et al., 2013), with both amplitude and period impacting evolutionary outcomes. For example, Donnelly et al. (2013) found that parasite evolution is not affected by fluctuations in the host birth rate in a standard model, but the inclusion of density-dependent virulence leads to an increase in the parasite's transmission as the amplitude of oscillations increases. Elsewhere, coevolution of both the host and parasite has been considered using genetic based methods that do not account for ecological factors (Nuismer et al., 2003; Mostowy & Engelstädter, 2011; but see Poisot et al., 2012). Of particular relevance, Poisot et al. (2012) showed that, for step-wise environmental oscillations implemented through a dynamic resource, the host evolved lowest resistance for intermediate amplitudes. This is in contrast to my results from Chapter 3 (Ferris & Best, 2018), where I found that, for a continuously varying birth rate in the presence of recovery, the host evolves monotonically decreasing resistance as amplitude increases. The differences between these predictions is likely due to how increasing the amplitude changes the environmental oscillations: in Chapter 3, the average birth rate stays the same while both the minimum and maximum change with amplitude; in Poisot et al. (2012), the minimum resource input remains the same for all amplitudes while the maximum, and therefore the average, increases with amplitude. Either prediction could be correct for different species under certain environmental oscillations, but the effect of amplitude on evolution has yet to be explored thoroughly in an experimental context.

In this chapter, I consider how a temporally oscillating nutrient resource affects coevolution of the bacterium *P. fluorescens* SBW25 with the lytic phage SBW25Φ2 (Buckling & Rainey, 2002; Brockhurst et al., 2007). I focus on the effect of changing the amplitude of environmental oscillations on coevolution of bacterial resistance and phage infectivity, using constant and oscillating treatments with the same mean resource level but increasing difference between the high and low nutrient concentrations. Recent theory predicts that the bacterial host would evolve monotonically decreasing resistance as amplitude increases (Chapter 3; Ferris & Best, 2018), and that the effect of resource oscillations on parasitic phage evolution would be indirect and mediated via the effect on the host (Best et al., 2010b; Donnelly et al., 2013). I also extend the model from Chapter 2 to include coevolution and growth rate parameters from the experiment, and then compare the new predictions with the experimental results. I found that, in

both the experiment and the coevolutionary model, the amplitude of environmental oscillations determines the degree of resistance evolution and counter adaptation by the phage, with greatest resistance and infectivity evolving at intermediate amplitudes of resource oscillation.

§ 5.2 Methods

In this section I describe the bacteria-phage experiment, where the oscillating environment is implemented through oscillating nutrient resource. I also introduce a coevolutionary model of host defence and parasite infectivity, which is investigated further in Chapter 6.

5.2.1 Culture Techniques

Cultures were grown in 30ml glass microcosms with loose plastic lids containing 6ml of King's Media B (KB) in M9 salt solution, incubated at 28°C with orbital shaking at 180rpm. A gradient of nutrient concentrations, chosen by influence on growth kinetics (see section 5.2.2), were prepared by diluting KB into M9 salt solution. Bacterial densities were measured as colony forming units (CFU/ml) by plating diluted cultures on standard KB agar plates, and phage densities as plague forming units (PFU/ml) by plating a serial dilution of filtered phage on a soft agar (0.8% agar) lawn of ancestral bacteria.

5.2.2 Resource Choice

Before beginning the evolution experiment, I produced growth curves for ancestral bacteria grown with ancestral phage in various media concentrations. This was to ensure that the resource concentrations chosen for the evolution experiment covered a range of bacterial growth kinetics. Three replicates of ancestral bacteria and phage populations were grown in a 96-well microtitre plate containing a range of concentrations of KB media in M9 salts (final volume 150μl). Bacterial overnight cultures were prepared from glycerol stocks by innoculation into microcosms containing the standard concentration of KB media for 24h (180rpm, 28^{o}C). Phage cultures were innoculated from glycerol stocks into microcosms containing ancestral bacteria for 24h (180 rpm, 28^{o}C) then filtered (0.22μm) to prepare phage stocks. Bacteria and phage were added to the

microtitre plate to achieve a 10^{-1} dilution from overnight cultures. The absorbance at OD600nm was measured every 30 minutes after 1 minute of shaking for 24h.

Figure 5.1 shows the mean maximum measured absorbance against $\log_{10}$(Resource Concentration). The minimum resource concentrations used for the evolution experiment described in section 5.2.3 are marked on the graph, showing a range of different growth potential.

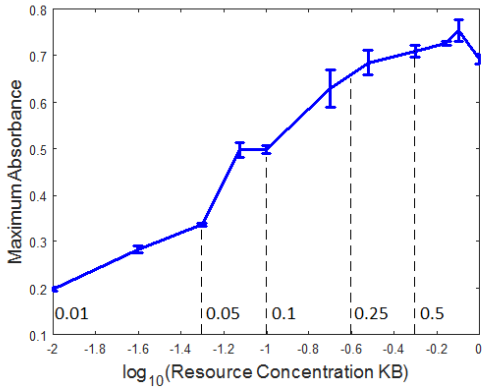

Figure 5.1: Mean maximum absorbance at OD600nm ± standard error (SE) for ancestral bacteria grown with ancestral phage against $\log_{10}$(resource concentration). The minimum and constant resources used for the evolution experiment described in section 5.2.3 are marked (minimum resources: 0.01, 0.05, 0.1, 0.25; contant resource: 0.5 KB).

5.2.3 Experiment Design

I used five treatments consisting of one constant (0.5KB constant) and four oscillating treatments with the same mean resource level but different magnitudes of oscillation between high and low nutrient concentrations, alternating every transfer (0.25/0.75KB, 0.1/0.9KB, 0.05/0.95KB, 0.01/0.99KB). Independent clones of the bacteria *P. fluorescens* SBW25 and bacteriophage SBW25Φ2 were used to inoculate initial populations (6 replicates) with $\sim 10^8$ *P. fluorescens* SBW25 cells and $\sim 10^7$ SBW25Φ2 particles. Phage were isolated from entire populations by filtration (0.22μm). One percent of the volume (60μl) was serially transferred every 48 hours into new media, with a total of 24 transfers. Population densities were measured every third transfer, whereupon samples of the whole population, phage population and 20 bacterial clones were collected for each replicate and frozen at -80^{o}C in 20% glycerol.

During the course of the experiment, some phage populations fell below detection levels

(minimum 200 PFU/ml) and densities could not be measured using the PFU method, and as such are shown as having zero phage particles in plots. In some cases, these phage populations later recovered to densities above the detection threshold. Phage populations that recovered in a later transfer were re-isolated from the undetectable time point for use in cross-infection assays by growth from frozen stocks with ancestral bacteria for 24h.

5.2.4 Population Density Analysis

The fluctuations in bacteria and phage population densities were analysed for magnitude of variation using the Fluctuation Index (FI, Vogwill et al., 2009):

$$\mathrm{FI} = \frac{1}{T\hat{N}} \Sigma_{t=0}^{T-1} |N(t+1) - N(t)| \tag{5.1}$$

where $N(t)$ is the population density at transfer t, and $\hat{N}$ is the mean population over T transfers. I also analysed the synchrony of the bacteria and phage population densities, i.e. how much the oscillations in densities between replicates were in time with each other. For this I define a synchrony measure ϕ_N (Loreau & de Mazancourt, 2008):

$$\phi_N = \frac{\sigma^2_{N_{\mathrm{sum}}}}{\left(\Sigma_i \sigma_{N_i}\right)^2} \tag{5.2}$$

where $N_i(t)$ is the population density time-series ($i = 1, 2, ..., S$), S is the number of populations being compared, $N_{\mathrm{sum}}(t) = \Sigma_{i=1}^{S} N_i(t)$, and $\sigma^2_{N_i}$ is the variance of $N_i(t)$. For the synchrony of the bacteria and phage population densities, I calculated the synchrony between replicates pairwise ($S = 2$), then found the mean and standard error (SE) of the resulting ϕ_N values for each treatment. For synchrony between the bacteria and phage populations, I calculated the synchrony measure ϕ_N per replicate population ($S = 2$), then averaged over all replicates for each treatment. Replicates where the phage died out were excluded where relevant.

5.2.5 Cross-infection Resistance Assay

Cross-infection assays were conducted to compare the resistance of the bacteria to phage from different treatments. As phage survival was variable across treatments (section 5.3.2), I selected 4 treatments where phage survived to the endpoint in at least 4 out of 6 replicates. For 4 replicates per treatment, I measured the resistance of end-point

bacterial clones against whole phage populations from each treatment and replicate (16 phage populations in total).

To measure resistance, 20 bacterial clones and whole phage populations were grown in 96-well microtitre plates containing the standard concentration of KB media in M9 salts (final volume 150μl). Bacterial overnight cultures were prepared directly from glycerol stocks by inoculation into KB 96 well microtitre plates, incubated for 24h at 28^{o}C, 80% humidity, static. Phage cultures were inoculated from glycerol stocks into microcosms containing ancestral bacteria for 24h (180 rpm, 28^{o}C) then filtered (0.22μm) to prepare phage stocks. Bacteria were added to achieve a 10^{-2} dilution and phage a 10^{-1} dilution from overnight cultures, to ensure phage density was greater than bacterial density (i.e. multiplicity of infection > 1). Bacterial growth was measured as the change in absorbance at OD600nm over 20h. Relative bacterial growth (RBG_{ij}) for bacteria i and phage j provides a metric of resistance to phage infection by describing growth in the presence versus absence of phage (Poullain et al., 2008; Wright et al., 2016). This is given by the following equation:

$$\mathrm{RBG}_{ij} = \frac{\mathrm{Abs}_{ij}(t=20) - \mathrm{Abs}_{ij}(t=0)}{\mathrm{Abs}_{i\,\mathrm{control}}(t=20) - \mathrm{Abs}_{i\,\mathrm{control}}(t=0)}\,, \tag{5.3}$$

where $\mathrm{Abs}_{ij}(t)$ denotes the absorbance for bacteria i grown with phage j at time t, while $\mathrm{Abs}_{i\,\mathrm{control}}(t)$ denotes the absorbance for bacteria i grown in the absence of phage at time t. RBG values were adjusted to restrict values to $[0, 1]$ to keep within biologically meaningful ranges (negative values suggest negative growth, while values greater than 1 suggest growth higher than the reference bacteria without phage).

5.2.6 Time-Shift Assay

Time-shift assays were conducted to measure the rate of coevolution between the bacteria and phage during the course of the experiment. Bacteria from transfers 6, 12 and 18 were grown with phage from the same population but three transfers in the past, the same transfer, or three transfers in the future. This was done for four replicates of four treatments where phage survived until the end of the experiment (note that different replicates were used for each treatment due to differences in phage survival). Bacteria overnight cultures were prepared as above for the cross-resistance assays. Phage cultures were inoculated from glycerol stocks into deep 96 well plates containing ancestral bacteria for 24h (28^{o}C, 80% humidity, static), then filtered via centrifuge (0.22μm) to prepare phage stocks. As above, bacterial growth was measured as the change in

absorbance at OD600nm over 20h, giving a relative bacterial growth measure RBG as a metric of resistance to phage infection (equation (5.3)).

5.2.7 Growth Curves

To assess the impact of phage resistance on adaptation to different resource levels, I compared growth kinetics of the ancestral bacteria to phage-resistant mutants of SBW25 (previously isolated by Harrison et al., 2013). Three independent clones of each strain were pre-conditioned in 12 different resource concentrations for 48h, then diluted by 10^{-2} in these KB concentrations into a 96-well microtitre plate (150μl final volume). The absorbance at OD600nm was measured every 30 minutes after 1 minute of shaking for 48h. The maximum growth rate was calculated as the maximum rate of increase in optical density within 48h.

5.2.8 Statistical Analysis

I use statistics to analyse the data collected during the experiments detailed above. I use linear mixed effect models, as these models allow for both fixed (parameters that are fixed) and random effects (parameters that may contribute to randomness in the data). These models are also useful when there is some non-independence within the data, for example here the replicates in each treatment are all from the same original colony and so are not independent. In these models, the response variable is the quantity that we have measured that we want to explain using fixed and random variables from the experiment. Here, I used the `lmer` program from the `lme4` package in R to form statistical models as described below.

The quantities used to analyse the population densities (Fluctuation Index FI and synchrony ϕ_N, equations (5.1) and (5.2) respectively) were statistically analysed with linear mixed effect models, with Fluctuation Index and synchrony as the response variables, bacteria and phage resource amplitudes fitted as fixed effects, and replicate as a random effect.

Linear mixed effect models were used to analyse the resistance assay data with RBG as the response variable. In plots, RBG is used for bacteria resistance, while 1− RBG represents phage infectivity. Bacteria and phage resource amplitudes were fitted as linear and quadratic fixed effects with no interaction, and replicate as a random effect, with phage replicate nested within bacteria replicate.

An individual linear mixed effect model was used to analyse the time-shift assay data with RBG as the response variable. Transfer, treatment, phage time-shift and their interactions were fitted as fixed effects and replicate as a random effect.

The maximum growth rates were analysed using a mixed effects model, with maximum growth rate as the response, resource concentration and phage resistance as fixed effects, and replicate as a random effect (no interaction between resource concentration and phage resistance was included, as the model was better without it: AIC $= -474.4$ with interaction, AIC $= -474.6$ without interaction).

To determine if the fixed effects explain a significant trend in the data, I used the `glht` program from the `multcomp` package in R to find p-values. These values describe the probability that, when the null hypothesis is true, the actual statistic is greater than or equal to the observed results. In the models described above, the null hypothesis is that none of the fixed effects (variables) describe the data. Very low p-values (usually less than 0.05) suggest that the null hypothesis is wrong, and thus the effect being tested plays a significant role in the collected data. In this chapter I also quote t-values from the mixed effect models, which are calculated as the model parameter over the standard deviation of that parameter, therefore giving a relative size of the impact of an effect in the model. These values are linked to p-values, in that large t-values provide evidence against the null hypothesis and thus suggest that the effect being tested is significant. When discussing phage survival in section 5.3.2 I use Z-values which describe how many standard deviations an observation is above or below the mean value of what is being observed. The null hypothesis is rejected if the Z-value is large, but is accepted if the Z-value is close to zero.

5.2.9 Mathematical Model

In this section I sketch a mathematical model to describe the bacteria-phage experiment above. This model is described in more detail in Chapter 6, including how the adaptive dynamics method from Chapter 2 is extended to study coevolution.

As the bacterial population dynamics are affected by the amplitude of resource oscillations (Figure 5.2), I use an ecological model for this interaction. I use a standard SIS infection model (Susceptible-Infected-Susceptible; Anderson & May, 1981; Ferris & Best, 2018; Chapter 2), which is described by the following equations:

$$\frac{dS}{dt} = aS(1 - qN) - bS - \beta SI + \gamma I \tag{5.4}$$

$$\frac{dI}{dt} = \beta SI - (\alpha + b + \gamma)I \tag{5.5}$$

where S, I are the susceptible and infected populations, and $N = S + I$ is the total population. The parameters are described in Chapters 2 and 6, with default values for this chapter given in Table 6.1. I assume that infected hosts cannot reproduce and that the bacteria can recover from infection ($\gamma > 0$). These assumptions are appropriate for this experimental study system, as bacteria infected with actively replicating phage are unlikely to divide (but see Ripp & Miller (1997) where this is not the case), and bacteria can 'recover' from infection (Westra et al., 2012; Koskella & Brockhurst, 2014). I checked the case where the bacteria cannot recover from infection ($\gamma = 0$), finding the same results as in the presence of recovery (Figure 6.10).

To imitate the oscillating media used in the experiment, I let the birth rate a depend on time through a periodic step function:

$$a = a_0(1 + \text{births}(t)) \tag{5.6}$$

where a_0 is the 'average' birth rate, and the function births(t) is a step function between a minimum and maximum (representing the low and high resource environments). Details about the function births(t) are given in section 5.3.5, where births(t) is defined in terms of the amplitude δ (equation (5.11)), and is plotted in Figure 5.8(a). An equal amount of time is spent in each environment, with the period of the oscillations equal to ϵ. The parameter a_0 only takes the average value of the birth rate a when the seasonal forcing births(t) is symmetric around zero, which is generally not the case here (equation (5.11)). However, a_0 is labelled the 'average birth rate' for consistency.

To model coevolution of the host and parasite, I use a range model that has been used previously to model eco-evolutionary dynamics with specificity in infection (Best et al., 2010b, 2017b; Boots et al., 2014). I use the following form for the transmission coefficient, incorporating evolutionary traits host defence u and parasite infectivity v:

$$\beta = \beta(u, v) = \beta_0(v)\left(1 - \frac{1}{1 + e^{-\kappa(u-v)}}\right), \tag{5.7}$$

where $\beta_0(v)$ describes a trade-off between broadness of infection and efficacy of transmission for the parasite, and κ denotes the steepness of the function. This transmission function allows for specificity in infection to occur. For example, when parasite infectivity v is large, the transmission coefficient is positive for most host defence strategies u, and so the parasite can infect a wide range of hosts. Similarly, when host defence u is

large, transmission $\beta(u, v)$ is low or zero for most parasite infectivities v, and the host can defend against a range of parasites. Chapter 6 gives more information about the transmission coefficient $\beta(u, v)$ and the trade-off functions $\beta_0(v)$, $a_0(u)$ (Figure 6.1).

I use the adaptive dynamics method to model coevolution (Geritz et al., 1998), investigating how the end-point of evolution varies with amplitude, i.e. I only consider singular points in the trait space that are both convergence stable and evolutionarily stable (Geritz et al., 1998) and are thus long-term attractors of evolution. In a coevolutionary context, a singular point (u^*, v^*) is defined as the point where both the host and parasite fitness gradients with respect to a rare mutant are zero, i.e.:

$$\left.\frac{\partial r_{\mathrm{H}}}{\partial u_{\mathrm{m}}}\right|_{u=u_{\mathrm{m}}=u^*} = 0 \tag{5.8}$$

$$\left.\frac{\partial r_{\mathrm{P}}}{\partial v_{\mathrm{m}}}\right|_{v=v_{\mathrm{m}}=v^*} = 0 \tag{5.9}$$

where r_{H} = host fitness, r_{P} = parasite fitness, u_{m} = mutant host resistance and v_{m} = mutant parasite infectivity (Best et al., 2010b). Second-order conditions on the two fitnesses for evolutionary and convergence stability can be found in Best et al. (2010b) (see also Chapter 6). The host fitness is found in the same way as in Chapter 2, using numerical Lyapunov exponents for $0 \leq \delta \leq 1$ (Metz et al., 1992; Ferris & Best, 2018). For the parasite fitness, I use the averaging method from Donnelly et al. (2013) and the equilibrium susceptible resident population $\hat{S} = (\alpha + b + \gamma)/\beta(u, v)$ to find:

$$r_{\mathrm{P}} = (\alpha + b + \gamma)\left(\frac{\beta(u, v_{\mathrm{m}})}{\beta(u, v)} - 1\right) \tag{5.10}$$

for all values of amplitude δ in $[0, 1]$ (see Chapter 6 for full derivation). Note that the parasite's evolution only depends on seasonality through the host's resistance, u.

§ 5.3 Results

In this section I present population density and evolutionary results from the bacteria-phage experiment. I found that only the bacteria population sizes were affected by the amplitude of the oscillating resource, and that the bacteria and phage evolved highest resistance/infectivity in the intermediate amplitude treatments. The coevolutionary model results match those from the experiment when bacterial growth rates in each environment are included in the seasonal forcing, and as such the model can be used

to explain the bacteria-phage evolutionary results.

5.3.1 Bacterial population dynamics were affected by resource amplitude

To quantify the effect of resource oscillations on the ecological dynamics of host and parasite populations I measured population densities of both species at every third transfer. The extent of fluctuation in bacterial population densities varied according to the amplitude of resource oscillations, such that density fluctuations increased with the amplitude of resource oscillations (Figure 5.2; Amplitude effect on bacteria density fluctuations: $t = 14.171$, $p < 10^{-16}$) whilst also becoming more synchronous among replicate populations (Figure 5.2; Amplitude effect on bacteria replicate synchrony: $t = 10.35$, $p < 10^{-16}$). By contrast, phage population densities were not significantly affected by resource amplitude either in terms of fluctuation (Figure 5.2; Amplitude effect on phage density fluctuations: $t = 1.103$, $p = 0.27$) or synchrony (Figure 5.2; Amplitude effect on phage replicate synchrony: $t = 0.547$, $p = 0.585$). Previously it has been shown that phage population sizes do not depend on resource quality (Harrison et al., 2013), and so it is perhaps unsurprising that phage densities were not significantly affected by the fluctuating resource concentrations. There was also no significant effect of amplitude on the synchrony between the bacteria and phage populations (Figure 5.3; Amplitude effect: $t = 1.33$, $p = 0.184$). Taken together, these data show that bacterial population dynamics were driven by the resource oscillations, whereas phage densities were not, suggesting that resource oscillations have a more direct effect on bacterial ecological dynamics.

5.3.2 Phage Survival

Phage survival was analysed using a survival model (fitted to a Weibull distribution) on the time of extinction given by the first transfer at which phage were undetectable using PFUs and were later unrecoverable, taking into account phage that survived until the end of the experiment. Phage death occurred in two or three replicates in each fluctuation regime (Figure 5.4), but treatment was not found to be a statistically significant factor (effect of treatment: $Z = -0.18$, $p = 0.85$).

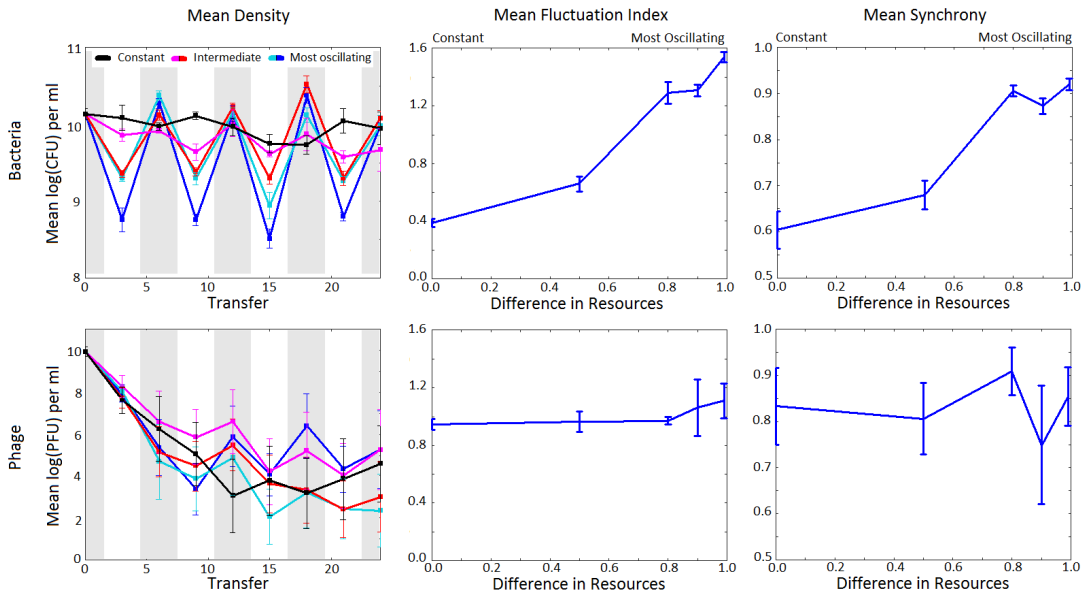

Figure 5.2: Effect of resource oscillation amplitude on the ecological dynamics of bacteria and phage. First row: Bacterial population dynamics. Second row: Phage population dynamics. Left column: Mean $\log_{10}$ population densities per ml ±SE. Grey shading indicates timepoints with high resource levels, whereas white shading indicates timepoints with low resource levels. Middle column: Mean fluctuation index FI ±SE (equation (5.1)). Right column: Mean synchrony between replicates ±SE (equation 5.2). Analysis of phage densities omitted extinct phage replicates.

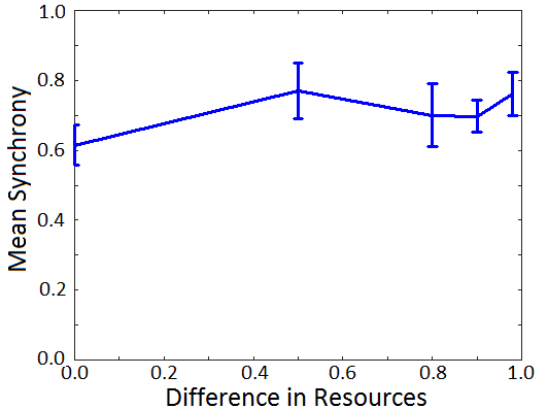

Figure 5.3: Mean pairwise synchrony (equation 5.2) between bacteria and phage populations ± SE as the difference in resources (amplitude) increases.

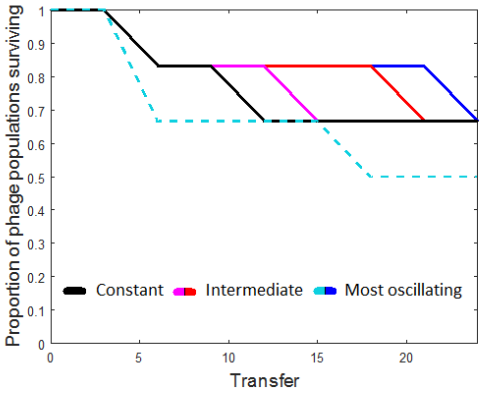

Figure 5.4: Proportion of surviving phage replicates against transfer number for each treatment. The dashed line indicates the treatment that was not used for the resistance assays due to fewer than four surviving phage replicates at the final transfer.

5.3.3 Resistance and infectivity ranges peak at intermediate resource amplitude

To explore how the amplitude of resource oscillations affected bacterial resistance evolution, I performed a cross-infection experiment using bacteria and phage isolated from the end of the coevolution experiment. Specifically, for each population I tested the resistance of multiple bacterial clones against infection by phage populations from all other treatments, thus gaining an overall measure of the change in resistance and infectivity traits that occurred during the experiment through coevolution. I found that bacteria from intermediate amplitude treatments evolved greater resistance against phage compared to bacteria from constant or high-amplitude oscillating environments (Figure 5.5(a); effect of quadratic bacteria resource amplitude term: $t = -2.334$, $p = 0.0499$). Phage evolved to counter-adapt against increased bacterial resistance, Figure 5.5(b), such that the highest infectivity arose in phage evolved under intermediate amplitude resource oscillations (effect of quadratic phage resource amplitude term: $t = 2.639$, $p = 0.022$), with the lowest infectivity observed in phage evolved under the highest amplitude oscillations.

5.3.4 Rates of Evolution of Resistance

The rate of resistance evolution in the bacteria slowed down through time in all treatments, shown by the decrease in slopes of resistance with phage shift (Figure 5.6; effect

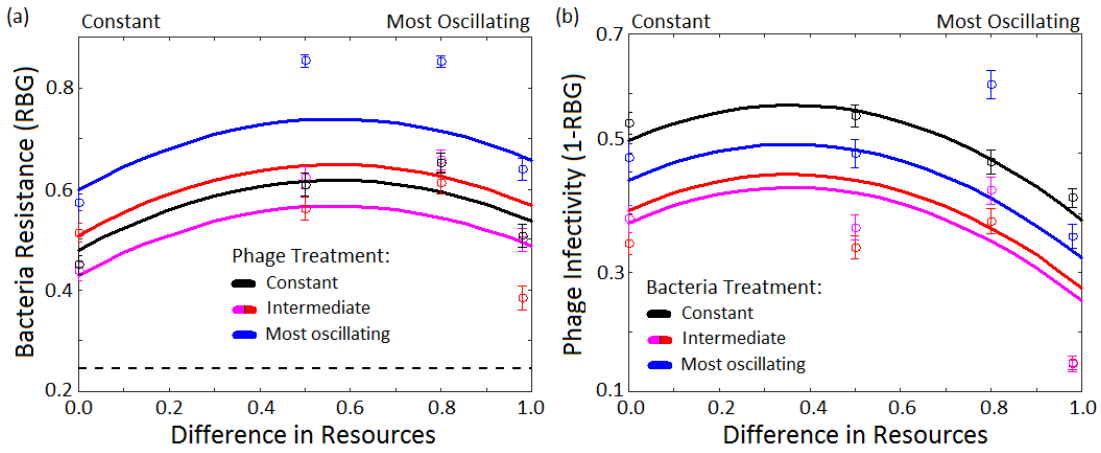

Figure 5.5: (a) Bacterial resistance (RBG) against phage populations evolved under four resource oscillation amplitude regimens. The black dashed line indicates the mean RBG for ancestral bacteria against all phage populations. (b) Phage infectivity (1−RBG) against bacterial populations evolved under four resource oscillation amplitude regimens. Circles mark mean resistance/infectivity ±SE for each bacteria and phage treatment.

of phage shift for all treatments at transfer 6 vs 12: $p = 0.0524$; 6 vs 18: $p = 0.0725$).

There was no clear effect of treatment amplitude on the rate of evolution, although the individual treatments can be compared pairwise. For example, for bacteria at transfer six, those from the 0.1/0.9KB treatment (intermediate amplitude) were overall more resistant than bacteria from the high amplitude treatment (0.01/0.99KB; $p = 0.0051$). Similarly, for bacteria from transfer eighteen, those from the highest amplitude treatment (0.01/0.99KB) were significantly more resistant than bacteria from one of the intermediate treatments (0.1/0.9KB; $p = 0.0011$) and the constant treatment (0.5KB; $p < 0.001$). Note that here resistance is measured against phage from the same population as the bacteria, and so does not represent the general range of resistance against different phage (for range of resistance see Figure 5.5). Therefore these results suggest that bacteria from the high amplitude treatment evolved specific resistance against their own phage, whereas bacteria from the intermediate amplitude treatment (0.1/0.9KB) evolved greater range of resistance (Figure 5.5) but lower specific resistance against their own phage.

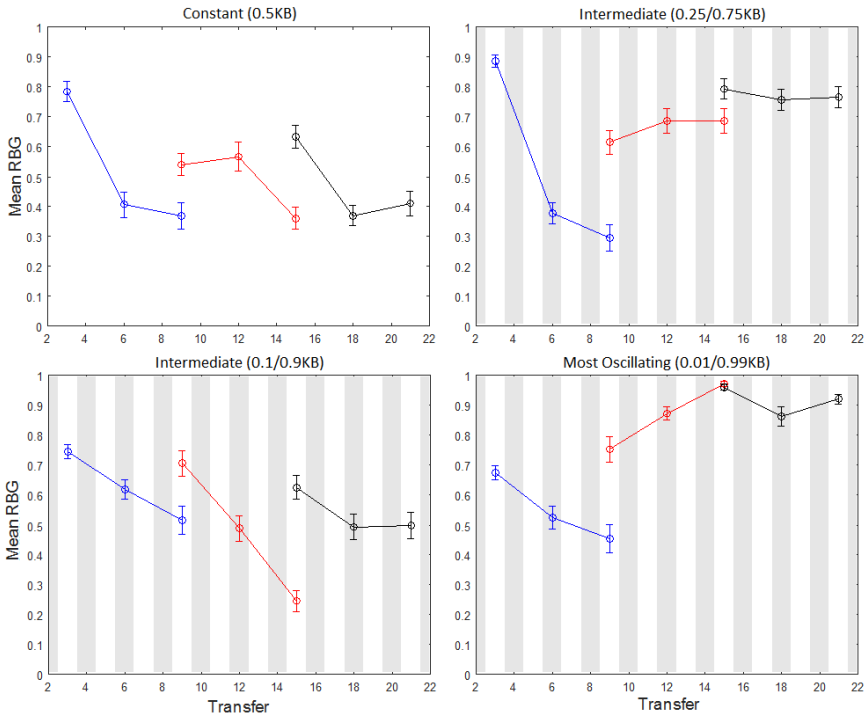

Figure 5.6: Time-shift assays for four treatments (constant 0.5KB, oscillating 0.25/0.75KB, 0.1/09KB, 0.01/0.99KB). Circles denote mean RBG ± SE for bacteria from transfers 6, 12 and 18 against past, contemporary and future phage from the same population. Grey bars indicate transfers with high resource.

5.3.5 Modelling the Evolutionary Results

In order to model the experimental system above, I adapted an SIS model with fluctuating growth rates (Ferris & Best, 2018) to include coevolution by way of a range model (Best et al., 2010b, 2017b; Boots et al., 2014). Initially, I assumed that the maximum (minimum) birth rates increased (decreased) linearly with resource concentrations. This model predicted monotonically decreasing investment in resistance and infectivity as the amplitude of the birth rate oscillations increased (Figures 6.3 and 6.7). However, the patterns of evolved resistance and infectivity traits observed in the experiment were non-monotonic and therefore this initial model did not capture the evolutionary behaviour of the system. The initial model will be discussed in more detail in Chapter 6, but here I will move on to the evidence-based seasonality case.

To better parameterise the model for the experimental system, I next experimentally measured the effect of resource level on the growth rates of phage-sensitive and phage-

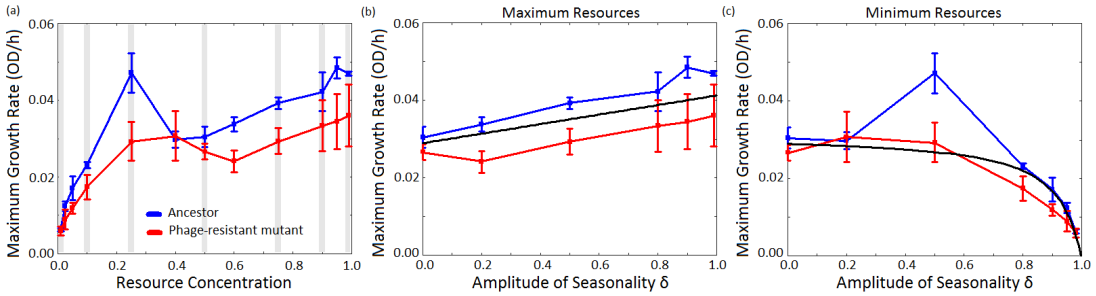

Figure 5.7: (a) Mean maximum growth rate of ancestral (blue) and phage-resistant mutant (red) bacteria in the absence of phage grown under different resource concentrations ±SE. Grey stripes indicate the resource concentrations used in the coevolution experiment. (b),(c) Mean maximum growth rates ±SE from (a) against the amplitude of oscillation, with black lines indicating the fitted birth rates from equation (5.11). (b) Maximum resources and birth rate function $\frac{0.3684\delta}{30} + 0.029$; (c) Minimum resources and birth rate function $\frac{-0.0699\delta}{30(1-0.9225\delta)} + 0.029$.

resistant genotypes of *P. fluorescens* (Figure 5.7(a)). The phage-resistant genotypes had lower growth across resource environments (Figure 5.7(a); effect of phage resistance: $t = -3.849$, $p = 0.0002$), but more importantly, the growth rates of both genotypes increased with resource level (resource effect on bacterial growth rate: $t = 10.447$, $p < 10^{-10}$) but not linearly – the growth rate gradient is much steeper at low resource levels (Figure 5.7(a)). Hence I incorporated the bacterial growth rates into the oscillating birth rate in the model by choosing functions for the high and low resource birth rates, that is, the maxima and minima of the function in equation (5.6) that imitate this trend of bacterial growth rate with resource as per Figure 5.7(a). Specifically, I still set the high resource birth rate in the model to increase linearly with amplitude, as this resembles the changes in bacterial growth rate in the high resource concentrations (resource concentrations ≥ 0.5 in Figure 5.7(a)). However, for the low resource birth rate in the model, I used a function that allows for changes in gradient with amplitude, so that it can decrease slowly at low amplitude oscillations (resource concentrations $0.25 - 0.5$ in Figure 5.7(a)), but rapidly declines at high amplitude oscillations (i.e. as the resource level decreases further; resource concentrations < 0.25 in Figure 5.7(a)). These functions relate to the overall trend of both genotypes in Figure 5.7(a), with resistance costs incorporated through a trade-off in the average birth rate a_0 that is the same for all amplitudes/resources (equation (6.9)).

I used a statistical curve fitting technique to determine the best fit for the maximum and minimum birth rate functions within a given functional form. This was done by

first plotting the maximum growth rates from Figure 5.7(a) against amplitude (rather than resource concentration), Figure 5.7(b), (c). I then assumed that the general form for the minimum birth rate was $\frac{x\delta}{1+y\delta} + 0.029$, and that the maximum was $m\delta + 0.029$, where 0.029 is the mean maximum growth rate over both bacteria genotypes in the constant environment (0.5KB concentration). The parameters x, y and m were found by minimising the sum of squares error with the bacterial growth data of both genotypes from Figures 5.7(b),(c), with a final error of 0.0023 for both functions. These functions are plotted against amplitude with the growth data in Figure 5.7(b),(c). To incorporate the maximum and minimum functions into the mathematical model, the functions plotted in Figure 5.7(b),(c) were scaled such that the maximum and minimum birth rates are zero in the constant environment ($\delta = 0$), and take significant values in the mathematical model. This resulted in the following seasonality function for the mathematical model:

$$\text{births}(t) = \text{births}_{\text{exp}}(t) = \begin{cases} 0.3684\delta & \text{if } n\epsilon \leq t < (n + \frac{1}{2})\epsilon\,, \\ \frac{-0.0699\delta}{(1-0.9225\delta)} & \text{otherwise,} \end{cases} \tag{5.11}$$

where δ is the amplitude, ϵ is the period, and n is a non-negative integer. This function is plotted in Figure 5.8(a). Additional details about the method used to derive these functions are given in Chapter 6.

I found that as the amplitude of oscillations δ increases, the model predicts that the host evolves resistance non-monotonically, with highest resistance evolving for intermediate amplitudes, Figure 5.8(b). This behaviour is similar to that found in the experiment, Figure 5.5(a), and can be explained by considering the effect of the oscillating birth rates as amplitude increases.

For low amplitudes in the model, the birth rate in the high resource environment increases faster than it decreases in the low environment (Figure 5.8(a)). Therefore the average birth rate over one oscillation increases with amplitude (Figure 5.8(a)), and so the host can afford to invest more in resistance. The increase in the average birth rate also increases the size of the infected population (Boots & Haraguchi, 1999; Ferris & Best, 2018; Figure 2.2), which further amplifies selection for resistance. A similar argument follows through to the experimental data: at low amplitudes the low resource environment has similar growth and resistance costs compared to the high environment (Figure 5.7(a),(b), resource concentrations 0.25 and 0.75), so average growth is greater than in the constant environment. Similarly to the model, this results in a high infected population density (Boots & Haraguchi, 1999; Ferris & Best, 2018;

Figure 2.2) and so greater selection for resistance. Therefore I find higher resistance evolving for intermediate amplitude oscillations due to increased selection for resistance, which is (relatively) cheap when amplitudes are low, boosting the selection effect.

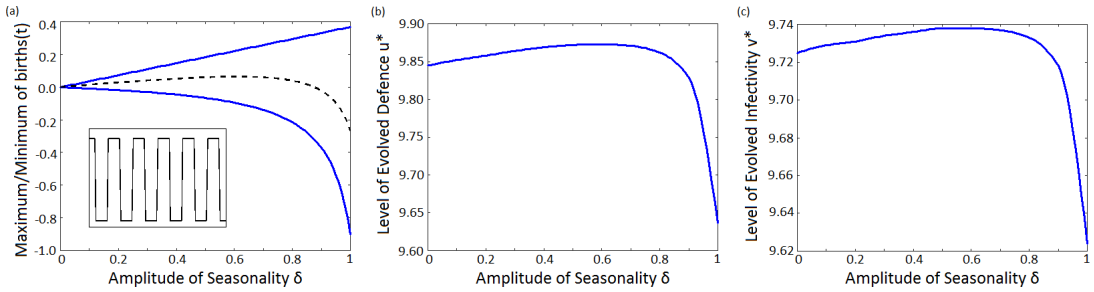

Figure 5.8: (a) Change in the maximum/minimum of the oscillating birth rate births(t), corresponding to growth in the high and low resource environments, as the amplitude of oscillations δ varies. Maximum $= 0.3684\delta$; Minimum $= -0.0699\delta/(1 - 0.9225\delta)$ (equation (5.11)). The black dashed line shows the average birth rate at amplitude δ. Insert: step function between minimum and maximum, with an equal amount of time spent in each environment. Insert: step function between minimum and maximum, with an equal amount of time spent in each environment. (b) Evolved host resistance u^* and (c) evolved parasite infectivity v^* as amplitude δ increases.

For high amplitude oscillations in the model, the birth rate in the low resource environment decreases faster than it increases in the high environment as the amplitude is increased further, Figure 5.8(a), giving an overall decrease in the average birth rate. This leads to a lower infected density, and so there is less selection for resistance. Therefore, as there is also a decrease in reproduction, the host can use the trade-off between birth rate a_0 and resistance u to invest more in growth, and so resistance decreases. For the bacteria, low resource concentrations at high amplitudes hindered growth in ancestral and spontaneous phage-resistant mutants (Figure 5.7(a)). This lack of growth means that the infected density is low and so there is less selection for resistance, but also that bacteria with high resistance are unlikely to survive the periodically low resource environment. Hence the overall bacterial resistance decreases at high amplitudes.

The model shows that the parasite's evolution only depends on the oscillations in host birth rate through the host's resistance u (see equation (5.10)), and so the parasite evolves similarly to the host with highest infectivity evolving for intermediate amplitudes (Figure 5.8(c)). This is similar to what I found experimentally for the phage (Figure 5.5(b)), i.e. the phage evolve in response to the bacteria only since phage population sizes were unaffected by the oscillating resource (Figure 5.2) and fluctuations in phage density did not significantly affect infectivity (effect of phage fluctuation index

on phage infectivity: $t = -0.779$, $p = 0.920$). Hence the phage have a similar evolution profile to bacterial resistance with respect to resource amplitude.

§ 5.4 Discussion

In this chapter I investigated how the amplitude of environmental oscillations affected the coevolution of host resistance and parasite infectivity both experimentally and theoretically. I showed that the bacterium *P. fluorescens* and its lytic phage SBW25Φ2 evolved highest resistance and infectivity for intermediate amplitude oscillations in nutrient resources. I also developed a coevolutionary model that incorporates evidence-based assumptions on the impact of seasonality on growth, which supported the empirical data by showing maximum investment in host resistance and parasite infectivity for intermediate amplitudes. The model reinforces the suggestion that the evolutionary results are due to differential growth costs in the different environments.

I used the theoretical model to explain the empirical results for varying amplitude when evidence-based growth rates are included in the oscillating birth rate function. The key to the non-monotonicity in these results is due to how the growth rates in the individual environments change with amplitude. Starting at low amplitudes, the birth rate in the high resource environment increases faster than it decreases in the low resource environment as the amplitude increases, leading to an increase in the average birth rate compared to the constant environment. This gives higher infected population densities, therefore increasing selection for resistance. Once the amplitude reaches a certain value, the birth rate in the low resource environment decreases more rapidly and the average birth rate decreases. Therefore the infected population size decreases, and so there is less selection for resistance. The host can no longer afford high resistance due to the decrease in birth rate, and since there is lower selection for resistance the host can invest more in births to maintain a large population size. I found this behaviour for a range of parameter values (Figures 6.10 - 6.13) and so it is not limited to the example shown. These arguments from the model explain the experimental pattern for bacterial resistance. Nutrient level determines the growth rate of the bacteria, with largest average growth rate in the oscillating treatments occurring for intermediate amplitudes. This, along with low competition for resources between the bacteria, leads to a greater infected population and therefore increased selection for resistance (Boots & Haraguchi, 1999; Ferris & Best, 2018; Figure 2.2). These factors combine such that bacteria in resource environments with intermediate oscillations benefit from high nutrient levels

(greater selection for resistance), but aren't as limited by low resources (low costs at low amplitudes), hence resistant mutants are able to survive better than in populations experiencing high amplitude oscillations of resource levels. The effect of population sizes can also be considered, with higher resource concentrations sustaining larger populations with greater genetic diversity. Therefore resistant mutants are more likely to occur in high resource concentrations, although their long-term survival depends on fitness costs in the periodically low resource environments. This result, that the bacteria evolve higher resistance in an oscillating environment with intermediate amplitude, appears contrary to existing evidence that a temporal environment constrains or has no effect on coevolution (Harrison et al., 2013; Duncan et al., 2017), including predator-prey interactions (Friman et al., 2011; Friman & Laakso, 2011; Hiltunen et al., 2015). These studies all use a fixed amplitude of oscillation, while I use a fixed period, and so there is likely to be an interacting effect of period and amplitude of oscillating environments on coevolution, although this has yet to be studied empirically.

For the phage, I found that highest infectivity evolved for intermediate amplitudes, and was limited by very high amplitude oscillations. The phage population sizes were unaffected by the amplitude of the resource oscillations, which suggests that phage infectivity was more strongly influenced by the strength of bacterial resistance than by nutrient availability. Therefore I find a non-linear response in phage infectivity as the amplitude of resource oscillations increases due to the behaviour of the evolved bacterial resistance. This result can also be seen in the model developed here. The parasite fitness is only affected by the oscillating environment through evolution of the host (equation (5.10), see also Best et al., 2010b; Donnelly et al., 2013), and so maximum infectivity evolves for intermediate amplitudes. A similar pattern was observed by Harrison et al. (2013), in that the phage population densities were not affected by the oscillating resource level and the phage evolved similarly to the host (broader range of resistance and infectivity in a constant environment). This experimental system and model are asymmetric in terms of how the oscillating environment impacts each species, since only the host densities are strongly affected. This in turn influences how evolution depends on the environment, leading to imbalances in coevolution and producing the similar evolutionary profiles with resource amplitude. However this effect, where only the host population is strongly impacted by the oscillations, is unlikely to be universal. In fact, there are many instances of environmental variation that strongly affect the parasite only (Mitchell et al., 2005; Fels & Kaltz, 2006; Laine, 2007; Vale et al., 2008; Duncan et al., 2017), both species (Hiltunen et al., 2015), or their interaction (Zhang & Buckling, 2011; Dallas & Drake, 2016). In these cases, we

may not expect similar resistance/infectivity evolutionary profiles, and mathematical models have already shown that such oscillations in environmental conditions can have a direct effect on parasite evolution (Koelle et al., 2005; Sorrell et al., 2009; Hamelin et al., 2011; van den Berg et al., 2011). Hence we need to understand how the environment influences each partner and their interaction in order to accurately predict the effect on coevolution, especially for use in theoretical models.

Previously, theoretical models have predicted that hosts evolved highest resistance for either constant or high amplitude oscillations in environment (Poisot et al., 2012; Ferris & Best, 2018; Chapter 3). Despite including a stepped resource and coevolution, previous models (Poisot et al., 2012) and the initial model extension (Chapter 6) failed to fully replicate the experimental set-up well enough to reproduce the evolutionary results. This is primarily due to how the minimum environment changes with amplitude. Poisot et al. (2012) keep the minimum constant while the maximum resource input increases, which does not match either the resource concentrations or growth rates in the experiment. For the initial model extension, I assumed that the maximum and minimum environments changed symmetrically, as this is how I altered the nutrient concentrations, and the average birth rate remained constant for all amplitudes. Again, this is not the case in the experiment, as I showed that growth rates decrease more rapidly as the resource concentration decreases. However, by incorporating experimentally derived growth kinetics, the coevolutionary model predicts evolution of highest resistance and infectivity at intermediate amplitudes, supporting the experimental results. Due to the default behaviour of the model, which produces a monotonic decrease in both traits for symmetric seasonality over a range of parameters (Figures 6.10 - 6.13), the main difference between the experimental and theoretical results is the predicted large drop in both resistance and infectivity for very high amplitudes. This could be due to the experimental oscillations being less extreme than the largest amplitude used in the model, and in fact the experimental data does suggest such a drop-off may occur, especially for the phage. This could be tested by using an even lower concentration of resource in the maximum amplitude environment, although this may come with an increased risk of phage extinction (Wright et al., 2016). The model could also be made more specific to the study system, for example by including free-living phage, more details about the lytic cycle or more realistic parameter values derived from experimental data. These alterations could make predictions more accurate, although the extra effort may not be necessary if results obtained from a simpler model are adequate. The co-evolutionary model could be applied to previous oscillating environment studies, provided that sufficient data about how the different individual environments affect

both species is available (for example how the period of oscillations affect coevolution (Harrison et al., 2013; Duncan et al., 2017)).

The vast majority of natural biological systems experience environmental oscillations due to a range of biotic and abiotic factors, not least regular climate variation. The impact of this seasonality on population dynamics in infectious disease systems has received considerable attention (Altizer et al., 2006). Population densities are crucial to shaping host-parasite coevolution (Papkou et al., 2016), yet until recently we have had little understanding of how fluctuating population densities, in any biological context, impact selection. This is now an emerging field of study; recent theoretical work (Koelle et al., 2005; Poisot et al., 2012; Donnelly et al., 2013; Ferris & Best, 2018) has laid the groundwork for us to be able to explore these impacts theoretically, and experimental tests of coevolution in oscillating environments are also emerging (Harrison et al., 2013; Duncan et al., 2017). This study has emphasized the importance of identifying underlying fitness costs to understand and better predict coevolution in a temporally oscillating environment. These findings suggest that in host-parasite systems where the hosts population growth dynamics are subject to seasonal forcing, coevolution will be most constrained in environments with extreme amplitudes of oscillation. Further, for oscillating environments that do not directly affect the parasite population, infectivity evolves in response to changes in host defence only.

Chapter 6

Coevolutionary Model of Host Defence and Parasite Infectivity

§ 6.1 Introduction

In this chapter, I present a more thorough analysis of the coevolutionary model from Chapter 5, which was used to predict the results from the bacteria-phage experiment (see also Ferris et al., in prep). The coevolutionary model is an extention of that from Chapter 2, where I considered evolution of the host only. In reality, both the host and the parasite are likely to coevolve due to their interaction with each other. This has been observed in many different host species, including invertebrates (Bérénos et al., 2011; Obbard & Dudas, 2014), plants (Laine, 2009; Edger et al., 2015) and bacteria (Lenski & Levin, 1985; Forde et al., 2004; Koskella & Brockurst, 2014) for a range of different parasite species. In particular, coevolution occurs between the bacteria *P. fluorescens* and its bacteriophage, i.e. the species used for the experimental study in Chapter 5 (Buckling & Rainey, 2002; Brockhurst et al., 2007), with Lopez-Pascua & Buckling (2008) showing that the rate of coevolution depends on the productivity of the environment. Therefore, to predict the evolutionary results from my experiment, it is pertinent to consider coevolution, as has been done elsewhere for these study species (Lopez-Pascua et al., 2014). Since coevolution is such a wide-spread and well recognised phenomenon, there is a wealth of theoretical research on the subject, from genetic based methods (Leonard, 1977; Sasaki, 2000; Agrawal & Otto, 2006; Lively, 2010b; Engelstädter, 2015) to adaptive dynamics studies (Restif & Koella, 2003; Boots et al., 2014; Ashby & Boots, 2015; Kada & Lion, 2015) on a wide range of evolutionary topics

(see Ashby et al. (2019) for an extensive list of theoretical host-parasite coevolution studies). Mathematically, coevolution of two (or more) species is generally more difficult than evolution of a single species, but as the results from coevolutionary studies may not be predictable from single-species evolution (Restif & Koella, 2003; Best et al., 2009), it is often necessary to include coevolution to obtain accurate predictions. For example, coevolution can lead to the emergence of more highly virulent parasites compared to parasite-only evolution due to branching in the host (Best et al., 2009), and so understanding the conditions that may lead to this scenario will be important for real world infection dynamics. Hence, while studies focussed on evolution of a single species are useful, coevolution is a fundamental process that may alter evolutionary outcomes.

Evolution studies often assume that host defence and parasite infectivity are 'universal', such that any parasite can infect any host with transmission rate depending on their overall infectivity and/or defence (Gandon et al., 2002; Bonds et al., 2005; Kada & Lion, 2015). There is empirical evidence for this assumption (Kover & Schaal, 2002; Mealor and Boots, 2006; Boots, 2011), however this is not always the case. For many host-parasite systems infection is specific, where particular parasite strains are able to infect only a certain range of hosts, and vice versa for host defence (Forde et al., 2008; Poland et al., 2009). In particular, it has been shown that this is the case for the interaction between the bacteria and phage in the experimental study in Chapter 5 (Buckling & Rainey, 2002; Poullain et al., 2008), and so a specific infection approach may be more appropriate for these species. Often, a gene-for-gene, inverse gene-for-gene or matching alleles method is used to study coevolution with specific infection (Sasaki, 2000; Agrawal & Lively, 2002; Tellier & Brown, 2007; Fenton et al., 2009, 2012; Best et al., 2014), however these models often exclude ecological factors and population dynamics which I showed to be key in the oscillating environment experiment (Chapter 5; Ferris et al., in prep). Instead, I am able to utilise a 'range' model, developed by Best et al. (2010b) and implemented for these study species by Lopez-Pascua et al. (2014) (see also Best et al., 2014, 2017b; Boots et al., 2014). This approach involves using an ecological infection model and adaptive dynamics, but also assumes an almost all-or-nothing infection process which depends on both the parasite infectivity and host defence traits. Specifically, when the host has high defence there is no transmission of almost all parasites, whereas a host with low defence can be infected by almost any parasite. Similarly, a parasite with high infectivity will be able to infect a wide range of different hosts (generalist), whereas a parasite with lower infectivity will only be able to infect a few hosts (specialist). Best et al. (2010b) use a continuous function to

approximate this specific infection process, allowing them to include important ecological dynamics and use the continuous evolutionary tools from adaptive dynamics. The same approach for continuous infection specificity can be found elsewhere (Boots et al., 2014; Best et al., 2017b), with Boots et al. (2014) finding that both specificity and incompatability between strains are needed to produce static diversity (i.e. a polymorphism of different host and parasite strains that, once evolved, is maintained through time). The inclusion of specificity makes adaptive dynamics results more comparable to those from genetic based studies, where it is common to have this type of infection interaction.

While there have been many theoretical host-parasite coevolution studies in a constant environment, a vast majority of species will experience heterogeneous conditions that affect life histories and infection dynamics. Investigating the effects of these environments on host-parasite coevolution is important, and in fact many have focussed on spatial heterogeneity (Hartvigsen & Levin, 1997; Hochberg & van Baalen, 1998; Damgaard, 1999; Thompson, 1999; Nuismer & Kirkpatrick, 2003; Moreno-Gámez et al., 2013). For example, Hochberg & van Baalen (1998) showed that greater dispersal can lead to an increase in the spatial range of strains otherwise dominant in the most productive environments, which decreases overall diversity. However, relatively few have considered the impact of a temporally variable environment (Nuismer et al., 2003; Mostowy & Engelstädter, 2011; Poisot et al., 2012), despite arguments that temporal changes in environment and/or population sizes will have an effect on coevolution (Wolinska & King, 2009; Papkou et al., 2016). These studies of temporal heterogeneity use genetic-based methods to study coevolution with specific infection, but only Poisot et al. (2012) include ecological factors, which could change evolutionary outcomes through eco-evolutionary feedbacks (Chapter 3; Ferris & Best, 2018; Ashby et al., 2019). Poisot et al. (2012) found that, for step-wise environmental fluctuations implemented through a dynamic resource, the host evolved lowest resistance for intermediate amplitudes and the parasite invested more in infectivity as the amplitude increased. While these predictions may hold for certain empirical systems, they certainly do not match the results from the bacteria-phage experiment in Chapter 5, where I found maximum investment in host resistance and parasite infectivity at intermediate amplitude oscillations in resource concentration (see also Ferris et al., in prep). As discussed in Chapter 5, the main reason for the difference between the experimental and Poisot et al.'s results is due to how the periodic forcing is implemented in their model, as it does not reflect the experimental conditions. Similarly the host-only evolution result, where defence decreases monotonically as amplitude increases (Chapter 3; Fer-

ris & Best, 2018), does not fit the resistance results from the experiment for the same reason. A parasite-only evolution prediction of monotonic increasing transmission by Donnelly et al. (2013) also does not match the empirical results for the phage. Therefore a reasonable next step would be to consider coevolution of the host and parasite with recovery, potentially using a specific seasonality function that takes into account bacterial growth in each individual environment. A model for this was presented in Chapter 5, which found that once the seasonal forcing is based on empirical data, the evolutionary outcomes better reflect those from the experiment.

In this chapter, I give a more thorough examination of the coevolutionary model from Chapter 5 that was used to predict the evolutionary outcomes observed in the bacteriaphage experiment (maximum resistance/infectivity for intermediate amplitudes; see also Ferris et al., in prep). I give more background to the development of the coevolutionary range model, based on that by Best et al. (2010b), that incorporates a periodic forcing in the host birth rate as a proxy for the oscillating resource concentration. Using previous studies and work from Chapter 3, I predicted that a continuous symmetric sinusoidal form for the seasonality would give a monotonic decrease in host defence (Ferris & Best, 2018; see also Chapter 3), and that the parasite's evolution would not directly depend on the seasonality (Donnelly et al., 2013). As expected, the host and parasite evolved monotonically decreasing defence and infectivity as the amplitude of seasonality increased, even when the seasonal forcing was discretized. As shown in Chapter 5, to obtain the results from the experiment I introduced a stepped forcing based on growth rates of the bacteria in each individual environment. This form for the seasonality produced evolutionary results that are much more similar to those from the experimental data, emphasizing that specific details about experimental systems may be needed to be able to predict evolutionary outcomes, especially in heterogeneous environments.

§ 6.2 Methods

Here I describe the model presented in Chapter 5 in more detail, and give more information about the coevolutionary method. The model is an extension of that from Chapter 2 to include a specific transmission process by considering host-parasite range (Best et al., 2010b, 2017b; Boots et al., 2014). I compare three different forms for the seasonal forcing in host birth rate, one of which is based on the maximum bacterial growth rates from the experiment in Chapter 5. In section 6.3, I explore how the sea-

sonal parameters affect the coevolutionary dynamics for each of the different types of seasonality.

6.2.1 Infection Model

To begin, I use the same SIS infection equations as in Chapter 2. To reiterate:

$$\frac{dS}{dt} = aS(1 - qN) - bS - \beta SI + \gamma I, \tag{6.1}$$

$$\frac{dI}{dt} = \beta SI - (\alpha + b + \gamma)I, \tag{6.2}$$

where S, I and N denote the susceptible, infected and total population sizes respectively. Since I am now using these equations to model specific species, I have to be careful about the underlying assumptions. In the experimental system, the hosts reproduce asexually (birth rate a; Koch, 2002), and since this is a lytic phage parasite I assume that once infected the hosts can no longer reproduce (Cairns et al., 2009; but see Ripp & Miller, 1997). The hosts are limited to a finite population size through competition for resources (Hui, 2006), which I implement in the birth term through a crowding coefficient q. The bacteria were transferred to fresh media before they reached the death phase of their growth (Monod, 1949), and so I assume that all hosts have a constant intrinsic death rate b (baseline mortality rate). In the model, susceptible hosts are infected with transmission coefficient β on contact with infected individuals using the mass action principle. In reality, the bacteria are infected by free-living phage particles. The model almost accounts for this discrepancy through the number of infected bacteria I, which is likely to be proportional to the number of free-living phage by way of the lytic phage bursting infected cells (but see Bull, 2006; Pagliarini & Korobeinikov, 2018 for models with free-living phage particles). This bursting process kills the infected host cells, and so I incorporate this in the model through an additional infected death rate α. I assume that the host can recover from the parasite and return to the susceptible class at rate γ, which is appropriate for the experimental system as there is evidence to suggest that bacteria can 'recover' from infection (Westra et al., 2012; Koskella & Brockhurst, 2014). I also consider the case with no recovery ($\gamma = 0$), finding the same qualitative results (Figure 6.10). Table 6.1 contains descriptions and default values used for all the parameters in the mathematical model, including those used in the trade-off functions described below.

Parameter	Definition	Default Value
a_0	Average birth rate	Varies
$\hat{a_0}$	Relative size of the average birth rate $a_0(u)$	22.7
p_u	Gradient of the average birth rate $a_0(u)$	5.7
c_u	Curvature of the average birth rate $a_0(u)$	-0.4
β	Transmission coefficient	Varies
κ	Steepness of transmission $\beta(u, v)$	2
β_0	Efficacy of transmission	Varies
$\hat{\beta}_0$	Relative size of the efficacy of transmission $\beta_0(v)$	261.4
p_v	Gradient of the efficacy of transmission $\beta_0(v)$	194
c_v	Curvature of the efficacy of transmission $\beta_0(v)$	0.5
$u_{\min}$	Minimum host defence	0
$u_{\max}$	Maximum host defence	10
$v_{\min}$	Minimum parasite infectivity	0
$v_{\max}$	Maximum parasite infectivity	10
u	Host defence	Varies
v	Parasite infectivity	Varies
δ	Amplitude of periodic forcing births(t)	Varies
ϵ	Period of periodic forcing births(t)	1
q	Crowding coefficient acting on births	0.1
b	Baseline mortality rate	1
γ	Recovery Rate	1
α	Virulence/additional death rate due to parasite	6

Table 6.1: Parameter definitions and default values for the coevolutionary model.

6.2.2 Seasonality

For this model, I focus on three different types of seasonality, namely a continuous sine function (Chapters 3 and 4, see also Ferris & Best, 2018), a discretized version of the sine function, and a periodic step function that imitates the bacterial growth rates in the oscillating resource concentrations (Figure 5.7; Ferris et al., in prep). In order to do this, I let the birth rate a depend on time through the function births(t):

$$a = a_0(1 + \text{births}(t)) \tag{6.3}$$

where a_0 is the 'average' birth rate, and births(t) is a periodic function of time. For the continuous sine function, as in Chapter 2, I use the following:

$$\text{births}(t) = \text{births}_{\text{cont}}(t) = \delta \sin(2\pi t/\epsilon) \tag{6.4}$$

where δ is the amplitude and ϵ the period of oscillations. I also consider a discontinuous version of this seasonality through a periodic step function. This is so that I can check the effect of including discontinuities in the seasonal forcing on the evolutionary outcomes. Hence I use the following:

$$\text{births}(t) = \text{births}_{\text{step}}(t) = \begin{cases} \delta & \text{if } n\epsilon \leq t < (n + \frac{1}{2})\epsilon\,, \\ -\delta & \text{otherwise,} \end{cases} \tag{6.5}$$

where n is a non-negative integer. Here the birth rate alternates between a positive maximum and negative minimum that depends on the amplitude δ, Figure 6.7(a), with the average birth rate constant for all δ and an equal amount of time ($\frac{\epsilon}{2}$) spent in each environment.

To imitate the bacterial growth rates in the different resource concentrations in the experiment, I chose to use a step function similar to that in equation (6.5) where the maximum and minimum birth rate functions were fitted to the maximum bacterial growth rate data from Figure 5.7. This was done by first plotting the maximum growth rates against amplitude (rather than resource concentration). I then assumed that the general form for the minimum birth rate was $\frac{x\delta}{1+y\delta} + 0.029$, and that the maximum was $m\delta + 0.029$, where 0.029 is the mean maximum growth rate over both bacteria genotypes in the constant environment (0.5KB concentration). These assumptions result in functions such that the maximum grows linearly with amplitude, while the minimum is non-linear and decreases more rapidly as the amplitude increases (i.e. less growth as the resource concentration decreases). The parameters x, y and m were found by minimising the sum of squares error with the maximum growth data for all three replicates of both the ancestral and phage-resistant bacteria. This was done by using the 'fminsearch' solver in MATLAB, with final error 0.0023 for both the minimum and maximum birth rate functions. If I assume that the maximum has the same form as the minimum (i.e. $\frac{x\delta}{1+y\delta} + 0.029$), the sum of squares error with the bacterial growth rate data is the same as for the linear function, hence I use the linear approximation for simplicity. The functions are plotted with the mean maximum growth rate data in Figure 5.7(b),(c). These functions were then scaled such that the maximum and minimum birth rates are zero in the constant environment ($\delta = 0$), and take significant values in the mathematical model. The periodic forcing births(t) is then given by the

following:

$$\text{births}(t) = \text{births}_{\text{exp}}(t) = \begin{cases} 0.3684\delta & \text{if } n\epsilon \leq t < (n+\frac{1}{2})\epsilon\,, \\ \frac{-0.0699\delta}{(1-0.9225\delta)} & \text{otherwise,} \end{cases} \tag{6.6}$$

where, again, n is a non-negative integer. The function $\text{births}_{\text{exp}}(t)$ is plotted in Figure 6.8(a), and an equal amount of time ($\frac{\epsilon}{2}$) spent in each environment.

6.2.3 Specific Infection and Trade-Offs

In contrast to the models in Chapter 3 and 4, I now define separate evolutionary parameters that do not immediately appear in the SIS equations above. Let u denote the level of host defence and v parasite infectivity such that $u \in [u_{\min}, u_{\max}]$ and $v \in [v_{\min}, v_{\max}]$ for some pre-defined limits (see Table 6.1). To include a specific infection process, I need to define the transmission coefficient β such that there is an almost "all-or-nothing" response where hosts (respectively parasites) can defend against (infect) only a certain range of parasite infectivities (host defences). Hence I use the following continuous function for transmission coefficient β (Best et al., 2010b; see also Nuismer et al., 2007; Boots et al., 2014; Best et al., 2017b):

$$\beta = \beta(u, v) = \beta_0(v)\left(1 - \frac{1}{1 + e^{-\kappa(u-v)}}\right), \tag{6.7}$$

where κ determines the level of specificity (i.e. the steepness of the curve), and $\beta_0(v)$ describes a trade-off between broadness of infection and efficacy of transmission for the parasite (see equation (6.8) below). Figure 6.1(a) shows how this $\beta(u, v)$ function varies with host defence u for two different parasite infectivity values v. For low u, transmission β is at its maximum and there is high transmission of the parasite. As defence increases, the host can defend itself against a wider range of parasites and so the transmission coefficient decreases, with gradient determined by the steepness κ (see Figure 6.1(b) for different κ values). Transmission rapidly decreases to zero once host defence is greater than parasite infectivity, so that for high u the host can defend against almost all parasites and there is little or no transmission ($\beta \approx 0$). For a parasite with high infectivity v (red line in Figure 6.1(a)), a broad range of hosts can be infected but with low efficacy due to the trade-off in $\beta_0(v)$. Meanwhile, a parasite with lower infectivity v (blue line in Figure 6.1(a)) can infect fewer hosts but with a much greater rate of success for those hosts. In particular, note that higher infectivity v does not

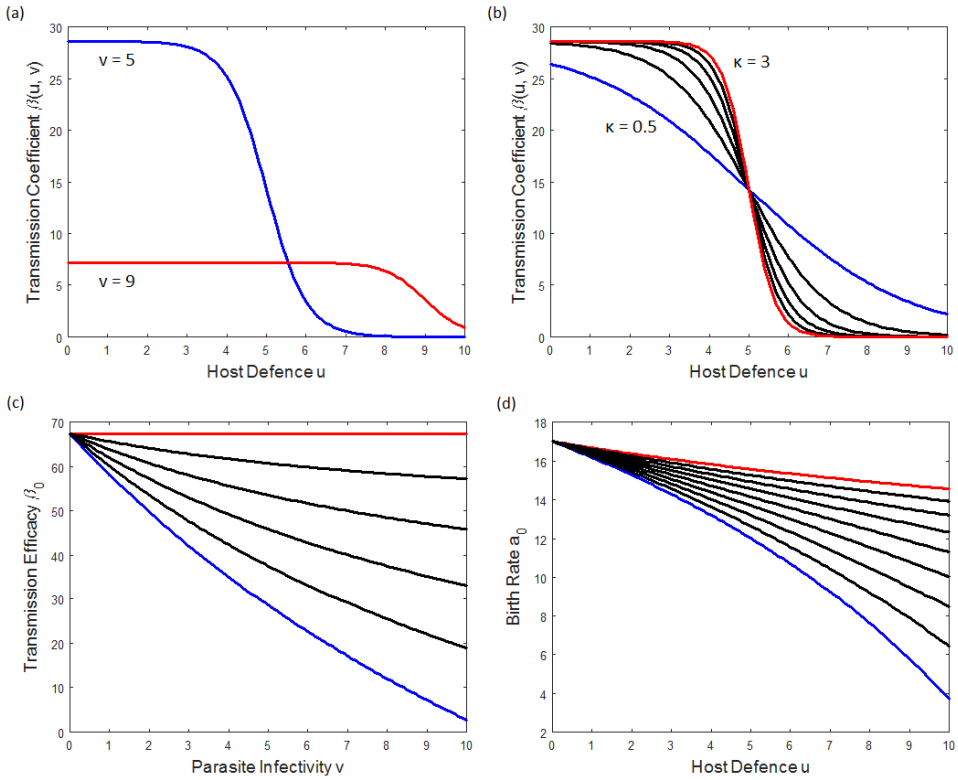

Figure 6.1: (a) Change in the transmission coefficient $\beta(u, v)$ as host defence u varies for parasite infectivity $v = 5$ (blue) and $v = 9$ (red). For higher v, the parasite can infect a wider range of hosts, but has a low efficacy as a result. Equally, a host with greater defence u can prevent infection by a wider range of parasites. (b) Change in transmission coefficient $\beta(u, v)$ as host defence u varies for parasite infectivity $v = 5$ and steepness κ varying between 0.5 (blue) and 3 (red) in steps of 0.5. The curve is steeper for higher κ, giving a more specific infection process. (c) Change in the efficacy of transmission $\beta_0(v)$ as parasite infectivity v varies for default parameter values with increasing c_v from 0.5 (blue) to 1 (red) in steps of size 0.1. (d) Change in the average birth rate $a_0(u)$ as host defence u varies for default parameter values with increasing c_u from -0.4 (blue) to 0.4 (red) in steps of size 0.1.

guarantee greater transmission depending on the level of host defence (e.g. compare the two values of v at $u = 4$ and $u = 8$).

As mentioned above, I assume that the parasite evolves infectivity v through the range of transmission, but I also include a cost in the efficacy of transmission $\beta_0(v)$. I use the

following equation to describe this:

$$\beta_0 = \beta_0(v) = \hat{\beta}_0 - p_{\mathrm{v}} \frac{1 + \frac{v - v_{\min}}{v_{\max} - v_{\min}}}{1 + c_{\mathrm{v}} \frac{v - v_{\min}}{v_{\max} - v_{\min}}}, \tag{6.8}$$

where p_{v}, c_{v} determine the gradient and curvature of $\beta_0(v)$ and $\hat{\beta}_0 - p_v$ is the minimum efficacy obtained. I choose parameters such that as the broadness of infection increases (v increases) the efficacy of transmission $\beta_0(v)$ decreases, as has been observed empirically (Thrall & Burdon, 2003; Poullain et al., 2008). Hence I need a negative gradient $\beta_0'(v) < 0$, which can be obtained by satisfying either $p_{\mathrm{v}} < 0$ and $c_{\mathrm{v}} > 1$, or $p_{\mathrm{v}} > 0$ and $-1 < c_{\mathrm{v}} < 1$. The parameter $\hat{\beta}_0$ is chosen such that $\beta_0(v) > 0$ for all v, i.e. $\hat{\beta}_0 > 2p_{\mathrm{v}}/(1 + c_{\mathrm{v}})$. Default parameters for this trade-off are given in Table 6.1, and this function is plotted against parasite infectivity v in Figure 6.1(c). Note that since the cost of increased transmission is through reduced range, there is no infectivity trade-off with virulence which has commonly been assumed elsewhere (Miller et al., 2006; Best et al., 2009, 2014; Svennungsen & Kisdi, 2009).

I assume that the host evolves defence u through lowered transmission coefficient β, however this comes at a cost to the average birth rate a_0 (equation (6.3)). Similarly to the models in Chapters 3 and 4, I use the following trade-off function to describe this cost:

$$a_0 = a_0(u) = \hat{a_0} - p_{\mathrm{u}} \frac{1 + \frac{u - u_{\min}}{u_{\max} - u_{\min}}}{1 + c_{\mathrm{u}} \frac{u - u_{\min}}{u_{\max} - u_{\min}}}, \tag{6.9}$$

where p_{u}, c_{u} determine the gradient and curvature of $a_0(u)$ and $\hat{a_0} - p_u$ is the minimum average birth rate. I choose trade-off parameter values such that as host defence u increases, the average birth rate decreases, giving a negative gradient $a_0'(u) < 0$. For this to hold, I need to satisfy either $p_{\mathrm{u}} < 0$ and $c_{\mathrm{u}} > 1$, or $p_{\mathrm{u}} > 0$ and $-1 < c_{\mathrm{u}} < 1$. The parameter $\hat{a_0}$ is chosen such that $a_0(u) > 0$ for all values of u, giving $\hat{a_0} > 2p_{\mathrm{u}}/(1 + c_{\mathrm{u}})$. Again, default parameters for this trade-off are given in Table 6.1, and this function is plotted against host defence u in Figure 6.1(d).

6.2.4 Coevolutionary Adaptive Dynamics

Here I provide details about how adaptive dynamics is used to study coevolution. In addition to the general assumptions for single-species evolution (Chapter 2; Geritz et al., 1998), I also assume that the host and parasite mutation speeds are equal. This assumption simplifies the coevolutionary dynamics, although the effect of different

mutation rates has been explored elsewhere (Dieckmann & Law, 1996; Haraguchi & Sasaki, 1996; Marrow et al., 1996; Nuismer et al., 2005; Best et al., 2009, 2010b).

6.2.4.1 Fitness

As for single-species evolution, I need to find the fitness for the host and the parasite to determine the direction of evolution. The host fitness is calculated in the same way as explained in Chapter 2. For no seasonality ($\delta = 0$), I use the negative determinant of the Jacobian to find:

$$r_{\mathrm{H}} = (\alpha + b + \gamma)\left[a_0(u_{\mathrm{m}})(1 - qN^*) - b\right] - (\alpha + b)\beta(u_{\mathrm{m}}, v)I^*, \tag{6.10}$$

where I^*, N^* denote the equilibrium infected and total population sizes respectively. This fitness is discussed in more detail in section 6.2.4.4. When seasonality is present ($0 < \delta \leq 1$), the form of the general solution to the mutant equations is different due to time-dependent coefficients, and so I use numerical Lyapunov exponents as the host fitness (Chapter 2; Metz et al., 1992; Klausmeier, 2008).

For the parasite fitness, I use the averaging method from Donnelly et al. (2013) which finds a fitness that is valid for all values of the amplitude δ. To start, I introduce a mutant parasite with infectivity v_{m}:

$$\frac{dI_{\mathrm{m}}}{dt} = \beta(u, v_{\mathrm{m}})S^*I_{\mathrm{m}} - (\alpha + b + \gamma)I_{\mathrm{m}}\,, \tag{6.11}$$

where $S^* = S^*(t)$ is the limit cycle of the susceptible resident host. I can then find the parasite fitness r_{P} as the average growth of the mutant parasite over one period:

$$r_{\mathrm{P}} = \frac{1}{T}\int_{P_0}^{P_1} \frac{1}{I_{\mathrm{m}}}\frac{dI_{\mathrm{m}}}{dt}dt \tag{6.12}$$

$$= \frac{1}{T}\int_{P_0}^{P_1} \left[\beta(u, v_{\mathrm{m}})S^*(t) - (\alpha + b + \gamma)\right]dt \tag{6.13}$$

$$= \beta(u, v_{\mathrm{m}})\hat{S} - (\alpha + b + \gamma)\,, \tag{6.14}$$

where $\hat{S} = \frac{1}{T}\int_{P_0}^{P_1} S^*(t)dt$ is the average susceptible resident population, P_0 is some arbitrarily chosen time, $P_1 = P_0 + T$ and T is some multiple of the period of the equilibrium dynamics (usually $T = \epsilon$). As shown in Chapter 2, I can calculate $\hat{S}$ by

integrating the equilibrium infected host equation over one period:

$$\frac{1}{T}\int_{P_0}^{P_1}\frac{1}{I}\frac{dI}{dt}dt = [ln(I)]_{t=P_0}^{t=P_1} = 0 \tag{6.15}$$

$$= \frac{1}{T}\int_{P_0}^{P_1}\beta S - (\alpha + b + \gamma)dt = \beta\hat{S} - (\alpha + b + \gamma) \tag{6.16}$$

giving $\hat{S} = (\alpha + b + \gamma)/\beta$. Now, substituting this into equation (6.12), I have the parasite fitness r_{P} for $\delta \in [0, 1]$:

$$r_{\mathrm{P}} = (\alpha + b + \gamma)\left(\frac{\beta(u, v_{\mathrm{m}})}{\beta(u, v)} - 1\right). \tag{6.17}$$

6.2.4.2 Singular Points

In a coevolutionary context, a singular point (u^*, v^*) is defined as the point at which both the host and parasite fitness gradients with respect to a rare mutant are zero:

$$\left.\frac{\partial r_{\mathrm{H}}}{\partial u_{\mathrm{m}}}\right]_{u=u_{\mathrm{m}}=u^*} = 0 \tag{6.18}$$

$$\left.\frac{\partial r_{\mathrm{P}}}{\partial v_{\mathrm{m}}}\right]_{v=v_{\mathrm{m}}=v^*} = 0 \tag{6.19}$$

where r_{H} = host fitness, r_{P} = parasite fitness, u_{m} = mutant host defence and v_{m} = mutant parasite infectivity (Geritz et al., 1998; Best et al., 2010b). I find the host fitness gradient numerically as described in Chapter 2, whereas I can find the parasite fitness gradient analytically for all δ:

$$\left.\frac{\partial r_{\mathrm{P}}}{\partial v_{\mathrm{m}}}\right|_{v=v_{\mathrm{m}}=v^*} = \left[\frac{(\alpha + b + \gamma)}{\beta(u, v)}\frac{\partial\beta(u, v_{\mathrm{m}})}{\partial v_{\mathrm{m}}}\right]_{v=v_{\mathrm{m}}=v^*} \tag{6.20}$$

$$= (\alpha + b + \gamma)\left[\frac{1}{\beta_0}\frac{\partial\beta_0}{\partial v} - \frac{1}{(1 - F)}\frac{\partial F}{\partial v}\right]_{v=v^*}, \tag{6.21}$$

where I have simplified the expression using $\beta(u, v) = \beta_0(v)(1 - F)$ for:

$$F = F(u, v) = \frac{1}{1 + e^{-\kappa(u-v)}}. \tag{6.22}$$

For any value of the amplitude δ, the numerical program I use to find the singular point (u^*, v^*) is slightly altered for coevolution, as I have to find not one but two values. The

fact that the parasite fitness is analytic for all δ greatly simplifies this issue, and so I use the following numerical scheme:

1. Pick a value of u and find its associated v^* using the analytic parasite fitness gradient in equation (6.20).
2. Using this value of v^*, find the host fitness gradient for the chosen u numerically (see Chapter 2).
3. Repeat for multiple values of u until the host fitness gradient changes sign. This gives the singular point (u^*, v^*).

6.2.4.3 Types of Singular Points

In this chapter I primarily consider singular points that are end-points of coevolution, i.e. the combinations of strategies at which the populations no longer evolve and continue to have those strategies for all time. These singular points are called CoESSs, which are similar to CSSs in single species evolution (see Chapter 2). This type of point occurs when evolutionary stability (ES, no local mutant can invade the current population) and convergence stability (CS, evolution towards the singular point) are satisfied for both the host and the parasite (Geritz et al., 1998). Coevolutionary singular points that do not satisfy these criteria do exist for this model (e.g. branching points, see Best et al., 2010b), but I do not focus on these outcomes in this work.

The singular point is evolutionarily stable when the following conditions are satisfied (Gertiz et al., 1998; Best et al., 2010b):

$$E_{\mathrm{H}} = \left.\frac{\partial^2 r_{\mathrm{H}}}{\partial u_{\mathrm{m}}^2}\right|_{u=u_{\mathrm{m}}=u^*} < 0, \tag{6.23}$$

$$E_{\mathrm{P}} = \left.\frac{\partial^2 r_{\mathrm{P}}}{\partial v_{\mathrm{m}}^2}\right|_{v=v_{\mathrm{m}}=v^*} < 0. \tag{6.24}$$

For the host, E_{H} can be calculated numerically when $\delta > 0$, as described in Chapter 2. In a constant environment ($\delta = 0$), E_{H} can be found analytically (section 6.2.4.4), the sign of which is plotted in Figure 6.2(a) for varying host defence u and parasite infectivity v. This shows where the host singular point is evolutionarily stable for $\delta = 0$, i.e. where $E_{\mathrm{H}} < 0$ (blue regions). These regions may change for $\delta > 0$.

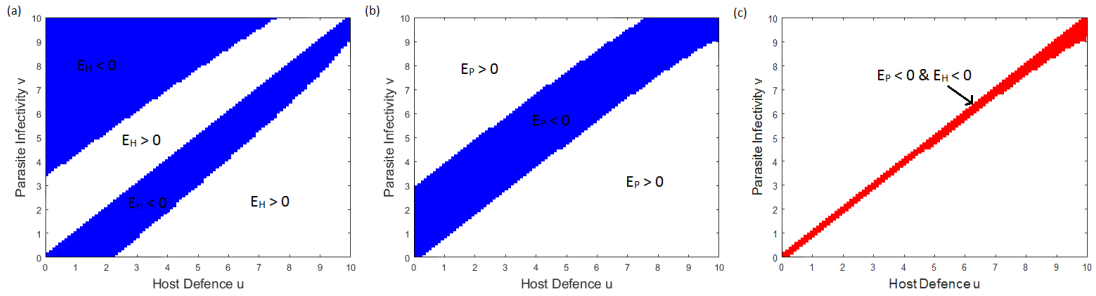

Figure 6.2: Sign of (a) E_{H} and (b) E_{P} as host defence u and parasite infectivity v vary for default parameters. Blue: $E_{\mathrm{H}}, E_{\mathrm{P}} < 0$, so host/parasite evolutionary stability is satisfied. White: $E_{\mathrm{H}}, E_{\mathrm{P}} > 0$, so host/parasite evolutionary stability is not satisfied. The region in (b) holds for all values of $\delta \in [0, 1]$, while that in (a) is only true for $\delta = 0$. (c) Overlap of the blue regions shown in (a) and (b), where red indicates the area such that both $E_{\mathrm{H}} < 0$ and $E_{\mathrm{P}} < 0$, i.e. where the singular point (u^*, v^*) is evolutionarily stable at $\delta = 0$. White areas show where at least one of the stability conditions is not satisfied, i.e. $E_{\mathrm{H}} > 0$ or $E_{\mathrm{P}} > 0$.

For the parasite, the derivative E_{P} becomes:

$$E_{\mathrm{P}} = \left.\frac{\partial^2 r_{\mathrm{P}}}{\partial v_{\mathrm{m}}^2}\right|_{v=v_{\mathrm{m}}=v^*} \tag{6.25}$$

$$= (\alpha + b + \gamma)\left[\frac{1}{\beta_0}\frac{\partial^2 \beta_0}{\partial v^2} - \frac{2}{\beta_0(1-F)}\frac{\partial F}{\partial v}\frac{\partial \beta_0}{\partial v} - \frac{1}{(1-F)}\frac{\partial^2 F}{\partial v^2}\right]_{v=v^*}. \tag{6.26}$$

While the middle term is always negative, the sign of the first term ($\frac{\partial^2 \beta_0}{\partial v^2}$) depends on the choice of trade-off parameters, and the third term ($\frac{\partial^2 F}{\partial v^2}$) depends on the singular point (u^*, v^*). Figure 6.2(b) shows where the evolutionary stability condition is satisfied for varying defence u and parasite v with default parameters. For all amplitudes δ, singular points inside the blue region satisfy $E_{\mathrm{P}} < 0$ and the parasite trait is evolutionarily stable.

When there is no seasonality ($\delta = 0$), the singular point (u^*, v^*) must be within the red region in Figure 6.2(c) for both host and parasite evolutionary stability to hold.

The conditions for convergence stability are more complicated. When I assume that the species mutate at the same rate, the eigenvalues of the following Jacobian matrix determine whether or not the singular point is convergence stable (Kisdi, 2006; Best et

al., 2010b):

$$\begin{bmatrix} S^*(E_{\mathrm{H}}+M_{\mathrm{H}}) & S^*A_{\mathrm{H}} \\ I^*A_{\mathrm{P}} & I^*(E_{\mathrm{P}}+M_{\mathrm{P}}) \end{bmatrix} = \begin{bmatrix} S^*\left(\frac{\partial^2 r_{\mathrm{H}}}{\partial u_{\mathrm{m}}^2}+\frac{\partial^2 r_{\mathrm{H}}}{\partial u_{\mathrm{m}}\partial u}\right) & S^*\frac{\partial^2 r_{\mathrm{H}}}{\partial u_{\mathrm{m}}\partial v} \\ I^*\frac{\partial^2 r_{\mathrm{P}}}{\partial v_{\mathrm{m}}\partial u} & I^*\left(\frac{\partial^2 r_{\mathrm{P}}}{\partial v_{\mathrm{m}}^2}+\frac{\partial^2 r_{\mathrm{P}}}{\partial v_{\mathrm{m}}\partial v}\right) \end{bmatrix}. \tag{6.27}$$

Due to the complexity of this condition, I used stochastic evolutionary simulations to check for convergence stability for all values of δ, including when there is no seasonality. These simulations were performed as in Chapter 2 with adjustments to incorporate coevolution:

1. Start with an initial population with traits (u_0, v_0) and run the population to equilibrium.
2. Add a rare host or parasite mutant (probability $\frac{1}{2}$ each for the first mutant) with small population size and trait close to u_0 or v_0 (probability $\frac{1}{2}$ above or below).
3. The dynamics of the whole population (initial and mutant) are run for a fixed length of time.
4. At the end of this run, if one or more of the populations is smaller than a fixed threshold, the population is removed.
5. A mutant from the other species is added, again with small population size and trait close to u_0 or v_0.
6. Steps 3 - 5 are repeated many times, alternating adding host and parasite mutants, where the traits of new mutants depend on the current population traits and their relative densities (if more than one strain persists).
7. The traits (u, v) are plotted through time, with shading showing the relative density of the population with each strain.

Examples of coevolutionary simulation outputs can be found in Figure 6.5 for default parameters with the continuous seasonal forcing.

6.2.4.4 Example: Coevolutionary Dynamics With No Seasonality

When there is no seasonality ($\delta = 0$) I can find the host fitness analytically, and therefore the derivatives needed for the coevolutionary dynamics above. To find the

host fitness, I use the negative determinant of the Jacobian of the simplified mutant equations (Chapter 2; Hoyle et al., 2012) to obtain:

$$r_{\mathrm{H}} = (\alpha + b + \gamma)\left[a_0(u_{\mathrm{m}})(1 - qN^*) - b\right] - (\alpha + b)\beta(u_{\mathrm{m}}, v)I^*, \tag{6.28}$$

where I^*, N^* denote the equilibrium infected and total population sizes respectively (see also equation (6.10)). This then gives the host fitness gradient:

$$\left.\frac{\partial r_{\mathrm{H}}}{\partial u_{\mathrm{m}}}\right|_{u=u_{\mathrm{m}}=u^*} = \left[(\alpha + b + \gamma)(1 - qN^*)\frac{da_0(u_{\mathrm{m}})}{du_{\mathrm{m}}} - (\alpha + b)I^*\frac{\partial\beta(u_{\mathrm{m}}, v)}{\partial u_{\mathrm{m}}}\right]_{u=u_{\mathrm{m}}=u^*} \tag{6.29}$$

$$= \left[(\alpha + b + \gamma)(1 - qN^*)\frac{da_0}{du} + (\alpha + b)I^*\beta_0(v)\frac{\partial F}{\partial u}\right]_{u=u^*}, \tag{6.30}$$

where I have simplified the expression for $\beta(u, v)$ using $F(u, v)$ as defined in equation (6.22). To determine if the host singular point u^* is evolutionarily stable, I need to find the sign of:

$$\left.\frac{\partial^2 r_{\mathrm{H}}}{\partial u_{\mathrm{m}}^2}\right|_{u=u_{\mathrm{m}}=u^*} = \left[(\alpha + b + \gamma)(1 - qN^*)\frac{\partial^2 a_0}{\partial u^2} + (\alpha + b)I^*\beta_0(v)\frac{\partial^2 F}{\partial u}\right]_{u=u^*} \tag{6.31}$$

For this to be negative, and therefore the host singular point to be ES, I need $\frac{\partial^2 a_0}{\partial u^2} < 0$ and/or $(2e^{-2(u-v)}F - 1) < 0$ for $u = u^*$ since the rest of the terms are positive. Given that default $p_{\mathrm{u}} > 0$, the first condition holds for all u when $-1 < c_u < 0$. For the second condition I need $e^{-2(u^*-v)} < 1$, i.e. $u^* > v$. Therefore I chose default c_{u} to satisfy the first condition, and $u^* > v^*$ at $\delta = 0$ to satisfy the second. The regions where $E_{\mathrm{H}} < 0$ is satisfied for varying u and v is plotted for default values and $\delta = 0$ in Figure 6.2(a), showing that we either need $u > v$ or $v \gg u$ for the host strategy to be evolutionarily stable. Note that I can find $u^* < v^*$ such that the singular point remains ES, for example for increased crowding coefficient q (Figure 6.12), although the traits have to be very close to each other to satisfy both ES conditions. This is shown in Figure 6.2(c) for $\delta = 0$, where the traits have to be within the red region to satisfy both $E_{\mathrm{P}} < 0$ and $E_{\mathrm{H}} < 0$, i.e. for the singular strategy to be evolutionary stable in both traits.

I used the stability conditions to find an initial singular point at $\delta = 0$ that was both ES (Figure 6.2) and CS (simulations). From there I explored how seasonality affected this singular point using the numerical methods detailed above, with simulations to confirm that the singular point remained a CoESS for all amplitudes. In some cases,

the singular point changed type as the amplitude increased, for example Figure 6.6, but this was not explored further as it was not relevent to the experimental study in Chapter 5.

§ 6.3 Results

Here I use the methodology above to investigate how changing the amplitude of oscillations alters host-parasite coevolution for the three types of seasonality defined in equations (6.4) - (6.6). I focus on singular points that are evolutionarily and convergence stable, which are end points of evolution (CoESSs). I compare the different types of seasonality with results from the experiment in Chapter 5, where I found maximal investment in host defence and parasite infectivity for intermediate amplitude oscillations.

6.3.1 Sinusoidal Seasonality

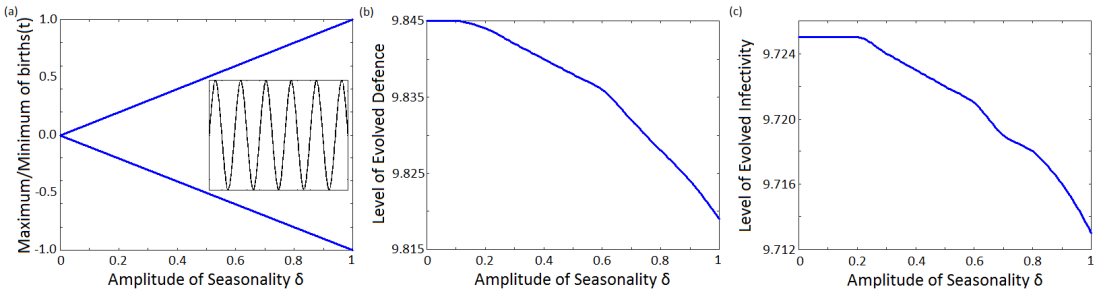

Figure 6.3: (a) Change in the minimum/maximum of $\text{births}_{\text{cont}}(t) = \delta \sin(2\pi t/\epsilon)$ (equation (6.4)) as the amplitude δ varies. Maximum $= \delta$; Minimum $= -\delta$. Insert: sine function seasonality with symmetric maxima and minima. (b) Evolved host defence u^* and (c) evolved parasite infectivity v^* as amplitude δ increases.

First, let us consider the continuous sinusoidal seasonality case $\text{births}_{\text{cont}}(t)$, i.e. the seasonality function used in Chapters 3 and 4. Figure 6.3 shows that for this seasonality, the host and parasite evolve monotonically decreasing defence and infectivity as the amplitude δ increases. This is not what I found in the experiment, but it is what I expected given results from my host-only evolution model with this type of seasonality and positive recovery (Chapter 3). The parasite infectivity trend is predictable from the host behaviour: as the amplitude increases, the host invests less in defence and so the parasite can afford to invest less in the broadness of infection. Overall, the transmission

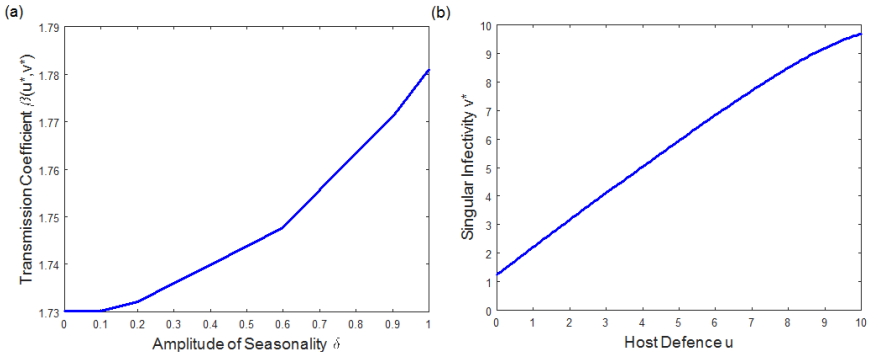

Figure 6.4: (a) Change in the transmission coefficient evaluated at the singular point $\beta(u^*, v^*)$ as the amplitude of seasonality δ increases for the sinusoidal forcing $\text{births}_{\text{cont}}(t)$. (b) Change in the infectivity singular point v^* as host defence u varies. This holds for all forms of births(t) and all values of the seasonal parameters δ and ϵ.

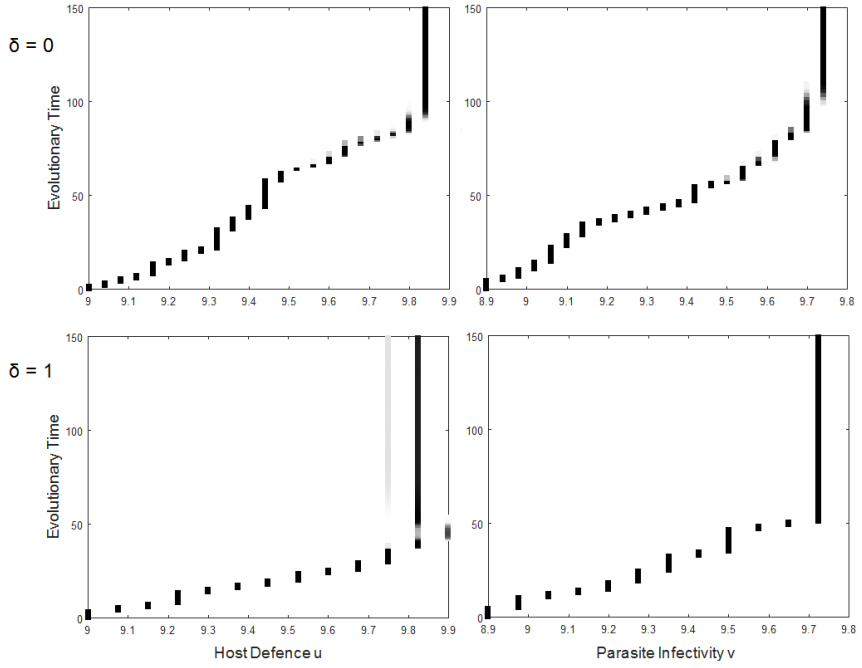

Figure 6.5: Examples of stochastic simulations used to confirm that the singular point is ES and CS for multiple values of the amplitude δ. Darker shading indicates a higher proportion of the population with defence u or infectivity v, and the initial population had trait values $(u_0, v_0) = (9, 8.9)$. Left column: Evolution of host defence u through time. Right column: Evolution of parasite infectivity v through time. Top row: No seasonality ($\delta = 0$). Bottom row: Maximum amplitude in the seasonality ($\delta = 1$).

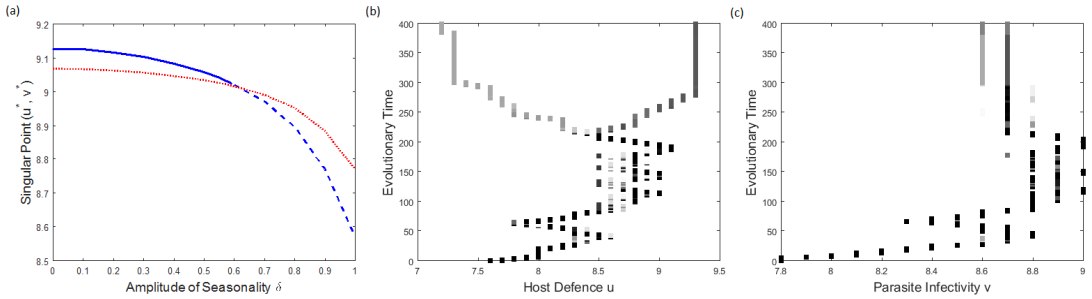

Figure 6.6: (a) Change in host defence u^* (blue) and parasite infectivity v^* (red dotted) as amplitude δ increases, showing where the host ES condition does (solid line) and does not (dashed line) hold. (b),(c) Stochastic simulations for amplitude $\delta = 1$ for (b) host defence u and (c) parasite infectivity v. Darker shading indicates a higher proportion of the population with defence u or infectivity v, and the initial population had trait values $(u_0, v_0) = (7.6, 7.8)$. Parameter values were taken to be $\hat{\beta}_0 = 86.9$, $p_v = 39.1$, $c_v = -0.1$, $\hat{a_0} = 72.2$, $p_u = 21$, but otherwise default values were used.

coefficient at the singular point increases with the amplitude (Figure 6.4(a)), since the parasite is able to invest more in transmission efficacy as defence decreases (Figure 6.4(b)). As discussed in section 6.2.4.3 above, I used numerical simulations to confirm that the singular point remained ES and CS as δ increased. Examples can be found in Figure 6.5 for the default parameter values and different amplitudes, showing that the host and parasite evolve towards the singular point (u^*, v^*) and stay there for all time.

It should be noted that the overall change in (u^*, v^*) over the range of δ values is not very large for default parameter values (~ 0.03 in Figure 6.3). This is largely due to the use of range transmission rather than universal transmission (Chapter 3), since small decreases in host defence may lead to relatively large increases in transmission when u and v are similar (Figure 6.1(a)). Hence there is increasing selection for host defence, which leads to a smaller selection gradient and lower overall changes in u^* when compared to host-only evolution. Different trade-off parameter sets can lead to larger changes in the singular point, however the host ES condition is often lost at high amplitudes, leading to branching in the host trait. This occurs for all three types of seasonality considered. An example is shown in Figure 6.6 for the sinusoidal seasonality, where the change in u^* from $\delta = 0$ to 1 is approximately 0.6 (compared to ~ 0.03 for the default parameters in Figure 6.3). At $\delta = 0.6$ in Figure 6.6, the host ES condition no longer holds and branching occurs in the host trait, as shown by simulations for $\delta = 1$ in Figure 6.6(b),(c). This change in behaviour could be due to the lack of direct dependence of the parasite infectivity on the seasonal amplitude,

meaning that v^* changes less than u^* over the range of δ values. This often leads to $v^* > u^*$ at high amplitudes, which I showed in Figure 6.2 is unlikely to satisfy the host ES condition. Hence the predominant cases where the singular point is a CoESS for all δ is for $u^* > v^*$ at $\delta = 0$, which results in smaller changes in the singular point over the range of δ values (e.g. Figure 6.3).

6.3.2 Stepping Seasonality

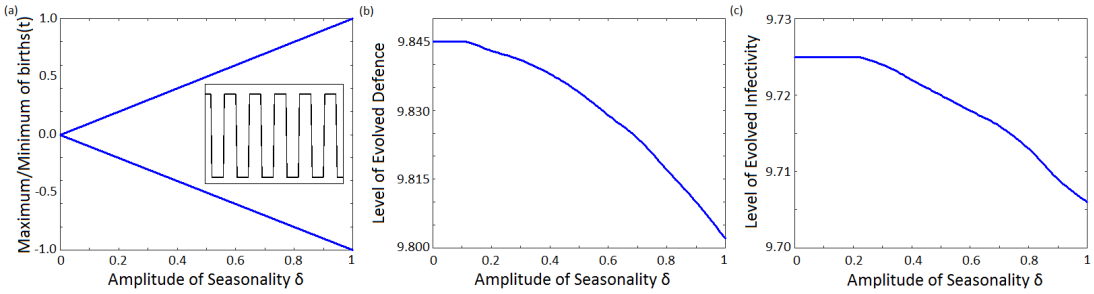

Figure 6.7: (a) Change in the minimum/maximum of the discontinuous stepping seasonality $\text{births}_{\text{step}}(t)$ (equation (6.5)) as the amplitude δ varies. Maximum $= \delta$; Minimum $= -\delta$. Insert: step function between minimum and maximum, with an equal amount of time spent in each environment. (b) Evolved host defence u^* and (c) evolved parasite infectivity v^* as amplitude δ increases.

Next, I consider a discontinuous version of the sinusoidal seasonality, i.e. a step function where the maxima and minima are linear with opposite gradients ($\pm\delta$; Figure 6.7(a)). For this seasonality I find that, similarly to the sinusoidal forcing above, both the host defence and parasite infectivity decrease as amplitude increases. I also found that transmission at the singular point changes with amplitude in a similar way to the sinusoidal seasonality above, Figure 6.4(a), where transmission is lowest in a constant environment when host defence and parasite infectivity are high. The defence and infectivity outcomes confirm that the experimental results are not due to discontinuous changes in environment, so I move on to the third, evidence-based, forcing.

From the growth data in Chapter 5, I know that the bacteria grow faster in media with higher resource concentrations, but importantly that this relationship is not linear. In particular Figure 5.7 shows that, for low resource concentrations, the growth rate decreases more rapidly as the concentration decreases. Hence I use the seasonality function defined in equation (6.6) (Figure 6.8(a)), which is an approximation of this non-linearity as amplitude δ increases (resource concentration increases in maximum

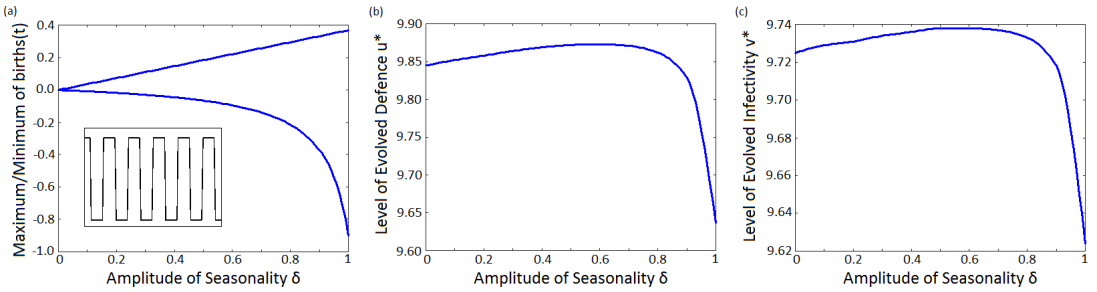

Figure 6.8: (a) Change in the minimum/maximum of $\text{births}_{\text{exp}}(t)$ from equation (6.6) as the amplitude δ varies. Maximum $= 0.3684\delta$; Minimum $= -0.0699\delta/(1 - 0.9225\delta)$. Insert: step function between minimum and maximum, with an equal amount of time spent in each environment. (b) Evolved host defence u^* and (c) evolved parasite infectivity v^* as amplitude δ increases.

environment but decreases in minimum environment).

As shown in Chapter 5, I find that as the amplitude δ increases, the host evolves resistance non-monotonically, with highest defence evolving for intermediate amplitudes, Figure 6.8(b), matching the empirical results. For low amplitudes, the average birth rate increases with amplitude, which in turn increases the infected population size (Figure 2.2). Therefore the host increases defence due to this selection pressure, but also because the periodically low environment isn't too costly (Figure 6.8(a)) and so the host can afford higher resistance. However, once the amplitude reaches a certain point, the low environment becomes increasingly costly and the average birth rate starts to decrease. This decreases the infected population size, and thus lowers selection for defence, which is boosted by greater selection for increased birth rate. Therefore the host decreases defence for large amplitudes. The parasite's evolution only depends on seasonality through the host's defence u, and so the parasite evolves similarly to the host with highest infectivity evolving for intermediate amplitudes, again predicting the empirical results from Chapter 5. Given the evolutionary results when seasonality changes symmetrically with amplitude (section 6.3.1), it is clear that using the empirical data for host birth rates is the key difference that enables us to recover the non-linear evolutionary behaviour observed in the bacteria-phage experiment in Chapter 5.

The combination of these evolutionary changes leads to the transmission coefficient $\beta(u^*, v^*)$ also varying with amplitude δ, Figure 6.9. Transmission is smallest for intermediate amplitudes where the host defence and parasite infectivity are highest (low transmission and small transmission efficacy). This and the result for symmetric seasonality suggests that, generally, transmission is largest in environments where evolved

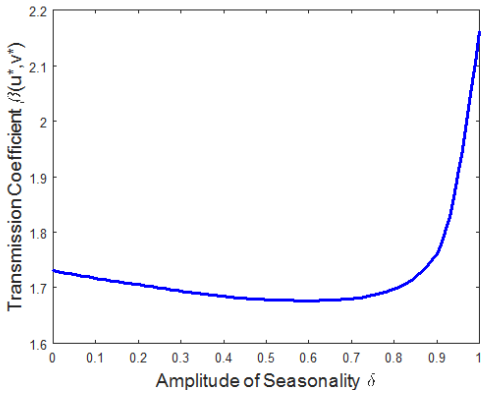

Figure 6.9: Change in the transmission coefficient evaluated at the singular point $\beta(u^*, v^*)$ as the amplitude of seasonality δ increases for the experimentally based forcing $\text{births}_{\text{exp}}(t)$.

defence/infectivity is highest.

Similar to the sinusoidal seasonality above, the overall change in defence and infectivity is larger when I use different trade-off parameters or lower specificity of the infection process. However, very often either the host ES condition is lost at high amplitudes (e.g. Figure 6.6 for sinusoidal seasonality, discussed above), or the non-monotonic evolutionary behaviour changes, with very low steepness κ giving maximum defence/infectivity at very low amplitudes (Figure 6.14; discussed in section 6.3.3). These parameter sets no longer recover the evolutionary results from Chapter 5, with the effect of lowered steepness κ suggesting that weak specificity in the infection process cannot predict the experimental evolutionary results.

6.3.3 Exploration of the Parameter Space

The results I presented in sections 6.3.1 and 6.3.2 are for a default parameter set defined in Table 6.1, so it is important to check that these results are robust for alternative parameter values. Figures 6.10-6.13 show how the singular point (u^*, v^*) changes as both the amplitude δ and other parameters in the model are varied, with the latter taking values on both sides of the default parameter set. I consider the sinusoidal and evidence-based seasonality functions, as the symmetric discontinuous seasonality gives similar results to the sinusoidal function. All singular points considered are CoESSs, i.e. final end-points of coevolution.

Overall, I found that the qualitative behaviour of the singular point with amplitude

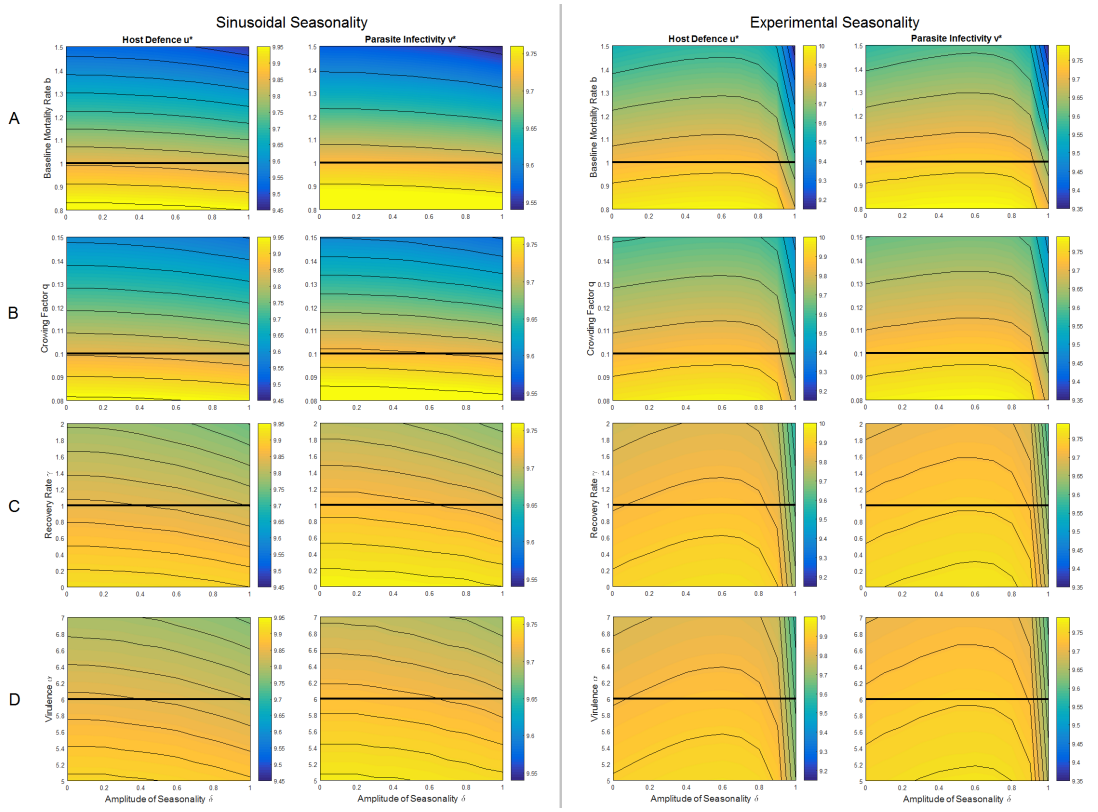

Figure 6.10: Contour plots showing host defence u^* and parasite infectivity v^* as the amplitude of seasonality δ and other parameters vary. A: Baseline mortality rate b; B: Crowding Factor q; C: Recovery rate γ; D: Virulence α. Left column: Sinusoidal seasonality $\text{births}_{\text{cont}}(t)$; Right column: Experimental seasonality $\text{births}_{\text{exp}}(t)$. Default parameters from Table 6.1 are marked with thick black lines.

δ remains the same for the range of parameters considered in Figures 6.10-6.13. This suggests that the results presented in sections 6.3.1 and 6.3.2 are robust, i.e. that symmetric seasonality leads to monotonic decreasing investment in defence/infectivity as the amplitude increases, while the experimentally based seasonality leads to maximum defence/infectivity at intermediate amplitudes.

Figures 6.10-6.13 can also be used to determine which conditions can lead to increased or decreased levels of resistance and infectivity. These changes in evolutionary endpoint are due to how the parameters affect the underlying population dynamics: for parameters that increase the size of the infected population (increases in $\hat{a_0}$ and c_u in Figure 6.11, $\hat{\beta_0}$ and c_v in Figure 6.12), the host invests more in defence to combat the greater risk of infection. Similiarly, parameters that decrease the infected population

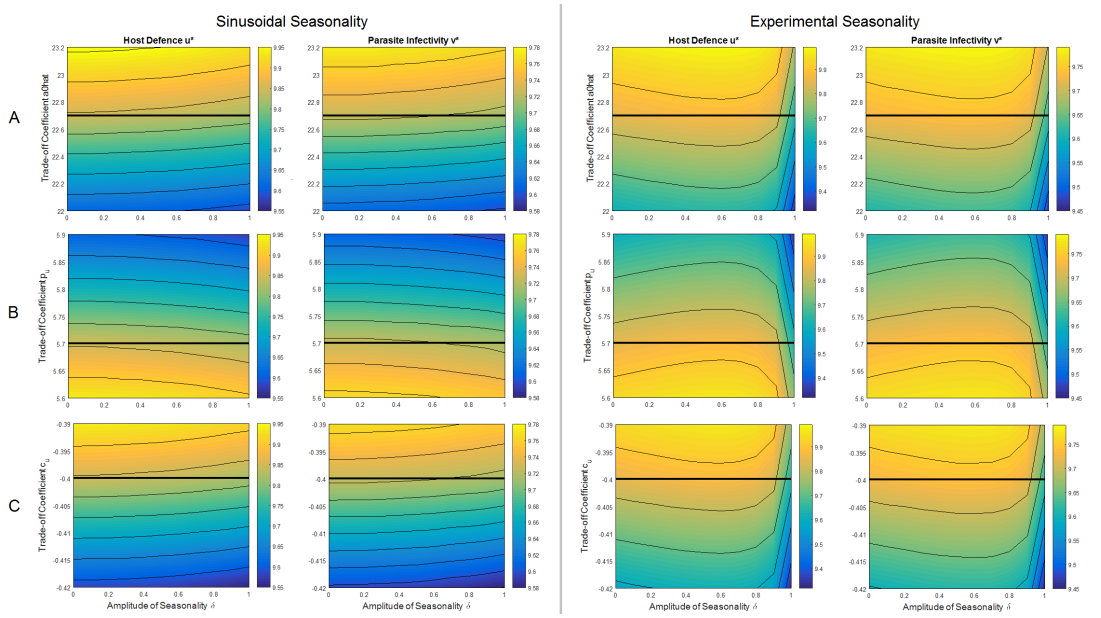

Figure 6.11: Contour plots showing host defence u^* and parasite infectivity v^* as the amplitude of seasonality δ and trade-off parameters in the average birth rate $a_0(u)$ vary. A: Relative size of the average birth rate $\hat{a_0}$; B: Gradient of the average birth rate p_u; C: Curvature of the average birth rate c_u. Left column: Sinusoidal seasonality $\text{births}_{\text{cont}}(t)$; Right column: Experimental seasonality $\text{births}_{\text{exp}}(t)$. Default parameters from Table 6.1 are marked with thick black lines.

size (increases in b, q, γ and α in Figure 6.10, p_u in Figure 6.11, p_v in Figure 6.12) mean that the host can afford to invest less in defence, and so u^* decreases. The parasite's evolution mirrors that of the host, with infectivity increasing with host defence.

Changing the model parameters can lead to different sensitivities of the evolved traits (u^*, v^*) to changes in the amplitude δ. Specifically, we can use Figures 6.10-6.13 to determine the conditions under which alterations to the seasonality will lead to larger changes in evolutionary outcome. For example, increased b, q, γ and α (Figure 6.10) lead to larger changes in (u^*, v^*) over the range of δ values. Additionally, increased efficacy of transmission (larger $\hat{\beta}_0$ and c_v, smaller p_v in Figure 6.12), decreased average birth rate (smaller $\hat{a_0}$ and c_u, larger p_u in Figure 6.11) and lower steepness κ (Figure 6.13) give greater changes in (u^*, v^*) over the range of values of δ. Overall, the sensitivity of the evolutionary outcome to changes in amplitude can be determined by how the size of the infected population is affected. Specifically, changes in parameters that lower the average infected population size lead to greater sensitivity in the evolutionary results to alterations in the seasonal amplitude. This is because selection for defence

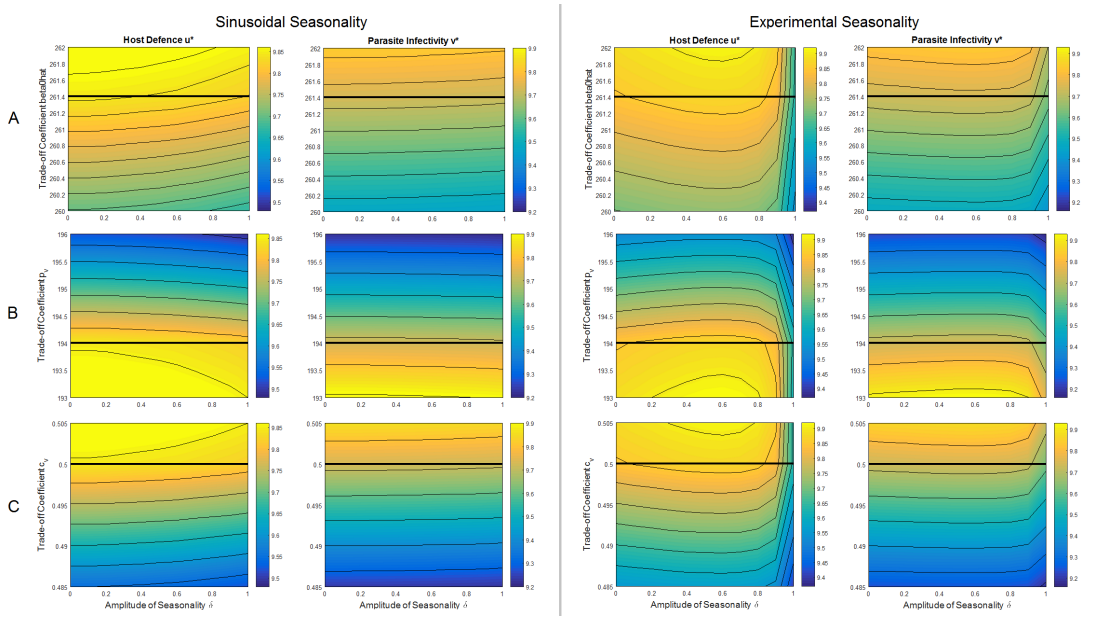

Figure 6.12: Contour plots showing host defence u^* and parasite infectivity v^* as the amplitude of seasonality δ and trade-off parameters in the efficacy of transmission $\beta_0(v)$ vary. A: Relative size of the efficacy of transmission $\hat{\beta}_0$; B: Gradient of the efficacy of transmission p_v; C: Curvature of the efficacy of transmission c_v. Left column: Sinusoidal seasonality $\text{births}_{\text{cont}}(t)$; Right column: Experimental seasonality $\text{births}_{\text{exp}}(t)$. Default parameters from Table 6.1 are marked with thick black lines.

is lower, which promotes investment in birth rate and thus amplifies the effect of the seasonal amplitude, giving greater evolutionary sensitivity to changes in δ. Hence the sensitivity of the evolutionary outcome to changes in the amplitude is due to how the periodic forcing affects the underlying dynamics, and so eco-evolutionary feedbacks are important when determining the sensitivity of evolutionary outcomes to changes in the seasonal amplitude.

We can also determine if constant or highly varying environments lead to larger/smaller changes in evolutionary outcomes as other parameters vary. I found that, for the majority of parameters, (u^*, v^*) varies the most in high amplitude environments when other parameters are altered. The exception to this rule occurs for the parameters in the efficacy of transmission trade-off $\beta_0(v)$ (Figure 6.12), in which case I find that the most change occurs in constant environments. Naively, we might expect the most change to occur in highly variable environments for all parameters, since the maximum infected population at high amplitudes should be more sensitive to changes in parameters than in a constant environment, hence impacting evolutionary outcomes. This is not the case

when considering the efficacy of transmission, because the parasite's trade-off is through this term. This means that decreasing v as the amplitude δ increases can give a greater infected population size at high amplitudes compared to the constant environment. Thus the selection pressure for host defence increases, leading to lower sensitivity in high amplitude environments. Hence eco-evolutionary feedbacks are, again, an influential factor that determines the sensitivity of evolution to changes in parameters.

Using the parasite fitness gradient in equation (6.20), note that the parasite's evolution is only directly impacted by changes in the transmission efficacy $\beta_0(v)$ and steepness κ, with other parameters affecting it indirectly through host defence u. Hence the contours of v^* are different to those of u^* in Figures 6.12 and 6.13 where the fitness is directly affected, although not enough to change the qualitative behaviour as the amplitude δ varies. Otherwise the parasite contours are exactly the same as the host (Figures 6.10 and 6.11).

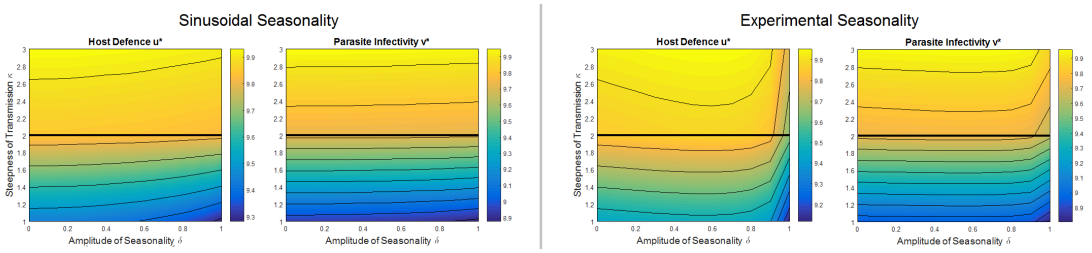

Figure 6.13: Contour plots showing host defence u^* and parasite infectivity v^* as the amplitude of seasonality δ and the steepness of transmission κ vary. Left column: Sinusoidal seasonality $\text{births}_{\text{cont}}(t)$; Right column: Experimental seasonality $\text{births}_{\text{exp}}(t)$. Default parameters from Table 6.1 are marked with thick black lines.

When I increase the steepness of transmission κ, the infected population decreases when $u > v$ (decrease in transmission, Figure 6.1), and so we might expect the host to invest less in defence. However, I found that the host invests more in defence (Figure 6.13). This is due to the fact that when κ is increased, the steepness of $\beta(u, v)$ is increased and the infection process is more specialist. Therefore, the host has to invest more in defence to keep transmission low. As for changes in the other parameters, the parasite increases infectivity in response to the host increasing defence (Figure 6.13). It is also worth noting that decreasing κ leads to larger overall changes in the singular point over the range of δ values, i.e. the seasonality has a larger effect on evolution when infection is less specific. This is because decreasing defence leads to a smaller increase in transmission when κ is lower, and so the host has more flexibility to evolve lower defences without increasing the infected population to such a degree.

When κ is reduced to 0.5, while the overall change in defence/infectivity is large for both types of seasonality, the peak for the experimental seasonality moves to smaller amplitudes and the predominant behaviour is a decrease in defence (Figure 6.14). In addition, the host evolutionary stability condition no longer holds for either seasonality function at high amplitudes (dashed lines in Figure 6.14), and thus the host will exhibit branching behaviour similar to that shown in Figure 6.6. The parasite strategies are CSSs for all values of δ, even after host evolutionary stability has been lost. This suggests that weak specificity in the infection process cannot predict the experimental results from Chapter 5, reinforcing evidence that the interaction between the bacteria and phage is specific (Buckling & Rainey, 2002; Poullain et al., 2008).

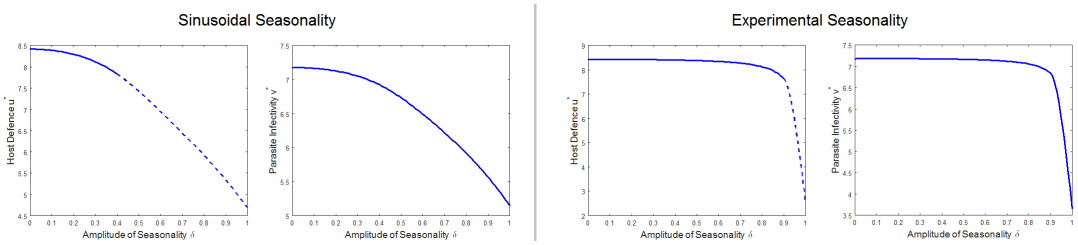

Figure 6.14: Host defence u^* and parasite infectivity v^* as the amplitude of seasonality δ varies for low steepness of transmission $\kappa = 0.5$ (default $\kappa = 2$). Dashed lines show where host evolutionary stability condition no longer holds. The parasite strategies are CSSs for all values of δ. Left column: Sinusoidal seasonality $\text{births}_{\text{cont}}(t)$; Right column: Experimental seasonality $\text{births}_{\text{exp}}(t)$. Parameters were otherwise fixed at default values from Table 6.1.

6.3.4 Period of the Forcing ϵ

In the results so far I have considered how the amplitude of the oscillations δ affects host-parasite coevolution while keeping the period constant ($\epsilon = 1$). However, I can also consider how the period ϵ impacts evolution, as I did for host-only evolution in Chapter 3. Figure 6.15 shows how investment in host defence varies as the period of oscillations increases for two different amplitudes and all three seasonality functions (parasite infectivity behaves similarly). I find that, similarly to host-only evolution, there is a trough in defence near $\epsilon = 2.5$ for all types of seasonality due to resonance with the natural timescale of the model. Overall, Figure 6.15 shows that, when the amplitude is high, fluctuations with very long periods appear to constrain coevolution of host defence and parasite infectivity when compared to very short periods, although intermediate periods ($\epsilon \sim 2.5$) appear to constrain coevolution the most. This be-

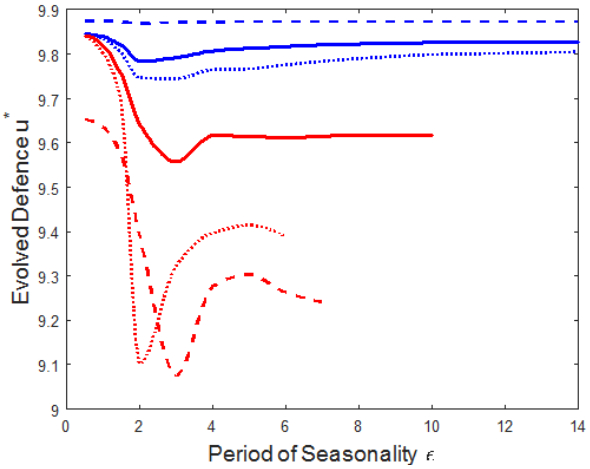

Figure 6.15: Evolved host defence u^* as the period of oscillations ϵ varies. Solid line: Sinusoidal seasonality $\text{births}_{\text{cont}}(t)$; Dotted line: Symmetric stepping seasonality $\text{births}_{\text{step}}(t)$; Dashed line: Experimental seasonality $\text{births}_{\text{exp}}(t)$. Parameters were otherwise fixed at default values with amplitude $\delta = 0.5$ (blue) or $\delta = 1$ (red).

haviour can also be found for intermediate amplitudes, although it is more difficult to see in Figure 6.15 because the impact of period on coevolution is much smaller than at larger amplitudes (see discussion below). The long period behaviour is likely due to large amounts of time spent in unfavourable conditions, leading to greater investment in average birth rate rather than defence.

For high amplitudes (red lines in Figure 6.15), there are no singular points for very high periods. This is because the infected population dies out for these combinations of seasonal parameters, so the host maximizes investment in births ($u = 0$, see Chapter 2). However, the main feature of the high amplitude behaviour is that the period ϵ has a much larger impact on coevolution than at smaller amplitudes. For high amplitude oscillations, the changes in the birth rate are more drastic, especially for the discontinuous seasonalities, and larger periods mean that a long time is spent at these extreme reproduction levels. Therefore the underlying dynamics will be affected by changes in period much more than at lower ampitudes, which in turn influences coevolution, and so there is a bigger impact of the period ϵ at higher amplitudes.

It is worth noting that for intermediate amplitudes, evolution in the experimental seasonality case is hardly affected by changes in the period (blue dashed line in Figure 6.15). This is because, when compared to the other seasonalities, the cost in the low environment is small. Hence, increasing the period ϵ means that greater periods of time

are spent in each of the conditions, which is more detrimental for hosts with the other seasonality functions that have greater costs at intermediate amplitudes. Therefore the population dynamics and thus the evolutionary dynamics are hardly altered by changes in the period ϵ for the experimental seasonality. This suggests that hosts in this type of seasonal environment are more able to cope with changes in period, although higher amplitudes lead to greater coevolutionary changes for all three types of seasonality.

§ 6.4 Discussion

In this chapter, I explored the coevolutionary model of host defence and parasite infectivity initially presented in Chapter 5, incorporating multiple types of seasonality in the host birth rate. I concentrated on stable end points of coevolution, finding that a continuous sinusoidal forcing affects evolution as I predicted, with monotonic decreases in both host defence and parasite infectivity as the amplitude of seasonality increases. This type of seasonality does not predict the results from the bacteria-phage experiment in Chapter 5, which instead found that maximum host defence and parasite infectivity evolved for intermediate amplitudes. When I altered the seasonal forcing to incorporate evidence-based assumptions on the seasonality of growth, the model predicted more accurate evolutionary results when compared to the experimental data.

The aim of this chapter was to investigate further the theoretical coevolution model from Chapter 5 (see also Ferris et al., in prep). Initially I used a sinusoidal and a symmetric step-wise seasonality function, with changes in maximum/minimum birth rate that mimic the resource concentrations from the experiment. For both of these seasonalities, I found that increasing the amplitude of the fluctuations led to monotonically decreasing host defence and parasite infectivity. This does not agree with the experimental results, but occurs for similar reasons as in Chapter 3: as the amplitude increases the minimum host population size decreases, and so the host invests more in birth rate to maintain a large population size. The parasite then evolves lower infectivity in response to the host, thus lowering the infected population size and decreasing selection for defence in the host. When I incorporated bacterial growth rates specific to the experimental conditions, the coevolutionary model predicts highest evolved resistance and infectivity for intermediate amplitudes and therefore better resembles the experimental results (see Chapter 5 for a full discussion). The key difference between the symmetric and experimental seasonalities occurs at low amplitudes (decrease in defence for symmetric, increase for experimental), which is primarily due to how the

minimum birth rate affects the host. In the symmetric case, the maximum/minimum birth rate gradients are the same and so the average birth rate is constant for all amplitudes. For the evidence-based seasonality, the magnitude of the gradient of the minimum birth rate is smaller than the maximum at low amplitudes, meaning that the average birth rate is greater than in the constant environment. This difference in how the seasonality affects the average birth rate leads to the different evolutionary outcomes observed, as a larger average birth rate means that there is greater selection for host defence.

In previous theoretical models of quantitative host defence in a temporal environment, only Poisot et al. (2012) found non-linear behaviour of evolved defence against amplitude of seasonality. However, they found that the host evolves minimum defence for intermediate amplitudes, compared to maximum here for the experimental seasonality. This difference can be attributed to how the periodic forcing is implemented, as discussed in Chapter 5, and highlights how individual environments within the model can alter host-parasite coevolution. It is therefore clear that the way in which seasonality is implemented can have direct effects on coevolution, and so models of specific empirical systems should take this into account.

In my coevolutionary model, the parasite fitness was only affected by oscillations in host birth rate indirectly through the host's defence (equation (6.17)), and so the parasite's evolution is strongly determined by that of the host. The dependence of parasite evolution on that of the host has also been observed in a constant environment. For a 'universal' infection process, the host can limit parasite diversity by not allowing branching in the parasite trait (Best et al., 2009; Svennungsen & Kisdi, 2009), or the population is limited to a dimorphism in both traits (Boots et al., 2014). For a specific infection process, a cascade of branching events can occur, with parasite diversity limited by the number of host populations that currently exist (Best et al., 2010b; Boots et al., 2014). Given that parasite evolution can be determined by coevolution with the host in a constant environment, it is perhaps unsurprising that similar interactions also occur in fluctuating environments. We can also consider how the host's evolutionary behaviour depends on that of the parasite, with the model here suggesting that coevolution may have altered host defence quantitatively, but overall the host's qualitative evolutionary behaviour remained the same (decrease in defence as amplitude increases, compare with Chapter 3). However, other studies have shown that coevolution with the parasite can impact host evolution (van Baalen, 1998; Restif & Koella, 2003; Best et al., 2009, 2010b, 2014), so my relatively simple model may miss some interactions,

perhaps due to the assumption of infected sterility, that could lead to coevolutionary outcomes where the parasite's evolution has a more significant impact on the host's defence.

I found that seasonality has a larger effect on the co-evolutionary singular point when infection is less specific. This is due to the fact that, for less specific infection, lowering defence leads to a smaller increase in transmission, and so the host can afford to invest even less in defence and more in birth rate. Therefore the level of specificity has an important impact on coevolutionary outcomes, with highly specific interactions leading to evolution of greater defence and infectivity. I also found that the non-monotonic evolutionary behaviour for the experimental seasonality changed at very low specificity, with maximum investment in defence occuring at lower amplitudes. This is due to very low specificity increasing transmission (Figure 6.1), therefore increasing the infection prevalence and decreasing the overall population size (Chapter 2). Therefore selection for increased birth rate is greater than for more specific infection processes, and so the amplitude at which investment in births becomes advantageous occurs at smaller values. This theoretical result reinforces empirical evidence that the interaction between the bacteria and phage is specific (Buckling & Rainey, 2002; Poullain et al., 2008), as specificity of infection is needed to predict the evolutionary results from the experiment in Chapter 5. In other theoretical work, the level of specificity has been shown to influence static and temporal diversity (Boots et al., 2014; Best et al., 2017b), with greater specificity leading to more polymorphic populations or unstable evolutionary fluctuations. Hence the nature of the interaction between hosts and parasites has a complicated effect on coevolution, and while there has been a great deal of research from a genetic perspective (Sasaki, 2000; Tellier & Brown, 2007; Best et al., 2014), there is still plenty of scope to investigate eco-evolutionary feedbacks within this framework (Ashby et al. (2019)).

I considered varying the period of the oscillations for fixed amplitude, finding that co-evolution was most constrained in environments at intermediate periods. This partially agrees with empirical data from Harrison et al. (2013), where they found that bacteria *P. fluorescens* evolved lower phage resistance in more rapidly fluctuating environments. I also found that amplitude and period have an interacting effect on coevolution, with lowest resistance evolving for high amplitudes and intermediate periods. This has yet to be investigated empirically, as many studies consider either varying amplitude (Blanford et al., 2003; Chapter 5; Ferris et al., in prep) or period (Hiltunen et al., 2012; Harrison et al., 2013; Duncan et al., 2017), so it is unclear how these seasonal

parameters may interact in experimental systems.

In spatial host-parasite evolution literature, there appears to be a consensus that local interactions lead to the evolution of less virulent parasites when compared to well-mixed populations (Hochberg & van Baalen, 1998; Boots & Sasaki, 1999; Haraguchi & Sasaki, 2000; Kamo et al., 2007; Best et al., 2011; Su & Boots, 2017). It has also been found that local interactions can lead to the parasite evolving increased transmission (Read & Keeling, 2003; Ashby et al., 2014), although there may be less variation within the parasite population (Damgaard, 1999). For host evolution, many have found that spatial structure gives lower resistance (Hochberg & van Baalen, 1998; Débarre et al., 2012; Ashby et al., 2014), although Best et al., (2011) found the opposite when transmission and reproduction are localized. A common thread throughout appears to be that greater spatial heterogeneity generally leads to more infection within the population, as lower virulence usually leads to greater infected population sizes (Chapter 2). This phenomenon extends to temporal heterogeneity studies, with greater amplitudes of environmental variation leading to more infection (Poisot et al., 2012; Ferris & Best, 2018; but see Donnelly et al., 2013). Greater levels of infection has also observed in heterogeneous environments for some empirical host-parasite (Brockhurst et al., 2006; Kerr et al., 2006) and predator-prey species (Friman & Laakso, 2011; Friman et al., 2011), but there isn't conclusive experimental evidence that this is a consistent trend. Indeed, this behaviour is by no means universal, as I found in this chapter that increased heterogeneity (amplitude) led to lower average infected population sizes despite an increase in transmission. Therefore more theoretical and empirical work could be done to investigate effect of heterogeneous environments and evolution on the occurrence of infection, as it could have important repercussions for real-world infection predictions.

In this chapter I made multiple assumptions to simplify the analysis and reduce computational time. First, I assumed that the host and parasite mutate at the same rate, despite evidence to the contrary for my experimental species (Samson et al., 2013; Lopez-Pascua et al., 2014). It is unclear how changing these mutation rates will alter the evolutionary outcomes, although elsewhere it has been shown that evolutionary cycles can emerge when the host evolves faster than the parasite (Best et al., 2010b; but see Best et al., 2017b). Second, I only considered CoESS singular points with parameters close to default values, including trade-off coefficients, even though other evolutionary outcomes exist that often depend on trade-off choice (Kisdi, 2006; Best et al., 2009). An extention of this study would be to consider a wider range of parameters, and in particular to consider other types of singular points and how seasonality

may affect when they emerge. Third, I only investigated the effects of two types of discontinuous seasonality specific to my previous theoretical and experimental work. Alternative forms for the different environments as the amplitude increases are likely to occur in different contexts, and could produce interesting coevolutionary behaviours not observed here.

This chapter has investigated host-parasite coevolution in a seasonal environment, with particular attention paid to incorporating empirically obtained information to predict experimental outcomes. I found that while coevolution is important, understanding underlying biological processes can be key to producing accurate predictions through mathematical modelling. There is plenty of scope to extend this work further, in a general theoretical context or for application to a different experimental system, but it is important to consider the impact of individual environments within temporally varying conditions as they can determine evolutionary outcomes.

Chapter 7

Conclusions

§ 7.1 Summary

Infectious diseases are a global issue, and as such are the focus of a rich area of research, with applications in public health, agriculture, conservation, and more. There are many factors that can determine the spread and impact of a disease, two of which are evolution and heterogeneous environments. Therefore investigating the combination of all three of these concepts (i.e. infection, evolution and heterogeneous environments) is likely to have important implications for real-world systems. In this thesis, I studied host-parasite evolution in a temporally heterogeneous environment, with a focus on how seasonal parameters change evolutionary outcomes. Previous to this work, there was little theoretical research investigating the evolution of quantitative host-parasite traits in seasonal environments, despite the fact that many species experience temporal environments that can cause fluctuating population and infection dynamics (Fenton et al., 2006a; Smith et al., 2008; Reynolds et al., 2013; Ewing et al., 2016). Here I summarize the main results and implications from this thesis, and consider possible directions for future research.

In Chapter 3 I investigated the evolution of host avoidance when the host birth rate was periodic in time. I found that seasonality affected host evolution, and that recovery had a significant interaction with the seasonal amplitude: the absence of recovery led to an increase in defence with amplitude; the presence of recovery generally gave lower evolved defence for greater seasonal amplitudes. Of particular relevance to previous work, the behaviour of host defence as other parameters were varied was not necessarily the same in constant and highly variable environments, although this effect was

dampened for long-lived hosts. In Chapter 4 I conducted a similar investigation, but instead considered evolutionary branching behaviour through three different host defence mechanisms, with a focus on mortality tolerance. I found that branching in tolerance could occur in a seasonal, but not constant, environment, and that the majority of simulations led to a temporary dimorphism (i.e. eventual extinction of a branch). This branching appeared due to fold-bifurctions in the adaptive dynamics singular point and a negative feedback with maximum infected population size, and branching tended to occur in parameter regions where the infected population was high. Similarly to previous studies that assume a constant environment, the evolutionary behaviour of resistance and tolerance were qualitatively different. In particular, greater amplitudes appeared to 'stabilise' tolerance evolution, but had the opposite effect for resistance evolution.

Previous theoretical work has considered how evolved host defence changes in a constant environment (Boots & Bowers, 1999, 2004; Restif & Koella, 2004), with some considering the evolutionary differences between long- and short-lived hosts (van Boven & Weissing, 2004; Lee, 2006; Miller et al., 2007; Boots et al., 2013; Donnelly et al., 2017). In particular, it has been found that innate resistance (avoidance, recovery or tolerance) tends to be greater in long- compared to short-lived hosts, although this behaviour can become more complex due to ecological feedbacks or acquired immunity (Miller et al., 2007; Donnelly et al., 2015, 2017). The greater investment in innate resistance tends to occur because long-lived hosts are more likely to become infected, increasing selection for resistance. However, acquired immunity means that the hosts are also more likely to recover to an immune class, thus reducing infection prevalence and selection for resistance, which complicates the evolutionary behaviour with life-span. Similarly, I found that longer-lived hosts without immunity evolved greater resistance through avoidance, but also that the effect of seasonality on host evolution was dampened for long- compared to short-lived hosts (compare Figures 3.8 and 3.9 in Chapter 3). I also found a similar trend for tolerance evolution, whereby maximization of tolerance was more likely to evolve for longer-lived hosts (Figure 4.7 in Chapter 4). As above, these evolutionary behaviours are due to increased selection for defence, as infection prevalence is higher for long-lived hosts. This can also explain the dampening of the effect of seasonality for long-lived hosts. High defence is traded-off against average birth rate, so long-lived hosts will have a smaller average birth rate than the short-lived hosts. Since the birth rate multiplies the periodic forcing, the long-lived hosts will have smaller amplitude oscillations in the population dynamics compared to short-lived hosts with higher birth rates, and so evolution is less affected by increasing the amplitude of the

forcing and the seasonal effect is dampened for long-lived hosts. This suggests that if the forcing or trade-off were to be implemented elsewhere then there might not be such a clear dampening effect for long-lived hosts, but this remains to be investigated. Therefore it appears to be a common result that longer-lived hosts evolve greater defence than their short-lived counterparts, even in fluctuating environments. However this behaviour is easily complicated by eco-evolutionary feedbacks, in particular by the potential for host immunity to the parasite.

There has been a disconnect between theoretical and empirical work about the possibility for diversity in host tolerance: empirical studies have often found diversity in host tolerance to parasitism (Koskela et al., 2002; Råberg et al., 2007; Blanchet et al., 2010; Sternberg et al., 2012; Hayward et al., 2014), whereas theoretical studies generally do not find polymorphic populations when the host evolves through tolerance (Roy & Kirchner, 2000; Miller et al., 2005; Best et al., 2014, 2017a; but see Fornoni et al., 2004; Best et al., 2008, 2010a; Carval & Ferriere, 2010). The work in this thesis suggests that temporal environments can allow for theoretical diversity in host tolerance, although whether or not diversity is maintained depends on the range of tolerance traits allowed. It has already been shown that the underlying ecology is crucial in determining the level of diversity in host resistance (Boots et al., 2012), so it is perhaps unsurprising that variable population dynamics can lead to the emergence different evolutionary behaviours, including branching. However, some experimental studies have found measurable tolerance diversity in a constant environment (Råberg et al., 2007; Kause et al., 2012), so temporal heterogeneity cannot account for this diversity. Therefore, while temporal heterogeneity may be a driver of tolerance diversity for some hosts, there will be other factors that have so far been missed in many theoretical models.

Throughout the host-parasite evolutionary literature, it has become clear that eco-evolutionary feedbacks are a key factor that determine host evolution (Roy & Kirchner, 2000; Restif & Koella, 2004; Miller et al., 2005, 2007; Boots et al., 2009, 2012; Best et al., 2017b; Theodosiou et al., 2019). I found that this remains the case in temporal environments for evolution through both resistance and tolerance, with potentially accentuated implications due to the cyclic nature of the populations. For example, in Chapter 3 I found that, when recovery was small, evolution in host avoidance could drive the population through a period-doubling bifurcation, which resulted in population dynamics with greater period. This has also been observed in constant environments, where the period-doubling bifurcation can lead to a discrete 'jump' in the level of evolved defence as parameters are varied (Hoyle et al., 2011; Best et al., 2013). For

evolving avoidance or tolerance, I found that seasonality can lead to the emergence of fold bifurcations, such that two or three singular points occur simultaneously (Figure 3.6 in Chapter 3, Figure 4.6 in Chapter 4). For avoidance, I found that two of the three singular points were CSSs (i.e. end-points of evolution), giving bistability between high and low levels of defence. For tolerance, the main effect studied here is the emergence of branching behaviour as the central strategy, which is intrinsically linked to these fold bifurcations. Similar bifurcations have also been observed in a constant environment as other parameters are varied, with Miller et al. (2007) finding that, with or without acquired immunity, increasing the host lifespan can lead to bistability between high and low levels of defence through either avoidance or tolerance. Therefore eco-evolutionary feedbacks can lead to bistability between different levels of defence in constant and temporal environments, so the periodic forcing does not eliminate this behaviour. For tolerance evolution, a key eco-evolutionary feedback is the negative feedback between tolerance and the maximum infected population size, which allows branching behaviour to emerge in a fluctuating environment. This result, and those above, emphasizes the amplified effects of eco-evolutionary feedbacks in seasonal environments, and that these feedbacks can often lead to complex host evolutionary behaviour that may not have been observed in a constant environment.

In Chapter 5 I presented an experimental evolution study using the bacteria *P. fluorescens* SBW25 and its parasitic phage SBW25Φ2 that investigated how seasonal amplitude might alter coevolution, as previous experimental work in temporal environments had not considered the effects of this seasonal trait (but see Blanford et al., 2003). I found that only the bacteria population sizes were directly affected by the amplitude of the oscillations in the resource, and that the bacteria and phage evolved maximum resistance/infectivity for intermediate amplitude oscillations. I also developed a coevolutionary model for the experimental system, which was introduced in Chapter 5 and explored further in Chapter 6. I found that bacterial growth rates in the individual environments and a specific infection process needed to be incorporated into the model to replicate the experimental results. In particular, maximum resistance/infectivity evolved for intermediate amplitudes due to changes in the growth rate in the low resource environment as the amplitude increased. When I explored the model more generally, I found that for seasonality functions where the maximum/minimum birth rate changed symmetrically with amplitude, the model predicted monotonically decreasing investment in defence and infectivity as the amplitude of seasonality increased, which is similar to predictions from the host-only evolutionary model in Chapter 3.

There is growing interest in experimental evolution in temporal environments, although much of this has focussed on the evolution of antibiotic resistance in parasites when treatment is applied cyclicly (Brown & Nathwani, 2005; Kim et al., 2014; van den Bergh et al., 2016). To date there have been few studies exploring host-parasite coevolution in temporal environments, and many have focussed on pulsed conditions (Friman et al., 2011; Friman & Laakso, 2011; Hiltunen et al., 2015) or changes in period (Harrison et al., 2013; Dallas & Drake, 2016; Duncan et al., 2017). In a bacteria-phage experiment, I found that maximum resistance/infectivity evolved for intermediate amplitude treatments. The coevolutionary model used to explain this result found that the growth of the bacteria in the individual environments was the main driver of this evolutionary trend. This suggests that if the experiment were to be repeated with a much lower mean resource level, then the growth rates of the bacteria in the low and high resource environments may change more symmetrically as the amplitude increases, which is likely to produce different evolutionary results (e.g. if the range of resource concentrations were taken to be $\leq$ 0.25KB from Figure 5.7 in Chapter 5). In a different temporal environment study, Blanford et al. (2003) found that pea aphids, *Acyrthosiphon pisum*, evolved highest resistance against a fungal pathogen, *Erynia neoaphidis*, for high amplitude oscillations in temperature. Similarly to my study, this is due to how the periodically high temperatures affects the population sizes, with reduced survival of the pathogen occuring at high amplitudes. Therefore specific details about how the environmental oscillations impact the host and/or parasite has important implications for coevolution, as has already been oberved by Harrison et al. (2013) and Duncan et al. (2017), where two different types of environmental variation led to contrasting evolutionary results. The relatively unique combination of experiment and theory presented in this thesis was essential to fully understand the coevolutionary results; the experimental data alone was indicative, but not conclusive, evidence of the underlying mechanisms driving coevolution, while the theoretical model may have missed the experimental results altogether without the specific growth information. In addition, the study presented here has emphasized the importance of understanding how individual environments and temporal conditions affect each species, as this will have important consequences for coevolution.

In previous theoretical coevolutionary work, it has been found that the introduction of coevolution can lead to outcomes that cannot be predicted from single species evolution alone (Restif & Koella, 2003; Best et al., 2009). For the model presented in this thesis with sinusoidal seasonality, coevolution appears to have little effect on the qualitative behaviour of host defence as the amplitude is increased (i.e. decrease as amplitude

increases; Chapters 3 and 6), although coevolution does lead to lower parasite infectivity at high amplitudes (Chapter 6). While it appears that the coevolution results here are predictable from the host-only results, this is not the whole story. For both cases, as amplitude increases the transmission coefficient at the singular point increases. In the host-only evolution model this led to increased infected population, however, for the coevolutionary model the average infected population actually decreases due to the specific infection process and changes in the parasite's infectivity. Therefore, while the evolutionary dynamics may be similar, the underlying epidemiological dynamics resulting from host-only evolution and coevolution can be very different, especially in a highly variable environment.

In relation to parasite evolution, the coevolutionary results here contrast against previous studies. For example, for parasite-only evolution in a temporal environment, Donnelly et al. (2013) found that, when virulence is density-dependent, the parasite evolves greater transmission and virulence as the amplitude increases. Therefore it appears that coevolution may alter the parasite evolutionary behaviour, although the inclusion of density-dependent virulence is an important factor which, if addded to the coevolutionary model here, may lead to different behaviour again. Elsewhere, Best et al. (2009) found that coevolution led to the emergence of more virulent parasites when compared to parasite-only evolution due to branching in the host population. Again, this contrasts against my model. When considering increasing amplitude environments, I found that the parasite's infectivity is constant when the host does not evolve, and is lower in a range of temporal environments when the host coevolves with the parasite. The differences between these results may be due to the type of infection process used (range here, universal in Best et al., 2009), or the trade-offs that are included (within transmission here, between transmission and virulence in Best et al., 2009). Hence underlying ecological assumptions and whether or not the host coevolves with the parasite has an important impact on the level of parasite infectivity that evolves, and so these factors should be taken into account when predicting the relative virulence or transmissibility of certain parasites.

In this thesis I have developed a mathematical method to explore evolution in a fluctuating environment, specifically investigating host-parasite evolution. Overall, the results here suggest that seasonal environments can have a significant impact on host-parasite evolution. This can be in terms of the level of evolved defence/infectivity, or the types of evolutionary behaviour that emerge. Eco-evolutionary feedbacks have already been shown to be important in constant environments (Boots et al., 2009; Ashby et al.,

2019), and the results here have demonstrated that these feedbacks can be even more influential in seasonal environments with oscillating population sizes. In particular, I found that eco-evolutionary feedbacks can lead to different evolutionary behaviour in highly variable environments, including bistability and branching, and evolution of host avoidance can drive the population dynamics through a period-doubling bifurcation into a cycle with a different period. The amplitude of the seasonal environment changes host-parasite coevolution experimentally and theoretically, and individual conditions within fluctuating environments can have a significant impact on coevolution. This work could be particularly important in relation to climate change, as it has been shown that not only are average temperatures increasing, but also that the amplitude of temporal fluctuations is growing (Schär et al., 2004; Alexander & Perkins, 2013; Vincze et al., 2017). Therefore models of host-parasite evolution in highly variable environments may be needed to predict the spread and impact of future outbreaks, especially in cases where changes in climate have a direct, or indirect, effect on infection dynamics.

§ 7.2 Future Work

The work in this thesis is part of a growing field of research investigating temporal environments and evolution in host-parasite systems, and contributes some important results to the field. However, there is plenty of scope for more theoretical and empirical explorations into this topic.

Throughout this thesis I considered a regular, deterministic time-varying birth rate as a proxy for a temporal environment. In reality there are many other types of temporal environment that can affect host-parasite populations, including, but not limited to, time-dependent infection (Fine & Clarkson, 1982; Aron & Schwartz, 1984; Knowles et al., 2012; Baracchini et al., 2016), periodic death (Shaw, 1994; Gehrt, 2005; Hamelin et al., 2011; van den Berg et al., 2010, 2011), stochastic temporal environments (Kaitala et al., 1997; Ives et al., 1999; Gómez-Corral & García, 2014; Fuentes & Ferrada, 2017), varying predation rates (Hilker & Malchow, 2006; Hsieh & Hsiao, 2008; Czaja et al., 2018), or seasonal vector population sizes (Altizer et al., 2006; Jian et al., 2014; Ewing et al., 2016). These temporal environments, and more, can influence host-parasite ecological dynamics, so it is likely that evolution will also be affected. Some of these environments have previously been investigated by others with regards to parasite evolution (Koelle et al., 2005; Sorrell et al., 2009; Hamelin et al., 2011; van den Berg

et al., 2010, 2011) and coevolution (Nuismer et al., 2003), although many still remain to be explored. In particular, I found no studies of host-only evolution that includes any of these alternative seasonalities. Unfortunately, the addition of many of these temporal environments complicates mathematical analysis, meaning that research on this topic is difficult and can take a long time to complete. For example, time-dependent transmission rates often lead to chaotic dynamics at high amplitudes (Grossman, 1980; Schwartz & Smith, 1983; Greenman et al., 2004; Grassly & Fraser, 2006). In this case, the numerical evolution method presented here is unlikely to work as it relies on the solution of the mutant population dynamics being a product of an exponential and a periodic function (but see Metz et al., 1992; Svardal et al., 2015). Alternatively, adding more dynamic equations to represent fluctuating conditions or vector densities could greatly improve the accuracy of evolutionary predictions, but this will come at a cost of increased computational time and, again, could lead to chaotic dynamics. Despite these potential problems, the investigation of these seasonalities would have important consequences for many different infection systems, and could be developed in collaboration with experimental studies in these environments. This could lead to interesting and unexpected coevolutionary outcomes, but also a deeper understanding about biological infection systems.

I have assumed that environmental fluctuations impact the species in only one way, i.e. only through the host birth rate. As detailed above, seasonality can affect host-parasite dynamics through a number of different mechanisms, which could occur concurrently (Anderson, 1974; Altizer et al., 2004, 2006; Hosseini et al., 2004). For example, Altizer et al. (2004) found that the seasonal prevalence of *Mycoplasma gallisepticum* in house finches (*Carpodacus mexicanus*) was likely determined by annual changes in host behaviour, reproduction and environmental effects on immunocompetence. While concurrent seasonality functions have been considered in infection models (Dorélien et al., 2013; Reynolds et al., 2013; Gómez-Corral & García, 2014; Baracchini et al., 2016), no mathematical studies have considered the effect of this type of environment on host-parasite evolution. Experimentally, only Hiltunen et al., (2015) have investigated multiple types of seasonality, using the bacteria *P. fluorescens* SBW25 and the protozoan *T. thermophila* 1630/1U with two oscillating environmental forcings that each impacted one of the coevolving species. They found that the rate of evolution of defence was smaller in oscillating compared to constant environments, but also that lower defence evolved when both fluctuating stressors were present, suggesting an additive effect that constrained the evolutionary response. Hence evolution may be affected in a particular way by one type of environmental fluctuations, but combinations of os-

cillating forcings may have more complicated effects. In particular, different seasonal conditions may not always lead to additive effects on evolution, and combinations of amplitudes/periods/synchronicity of various temporal forcings could affect evolution in a variety of ways. Therefore the combination of multiple oscillating forcings and evolution could be explored in greater depth, both theoretically and experimentally, and in particular the effects of seasonalities that impact the host and parasite in different ways could be investigated.

For the majority of this work, I investigated how stable end-points of evolution (CSSs or CoESSs) varied with seasonal parameters. However, as seen in Chapter 4, seasonality could lead to changes in the type of evolutionary behaviour observed, including the level of diversity in the population. For example, branching in tolerance could only occur when the amplitude of seasonality was high enough, and increasing the amplitude generally led to more stable (unstable) evolutionary behaviour in tolerance (resistance). This was also touched on in Chapter 6, where I found that for alternative trade-off parameters, the host loses evolutionary stability and branches when the amplitude is high. I did not investigate this result further as it did not reflect the experimental data, but there is scope for this to be explored in more detail in a coevolutionary context. For example, when considering specific infection in a constant environment, Best et al., (2010b) found that the specificity can lead to a cascade of branching events. Similarly, Boots et al. (2014) investigated different types of infection specificity, finding that diversity is limited to dimorphism in both the host and parasite unless there is some level of incompatability between strains, in which case static polymorphisms of multiple traits can emerge through branching. However, both of these studies assumed a constant environment, and so it is unclear if a seasonal environment would have an effect on these results. In particular, one could consider how seasonality affects the possibility for coevolutionary branching, the level of diversity obtained, and, similarly to Boots et al. (2014), the restrictions on the transmission process that lead to static polymorphisms. Additionally, the branching results for the evolution of host tolerance presented in Chapter 4 does not take into account coevolution, which could eliminate or promote tolerance diversity in the population. Hence there are many avenues to explore the evolution of host-parasite diversity in temporal environments, which could help to identify circumstances under which diversity is promoted and maintained in seasonal infection systems, and therefore predict the potential risk of future outbreaks.

Overall, the few studies that consider evolution in fluctuating environments tend to investigate resistance rather than tolerance (Hiltunen et al., 2015; Poisot at al., 2012;

Harrison et al., 2013; Duncan et al., 2017). The work in Chapter 4 provides a starting point for the exploration of tolerance in seasonal environments, especially in terms of host diversity, but there is plenty more that could be done. In particular, I found that branching in tolerance occured in parameter regions that gave larger infected population sizes. Of the previous studies that find branching in tolerance, Best et al. (2010a) found that low mortality rates, which cause greater infected population sizes, led to a wider range of trade-offs that give branching behaviour for evolving sterility tolerance. This suggests that infected population size may be a consistent driver of tolerance branching in constant and temporal environments, although more evidence is needed to support this theory. There is also a lack of empirical work studying the effects of temporal environments on the evolution of host tolerance, which may provide important information for future modelling work. Hence experimental and theoretical work could investigate tolerance and seasonal environments further, with a fully collaborative study potentially providing even more insight into the drivers of tolerance evolution and diversity.

In this thesis I have concentrated on the evolution of resistance (avoidance and recovery) and mortality tolerance, but hosts can also evolve through infected sterility tolerance (Simms & Triplett, 1994; Stowe, 1998; Hochwender et al., 2000; Restif & Koella, 2004; Best et al., 2008, 2010a) or acquired immunity (Deerenberg et al., 1997; Zuk & Stoehr, 2002; Boots & Bowers, 2004; Gerardo et al., 2010; Donnelly et al., 2017). For example, in a constant environment, sterility tolerance has distinct evolutionary behaviour when compared to mortality tolerance (Best et al., 2008), while acquired immunity may evolve in a similarly way to resistance mechanisms (Miller et al., 2007; Donnelly et al., 2017). The evolutionary dynamics of these defences has not been explored in a seasonal context, and may provide different results to those found in this thesis for resistance or mortality tolerance evolution. In addition, defence mechanisms are often linked (e.g. resistance and tolerance: Restif & Koella, 2004; Råberg et al., 2007; Carval & Ferriere, 2010; Howick & Lazzaro, 2017; Klemme & Karvonen, 2017), although experimental studies are sometimes unable to untangle the costs of individual defence mechanisms (Simms & Triplett, 1994; Frank, 2000), and it has been shown theoretically that simultaneous evolution of multiple defences can obscure their actual costs (Restif & Koella, 2004). Therefore it may be pertinent to consider a range of trade-offs between different types of defence and the environment, which could improve our understanding of empirical results and determine which mechanisms may be most beneficial in constant and variable environments.

In this work I considered temporal environments, but this is only one way in which habitats and infection dynamics are heterogeneous. Spatial heterogeneity also plays an important role, and the intersection between time and space is often an influential factor in infection dynamics. For example, empirical evidence suggests that temporal spatial clustering of hosts can lead to outbreaks of disease (Dhondt et al., 2005, 2012; Caillaud et al., 2006; Bharti et al., 2011; Silk et al., 2017). Host-parasite evolution has yet to be studied in a temporal and spatial environment, however, the theoretical spatial evolutionary literature has generally found that more localized interactions lead to lower virulence (Hochberg & van Baalen, 1998; Boots & Sasaki, 1999; Haraguchi & Sasaki, 2000; Kamo et al., 2007; Su & Boots, 2017) or greater transmission (Read & Keeling, 2003; Débarre et al., 2012; Ashby et al., 2014), which generally leads to greater infection in the population. In contrast, when considering host-only evolution and coevolution in a temporal environment, I found contradictory results as to how increasing the level of heterogeneity (amplitude of the fluctuations) affected the infected population size. Host-only evolution led to increased infection (Chapter 3), but coevolution gave lower infected population sizes (Chapter 6). Therefore an evolutionary and fully heterogeneous environment model, perhaps with interacting effects of the two heterogeneities, could be developed to investigate the general effect of heterogeneity on infection prevalence. Evolution for other ecological systems has been considered in this type of environment (Cohen & Levin, 1991; Massol, 2013; Massol & Débarre, 2015; Svardal et al., 2015), and so these studies could be altered to include host-parasite dynamics, with the resulting model able to encompass many real-world infection systems. Alternatively, some have already studied infection models with spatial and temporal heterogeneity (Sari & Augeraud-Véron, 2015; Hirsch et al., 2016), with Duke-Sylvester et al. (2011) applying such a model to the spread of raccoon rabies in the USA. They found that, for spatial patches with synchronous periodic reproduction, changing the variation in the timing of host births across the patches led to differences in the spatial synchronization of epidemics. These infection models could be extended to include evolution, however, such complexity would likely come at a cost of increased computational time and broad simplifying assumptions.

There are number of ways in which the temporal environment experiment presented in Chapter 5 could be extended to include spatial hetergeneity. For example, it would be relatively simple to expand the experiment to consider local-interactions through static microcosms (Brockhurst et al., 2003, 2006; Lopez-Pascua et al., 2012), which could show if the temporal environment has a larger/smaller impact on coevolution when host-parasite interactions are locally determined. Alternatively, a more compli-

cated way to include both temporal and spatial environments would be to combine the periodic treatment presented in Chapter 5 with spatial heterogeneity specified by migration between patches (e.g. Vogwill et al., 2008, 2009, 2010, 2011), or by migration along a productivity gradient (Lopez-Pascua et al., 2010). Great care would be needed when designing and setting up these migration experiments with temporal environments, so that the experiment itself is possible practically and the results can be clearly understood. Therefore, there are a few ways in which evolution could be studied experimentally in a spatial and temporal environment, although high levels of complexity may reduce tractability and so experiment design will be especially important to gain clear results.

I found that there is a strong interaction between the amplitude and period of the seasonal forcing on the host-parasite population dynamics, which influenced the evolution of host defence (Chapter 3 and 4) and coevolution (Chapter 6). However, I did not find any studies in the experimental literature that considered both varying the amplitude and period in a temporal environment. While considering these quantities separately is useful, it is unclear if theoretical results about their interaction are realistic. The experiment from Chapter 5 could easily be extended to include additional treatments that vary both the amplitude and the period of resource oscillations, as the effect of changing the period alone has already been investigated by Harrison et al. (2013). This would provide experimental evolution evidence for the interaction of the seasonal parameters, and could show behaviour that is not obvious from studies of only one variable. The results could also be compared to theoretical coevolutionary outcomes from the models presented here and elsewhere (Poisot et al., 2012), which may prompt the addition of more evidence-based assumptions in order to achieve better evolutionary predictions. Such a combination of experimental and theoretical work could provide a deeper understanding of the drivers of infection dynamics in seasonal environments, and how the amplitude/period of environmental fluctuations may affect this.

There are many aspects of infection dynamics and evolution that have yet to be explored in a seasonal environment. One example is the parasite-mutualist continuum, whereby some parasite species can be beneficial to the host in certain contexts (Michalakis et al., 1992; Hughes et al., 2011; Sternberg et al., 2011; Vorburger & Gouskov, 2011; Ford & King, 2016). This has been studied theoretically in a constant environment, where trade-offs and characteristics of the species determined the evolutionary outcomes (Jones et al., 2011; Ashby & King, 2017). However, a seasonal environment could

change these characteristics and therefore alter the potential for evolved host protection by a parasite. Alternatively, hosts and parasites can adapt through plasticity, whereby defence/infectivity can vary quickly in response to ecological or environmental cues (Via & Lande, 1987; Gillespie & Turelli, 1989; West-Eberhard, 2003; Leimar, 2005; McLeod & Day, 2015). This could be especially important in fluctuating environments, as the host and parasite would be able to plastically respond to seasonal changes in the environment rather than evolve a fixed trait that may only be beneficial for part of the season. Plasticity has already been studied for other systems in spatial (Ernande & Dieckmann, 2004; Leimar et al., 2006) and temporal environments (Leimar, 2009; Herron & Doebeli, 2011; Svardal et al., 2011, 2015), but not yet for host-parasite coevolution in a temporal environment. Elsewhere, many have considered the evolution of drug-resistance in parasites when treatment is applied periodically (Baker et al., 2018), but it may be important to consider the timing of treatment strategies if the infection system is already seasonal, and how the parasite may evolve in response. Therefore there are many possible directions that are not explored in this thesis, but could provide interesting and important predictions for host-parasite coevolution in a range of different contexts.

The study of host-parasite evolution in temporal environments is an expanding area of research, with many aspects yet to be explored. The results from this thesis build upon previous research, and raise questions that could be investigated in the future. In particular, the work here highlights the benefits of developing experimental and theoretical work together, which can result in a more cohesive understanding of host-parasite evolution. Further work in this area could deepen our understanding of infection dynamics, especially in increasingly variable and uncertain climates.

References

P.A. Abrams. Character shifts of prey species that share predators. *Am. Nat.*, 156:S45–S61, 2000.

P.A. Abrams, H. Matsuda, and Y. Harada. Evolutionarily unstable fitness maxima and stable fitness minima of continuous traits. *Evol. Ecol.*, 7:465–487, 1993. doi: 10.1007/BF01237642.

M.A. Acevedo, F.P. Dillemuth, A.J. Flick, M.J. Faldyn, and B.D. Elderd. Virulence-driven trade-offs in disease transmission: A meta-analysis. *Evolution*, 73:636–647, 2019. doi: 10.1111/evo.13692.

A.F. Agrawal and C.M. Lively. Infection genetics: Gene-for-gene versus matching-alleles models and all points in between. *EER*, 4:79–90, 2002.

A.F. Agrawal and S.P. Otto. Host-parasite coevolution and selection on sex through the effects of segregation. *Am. Nat.*, 168:617–629, 2006. doi: 10.1086/508029.

L. Alexander and S. Perkins. Debate heating up over changes in climate variability. *Environ. Res. Lett.*, 8:041001, 2013. doi: 10.1088/1748-9326/8/4/041001.

S. Alizon and M. van Baalen. Transmission–virulence trade-offs in vector-borne diseases. *Theor. Pop. Biol.*, 74:6–15, 2008. doi: 10.1016/j.tpb.2008.04.003.

S. Altizer, A. Dobson, P. Hosseini, P. Hudson, M. Pascual, and P. Rohani. Seasonality and the dynamics of infectious diseases. *J. Anim. Ecol.*, 9:467–484, 2006. doi: 10.1111/j.1461-0248.2005.00879.x.

S. Altizer, W.M. Hochachka, and A.A. Dhondt. Seasonal dynamics of mycoplasmal conjunctivitis in eastern north american house finches. *Journal of Animal Ecology*, 73:309–322, 2004. doi: 10.1111/j.0021-8790.2004.00807.x.

R.M. Anderson. Population dynamics of the cestode caryophyllaeus laticeps (pallas, 1781) in the bream (aramis brama l.). *J. Anim. Ecol.*, 43:305–321, 1974.

R.M. Anderson and R.M. May. Population biology of infectious diseases: Part i. *Nature*, 280:361–367, 1979. doi: 10.1038/280361a0.

R.M. Anderson and R.M. May. The population dynamics of microparasites and their invertebrate hosts. *Phil. Trans. R. Soc. B*, 291:451–524, 1981. doi: 10.1098/rstb.1981.0005.

R.M. Anderson and R.M. May. Directly transmitted infectious diseases: Control by vaccination. *Science*, 215:1053–1060, 1982. doi: 10.1126/science.7063839.

R.M. Anderson and R.M. May. Age-related changes in the rate of disease transmission: implications for the design of vaccination programmes. *J. Hyg. Camb.*, 94:365–436, 1985. doi: 10.1017/S002217240006160X.

J.L. Aron and I.B. Schwartz. Seasonality and period-doubling bifurcations in an epidemic model. *J. Theor. Biol.*, 110:665–679, 1984. doi: 10.1016/S0022-5193(84)80150-2.

B. Ashby and M. Boots. Coevolution of parasite virulence and host mating strategies. *PNAS*, 112:13290–13295, 2015. doi: 10.1073/pnas.1508397112.

B. Ashby and E. Bruns. The evolution of juvenile susceptibility to infectious disease. *Proc. R. Soc. B*, 285:20180844, 2018. doi: 10.1098/rspb.2018.0844.

B. Ashby and S. Gupta. Parasitic castration promotes coevolutionary cycling but also imposes a cost on sex. *Evolution*, 68:2234–2244, 2014. doi: 10.1111/evo.12425.

B. Ashby, S. Gupta, and A. Buckling. Spatial structure mitigates fitness costs in host-parasite coevolution. *Am. Nat.*, 183:E64–E74, 2014. doi: 10.1086/674826.

B. Ashby, R. Iritani, A. Best, A. White, and M. Boots. Understanding the role of eco-evolutionary feedbacks in host-parasite coevolution. *J. Theor. Biol.*, 464:115–125, 2019. doi: 10.1016/j.jtbi.2018.12.031.

B. Ashby and K.C. King. Friendly foes: The evolution of host protection by a parasite. *Evol. Lett.*, 1:211–221, 2017. doi: 10.1002/evl3.19.

C.M. Baker, M.J. Ferrari, and K. Shea. Beyond dose: Pulsed antibiotic treatment schedules can maintain individual benefit while reducing resistance. *Scientific Reports*, 8:5866, 2018. doi: 10.1038/s41598-018-24006-w.

T. Baracchini, A.A. King, M.J. Bouma, X. Rodó, E. Bertuzzo, and M. Pascual. Seasonality in cholera dynamics: A rainfall-driven model explains the wide range of patterns in endemic areas. *Advances in Water Resources*, 000:1–10, 2016.

T.G. Barraclough. How do species interactions affect evolutionary dynamics across whole communities? *Annu. Rev. Ecol. Evol. Syst.*, 46:25–48, 2015. doi: 10.1146/annurev-ecolsys-112414-054030.

L.J. Bartlett, L. Wilfert, and M. Boots. A genotypic trade-off between constitutive resistance to viral infection and host growth rate. *Evolution*, 72:2749–2757, 2018. doi: 10.1111/evo.13623.

R.S. Baucom and J.C. de Roode. Ecological immunology and tolerance in plants and animals. *Func. Ecol.*, 25:18–28, 2011. doi: 65-2435.2010.01742.x.

M. Begon, M. Bennett, R.G. Bowers, N.P. French, S.M. Hazel, and J. Turner. A clarification of transmission terms in host-microparasite models: numbers, densities and areas. *Epidemiol. Infect.*, 129:147–153, 2002. doi: 10.1017/S0950268802007148.

M. Begon, S. Telfer, M.J. Smith, S. Burthe, S. Paterson, and X. Lambin. Seasonal host dynamics drive the timing of recurrent epidemics in a wildlife population. *Proc. R. Soc. B*, 276:1603–1610, 2009. doi: 10.1098/rspb.2008.1732.

C. Bérénos, K.M. Wegner, and P. Schmid-Hempel. Antagonistic coevolution with parasites maintains host genetic diversity: an experimental test. *Proc. R. Soc. B*, 278:218–224, 2011. doi: 10.1098/rspb.2010.1211.

G. Berg. Plant-microbe interactions promoting plant growth and health: perspectives for controlled use of microorganisms in agriculture. *Appl. Microbiol. Biotechnol.*, 84:11–18, 2009. doi: 10.1007/s00253-009-2092-7.

V. Bernhauerova. Vaccine-driven evolution of parasite virulence and immune evasion in age-structured population: the case of pertussis. *Theor. Ecol.*, 9:431–442, 2016. doi: 10.1007/s12080-016-0300-5.

A. Best. The effects of seasonal forcing on invertebrate-disease interactions with immune priming. *Bull. Math. Biol.*, 75:2241–2256, 2013. doi: 10.1007/s11538-013-9889-3.

A. Best, R.G. Bowers, and A. White. Evolution, the loss of diversity and the role of trade-offs. *Mathematical Biosciences.*, 264:86–93, 2015. doi: 10.1016/j.mbs.2015.03.011.

A. Best and A. Hoyle. A limited host immune range facilitates the creation and maintenance of diversity in parasite virulence. *Interface Focus*, 3:20130024, 2013. doi: 10.1098/rsfs.2013.0024.

A. Best, H. Tidbury, A. White, and M. Boots. The evolutionary dynamics of within-generation immune priming in invertebrate hosts. *J. R. Soc. Interface*, 10:20120887, 2013. doi: 10.1098/rsif.2012.0887.

A. Best, S. Webb, A. White, and M. Boots. Host resistance and coevolution in spatially structured populations. *Proc. R. Soc. B*, 278:2216–2222, 2011. doi: 10.1098/rspb.2010.1978.

A. Best, A. White, and M. Boots. Maintenance of host variation in tolerance to pathogens and parasites. *PNAS*, 105:20786–20791, 2008. doi: 10.1073/pnas.0809558105.

A. Best, A. White, and M. Boots. The implications of coevolutionary dynamics to host-parasite interactions. *Am. Nat.*, 173:779–791, 2009. doi: 10.1086/598494.

A. Best, A. White, and M. Boots. Resistance is futile but tolerance can explain why parasites do not always castrate their hosts. *Evolution*, 64:348–357, 2010a. doi: 10.1111/j.1558-5646.2009.00819.x.

A. Best, A. White, and M. Boots. The coevolutionary implications of host tolerance. *Evolution*, 68:1426–1435, 2014. doi: 10.1111/evo.12368.

A. Best, A. White, and M. Boots. The evolution of host defence when parasites impact reproduction. *EER*, 18:393–409, 2017a.

A. Best, A. White, E. Kisdi, J. Antonvics, M.A. Brockhurst, and M. Boots. The evolution of host-parasite range. *Am. Nat.*, 176:63–71, 2010b. doi: 10.1086/653002.

A. Best, A. White, Bowers R.G., A. Buckling, B. Koskella, and M. Boots. Host–parasite fluctuating selection in the absence of specificity. *Proc. R. Soc. B*, 284:20171615, 2017b. doi: 10.1098/rspb.2017.1615.

N. Bharti, A.J. Tatem, M.J. Ferrari, R.F. Grais, A. Djibo, and B.T. Grenfell. Explaining seasonal fluctuations of measles in niger using nighttime lights imagery. *Science*, 334:1424–1427, 2011. doi: 10.1126/science.1210554.

S. Bhatt et al. The global distribution and burden of dengue. *Nature*, 496:504–507, 2013. doi: 10.1038/nature12060.

M. Biggerstaff, S. Cauchemez, C. Reed, M. Gambhir, and L. Finelli. Estimates of the reproduction number for seasonal, pandemic, and zoonotic influenza: a systematic review of the literature. *BMC Infectious Diseases*, 14:480, 2014. doi: 10.1186/1471-2334-14-480.

O.N. Bjørnstad, W. Falck, and N.C. Stenseth. A geographic gradient in small rodent density fluctuations: a statistical modelling approach. *Proc. R. Soc. Lond. B*, 262:127–133, 1995. doi: 10.1098/rspb.1995.0186.

S. Blanchet, O. Rey, and G. Loot. Evidence for host variation in parasite tolerance in a wild fish population. *Evol. Ecol.*, 24:1129–1139, 2010. doi: 10.1007/s10682-010-9353-x.

S. Blanford, M.B. Thomas, C. Pugh, and J.K. Pell. Temperature checks the red queen? Resistance and virulence in a fluctuating environment. *Ecology Letters*, 6:2–5, 2003. doi: 10.1046/j.1461-0248.2003.00387.x.

M.H. Bonds. Host life-history strategy explains pathogen-induced sterility. *Am. Nat.*, 168:281–293, 2006. doi: 10.1086/506922.

M.H. Bonds, D.C. Keenen, A.J. Leidner, and P. Rohani. Higher disease prevalence can induce greater sociality: A game theoretic coevolutionary model. *Evolution*, 59:1859–1866, 2005. doi: 10.1111/j.0014-3820.2005.tb01056.x.

M.B. Bonsall and B. Raymond. Lethal pathogens, non-lethal synergists and the evolutionary ecology of resistance. *J. Theor. Biol.*, 254:339–349, 2008. doi: 10.1016/j.jtbi.2008.05.036.

M. Boots. Modelling insect diseases as functional predators. *Physiological Entomology*, 29:237–239, 2004. doi: 10.1111/j.0307-6962.2004.00403.x.

M. Boots. Fight or learn to live with the consequences? *TREE*, 23:248–250, 2008. doi: 10.1016/j.tree.2008.01.006.

M. Boots. The evolution of resistance to a parasite is determined by resources. *Am. Nat.*, 178:214–220, 2011. doi: 10.1086/660833.

M. Boots and M. Begon. Trade-offs with resistance to a granulosis virus in the indian meal moth, examined by a laboratory evolution experiment. *Functional Ecology*, 7:528–534, 1993. doi: 10.2307/2390128.

M. Boots, A. Best, M.R. Miller, and A. White. The role of ecological feedbacks in the evolution of host defence: what does the theory tell us? *Phil. Trans. R. Soc. B*, 364:27–36, 2009. doi: 10.1098/rstb.2008.0160.

M. Boots and R.G. Bowers. Three mechanisms of host resistance to microparasites - avoidance, recovery and tolerance - show different evolutionary dynamics. *J. Theor. Biol.*, 201:13–23, 1999. doi: 10.1006/jtbi.1999.1009.

M. Boots and R.G. Bowers. The evolution of resistance through costly acquired immunity. *Proc. R. Soc. Lond. B*, 271:715–723, 2004. doi: 10.1098/rspb.2003.2655.

M. Boots, R. Donnelly, and A. White. Optimal immune defence in the light of variation in lifespan. *Parasite Immunology*, 35:331–338, 2013. doi: 10.1111/pim.12055.

M. Boots and Y. Haraguchi. The evolution of costly resistance in host-parasite systems. *Am. Nat.*, 153:359–370, 1999. doi: 10.1086/303181.

M. Boots and M. Mealor. Local interactions select for lower pathogen infectivity. *Science*, 315:1284–1286, 2007. doi: 10.1126/science.1137126.

M. Boots and A. Sasaki. 'Small worlds' and the evolution of virulence: Infection occurs locally and at a distance. *Proc. R. Soc. Lond. B*, 266:1933–1938, 1999. doi: 10.1098/rspb.1999.0869.

M. Boots, A. White, A. Best, and R. Bowers. The importance of who infects whom: the evolution of diversity in host resistance to infectious disease. *Ecology Letters*, 15:1104–1111, 2012. doi: 10.1111/j.1461-0248.2012.01832.x.

M. Boots, A. White, A. Best, and R.G. Bowers. How specificity and epidemiology drive the coevolution of static trait diversity in hosts and parasites. *Evolution*, 68:1594–1606, 2014. doi: 10.1111/evo.12393.

R.G. Bowers, A. Hoyle, A. White, and M. Boots. The geometric theory of adaptive evolution: trade-off and invasion plots. *J. Theor. Biol.*, 233:363–377, 2005. doi: 10.1016/j.jtbi.2004.10.017.

R.G. Bowers, A. White, M. Boots, S.A.H. Geritz, and E. Kisdi. Evolutionary branching/speciation: contrasting results from systems with explicit or emergent carrying capacities. *EER*, 5:883–891, 2003.

H.J. Bremermann and J. Pickering. A game-theoretical model of parasite virulence. *J. Theor. Biol.*, 100:411–426, 1983. doi: 10.1016/0022-5193(83)90438-1.

H.J. Bremermann and H.R. Thieme. A competitive exclusion principle for pathogen virulence. *J. Math. Biol.*, 27:179–190, 1989. doi: 10.1007/BF00276102.

M.A. Brockhurst, A. Buckling, and P.B. Rainey. Spatial heterogeneity and the stability of host-parasite coexistence. *J. Evol. Biol.*, 19:374–379, 2006. doi: 10.1111/j.1420-9101.2005.01026.x.

M.A. Brockhurst, T. Chapman, K.C. King, J.E. Mank, S. Paterson, and G.D.D. Hurst. Running with the red queen: the role of biotic conflicts in evolution. *Proc. R. Soc. B*, 281:20141382, 2014. doi: 10.1098/rspb.2014.1382.

M.A. Brockhurst, A.D. Morgan, A. Fenton, and A. Buckling. Experimental coevolution with bacteria and phage: The pseudomonas fluorescens–ϕ2 model system. *Genetics and Evolution.*, 7:547–552, 2007. doi: 10.1016/j.meegid.2007.01.005.

M.A. Brockhurst, A.D. Morgan, P.B. Rainey, and A. Buckling. Population mixing accelerates coevolution. *Ecology Letters*, 6:975–979, 2003. doi: 10.1046/j.1461-0248.2003.00531.x.

E.M. Brown and D. Nathwani. Antibiotic cycling or rotation: a systematic review of the evidence of efficacy. *Journal of Antimicrobial Chemotherapy*, 55:6–9, 2005. doi: 10.1093/jac/dkh482.

F.Z. Brunner and C. Eizaguirre. Can environmental change affect host/parasite-mediated speciation? *Zoology*, 119:384–394, 2016. doi: 10.1016/j.zool.2016.04.001.

A. Buckling and P.B. Rainey. Antagonistic coevolution between a bacterium and a bacteriophage. *Proc. R. Soc. Lond. B*, 269:931–936, 2002. doi: 10.1098/rspb.2001.1945.

J.J. Bull. Optimality models of phage life history and parallels in disease evolution. *J. Theor. Biol.*, 241:928–938, 2006. doi: 10.1016/j.jtbi.2006.01.027.

J.J. Burdon. Phenotypic and genetic patterns of resistance to the pathogen phakopsora pachyrhizi in populations of glycine canescens. *Oecologia*, 73:257–267, 1987. doi: 10.1007/BF00377516.

D.L. Byers. Evolution in heterogeneous environments and the potential of maintenance of genetic variation in traits of adaptive significance. *Genetica.*, 123:107–124, 2005. doi: 10.1007/s10709-003-2721-5.

L-M. Cai, C. Modnak, and J. Wang. An age-structured model for cholera control with vaccination. *Applied Mathematics and Computation*, 299:127–140, 2017. doi: 10.1016/j.amc.2016.11.013.

D. Caillaud, F. Levréro, R. Cristescu, S. Gatti, M. Dewas, M. Douadi, A. Gautier-Hion, M. Raymond, and N. Ménard. Gorilla susceptibility to ebola virus: The cost of sociality. *Current biology*, 16:R489–R491, 2006. doi: 10.1016/j.cub.2006.06.017.

B.J. Cairns, A.R. Timms, V.A.A. Jansen, I.F. Connerton, and R.J.H. Payne. Quantitative models of *In Vitro* bacteriophage–host dynamics and their application to phage therapy. *PLoS Pathog.*, 5:e1000253, 2009. doi: 10.1371/journal.ppat.1000253.

D. Carval and R. Ferriere. A unified model for the coevolution of resistance, tolerance and virulence. *Evolution*, 64:2988–3009, 2010. doi: 10.1111/j.1558-5646.2010.01035.x.

V. Charu, S. Zeger, J. Gog, O.N. Bjørnstad, S. Kissler, L. Simonsen, B.T. Grenfell, and C. Viboud. Human mobility and the spatial transmission of influenza in the united states. *PLoS Comput. Biol.*, 13:e1005382, 2017. doi: 10.1371/journal.pcbi.1005382.

D.Z. Childs and M. Boots. The interaction of seasonal forcing and immunity and the resonance dynamics of malaria. *J. R. Soc. Interface*, 7:309–319, 2010. doi: 10.1098/rsif.2009.0178.

M. Choisy, J-F. Guégan, and P. Rohani. Dynamics of infectious diseases and pulse vaccination: Teasing apart the embedded resonance effects. *Physica D*, 223:26–35, 2006. doi: 10.1016/j.physd.2006.08.006.

F.B. Christiansen. On conditions for evolutionary stability for a continuously varying character. *Am. Nat.*, 138:37–50, 1991. doi: 10.1086/285203.

D. Cohen and S.A. Levin. Dispersal in patchy environments: The effects of temporal and spatial structure. *Theor. Pop. Biol.*, 39:63–99, 1991. doi: 10.1016/0040-5809(91)90041-D.

G.A. Colditz, T.F. Brewer, C.S. Berkey, M.E. Wilson, E. Burdick, H.V. Fineberg, and F. Mosteller. Efficacy of BCG vaccine in the prevention of tuberculosis. *JAMA*, 271:698–702, 1994. doi: 10.1001/jama.1994.03510330076038.

J. Crossan, S. Paterson, and A. Fenton. Host availability and the evolution of parasite life-history strategies. *Evolution*, 61:675–684, 2007. doi: 10.1111/j.1558-5646.2007.00057.x.

R.A. Czaja, A. Kanonik, and R.L. Burke. The effect of rainfall on predation of diamond-backed terrapin (malaclemys terrapin) nests. *Journal of Herpetology*, 52:402–405, 2018. doi: 10.1670/17-167.

T. Dallas and J.M. Drake. Fluctuating temperatures alter environmental pathogen transmission in a *Daphnia*pathogen system. *Ecology and Evolution*, 6:7931–7938, 2016. doi: 10.1002/ece3.2539.

C. Damgaard. Coevolution of a plant host-pathogen gene-for-gene system in a metapopulation model without cost of resistance or cost of virulence. *J. Theor. Biol.*, 201:1–12, 1999. doi: 10.1006/jtbi.1999.1007.

C. Darwin. *On the Origin of Species by Means of Natural Selection, or the Preservation of Favoured Races in the Struggle for Life (1st ed.)*. London: John Murray., 1859. LCCN 06017473. OCLC 741260650.

C. Darwin and A.R. Wallace. On the tendency of species to form varieties; and on the perpetuation of varieties and species by natural means of selection. *Zoological Journal of the Linnean Society*, 3:46–62, 1858. doi: 10.1111/j.1096-3642.1858.tb02500.x.

D.R. Daversa, A. Fenton, A.I. Dell, T.W.J. Garner, and A. Manica. Infections on the move: how transient phases of host movement influence disease spread. *Proc. R. Soc. B*, 84:20171807, 2017. doi: 10.1098/rspb.2017.1807.

J. Davies and D. Davies. Origins and evolution of antibiotic resistance. *Microbiology and Molecular Biology Reviews*, 74:417–433, 2010. doi: 10.1128/MMBR.00016-10.

C. de Mazancourt and U. Dieckmann. Trade-off geometries and frequency-dependent selection. *Am. Nat.*, 164:765–778, 2004. doi: 10.1086/424762.

F. Débarre, S. Lion, M. van Baalen, and S. Gandon. Evolution of host life-history traits in a spatially structured host-parasite system. *Am. Nat.*, 179:52–63, 2012. doi: 10.1086/663199.

C. Deerenberg, V. Arpanius, S. Daan, and N. Bos. Reproductive effort decreases antibody responsiveness. *Proc. R. Soc. B*, 264:1021–1029, 1997. doi: 10.1098/rspb.1997.0141.

S. Dey and A. Joshi. Stability via asynchrony in *Drosophila* metapopulations with low migration rates. *Science*, 312:434–436, 2006. doi: 10.1126/science.1125317.

A.A. Dhondt et al. Dynamics of a novel pathogen in an avian host: Mycoplasmal conjunctivitis in house finches. *Acta Tropica*, 94:77–93, 2005. doi: 10.1016/j.actatropica.2005.01.009.

A.A. Dhondt, S.L. States, K.V. Dhondt, and K.A. Schat. Understanding the origin of seasonal epidemics of mycoplasmal conjunctivitis. *Journal of Animal Ecology*, 81:996–1003, 2012. doi: 10.1111/j.1365-2656.2012.01986.x.

U. Dieckmann and R. Law. The dynamical theory of coevolution: a derivation from stochastic ecological processes. *J. Math. Biol.*, 34:579–612, 1996. doi: 10.1007/BF02409751.

O. Diekmann, J.A.P. Heesterbeek, and J.A.J. Metz. On the definition and the computation of the basic reproduction ratio R_0 in models for infectious diseases in heterogeneous populations. *J. Math. Biol.*, 28:365–382, 1990. doi: 10.1007/BF00178324.

K. Dietz. The incidence of infectious diseases under the influence of seasonal fluctuations. *Mathematical Models in Medicine*, 11:1–15, 1976. doi: 10.1007/978-3-642-93048-5_1.

I. Díez-Delgado et al. Impact of piglet oral vaccination against tuberculosis in endemic freeranging wild boar populations. *Preventive Veterinary Medicine*, 155:11–20, 2018. doi: 10.1016/j.prevetmed.2018.04.002.

M. Doebeli and G.D. Ruxton. Evolution of dispersal rates in metapopulation models: Branching and cyclic dynamics in phenotype space. *Evolution*, 51:1730–1741, 1997.

E. Doedel and B. Oldman. *AUTO 07-p: Continuation and bifurcation software for ordinary differential equations.* Concordia University., 2009.

R. Donnelly, A. Best, A. White, and M. Boots. Seasonality selects for more acutely virulent parasites when virulence is density dependent. *Proc. R. Soc. B*, 280:20122464, 2013. doi: 10.1098/rspb.2012.2464.

R. Donnelly, A. White, and M. Boots. The epidemiological feedbacks critical to the evolution of host immunity. *J. Evol. Biol.*, 28:2042–2053, 2015. doi: 10.1111/jeb.12719.

R. Donnelly, A. White, and M. Boots. Host lifespan and the evolution of resistance to multiple parasites. *J. Evol. Biol.*, 30:561–570, 2017. doi: 10.1111/jeb.13025.

A.M. Dorélien, S. Ballesteros, and B.T. Grenfell. Impact of birth seasonality on dynamics of acute immunizing infections in sub-saharan africa. *PLoS ONE*, 8:e75806, 2013. doi: 10.1371/journal.pone.0075806.

S.M. Duke-Sylvester, L. Bolzoni, and L.A. Real. Strong seasonality produces spatial asynchrony in the outbreak of infectious diseases. *J. R. Soc. Interface*, 8:817–825, 2011. doi: 10.1098/rsif.2010.0475.

A.B. Duncan, E. Dusi, F. Jacob, J. Ramsayer, M.E. Hochberg, and O. Kaltz. Hot spots become cold spots: coevolution in variable temperature environments. *J. Evol. Biol.*, 30:55–65, 2017. doi: 10.1111/jeb.12985.

P.P. Edger et al. The butterfly plant arms-race escalated by gene and genome duplications. *PNAS*, 112:8362–8366, 2015. doi: 10.1073/pnas.1503926112.

J. Engelstädter. Host-parasite coevolutionary dynamics with generalized success/failure infection genetics. *Am. Nat.*, 185:E117–E129, 2015. doi: 10.1086/680476.

P.M. Enriquez-Navas et al. Exploiting evolutionary principles to prolong tumor control in preclinical models of breast cancer. *Sci. Transl. Med.*, 8:327ra24, 2016. doi: 10.1126/scitranslmed.aad7842.

B. Ernande and U. Dieckmann. The evolution of phenotypic plasticity in spatially structured environments: implications of intraspecific competition, plasticity costs and environmental characteristics. *J. Evol. Biol.*, 17:613–628, 2004. doi: 10.1111/j.1420-9101.2004.00691.x.

I. Eshel. Evolutionary and continuous stability. *J. Theor. Biol.*, 103:99–111, 1983. doi: 10.1016/0022-5193(83)90201-1.

D.A. Ewing, C.A. Cobbold, B.V. Purse, M.A. Nunn, and S.M. White. Modelling the effect of temperature on the seasonal population dynamics of temperate mosquitoes. *J. Theor. Biol.*, 400:65–79, 2016. doi: 10.1016/j.jtbi.2016.04.008.

D. Fels and O. Kaltz. Temperature dependent transmission and latency of *Holospora-raundulata*, a micronucleus-specific parasite of the ciliate *Paramecium caudatum*. *Proc. R. Soc. B*, 273:1031–1038, 2006. doi: 10.1098/rspb.2005.3404.

A. Fenton, J. Antonovics, and M.A. Brockhurst. Inverse-gene-for-gene infection genetics and coevolutionary dynamics. *Am. Nat.*, 174:E230–E242, 2009. doi: 10.1086/645087.

A. Fenton, J. Antonovics, and M.A. Brockhurst. Two-step infection processes can lead to coevolution between functionally independent infection and resistance pathways. *Evolution*, 66:2030–2041, 2012. doi: 10.1111/j.1558-5646.2012.01578.x.

A. Fenton and M.A. Brockhurst. Epistatic interactions alter dynamics of multi-locus gene-for-gene coevolution. *PLoS ONE*, 2:e1156, 2007. doi: 10.1371/journal.pone.0001156.

A. Fenton, T. Hakalahti, M. Bandilla, and E.T. Valtonen. The impact of variable hatching rates on parasite control: A model of an aquatic ectoparasite in a finnish fish farm. *Journal of Applied Ecology*, 43:660–668, 2006a. doi: 10.1111/j.1365-2664.2006.01176.x.

A. Fenton, K.N. Johnson, Brownlie J.C., and G.D.D. Hurst. Solving the wolbachia paradox: Modeling the tripartite interaction between host, wolbachia, and a natural enemy. *Am. Nat.*, 178:333–342, 2011. doi: 10.1086/661247.

A. Fenton, J. Lello, and M.B. Bonsall. Pathogen responses to host immunity: The impact of time delays and memory on the evolution of virulence. *Proc. R. Soc. B*, 273:2083–2090, 2006b. doi: 10.1098/rspb.2006.3552.

N.M. Ferguson, D.A.T. Cummings, C. Fraser, J.C. Cajka, P.C. Cooley, and D.S. Burke. Strategies for mitigating an influenza pandemic. *Nature*, 442:448–452, 2006. doi: 10.1038/nature04795.

C. Ferris and A. Best. The evolution of host defence to parasitism in fluctuating environments. *J. Theor. Biol.*, 440:58–65, 2018. doi: 10.1016/j.jtbi.2017.12.006.

C.E. Ferris and A. Best. Can temporal fluctuations select for diversity in host tolerance to parasitism? Submitted.

C.E. Ferris, R.C.T. Wright, A. Best, and M.A. Brockhurst. The intensity of host-parasite coevolution peaks in seasonal environments that oscillate at intermediate amplitudes. In prep.

P.E.M. Fine and J.A. Clarkson. Measles in england and walesi: an analysis of factors underlying seasonal patterns. *Int. J. Epidemiol.*, 11:5–14, 1982. doi: 10.1093/ije/11.1.15.

B.F. Finkenstädt and B.T. Grenfell. Time series modelling of childhood diseases: a dynamical systems approach. *Appl. Stat.*, 49:182–205, 2000. doi: 10.1111/1467-9876.00187.

H.H. Flor. The complementary genic systems in flax and flax rust. *Advanced Genetics*, 8:29–54, 1956.

S.A. Ford and K.C. King. Harnessing the power of defensive microbes: Evolutionary implications in nature and disease control. *PLoS Pathog.*, 12:e1005465, 2016. doi: 10.1371/journal.ppat.1005465.

S.E. Forde, R.E. Beardmore, I. Gudelj, S.S. Arkin, J.N. Thompson, and L.D. Hurst. Understanding the limits to generalizability of experimental evolutionary models. *Nature*, 455:220–223, 2008. doi: 10.1038/nature07152.

S.E. Forde, J.N. Thompson, and B.J.M. Bohannan. Adaptation varies through space and time in a coevolving hostparasitoid interaction. *Nature*, 431:841–844, 2004. doi: 10.1038/nature02906.

J. Fornoni, J. Núñez-Farfán, P.L. Valverde, and M.D. Rausher. Evolution of mixed strategies of plant defense allocation against natural enemies. *Evolution*, 58:1685–1695, 2004.

S.A. Frank. Evolution of host-parasite diversity. *Evolution*, 47:1721–1732, 1993. doi: 10.2307/2410216.

S.A. Frank. Specific and non-specific defense against parasitic attack. *J. Theor. Biol.*, 202:283–304, 2000. doi: 10.1006/jtbi.1999.1054.

V-P. Friman and J. Laakso. Pulsed-resource dynamics constrain the evolution of predator–prey interactions. *Am. Nat.*, 177:334–345, 2011. doi: 10.1086/658364.

V-P. Friman, J. Laakso, M. Koivu-Orava, and T. Hiltunen. Pulsed-resource dynamics increase the asymmetry of antagonistic coevolution between a predatory protist and a prey bacterium. *J. Evol. Biol.*, 24:2563–2573, 2011. doi: 10.1111/j.1420-9101.2011.02379.x.

M.A. Fuentes and E. Ferrada. Environmental fluctuations and their consequences for the evolution of phenotypic diversity. *Front. Phys.*, 5:16, 2017. doi: 10.3389/fphy.2017.00016.

A.I. Furness. The evolution of an annual life cycle in killifish: adaptation to ephemeral aquatic environments through embryonic diapause. *Biol. Rev.*, 91:796–812, 2016. doi: 10.1111/brv.12194.

J.R. Fuxa and A.R. Richter. Reversion of resistance by *Spodoptera frugiperda* to nuclear polyhedrosis virus. *Journal of Invertebrate Pathology*, 53:52–56, 1989. doi: 10.1016/0022-2011(89)90073-6.

S. Gandon, P. Agnew, and Y. Michalakis. Coevolution between parasite virulence and host life-history traits. *Am. Nat.*, 160:374–388, 2002. doi: 10.1086/341525.

S. Gandon, A. Buckling, E. Decaestecker, and T. Day. Host–parasite coevolution and patterns of adaptation across time and space. *J. Evol. Biol.*, 21:1861–1866, 2008. doi: 10.1111/j.1420-9101.2008.01598.x.

S. Gandon and T. Day. Evolutionary epidemiology and the dynamics of adaptation. *Evolution*, 63:826–838, 2009. doi: 10.1111/j.1558-5646.2009.00609.x.

A.J. Garrison, A.D. Miller, M.R. Ryan, S.H. Roxburgh, and K. Shea. Stacked crop rotations exploit weed-weed competition for sustainable weed management. *Weed Science*, 62:166–176, 2014. doi: 10.1614/WS-D-13-00037.

S.D. Gehrt. Seasonal survival and cause-specific mortality of urban and rural striped skunks in the absence of rabies. *Journal of Mammalogy*, 86:1164–1170, 2005. doi: 10.1644/04-MAMM-A-173R2.1.

N.M. Gerardo et al. Immunity and other defenses in pea aphids, acyrthosiphon pisum. *Genome Biology*, 11:R21, 2010. doi: 10.1186/gb-2010-11-2-r21.

S.A.H. Geritz, E. Kisdi, G. Meszéna, and J.A.J. Metz. Evolutionarily singular strategies and the adaptive growth and branching of the evolutionary tree. *Evol. Ecol.*, 12:35–57, 1998. doi: 10.1023/A:1006554906681.

S.A.H. Geritz, E. Kisdi, and P. Yan. Evolutionary branching and long-term coexistence of cycling predators: critical function analysis. *Theor. Pop. Biol.*, 71:424–435, 2007. doi: 10.1016/j.tpb.2007.03.006.

A.K. Gibson, K.S. Stoy, and C.M. Lively. Bloody-minded parasites and sex: the effects of fluctuating virulence. *J. Evol. Biol.*, 31:611–620, 2018. doi: 10.1111/jeb.13252.

J.H. Gillespie and M. Turelli. Genotype-environment interactions and the maintenance of polygenic variation. *Genetics*, 141:129–138, 1989.

J.R. Gog. The impact of evolutionary constraints on influenza dynamics. *Vaccine*, 26S:C15–C24, 2008. doi: 10.1016/j.vaccine.2008.04.008.

J.R. Gog, S. Ballesteros, C. Viboud, L. Simonsen, O.N. Bjornstad, J. Shaman, D.L. Chao, F. Khan, and B.T. Grenfell. Spatial transmission of 2009 pandemic influenza in the us. *PLoS Comput. Biol.*, 10:e1003635, 2014. doi: 10.1371/journal.pcbi.1003635.

J.F. Gogarten et al. Seasonal mortality patterns in non-human primates: implications for variation in selection pressures across environments. *Evolution*, 66:3252–3266, 2012. doi: 10.1111/j.1558-5646.2012.01668.x.

P. Gomez and A. Buckling. Bacteria-phage antagonistic coevolution in soil. *Science*, 332:106–109, 2011. doi: 10.1126/science.1198767.

A. Gómez-Corral and M.L. García. Control strategies for a stochastic model of host–parasite interaction in a seasonal environment. *J. Theor. Biol.*, 354:1–11, 2014. doi: 10.1016/j.jtbi.2014.03.021.

N.C. Grassly and C. Fraser. Seasonal infectious disease epidemiology. *Proc. R. Soc. B*, 273:2541–2550, 2006. doi: 10.1098/rspb.2006.3604.

J. Greenman, M. Kamo, and M. Boots. External forcing of ecological and epidemiological systems: a resonance approach. *Physica D*, 190:136–151, 2004. doi: 10.1016/j.physd.2003.08.008.

E.C. Griffiths, A.B. Pedersen, A. Fenton, and O.L. Petchey. Analysis of a summary network of co-infection in humans reveals that parasites interact most via shared resources. *Proc. R. Soc. B*, 281:20132286, 2014. doi: 10.1098/rspb.2013.2286.

R. Grimshaw. *Nonlinear Ordinary Differential Equations.* Blackwell Scientific Publications, 1990. ISBN 0-632-02708-8.

Z. Grossman. Oscillatory phenomena in a model of infectious diseases. *Theor. Pop. Biol.*, 18:204–243, 1980.

F.M. Guerra, B. Bolotin, G. Lim, J. Heffernan, S.L. Deeks, Y. Li, and N.S. Crowcroft. The basic reproduction number (R_0) of measles: a systematic review. *Lancet Infect. Dis.*, 17:e420–28, 2017. doi: 10.1016/S1473-3099(17)30307-9.

S.C. Hackett and M.B. Bonsall. Type of fitness cost influences the rate of evolution of resistance to transgenic bt crops. *Journal of Applied Ecology*, 53:1391–1401, 2016. doi: 10.1111/1365-2664.12680.

A.R. Hall, P.D. Scanlan, A.D. Morgan, and A. Buckling. Host–parasite coevolutionary arms races give way to fluctuating selection. *Ecology Letters*, 14:635–642, 2011. doi: 10.1111/j.1461-0248.2011.01624.x.

S.L. Haller, C. Peng, G. McFadden, and S. Rothenburg. Poxviruses and the evolution of host range and virulence. *Infection, Genetics and Evolution*, 21:15–40, 2014. doi: 10.1016/j.meegid.2013.10.014.

F.M. Hamelin, M. Castel, S. Poggi, D. Andrivon, and L. Mailleret. Seasonality and the evolutionary divergence of plant parasites. *Ecology*, 92:2159–2166, 2011. doi: 10.1890/10-2442.1.

W.D. Hamilton. Extraordinary sex ratios. *Science*, 156:477–488, 1967. doi: 10.1126/science.156.3774.477.

I. Hanski, L. Hansson, and H. Henttonen. Specialist predators, generalist predators, and the microtine rodent cycle. *Journal of Animal Ecology*, 60:353–367, 1991. doi: 10.2307/5465.

L. Hansson and H. Henttonen. Rodent dynamics as community processes. *TREE*, 3:195–200, 1988. doi: 10.1016/0169-5347(88)90006-7.

Y. Haraguchi and A. Sasaki. Host-parasite arms race in mutation modifications: Indefinite escalation despite a heavy load? *J. Theor. Biol.*, 183:121–137, 1996. doi: 10.1006/jtbi.1996.9999.

Y. Haraguchi and A. Sasaki. The evolution of parasite virulence and transmission rate in a spatially structured population. *J. Theor. Biol.*, 203:85–96, 2000. doi: 10.1006/jtbi.1999.1065.

E. Harrison, A-L. Laine, M. Hietala, and M.A. Brockhurst. Rapidly fluctuating environments constrain coevolutionary arms races by impeding selective sweeps. *Proc. R. Soc. B*, 280:20130937, 2013. doi: 10.1098/rspb.2013.0937.

N.A. Hartemink, S.E. Randolph, S.A. Davis, and J.A.P. Heesterbeek. The basic reproduction number for complex disease systems: Defining R_0 for tick-borne infections. *Am. Nat.*, 171:734–754, 2008. doi: 10.1086/587530.

G. Hartvigsen and S. Levin. Evolution and spatial structure interact to influence plant-herbivore population and community dynamics. *Proc. R. Soc. Lond. B*, 264:1677–1685, 1997. doi: 10.1098/rspb.1997.0233.

A.D. Hayward, D.H. Nussey, A.J. Wilson, C. Berenos, J.G. Pilkington, K.A. Watt, J.M. Pemberton, and A.L. Graham. Natural selection on individual variation in tolerance of gastrointestinal nematode infection. *PLOS Biol.*, 12:e1001917, 2014. doi: 10.1371/journal.pbio.1001917.

D. He and D.J.D. Earn. Epidemiological effects of seasonal oscillations in birth rates. *Theor. Pop. Biol.*, 72:274–291, 2007. doi: 10.1016/j.tpb.2007.04.004.

S. Heilmann, K. Sneppen, and S. Krishna. Sustainability of virulence in a phage-bacterial ecosystem. *Journal of Virology*, 84:3016–3022, 2010. doi: 10.1128/JVI.02326-09.

S. Heilmann, K. Sneppen, and S. Krishna. Coexistence of phage and bacteria on the boundary of self-organized refuges. *PNAS*, 109:12828–12833, 2012. doi: 10.1073/pnas.1200771109.

M.D. Herron and M. Doebeli. Adaptive diversification of a plastic trait in a predictably fluctuating environment. *J. Theor. Biol.*, 285:58–68, 2011. doi: 10.1016/j.jtbi.2011.06.007.

F. Hilker and H. Malchow. Strange periodic attractors in a prey-predator system with infected prey. *Mathematical Population Studies*, 13:119–134, 2006. doi: 10.1080/08898480600788568.

T. Hiltunen, G.B. Ayan, and L. Becks. Environmental fluctuations restrict eco-evolutionary dynamics in predator–prey system. *Proc. R. Soc. B*, 282:20150013, 2015. doi: 10.1098/rspb.2015.0013.

T. Hiltunen, V-P. Friman, V. Kaitala, J. Mappes, and J. Laakso. Predation and resource fluctuations drive eco-evolutionary dynamics of a bacterial community. *Acta Oecol.*, 38:77–83, 2012. doi: 10.1016/J.Actao.2011.09.010.

B.T. Hirsch, J.J.H. Reynolds, S.D. Gehrt, and M.E. Craft. Which mechanisms drive seasonal rabies outbreaks in raccoons? A test using dynamic social network models. *Journal of Applied Ecology*, 53:804–813, 2016. doi: 10.1111/1365-2664.12628.

M.E. Hochberg and M. van Baalen. Antagonistic coevolution over productivity gradients. *Am. Nat.*, 152:620–634, 1998. doi: 10.1086/286194.

C.G. Hochwender, R.J. Marquis, and K.A. Stowe. The potential for and constraints on the evolution of compensatory ability in *Asclepias syriaca*. *Oecologia*, 122:361–370, 2000. doi: 10.1007/s004420050042.

F. Horns and M.E. Hood. The evolution of disease resistance and tolerance in spatially structured populations. *Ecol. and Evol.*, 2:1705–1711, 2012. doi: 10.1002/ece3.290.

P.R. Hosseini, A.A. Dhondt, and A. Dobson. Seasonality and wildlife disease: How seasonal birth, aggregation and variation inimmunity affect the dynamics of mycoplasma gallisepticum in house finches. *Proc. R. Soc. Lond. B*, 271:2569–2577, 2004. doi: 10.1098/rspb.2004.2938.

V.M. Howick and B.P. Lazzaro. The genetic architecture of defence as resistance to and tolerance of bacterial infection in *Drosophila melanogaster*. *Molecular Ecology*, 26:1533–1546, 2017. doi: 10.1111/mec.14017.

A. Hoyle, A. Best, and R.G. Bowers. Evolution of host resistance towards pathogen exclusion: the role of predators. *EER*, 14:125–146, 2012.

A. Hoyle, R.G. Bowers, and A. White. Evolutionary behaviour, trade-offs and cyclic and chaotic population dynamics. *Bull. Math. Biol.*, 73:1154–1169, 2011. doi: 10.1007/s11538-010-9567-7.

A. Hoyle, R.G. Bowers, A. White, and M. Boots. The influence of trade-off shape on evolutionary behaviour in classical ecological scenarios. *J. Theor. Biol.*, 250:498–511, 2008. doi: 10.1016/j.jtbi.2007.10.009.

Y-H. Hsieh and C-K. Hsiao. Predatorprey model with disease infection in both populations. *Mathematical Medicine and Biology*, 25:247–266, 2008. doi: 10.1093/imammb/dqn017.

G.L. Hughes, R. Koga, P. Xue, T. Fukatsu, and J.L. Rasgon. *Wolbachia* infections are virulent and inhibit the human malaria parasite *Plasmodium Falciparum* in *Anopheles Gambiae*. *PLoS Pathog.*, 7:e1002043, 2011. doi: 10.1371/journal.ppat.1002043.

C. Hui. Carrying capacity, population equilibrium, and environment's maximal load. *Ecological Modelling.*, 192:317–320, 2006. doi: 10.1016/j.ecolmodel.2005.07.001.

G.D.D. Hurst, E.L. Purvis, J.J. Sloggett, and M.E.N. Majerus. The effect of infection with male-killing rickettsia on the demography of female *Adalia bipunctata* l. (two spot ladybird). *Heredity*, 73:309–316, 1994. doi: 10.1038/hdy.1994.138.

N. Imai, I. Dorigatti, S. Cauchemez, and N.M. Ferguson. Estimating dengue transmission intensity from case-notification data from multiple countries. *PLoS Negl. Trop. Dis.*, 10:e0004833, 2016. doi: 10.1371/journal.pntd.0004833.

H. Inaba. Endemic threshold analysis for the Kermack-McKendrick reinfection model. *Josai Mathematical Monographs*, 9:105–133, 2016.

A. Ives, K. Gross, and J. Klug. Stability and variability in competitive communities. *Science*, 286:542–544, 1999. doi: 10.1126/science.286.5439.542.

J. Jaenike, R. Unckless, S.N. Cockburn, L.M. Boelio, and S.J. Perlman. Adaptation via symbiosis: Recent spread of a *Drosophila* defensive symbiont. *Science*, 329:212–215, 2010. doi: 10.1126/science.1188235.

S.D. Jayakar. A mathematical model for interaction of gene frequencies in a parasite and its host. *Theor. Pop. Biol.*, 1:140–164, 1970. doi: 10.1016/0040-5809(70)90032-8.

Y. Jian, S. Silvestri, E. Belluco, A. Saltarin, G. Chillemi, and M. Marani. Environmental forcing and density-dependent controls of *Culex pipiens* abundance in a temperate climate (northeastern italy). *Ecological Modelling*, 272:301–310, 2014. doi: 10.1016/j.ecolmodel.2013.10.019.

J. Johansson and J. Ripa. Will sympatric speciation fail due to stochastic competitive exclusion? *Am. Nat.*, 168:572–578, 2006. doi: 10.1086/507996.

M.A. Johansson, J. Hombach, and D.A.T. Cummings. Models of the impact of dengue vaccines: A review of current research and potential approaches. *Vaccine*, 29:5860–5868, 2011. doi: 10.1016/j.vaccine.2011.06.042.

E.O. Jones, A. White, and M. Boots. The evolution of host protection by vertically transmitted parasites. *Proc. R. Soc. B*, 278:863–870, 2011. doi: 10.1098/rspb.2010.1397.

S.C. Jung, A. Martinez-Medina, J.A. Lopez-Raez, and M.J. Pozo. Mycorrhiza-induced resistance and priming of plant defenses. *J. Chem. Ecol.*, 38:651–664, 2012. doi: 10.1007/s10886-012-0134-6.

S. Kada and S. Lion. Superinfection and the coevolution of parasite virulence and host recovery. *J. Evol. Biol.*, 28:2285–2299, 2015. doi: 10.1111/jeb.12753.

V. Kaitala, P. Lundberg, J. Ripa, and J. Ylikarjula. Red, blue and green: Dyeing population dynamics. *Ann. Zool. Fennici.*, 34:217–228, 1997.

M. Kamo and A. Sasaki. The effect of cross-immunity and seasonal forcing in a multi-strain epidemic model. *Physica D*, 165:228–241, 2002. doi: 10.1016/S0167-2789(02)00389-5.

M. Kamo, A. Sasaki, and M. Boots. The role of trade-off shapes in the evolution of parasites in spatial host populations: An approximate analytical approach. *J. Theor. Biol.*, 244:588–596, 2007. doi: 10.1016/j.jtbi.2006.08.013.

S.M. Karve, D. Bhave, D. Nevgi, and S. Dey. *Escherichia coli* populations adapt to complex, unpredictable fluctuations by minimizing trade-offs across environments. *J. Evol. Biol.*, 29:2545–2555, 2016. doi: 10.1111/jeb.12972.

A. Kause, S. van Dalen, and H. Bovenhuis. Genetics of ascites resistance and tolerance in chicken: A random regression approach. *G3*, 2:527–535, 2012. doi: 10.1534/g3.112.002311/-/DC1.

M.J. Keeling and K.T.D. Eames. Networks and epidemic models. *J. R. Soc. Interface*, 2:295–307, 2005. doi: 10.1098/rsif.2005.0051.

M.J. Keeling, P. Rohani, and B.T. Grenfell. Seasonally forced disease dynamics explored as switching between attractors. *Physica D*, 148:317–335, 2001. doi: 10.1016/S0167-2789(00)00187-1.

W.O. Kermack and A.G. McKendrick. Contributions to the mathematical theory of epidemics I. *Proceedings of the Royal Society*, 115A:700–721, 1927. (reprinted in Bulletin of Mathematical Biology 53(1/2): 33-55, 1991).

W.O. Kermack and A.G. McKendrick. Contributions to the mathematical theory of epidemics II. the problem of endemicity. *Proceedings of the Royal Society*, 138A:55–83, 1932. (reprinted in Bulletin of Mathematical Biology 53(1/2): 57-87, 1991).

W.O. Kermack and A.G. McKendrick. Contributions to the mathematical theory of epidemics [iii]. further studies of the problem of endemicity. *Proceedings of the Royal Society*, 141A:94–122, 1933. (reprinted in Bulletin of Mathematical Biology 53(1/2): 89-118, 1991).

B. Kerr, C. Neuhauser, B.J.M. Bohannan, and A.M. Dean. Local migration promotes competitive restraint in a host-pathogen tragedy of the commons. *Nature*, 442:75–78, 2006. doi: 10.1038/nature04864.

E.D. Ketterson, A.M. Fudickar, J.W. Atwell, and T.J. Greives. Seasonal timing and population divergence: when to breed, when to migrate. *Current Opinion in Behavioral Sciences*, 6:50–58, 2015. doi: 10.1016/j.cobeha.2015.09.001.

S. Kim, T.D. Lieberman, and R. Kishony. Alternating antibiotic treatments constrain evolutionary paths to multidrug resistance. *PNAS*, 111:14494–14499, 2014. doi: 10.1073/pnas.1409800111.

E. Kisdi. Evolutionary branching under asymmetric competition. *J. Theor. Biol.*, 197:149–162, 1999. doi: 10.1006/jtbi.1998.0864.

E. Kisdi. Trade-off geometries and the adaptive dynamics of two co-evolving species. *EER*, 8:959–973, 2006.

E. Kisdi and S.A.H. Geritz. Adaptive dynamics in allele space: Evolution of genetic polymorphism by small mutations in a heterogeneous environment. *Evolution*, 53:993–1008, 1999.

C.A. Klausmeier. Floquet theory: a useful tool for understanding nonequilibrium dynamics. *Theor. Ecol.*, 1:153–161, 2008. doi: 10.1007/s12080-008-0016-2.

I. Klemme and A. Karvonen. Vertebrate defense against parasites: Interactions between avoidance, resistance, and tolerance. *Ecology and Evolution*, 7:561–571, 2017. doi: 10.1002/ece3.2645.

D. Klinkenberg, S.J.M. Hahné, T. Woudenberg, and J. Wallinga. The reduction of measles transmission during school vacations. *Epidemiology*, 29:562–570, 2018. doi: 10.1097/EDE.0000000000000841.

S.C.L. Knowles, A. Fenton, and A.B. Pedersen. Epidemiology and fitness effects of wood mouse herpesvirus in a natural host population. *Journal of General Virology*, 93:2447–2456, 2012. doi: 10.1099/vir.0.044826-0.

A.L. Koch. Control of the bacterial cell cycle by cytoplasmic growth. *Critical Reviews in Microbiology*, 28:61–77, 2002. doi: 10.1080/1040-840291046696.

K. Koelle, M. Pascual, and M. Yunus. Pathogen adaptation to seasonal forcing and climate change. *Proc. R. Soc. B*, 272:971–977, 2005. doi: 10.1098/rspb.2004.3043.

T. Koskela, S. Puustinen, V. Salonen, and P. Mutikainen. Resistance and tolerance in a host plant-holoparasitic plant interaction: Genetic variation and costs. *Evolution*, 56:899–908, 2002.

B. Koskella and M.A. Brockhurst. Bacteriaphage coevolution as a driver of ecological and evolutionary processes in microbial communities. *FEMS, Microbiol. Rev.*, 38:916–931, 2014. doi: 10.1111/1574-6976.12072.

R.D. Kouyos, M. Salathé, and S. Bonhoeffer. The red queen and the persistence of linkage-disequilibrium oscillations in finite and infinite populations. *BMC Evolutionary Biology*, 7:211, 2007. doi: 10.1186/1471-2148-7-211.

R.D. Kouyos, M. Salathé, S.P. Otto, and S. Bonhoeffer. The role of epistasis on the evolution of recombination in host-parasite coevolution. *Theor. Pop. Biol.*, 75:1–13, 2009. doi: 10.1016/j.tpb.2008.09.007.

P.X. Kover and B.A. Schaal. Genetic variation for disease resistance and tolerance among *Arabidopsis thaliana* accessions. *PNAS*, 99:11270–11274, 2002. doi: 10.1073/pnas.102288999.

A.R. Kraaijeveld and H.C.J. Godfray. Trade-off between parasitoid resistance and larval competitive ability in *Drosophila melanogaster*. *Nature*, 389:278–280, 1997. doi: 10.1038/38483.

A. Kucharski and J.R. Gog. Influenza emergence in the face of evolutionary constraints. *Proc. R. Soc. B*, 279:645–652, 2012. doi: 10.1098/rspb.2011.1168.

Y.A. Kuznetsov. *Elements of Applied Bifurcation Theory.* Springer, 2nd edition, 1998.

A-L. Laine. Pathogen fitness components and genotypes differ in their sensitivity to nutrient and temperature variation in a wild plant–pathogen association. *J. Evol. Biol.*, 20:2371–2378, 2007. doi: 10.1111/j.1420-9101.2007.01406.x.

A-L. Laine. Role of coevolution in generating biological diversity: spatially divergent selection trajectories. *Journal of Experimental Botany*, 60:2957–2970, 2009. doi: 10.1093/jxb/erp168.

L. Lambrechts, J-M. Chavatte, G. Snounou, and J.C. Koella. Environmental influence on the genetic basis of mosquito resistance to malaria parasites. *Proc. R. Soc. B*, 273:1501–1506, 2006. doi: 10.1098/rspb.2006.3483.

D.A. Landis, S.D. Wratten, and G.M. Gurr. Habitat management to conserve natural enemies of arthropod pests in agriculture. *Annu. Rev. Entomol.*, 45:175–201, 2000. doi: 10.1146/annurev.ento.45.1.175.

B.P. Lazzaro and T.J. Little. Immunity in a variable world. *Phil. Trans. R. Soc. B*, 364:15–26, 2009. doi: 10.1098/rstb.2008.0141.

B.P. Lazzaro, T.B. Sackton, and A.G. Clark. Genetic variation in *Drosophila melanogaster* resistance to infection: A comparison across bacteria. *Genetics*, 174:1539–1554, 2006. doi: 10.1534/genetics.105.054593.

B.P. Lazzaro, B.K. Sceurman, and A.G. Clark. Genetic basis of natural variation in *D. melanogaster* antibacterial immunity. *Science*, 303:1873–1876, 2004. doi: 10.1534/genetics.105.054593.

K.A. Lee. Linking immune defenses and life history at the levels of the individual and the species. *Integrative and Comparative Biology*, 46:1000–1015, 2006. doi: 10.1093/icb/iclO49.

S. Lee and G. Chowell. Exploring optimal control strategies in seasonally varying flu-like epidemics. *J. Theor. Biol.*, 412:36–47, 2017. doi: 10.1016/j.jtbi.2016.09.023.

T. Lefèvre, A.J. Williams, and J.C. de Roode. Genetic variation in resistance, but not tolerance, to a protozoan parasite in the monarch butterfly. *Proc. R. Soc. B*, 278:751–759, 2011. doi: 10.1098/rspb.2010.1479.

O. Leimar. The evolution of phenotypic polymorphism: Randomized strategies versus evolutionary branching. *Am Nat.*, 165:669–681, 2005. doi: 10.1086/429566.

O. Leimar. Environmental and genetic cues in the evolution of phenotypic polymorphism. *Evol. Ecol.*, 23:125–135, 2009. doi: 10.1007/s10682-007-9194-4.

O. Leimar, P. Hammerstein, and T.J.M. Van Dooren. A new perspective on developmental plasticity and the principles of adaptive morph determination. *Am. Nat.*, 167:367–376, 2006. doi: 10.1086/499566.

J. Lello, R.A. Norman, B. Boag, P.J. Hudson, and A. Fenton. Pathogen interactions, population cycles, and phase shifts. *Am. Nat.*, 171:176–182, 2008. doi: 10.1086/525257.

R.E. Lenski and B.R. Levin. Constraints on the coevolution of bacteria and virulent phage: A model, some experiments, and predictions for natural communities. *Am. Nat.*, 125:585–602, 1985. doi: 10.1086/284364.

K.J. Leonard. Selection pressures and plant pathogens. *Annals of the New York Academy of Sciences*, 1:207–222, 1977. doi: 10.1111/j.1749-6632.1977.tb34240.x.

S. Levin and D. Pimental. Selection of intermediate rates of increase in parasite-host systems. *Am. Nat.*, 117:308–315, 1981.

S.B. Levy and B. Marshall. Antibacterial resistance worldwide: causes, challenges and responses. *Nature medicine*, 10:S122–S129, 2004. doi: 10.1038/nm1145.

C-J. Lin, K.A. Deger, and J.H. Tien. Modeling the trade-off between transmissibility and contact in infectious disease dynamics. *Mathematical Biosciences*, 277:15–24, 2016. doi: 10.1016/j.mbs.2016.03.010.

S. Lion and J.A.J. Metz. Beyond R0 maximisation: On pathogen evolution and environmental dimensions. *Trends in Ecology and Evolution*, 33:458–473, 2018. doi: 10.1016/j.tree.2018.02.004.

M. Lipsitch et al. Transmission dynamics and control of severe acute respiratory syndrome. *Science*, 300:1966–1970, 2003. doi: 10.1126/science.1086616.

E. Litchman and C.A. Klausmeier. Trait-based community ecology of phytoplankton. *Annu. Rev. Ecol. Evol. Syst.*, 39:615–639, 2008. doi: 10.1146/annurev.ecolsys.39.110707.173549.

C.M. Lively. The effect of host genetic diversity on disease spread. *Am. Nat.*, 175:E149–E152, 2010a. doi:010.1086/652430.

C.M. Lively. An epidemiological model of host–parasite coevolution and sex. *J. Evol. Biol.*, 23:1490–1497, 2010b. doi: 10.1111/j.1420-9101.2010.02017.x.

D.M. Livermore. Bacterial resistance: Origins, epidemiology, and impact. *Clinical Infectious Diseases*, 36:S11–S23, 2003. doi: 10.1086/344654.

W.P. London and J.A. Yorke. Recurrent outbreaks of measles, chickenpox and mumps: I. seasonal variation in contact rates. *American Journal of Epidemiology*, 98:453–468, 1973. doi: 10.1093/oxfordjournals.aje.a121575.

L.D.C. Lopez-Pascua, M.A. Brockhurst, and A. Bucling. Antagonistic coevolution across productivity gradients: an experimental test of the effects of dispersal. *J. Evol. Biol.*, 23:207–211, 2010. doi: 10.1111/j.1420-9101.2009.01877.x.

L.D.C. Lopez-Pascua and A. Buckling. Increasing productivity accelerates host-parasite coevolution. *J. Evol. Biol.*, 21:853–860, 2008. doi: 10.1111/j.1420-9101.2008.01501.x.

L.D.C. Lopez-Pascua, S. Gandon, and A. Bucling. Abiotic heterogeneity drives parasite local adaptation in coevolving bacteria and phages. *J. Evol. Biol.*, 25:187–195, 2012. doi: 10.1111/j.1420-9101.2011.02416.x.

L.D.C. Lopez-Pascua, A.R. Hall, A. Best, A.D. Morgan, M. Boots, and A. Buckling. Higher resources decrease fluctuating selection during host–parasite coevolution. *Ecol. Lett.*, 17:1380–1388, 2014. doi: 10.1111/ele.12337.

M. Loreau and C. de Mazancourt. Species synchrony and its drivers: Neutral and nonneutral community dynamics in fluctuating environments. *Am. Nat.*, 172:E48–E66, 2008. doi: 10.1086/589746.

M.F. Macpherson, R.S. Davidson, D.B. Duncan, P.W. Lurz, A. Jarrott, and A. White. Incorporating habitat distribution in wildlife disease models: conservation implications for the threat of squirrelpox on the Isle of Arran. *Animal Conservation*, 19:3–14, 2016. doi: 10.1111/acv.12219.

P. Marrow, U. Dieckmann, and R. Law. Evolutionary dynamics of predator–prey systems: an ecological perspective. *J. Math. Biol.*, 34:556–578, 1996.

F. Massol. A framework to compare theoretical predictions on trait evolution in temporally varying environments under different life cycles. *Ecological complexity*, 16:9–19, 2013. doi: 10.1016/j.ecocom.2012.05.004.

F. Massol and F. Débarre. Evolution of dispersal in spatially and temporally variable environments: The importance of life cycles. *Evolution*, 69:1925–1937, 2015. doi: 10.1111/evo.12699.

C.F. Maurice, S.C.L. Knowles, J. Ladau, K.S. Pollard, A. Fenton, A.B. Pedersen, and P.J. Turnbaugh. Marked seasonal variation in the wild mouse gut microbiota. *The ISME Journal*, 9:2423–2434, 2015. doi: 10.1038/ismej.2015.53.

R.M. May and R.M. Anderson. Population biology of infectious diseases: Part II. *Nature*, 280:455–461, 1979. doi: 10.1038/280455a0.

R.M. May and R.M. Anderson. Epidemiology and genetics in the coevolution of parasites and hosts. *Proc. R. Soc. B*, 219:281–313, 1983. doi: 10.1098/rspb.1983.0075.

J. Maynard Smith and G.R. Price. The logic of animal conflict. *Nature*, 246:15–18, 1973.

E. Mazé-Guilmo, S. Blanchet, O. Rey, N. Canto, and G. Loot. Local adaptation drives thermal tolerance among parasite populations: a common garden experiment. *Proc. R. Soc. B*, 283:20160587, 2016. doi: 10.1098/rspb.2016.0587.

E. Mazé-Guilmo, G. Loot, D.J. Páez, T. Lefèvre, and S. Blanchet. Heritable variation in host tolerance and resistance inferred from a wild host-parasite system. *Proc. R. Soc. B.*, 281:20132567, 2014. doi: 10.1098/rspb.2013.2567.

H. McCallum, N. Barlow, and J. Hone. How should pathogen transmission be modelled? *TRENDS in Ecology and Evolution*, 16:295–300, 2001. doi: 10.1016/S0169-5347(01)02144-9.

H. McCallum, A. Fenton, P.J. Hudson, B. Lee, B. Levick, R. Norman, S.E. Perkins, M. Viney, A.J. Wilson, and J. Lello. Breaking beta: deconstructing the parasite transmission function. *Phil. Trans. R. Soc. B*, 372:20160084, 2017. doi: 10.1098/rstb.2016.0084.

D.V. McLeod and T. Day. Pathogen evolution under host avoidance plasticity. *Proc. R. Soc. B*, 282:20151656, 2015. doi: 10.1098/rspb.2015.1656.

M.A. Mealor and M. Boots. An indirect approach to imply trade-off shapes: population level patterns in resistance suggest a decreasingly costly resistance mechanism in a model insect system. *J. Evol. Biol.*, 19:326–330, 2006. doi: 10.1111/j.1420-9101.2005.01031.x.

I. Medina and N.E. Langmore. The evolution of acceptance and tolerance in hosts of avian brood parasites. *Biol. Rev.*, 91:569–577, 2016. doi: 10.1111/brv.12181.

J.A.J. Metz, S.A.H. Geritz, G. Meszéna, F.J.A. Jacobs, and J.S. Van Heerwaarden. Adaptive dynamics: A geometrical study of the consequences of nearly faithful reproduction. In S.J. van Strien and S.M. Verduyn Lunel, editors, *Stochastic and Spatial Structures of Dynamical Systems.*, pages 183–231. Elsevier, North-Holland, 1996.

J.A.J. Metz, R.M. Nisbet, and S.A.H. Geritz. How should we define 'fitness' for general ecological scenarios? *TREE*, 7:198–202, 1992. doi: 10.1016/0169-5347(92)90073-K.

Y. Michalakis, I. Olivieri, F. Renaud, and M. Raymond. Pleiotropic action of parasites: How to be good for the host. *TREE*, 7:59–62, 1992. doi: 10.1016/0169-5347(92)90108-N.

M.R. Miller, A. White, and M. Boots. The evolution of host resistance: Tolerance and control as distinct strategies. *J. Theor. Biol.*, 236:198–207, 2005. doi: 10.1016/j.jtbi.2005.03.005.

M.R. Miller, A. White, and M. Boots. The evolution of parasites in response to tolerance in their hosts: The good, the bad, and apparent commensalism. *Evolution*, 60:945–956, 2006. doi: 10.1554/05-654.1.

M.R. Miller, A. White, and M. Boots. Host life span and the evolution of resistance characteristics. *Evolution*, 61:2–14, 2007. doi: 10.1111/j.1558-5646.2007.00001.x.

S.E. Mitchell, E.S. Rogers, T.J. Little, and A.F. Read. Host–parasite and genotype-by-environment interactions: temperature modifies potential for selection by a sterilizing pathogen. *Evolution*, 59:70–80, 2005. doi: 10.1111/j.0014-3820.2005.tb00895.x.

J. Monod. The growth of bacterial cultures. *Annu. Rev. Microbiol.*, 3:371–394, 1949.

S. Moreno-Gámez, W. Stephan, and A. Tellier. Effect of disease prevalence and spatial heterogeneity on polymorphism maintenance in host–parasite interactions. *Plant Pathology*, 62:133–141, 2013. doi: 10.1111/ppa.12131.

A. Morozov and A. Best. Predation on infected host promotes evolutionary branching of virulence and pathogens biodiversity. *J. Theor. Biol.*, 307:29–36, 2012. doi: 10.1016/j.jtbi.2012.04.023.

R. Mostowy and J. Engelstädter. The impact of environmental change on host-parasite coevolutionary dynamics. *Proc. R. Soc. B*, 278:2283–2292, 2011. doi: 10.1098/rspb.2010.2359.

H.C. Neu. The crisis in antibiotic resistance. *Science*, 257:1064–1073, 1992. doi: 10.1126/science.257.5073.1064.

O. Niaré et al. Genetic loci affecting resistance to human malaria parasites in a west african mosquitovector population. *Science*, 289:213–216, 2002. doi: 10.1126/science.1073420.

S.L. Nuismer, M. Doebeli, and D. Browning. The coevolutionary dynamics of antagonistic interactions mediated by quantitative traits with evolving variances. *Evolution*, 59:2073–2082, 2005. doi: 10.1554/05-141.1.

S.L. Nuismer, R. Gomulkiewicz, and M.T. Morgan. Coevolution in temporally variable environments. *Am. Nat.*, 162:195–204, 2003. doi: 10.1086/376582.

S.L. Nuismer and M. Kirkpatrick. Gene flow and the coevolution of parasite range. *Evolution*, 57:746–754, 2003. doi: 10.1111/j.0014-3820.2003.tb00286.x.

S.L. Nuismer, B.J. Ridenhour, and B.P. Oswald. Antagonistic coevolution mediated by phenotypic differences between quantitative traits. *Evolution*, 61:1823–1834, 2007. doi: 10.1111/j.1558-5646.2007.00158.x.

D.J. Obbard and G. Dudas. The genetics of hostvirus coevolution in invertebrates. *Current Opinion in Virology*, 8:73–78, 2014. doi: 10.1016/j.coviro.2014.07.002.

L.F. Olsen and W.M. Schaffer. Chaos versus noisy periodicity: alternative hypotheses for childhood epidemics. *Science*, 249:499–504, 1990. doi: 10.1126/science.2382131.

S.A. Orlofske, S.M. Flaxman, M.B. Joseph, A. Fenton, B.A. Melbourne, and P.T.J. Johnson. Experimental investigation of alternative transmission functions: Quantitative evidence for the importance of nonlinear transmission dynamics in host–parasite systems. *Journal of Animal Ecology*, 87:703–715, 2018. doi: 10.1111/1365-2656.12783.

S. Pagliarini and A. Korobeinikov. A mathematical model of marine bacteriophage evolution. *R. Soc. open sci.*, 5:171661, 2018. doi: 10.1098/rsos.171661.

A. Papkou, C.S. Gokhale, A. Traulsen, and H. Schulenburg. Host–parasite coevolution: why changing population size matters. *Zoology*, 119:330–338, 2016. doi: 10.1016/j.zool.2016.02.001.

B.J. Parker, J.R. Garcia, and N.M. Gerardo. Genetic variation in resistance and fecundity tolerance in a natural host-pathogen interaction. *Evolution*, 68:2421–2429, 2014. doi: 10.1111/evo.12418.

S.R. Parratt, E. Numminen, and A-L. Laine. Infectious disease dynamics in heterogeneous landscapes. *Annu. Rev. Ecol. Evol. Syst.*, 47:283–306, 2016. doi: 10.1146/annurev-ecolsys-121415-032321.

S. Paterson et al. Antagonistic coevolution accelerates molecular evolution. *Nature*, 464:275–278, 2010. doi: 10.1038/nature08798.

A.J. Peel, J.R.C. Pulliam, A.D. Luis, R.K. Plowright, T.J. OShea, D.T.S. Hayman, J.L.N. Wood, C.T. Webb, and O. Restif. The effect of seasonal birth pulses on pathogen persistence in wild mammal populations. *Proc. R. Soc. B*, 281:20132962, 2014. doi: 10.1098/rspb.2013.2962.

R.M. Penczykowski, A-L. Laine, and B. Koskella. Understanding the ecology and evolution of host–parasite interactions across scales. *Evolutionary Applications*, 9:37–52, 2016. doi: 10.1111/eva.12294.

A.D. Peters and C.M. Lively. Short- and long-term benefits and detriments to recombination under antagonistic coevolution. *J. Evol. Biol.*, 20:1206–1217, 2007. doi: 10.1111/j.1420-9101.2006.01283.x.

T. Poisot, P.H. Thrall, and M.E. Hochberg. Trophic network structure emerges through antagonistic coevolution in temporally varying environments. *Proc. R. Soc. B*, 279:299–308, 2012. doi: 10.1098/rspb.2011.0826.

J.A. Poland, P.J. Balint-Kurti, R.J. Wisser, R.C. Pratt, and R.J. Nelson. Shades of gray: the world of quantitative disease resistance. *Trends in Plant Science*, 14:21–29, 2009. doi: 10.1016/j.tplants.2008.10.006.

R. Porter, R.A. Norman, and L. Gilbert. An alternative to killing? Treatment of reservoir hosts to control a vector and pathogen in a susceptible species. *Parasitology*, 140:247–257, 2012. doi: 10.1017/S0031182012001400.

V. Poullain, S. Gandon, M.A. Brockhurst, A. Buckling, and M.E. Hochberg. The evolution of specificity in evolving and coevolving antagonistic interactions between a bacteria and its phage. *Evolution*, 62:1–11, 2008. doi: 10.1111/j.1558-5646.2007.00260.x.

L. Råberg. How to live with the enemy: Understanding tolerance to parasites. *PLoS Biol.*, 12:e1001989, 2014. doi: 10.1371/journal.pbio.1001989.

L. Råberg, A.L. Graham, and A.F. Read. Decomposing health: Tolerance and resistance to parasites in animals. *Phil. Trans. R. Soc. B*, 364:37–49, 2009. doi: 10.1098/rstb.2008.0184.

L. Råberg, D. Sim, and A. Read. Disentangling genetic variation for resistance and tolerance to infectious diseases in animals. *Science*, 318:812–814, 2007. doi: 10.1126/science.1148526.

C. Rafaluk-Mohr. The relationship between parasite virulence and environmental persistence: a meta-analysis. *Parasitology*, pages 1–6, 2019. doi: 10.1017/S0031182019000015.

F.S. Ramalho, J.B. Malaquias, A.C.S. Lira, F.Q. Oliveira, J.C. Zanuncio, and F.S. Fernandes. Temperature-dependent fecundity and life table of the fennel aphid hyadaphis foeniculi (passerini) (hemiptera: Aphididae). *PLoS ONE*, 10:e0122490, 2015. doi: 10.1371/journal.pone.0122490.

D.A. Rand, M. Keeling, and H.B. Wilson. Invasion, stability and evolution to criticality in spatially extended, artificial host-pathogen ecologies. *Proc. R. Soc. Lond B*, 259:55–63, 1995. doi: 10.1098/rspb.1995.0009.

J.M. Read and M.J. Keeling. Disease evolution on networks: The role of contact structure. *Proc. R. Soc. Lond. B*, 270:699–708, 2003. doi: 10.1098/rspb.2002.2305.

O. Restif and B.T. Grenfell. Vaccination and the dynamics of immune evasion. *J. R. Soc. Interface*, 4:143–153, 2007. doi: 10.1098/rsif.2006.0167.

O. Restif and J.C. Koella. Shared control of epidemiological traits in a coevolutionary model of host-parasite interactions. *Am. Nat.*, 161:827–836, 2003. doi: 10.1086/375171.

O. Restif and J.C. Koella. Concurrent evolution of resistance and tolerance to pathogens. *Am. Nat.*, 164:E90–E102, 2004. doi: 10.1086/423713.

J.J.H. Reynolds, J.A. Sherratt, A. White, and X. Lambin. A comparison of the dynamical impact of seasonal mechanisms in a herbivore–plant defence system. *Theor. Ecol.*, 6:225–239, 2013. doi: 10.1007/s12080-012-0173-1.

J. Rimer, I.R. Cohen, and N. Friedman. Do all creatures possess an acquired immune system of some sort? *Bioessays*, 36, 2014. doi: 10.1002/bies.201300124.

S. Ripp and R.V. Miller. The role of pseudolysogeny in bacteriophage-host interactions in a natural freshwater environment. *Microbiology*, 143:2065–2070, 1997. doi: 10.1099/00221287-143-6-2065.

M.G. Roberts. The pluses and minuses of R_0. *J. R. Soc. Interface*, 4:949–961, 2007. doi: 10.1098/rsif.2007.1031.

D. Roff. *Life history evolution.* Sinauer, Sunderland, MA., 2002. ISBN 9780878937561.

J.R. Rohr, T.R. Raffel, and C.A. Hall. Developmental variation in resistance and tolerance in a multi-host-parasite system. *Functional Ecology*, 24:1110–1121, 2010. doi: 10.1111/j.1365-2435.2010.01709.x.

W. Rowan. Light and seasonal reproduction in animals. *Biol. Rev.*, 13:374–401, 1938. doi: 10.1111/j.1469-185X.1938.tb00523.x.

B. Roy and J. Kirchner. Evolutionary dynamics of pathogen resistance and tolerance. *Evolution*, 54:51–63, 2000.

C. Rueffler, T.J.M. van Dooren, O. Leimar, and P.A. Abrams. Disruptive selection and then what? *TREE*, 21:238–245, 2006. doi: 10.1016/j.tree.2006.03.003.

J.E. Samson, A.H. Magadan, M. Sabri, and S. Moineau. Revenge of the phages: defeating bacterial defences. *Nat. Rev. Microbiol.*, 11:675–687, 2013. doi: 10.1038/nrmicro3096.

N. Sari and E. Augeraud-Véron. Periodic orbits of a seasonal SIS epidemic model with migration. *J. Math. Anal. Appl.*, 423:1849–1866, 2015. doi: 10.1016/j.jmaa.2014.10.084.

A. Sasaki. Host-parasite coevolution in a multilocus gene-for-gene system. *Proc. R. Soc. Lond. B*, 267:2183–2188, 2000. doi: 10.1098/rspb.2000.1267.

C. Schär, P.L. Vidale, D. Lüthi, C. Frei, C. Häberli, M.A. Liniger, and C. Appenzeller. The role of increasing temperature variability in european summer heatwaves. *Nature*, 427:332–336, 2004. doi: 10.1038/nature02300.

P. Schmid-Hempel. Evolutionary ecology of insect immune defences. *Annu. Rev. Entomol.*, 50:529–51, 2005. doi: 10.1146/annurev.ento.50.071803.130420.

P. Schmid-Hempel. *Evolutionary parasitology : the integrated study of infections, immunology, ecology, and genetics.* Oxford University Press, Oxford., 2011. ISBN 9780199229482.

I.B. Schwartz. Multiple stable recurrent outbreaks and predictability in seasonally forced nonlinear epidemic models. *J. Math. Biol.*, 21:347–361, 1985. doi: 10.1007/BF00276232.

I.B. Schwartz and H.L. Smith. Infinite subharmonic bifurcation in an SEIR epidemic model. *J. Math. Biol.*, 18:233–253, 1983. doi: 10.1007/BF00276090.

M.W. Shaw. Seasonally induced chaotic dynamics and their implications in models of plant disease. *Plant Pathology*, 43:790–801, 1994. doi: 10.1111/j.1365-3059.1994.tb01623.x.

C.W. Shepard, E.P. Simard, L. Finelli, A.E. Fiore, and B.P. Bell. Hepatitis B virus infection: Epidemiology and vaccination. *Epidemiologic Reviews*, 28:112–125, 2006. doi: 10.1093/epirev/mxj009.

M.J. Silk, N. Weber, L.C. Steward, R.J. Delahay, D.P. Croft, D.J. Hodgson, M. Boots, and R.A. McDonald. Seasonal variation in daily patterns of social contacts in the

european badger *Meles meles*. *Ecology and Evolution*, 7:9006–9015, 2017. doi: 10.1002/ece3.3402.

C.P. Simmons, J.J. Farrar, N. van Vinh Chau, and B. Wills. Dengue. *N. Engl. J. Med.*, 366:1423–32, 2012. doi: 10.1056/NEJMra1110265.

E.L. Simms and J. Triplett. Costs and benefits of plant responses to disease: resistance and tolerance. *Evolution*, 48:1973–1985, 1994.

H.L. Smith. Multiple stable subharmonics for a periodic epidemic model. *J. Math. Biol.*, 17:179–190, 1983. doi: 10.1007/BF00305758.

M.J. Smith, A. White, J.A. Sherratt, S. Telfer, M. Begon, and X. Lambin. Disease effects on reproduction can cause population cycles in seasonal environments. *Journal of Animal Ecology*, 77:378–389, 2008. doi: 10.1111/j.1365-2656.2007.01328.x.

R.J. Smith?, A.B. Hogan, and G.N. Mercer. Unexpected infection spikes in a model of respiratory syncytial virus vaccination. *Vaccines*, 5:12, 2017. doi: 10.3390/vaccines5020012.

M.T. Sofonea, S. Alizon, and Y. Michalakis. From within-host interactions to epidemiological competition: a general model for multiple infections. *Phil. Trans. R. Soc. B*, 370:20140303, 2015. doi: 10.1098/rstb.2014.0303.

I. Sorrell, A. White, A.B. Pedersen, R.S. Hails, and M. Boots. The evolution of covert, silent infection as a parasite strategy. *Proc. R. Soc. B*, 276:2217–2226, 2009. doi: 10.1098/rspb.2008.1915.

A.J. Spiers, A. Buckling, and P.B. Rainey. The causes of *Pseudomonas* diversity. *Microbiology*, 146:2345–2350, 2000. doi: 10.1099/00221287-146-10-2345.

C. Stawski, C.K.R. Willis, and F. Geiser. The importance of temporal heterothermy in bats. *J. Zool.*, 292:86–100, 2014. doi: 10.1111/jzo.12105.

S.C. Stearns. *The evolution of life histories.* Oxford University Press, Oxford., 1992. ISBN 9780198577416.

E.D. Sternberg, T. Lefèvre, J. Li, C.L.F. de Castillejo, H. Li, M.D. Hunter, and J.C. de Roode. Food plant-derived disease tolerance and resistance in a natural butterfly-plant-parasite interactions. *Evolution*, 66:3367–3376, 2012. doi: 10.1111/j.1558-5646.2012.01693.x.

E.D. Sternberg, T. Lefévre, A.H. Rawstern, and J.C. de Roode. A virulent parasite can provide protection against a lethal parasitoid. *Infection, Genetics and Evolution*, 11:399–406, 2011. doi: 10.1016/j.meegid.2010.11.017.

K.A. Stowe. Experimental evolution of resistance in *Brassica rapa*: Correlated response of tolerance in lines selected for glucosinolate content. *Evolution*, 52:703–712, 1998.

J.F. Strauß and A. Telschow. Modeling the indirect effect of *Wolbachia* on the infection dynamics of horizontally transmitted viruses. *Front. Microbiol.*, 6:378, 2015. doi: 10.3389/fmicb.2015.00378.

S.Y. Strauss and A.A. Agrawal. The ecology and evolution of plant tolerance to herbivory. *TREE*, 14:179–185, 1999. doi: 10.1016/S0169-5347(98)01576-6.

M. Su and M. Boots. The impact of resource quality on the evolution of virulence in spatially heterogeneous environments. *J. Theor. Biol.*, 416:1–7, 2017. doi: 10.1016/j.jtbi.2016.12.017.

D. Summers-Smith. Mortality of the house sparrow. *Bird Study*, 3:265–270, 1956. doi: 10.1080/00063655609475858.

H. Svardal, C. Rueffler, and J. Hermisson. Comparing environmental and genetic variance as adaptive response to fluctuating selection. *Evolution*, 65:2492–2513, 2011. doi: 10.1111/j.1558-5646.2011.01318.x.

H. Svardal, C. Rueffler, and J. Hermisson. A general condition for adaptive genetic polymorphism in temporally and spatially heterogeneous environments. *Theor. Pop. Biol.*, 99:76–97, 2015. doi: 10.1016/j.tpb.2014.11.002.

T.O. Svennungsen and E. Kisdi. Evolutionary branching of virulence in a single-infection model. *J. Theor. Biol.*, 257:408–418, 2009. doi: 10.1016/j.jtbi.2008.11.014.

E.I. Svensson and L. Råberg. Resistance and tolerance in animal enemy–victim coevolution. *TREE*, 25:267–274, 2010. doi: 10.1016/j.tree.2009.12.005.

P.D. Taylor. Evolutionary stability in one-parameter models under weak selection. *Theor. Pop. Biol.*, 36:125–143, 1989. doi: 10.1016/0040-5809(89)90025-7.

R.A. Taylor, A. White, and J.A. Sherratt. How do variations in seasonality affect population cycles? *Proc. R. Soc. B*, 280:20122714, 2013b. doi: 10.1098/rspb.2012.2714.

R.A. Taylor, A. White, and J.A. Sherratt. Seasonal forcing in a host–macroparasite system. *J. Theor. Biol.*, 365:55–66, 2015. doi: 10.1016/j.jtbi.2014.10.007.

L. Teixeira, A. Ferreira, and M. Ashburner. The bacterial symbiont wolbachia induces resistance to rna viral infections in *Drosophila melanogaster*. *PLoS Biology*, 6:e1000002, 2008. doi: 10.1371/journal.pbio.1000002.

A. Tellier and J.K.M. Brown. Stability of genetic polymorphism in host-parasite interactions. *Proc. R. Soc. Lond. B*, 274:809–817, 2007. doi: 10.1098/rspb.2006.0281.

L. Theodosiou, T. Hiltunen, and L. Becks. The role of stressors in altering ecoevolutionary dynamics. *Functional Ecology*, 33:73–83, 2019. doi: 10.1111/1365-2435.13263.

M.B. Thomas and S. Blanford. Thermal biology in insect-parasite interactions. *Trends Ecol. Evol.*, 18:344–350, 2003. doi: 10.1016/S0169-5347(03)00069-7.

J.N. Thompson. *The Coevolutionary Process.* University of Chicago Press., 1994.

J.N. Thompson. Specific hypotheses on the geographic mosaic of coevolution. *Am. Nat.*, 153:S1–S14, 1999. doi: 10.1086/303208.

J.N. Thompson. *The Geographic Mosaic of Coevolution.* University of Chicago Press., 2005.

J.N. Thompson and J.J. Burdon. Gene-for-gene coevolution between plants and parasites. *Nature*, 360:121–125, 1992. doi: 10.1038/360121a0.

P.H. Thrall, L.G. Barrett, P.N. Dodds, and J.J. Burdon. Epidemiological and evolutionary outcomes in gene-for-gene and matching allele models. *Front. Plant Sci.*, 6:1084, 2016. doi: 10.3389/fpls.2015.01084.

P.H. Thrall and J.J. Burdon. Evolution of virulence in a plant host-pathogen metapopulation. *Science*, 299:1735–1737, 2003. doi: 10.1126/science.1080070.

H.J. Tidbury, A. Best, and M. Boots. The epidemiological consequences of immune priming. *Proc. R. Soc. B*, 279:4505–4512, 2012. doi: 10.1098/rspb.2012.1841.

J. Toor and A. Best. The evolution of host resistance to disease in the presence of predators. *J. Theor. Biol.*, 365:104–111, 2015. doi: 10.1016/j.jtbi.2014.10.009.

J. Toor and A. Best. Evolution of host defense against multiple enemy populations. *Am. Nat.*, 187:308–319, 2016. doi: 10.1086/684682.

M.J. Turell, M.L. O'Guinn, D.J. Dohm, and J.W. Jones. Vector competence of north american mosquitoes (diptera: Culicidae) for west nile virus. *J. Med. Entomol.*, 38:130–134, 2001. doi: 10.1603/0022-2585-38.2.130.

A. Uziel and L. Stone. Determinants of periodicity in seasonally driven epidemics. *J. Theor. Biol.*, 305:88–95, 2012. doi: 10.1016/j.jtbi.2012.02.031.

P.F. Vale, A. Fenton, and S.P. Brown. Limiting damage during infection: Lessons from infection tolerance for novel therapeutics. *PLoS Biol.*, 12:e1001769, 2014. doi: 10.1371/journal.pbio.1001769.

P.F. Vale, M. Stjernman, and T.J. Little. Temperature dependent costs of parasitism and maintenance of polymorphism under genotype-by-environment interactions. *J. Evol. Biol.*, 21:1318–1427, 2008. doi: 10.1111/j.1420-9101.2008.01555.x.

M. van Baalen. Coevolution of recovery ability and virulence. *Proc. R. Soc. Lond. B*, 265:317–325, 1998. doi: 10.1098/rspb.1998.0298.

M. van Boven and F.J. Weissing. The evolutionary economics of immunity. *Am. Nat.*, 163:277–294, 2004. doi: 10.1086/381407.

F. van den Berg, N. Bacaer, C. Metz, J.A.J. Lannou, and F. van den Bosch. Periodic host absence can select for higher or lower parasite transmission rates. *Evol. Ecol.*, 25:121–137, 2011. doi: 10.1007/s10682-010-9387-0.

F. van den Berg, C.A. Gilligan, D.J. Bailey, and F. van den Bosch. Periodicity in host availability does not account for evolutionary branching as observed in many plant pathogens: An application to *Gaeumannomyces graminis* var. *tritici*. *Ecology and Epidemiology*, 100:1169–1175, 2010. doi: 10.1094/PHYTO-10-09-0282.

B. van den Bergh, J.E. Michiels, and J. Michiels. Experimental evolution of escherichia coli persister levels using cyclic antibiotic treatments. *Methods Mol. Biol.*, 1333:131–43, 2016. doi: 10.1007/978-1-4939-2854-5_12.

E. Venturino. The effects of diseases on competing species. *Mathematical Biosciences*, 174:111–131, 2001. doi: 10.1016/S0025-5564(01)00081-5.

E. Venturino. Epidemics in predator–prey models: disease in the predators. *IMA Journal of Mathematics Applied in Medicine and Biology*, 19:185–205, 2002.

S. Via and R. Lande. Evolution of genetic variability in a spatially heterogeneous environment: effects of genotype-environment interaction. *Genet. Res.*, 49:147–156, 1987. doi: 10.1017/S001667230002694X.

M. Vincze, I.D. Borcia, and U. Harlander. Temperature fluctuations in a changing climate: an ensemble-based experimental approach. *Scientific Reports*, 7:254, 2017. doi: 10.1038/s41598-017-00319-0.

T. Vogwill, A. Fenton, and M.A. Brockhurst. The impact of parasite dispersal on antagonistic host–parasite coevolution. *J. Evol. Biol.*, 21:1252–1258, 2008. doi: 10.1111/j.1420-9101.2008.01574.x.

T. Vogwill, A. Fenton, and M.A. Brockhurst. Dispersal and natural enemies interact to drive spatial synchrony and decrease stability in patchy populations. *Ecology Letters*, 12:1194–1200, 2009. doi: 10.1111/j.1461-0248.2009.01374.x.

T. Vogwill, A. Fenton, and M.A. Brockhurst. How does spatial dispersal network affect the evolution of parasite local adaptation? *Evolution*, 64:1795–1801, 2010. doi: 10.1111/j.1558-5646.2009.00937.x.

T. Vogwill, A. Fenton, and M.A. Brockhurst. Coevolving parasites enhance the diversity-decreasing effect of dispersal. *Biol. Lett.*, 7:578–580, 2011. doi: 10.1098/rsbl.2011.0071.

C. Vorburger and A. Gouskov. Only helpful when required: a longevity cost of harbouring defensive symbionts. *J. Evol. Biol.*, 24:1611–1617, 2011. doi: 10.1111/j.1420-9101.2011.02292.x.

S.D. Webb, M.J. Keeling, and M. Boots. Spatially extended hostparasite interactions: The role of recovery and immunity. *Theor. Pop. Biol.*, 71:251–266, 2007. doi: 10.1016/j.tpb.2006.07.010.

M.J. West-Eberhard. *Developmental Plasticity and Evolution.* Oxford University Press, 2003. ISBN: 9780195122350.

E.R. Westra, D.C. Swarts, R.H. Staals, M.M. Jore, S.J. Brouns, and J. van der Oost. The CRISPRs, they are a-changin: how prokaryotes generate adaptive immunity. *Annu. Rev. Genet.*, 46:311–339, 2012. doi: 10.1146/annurev-genet-110711-155447.

A. White, J.V. Greenman, T.G. Benton, and M. Boots. Evolutionary behaviour in ecological systems with trade-offs and non-equilibrium population dynamics. *EER*, 8:387–398, 2006.

A. White, P.W.W. Lurz, J. Bryce, M. Tonkin, K. Ramoo, L. Bamforth, A. Jarrott, and M. Boots. Modelling disease spread in real landscapes: Squirrelpox spread in southern scotland as a case study. *Hystrix*, 27, 2016. doi: 10.4404/hystrix-27.1-11657.

K.A.J. White, B.T. Grenfell, R.J. Hendry, O. Lejeune, and J.D. Murray. Effect of seasonal host reproduction on host-macroparasite dynamics. *Math. Biolsci.*, 137:79–99, 1996. doi: 10.1016/S0025-5564(96)00061-2.

N.J. White, S. Pukrittayakamee, T.T. Hien, M.A. Faiz, O.A. Mokuolu, and A.M. Dondorp. Malaria. *Lancet*, 383:723–35, 2014. doi: 10.1016/S0140-6736(13)60024-0.

A.J. Wilson, E.R. Morgan, M. Booth, R. Norman, S.E. Perkins, H.C. Hauffe, N. Mideo, J. Antonovics, H. McCallum, and A. Fenton. What is a vector? *Phil. Trans. R. Soc. B*, 372:20160085, 2017. doi: 10.1098/rstb.2016.0085.

J. Wolinska and K.C. King. Environment can alter selection in host-parasite interactions. *Trends in Parasitology*, 25:236–244, 2009. doi: 10.1016/j.pt.2009.02.004.

K.E. Wommack and R.R. Colwell. Virioplankton: Viruses in aquatic ecosystems. *Microbiology and Molecular Biology Reviews*, 64:69–114, 2000. doi: 10.1128/MMBR.64.1.69-114.2000.

R.C.T. Wright, M.A. Brockhurst, and E. Harrison. Ecological conditions determine extinction risk in co-evolving bacteria-phage populations. *BMC Evol. Biol.*, 16:227, 2016. doi: 10.1186/s12862-016-0808-8.

Y. Yang, Z. Feng, D. Xu, G.J. Sandland, and D.J. Minchella. Evolution of host resistance to parasite infection in the snail–schistosome–human system. *J. Math. Biol.*, 65:201–236, 2012. doi: 10.1007/s00285-011-0457-x.

M. Zbinden, C.R. Haag, and D. Ebert. Experimental evolution of field populations of *Daphnia magna* in response to parasite treatment. *J. Evol. Biol.*, 21:1068–1078, 2008. doi: 10.1111/j.1420-9101.2008.01541.x.

M. Zeller and J.C. Koella. The role of the environment in the evolution of tolerance and resistance to a pathogen. *Am. Nat.*, 190:389–397, 2017. doi: 10.1086/692759.

Q-G. Zhang and A. Buckling. Antagonistic coevolution limits population persistence of a virus in a thermally deteriorating environment. *Ecol. Lett.*, 14:282–288, 2011. doi: 10.1111/j.1461-0248.2010.01586.x.

X-S. Zhang and G.L. Iacono. Estimating human-to-human transmissibility of hepatitis a virus in an outbreak at an elementary school in china, 2011. *PLoS ONE*, 13:e0204201, 2018. doi: 10.1371/journal.pone.0204201.

L. Zhou, Y. Wang, Y. Xiao, and M.Y. Li. Global dynamics of a discrete age-structured SIR epidemic model with applications to measles vaccination strategies. *Mathematical Biosciences*, 308:27–37, 2019. doi: 10.1016/j.mbs.2018.12.003.

M. Zuk and A.M. Stoehr. Immune defense and host life history. *Am. Nat.*, 160:S9–S22, 2002. doi: 10.1086/342131.